Study and RTDS Implementation of Some Controllers for Performance and Power Quality Improvement of an Induction Motor Drive System

A Thesis submitted to National Institute of Technology, Rourkela

In partial fulfilment of the requirements for of the degree of

Doctor of Philosophy
In
Electrical Engineering

By
Madhu Singh
Roll. No. 509EE705

Under the Guidance of
Dr. K.B. Mohanty

Department of Electrical Engineering
National Institute Technology
Rourkela-769008
India
May, 2013

Department of Electrical Engineering

National Institute of Technology, Rourkela-769008

India

CERTIFICATE

This is to certify that the thesis titled "**Study and RTDS Implementation of Some Controllers for Performance and Power Quality Improvement of an Induction Motor Drive System**", submitted to the National Institute of Technology, Rourkela by Mrs. Madhu Singh, Roll. No. 509EE705 for the award of **Doctor of Philosophy** in Electrical Engineering is a bonafide record of research work carried out by her under my supervision and guidance from August 2009 to May 2013. The candidate has fulfilled all the prescribed requirements. The thesis which is based on candidate's own work or any part of it has not been submitted elsewhere for award of any degree/diploma. In my opinion the thesis is of standard required for the award of a **Doctor of Philosophy** in Electrical Engineering.

Prof. Kanungo Barada Mohanty

Associate Professor

Department of Electrical Engineering

Natinal Institute of Technology

Rourkela-769008 (ODISHA)

Acknowledgements

The author wishes to express profound gratitude and indebtness to her supervisor, Prof. K. B. Mohanty, who introduced to her the area of the present research and guided her effectively to successful completion. Prof. Mohanty was always available for discussion and suggestion for simulation and real time implementation of the drive system.

The author expresses her sincere gratitude to Doctorate Scrutiny Committee Members, Prof. P.C. Panda, Prof. K.K. Mahapatra and Prof. K. P. Maity for their critical comments and valuable suggestions at various stages of the programme. Prof. Santanu Bhattacharya, Dean (Academic) has been very cooperative and supportive, and she is grateful to him.

The author gratefully acknowledges Prof. A. K. Panda**,** the Head of the Department, for his gentle and supportive attitude and providing all possible facilities in the Power Electronics and Drive laboratory whilst pursuing present research work.

Words fail to acknowledge the encouragement and personal attention given by Prof. Bhidyadhar Subudhi**,** Ex-Head of the Department during his tenure.

The author owes her deep sense of indebtness to Prof. S. K. Sarangi**,** Director, NIT Rourkela, for providing an excellent and an ideal academic environment. Life at NIT Rourkela is ever fluid and progressive. As a Research Scholar of NIT Rourkela, she has been surrounded by intellect professors, colleagues and students, these communities have provided a rich interacting and fertile environment to study and explore new ideas. Because of them, her work accomplished in fruitful way.

The author also thanks the staff in the Electrical Engineering Department as well as in other departments NIT Rourkela for always being so helpful and friendly.

The author extends her sincere thanks to Prof. Rambabu Kodali, Director and Prof. Rajnish Srivastav, Ex-Director, NIT Jamshedpur for sponsoring her under Quality Improvement Programme (QIP) and granting leave to carry out and to complete this work at NIT Rourkela.

The author is deeply obliged to Prof. A.N.Thakur, Mrs Reeta Thakur, Prof. Prahlad Prasad, Mrs. Chetna Sumedha, Prof. Ranjit Prasad and Mrs. Anita Prasad, for their continual support and encouragement.

Last but not the least, the author would like to thank her parents, Shri I. N. Singh, Smt. Shail Kumari Singh, Shri S.D. Singh and Smt. Munni Singh for their love and moral support. She is grateful to her husband Shri Rajiv Ranjan Singh, son Survesh Ranjan and daughter Srishti, for their sacrifices, earnest support and patience during entire period of this work.

NIT Rourkela

Date: (Madhu Singh)

This research work is dedicated to

My children

Sarvesh Ranjan and Srishti

and husband

Rajiv Ranjan Singh

Abstract

The present research work is directed to study of some controllers for design, modelling, simulation and RTDS implementation of induction motor (IM) drive system to identify suitable controller for high performance. Initially dynamic modelling and simulation of a feedback linearization scheme for high performance IM drive is carried out. The flux measurement required in this scheme is achieved using flux estimator rather sensor to simplify the system. The complexity and calculation involved in reference frame transformation is taken care by implementing the scheme in stationary reference frame. Two linear and independent subsystems: (i) Electrical and (ii) Mechanical are created by linearizing control scheme. The systematic design of closed loop control scheme using Proportional Integral (PI) controller is developed for implementation. To take care of uncertainties in the system the Fuzzy controller is added to speed controller.

Sliding Mode (SM) controller considered to be a robust control strategy is designed and developed for IM drive. A procedure of finding gain and bandwidth of the controller is developed to take care of model inaccuracies, load disturbances and rotor resistance variation. During practical implementation of this controller for IM leads to oscillations and of state variable chattering due to presence of limiter and PWM inverter in the system.

Iterative Learning controller (ILC) introduced in recent time is gaining popularity due to capability to take care of short comings of Sliding Mode controller. Feedback and feed forward Iterative Learning controller combining fuzzy logic is designed and developed. The MATLAB/SIMULINK model of IM drive with controllers designed are simulated under various possible operating conditions. A comparative study of three controllers is carried out in similar situation and the response of the drive system is presented.

Normally we neglect stability aspect of IM while investigating procedure for performance improvement of IM drive. Stability study of IM in open loop and closed

loop conditions using Lyapunov criteria and also considering the power balance equation are presented. Subsequently Lyapunov based controller for IM is designed and developed. Another set of three controllers PI, SM and Lyapunov function based controllers for comparative study are taken for higher speed and heavy load. The simulation results obtained from MATLAB are verified on Real Time Digital Simulator (RTDS). The simulation results obtained here are similar to previous results which justify the accuracy in design and modelling of the system.

The research work on drive system has been extended for small contribution to minimize the distortion/ pollution in ac mains due to converter based drive. Initially passive shunt, series and hybrid filters are tested at the point of common coupling (PCC) for harmonic mitigation. A thyristor switched capacitor (TSC) based hybrid filter is designed for variable reactive power demand due to load change. Model Reference Adaptive Control Law is implemented to optimize the switching current of capacitor. The designed filter has been tested in MATLAB/ SIMULINK environment and overall performance of this filter at PCC is found to be better than other types of filter.

Key words: *Induction Motor, Controllers, High performance drive, Fuzzy logic, MATLAB simulation, Real Time Digital Simulation, Uncontrolled ac-dc converter, Power filter, Thyristor switched capacitor, Harmonic mitigation, Reactive power.*

Contents

		Page No.
Abstract		**vi**
List of symbols		**xiii**
List of Figures		**xvi**
List of Tables		**xxii**
1. Introduction		**1**
1.1	General	1
1.2	Literature Survey	2
1.3	Aims and Objectives of the Thesis	8
1.4	Scope of the Thesis	8
2. Stability Study and Feedback Linearization of Induction Motor Drive with PI Controller and PI with Fuzzy Torque Compensator		**11**
2.1	General	11
2.2	Induction Motor Modeling	11
2.3	Study of Stability of Induction Motor in Lyapunov Sense	16
2.3.1	Perturbation Model about Equilibrium Point	16
2.3.2	Energy and Power Balance Equations	19
2.3.3	Stability Analysis of the Induction Motor in the Sense of Lyapunov	23
2.3.4	Global Stability of Induction Motor	24
2.3.5	Global Asymptotic Stability of the Unloaded Induction Motor	24
2.3.6	Global Stability of Loaded Induction Motor	27
2.3.6.1	A Case Study	28
2.4	Feedback Linearization Control	31
2.5	Design of PI Controllers	34
2.5.1	PI Controller for Electrical Subsystem	35
2.5.2	PI Controller for Mechanical Subsystem	37
2.5.3	Fuzzy Torque Compensator for Speed Response Improvement	39
2.6	Summary of the Chapter	44

3. Design of SM, IL and Lyapunov Function Based Controller for the Induction Motor Drive **45**

3.1 General 45

3.2 Sliding Mode Controller 46

3.2.1 A Case Study 51

3.3 Iterative Learning Controller 54

3.4 Lyapunov Function Based Controller 58

3.4.1 State-space model of Induction Motor 58

3.4.2 Energy and Power Balance Equations 60

3.4.3 Controller Design and Stability Analysis of the Induction Motor 64

3.4.3.1 Selection of the Lyapunov Function 64

3.4.3.2 Global Stability analysis of the Induction Motor drive 66

3.4.4 System Description 67

3.5 Summary of the Chapter 68

4. Simulation and Performance Comparison of Induction Motor Drive With PI, Sliding Mode, Iterative Learning and Lyapunov Function based controller **69**

4.1 General 69

4.2 Description of the Proposed Induction Motor Drive System 70

4.2.1 Speed Controller 71

4.2.1.1 Proportional Integral Speed Controller 71

4.2.1.2 Fuzzy Torque Compensator 72

4.2.1.3 Sliding Mode Speed Controller 72

4.2.1.4 Iterative Learning Controller 73

4.2.1.5 Limiter 74

4.2.2 Flux Controller 74

4.2.2.1 Field Weakening 74

4.2.2.2 Proportional Integral Flux Controller 75

4.2.2.3 Sliding Mode Flux Controller 76

4.2.3 Rotor Flux Estimator 76

4.2.4 Feedback Linearizing Controller 77

4.2.5 Current Controlled Voltage Source Inverter 78

4.2.6 PWM Current Controller 79
4.3 MATLAB Model of the Induction Motor Drive System 80
4.3.1 Speed and Flux controller 81
4.3.2 Fuzzy Torque Compensator 82
4.3.3 Sliding Mode Controller 83
4.3. 4 Iterative Learning Controller 84
4.3.5 Feedback Linearizing Controller 84
4.3.6 Rotor Flux and Electromagnetic Torque Estimator 85
4.3.7 Two Phase Stationary to Three Phase Stationary Converter 86
4.3.8 Current Regulator 87
4.4 Simulation Results and Discussions 87
4.4.1 Performance Comparison between PI and PI with Fuzzy Torque Compensator 87
4.4.2 Performance Analysis of IM Drive with PI, SM and ILC 92
4.4.3 Performance Analysis of IM Drive with PI. SM and Lyapunov Function Based Controller 100
4.5 Summary of the Chapter 104

5. Real-Time Simulation of The Induction Motor Drive 105
5.1 General 105
5.2 RT-LAB Simulator 106
5.3 Full Real -Time Simulation of the IM Drive 108
5.4 Real- Time Simulation Results and Discussions 114
5.4.1 Performance Comparison of IM Drive between PI and PI with Torque Compensator 115
5.4.2 Performance Analysis of IM Drive with PI, SM and ILC 116
5.4.3 Performance Analysis of IM Drive with PI, SM and Lyapunov Function based Controllers 118
5.5 Summary of the Chapter 126
6. Power Quality Improvement at Ac Mains for the Induction Motor Drive System 127
6.1 General 127
6.2 Classification of Passive Filter 128

6.2.1 Passive Shunt Filter 128
6.2.2 Passive Series Filter 128
6.2.3 Passive Hybrid Filter 129
6.3 Compensation Principle and Design of Passive Filters 130
6.3.1 Compensation Principle of Passive Shunt Filters 131
6.3.2 Compensation Principle of Passive Series Filters 132
6.3.2 Compensation Principle of Passive Hybrid Filters 132
6.4 Design of Passive and TSC-Hybrid Filter 133
6.4.1 Filter design constraints 133
6.4.2 Design of Passive Shunt Filter 134
6.4.3 Design of Passive Series Filter 136
6.4.4 Design of Passive Hybrid Filter 137
6.4.5 Design of TSC- Hybrid filter 137
6.5 Thyristor Switched Capacitor System 138
6.5.1 Dynamic Modeling of Thyristor Switched Capacitor 138
6.5.2 Model Reference Adaptive Controller 140
6.6 MATLAB Model of the IM Drive System fed from Three-Phase Uncontrolled ac-dc Converter without and with Filter 145
6.6.1 MATLAB Model of the IM Drive System fed from Uncontrolled ac-dc Converter without Filter 146
6.6.2 MATLAB Model of the IM Drive System fed from three-phase Uncontrolled ac-dc Converter with Passive Shunt Filter 146
6.6.3 MATLAB Model of the IM Drive System fed from three-phase Uncontrolled ac-dc Converter with Passive Series Filter 146
6.6.4 MATLAB Model of the IM Drive System fed from three-phase Uncontrolled ac-dc Converter with Passive Hybrid Filter 147
6.6.5 MATLAB Model of the IM Drive System fed from three-phase Uncontrolled AC-DC Converter with TSC-Hybrid Filter 147
6.7 Results and Discussions 148
6.8 Summary of the chapter 165
7. Main Conclusions and Suggestions for Future Works 166
7.1 General 166
7.2 Summary of the Present Research 166

7.3 Main Contributions of the Thesis 167
7.4 Scope for Future Research 168
8. References 170
9. Publications 182

List of Symbols

$i_{as}, i_{bs}\ i_{cs}$	Three phase stator currents
$i_{as}^*, i_{bs}^*\ i_{cs}^*$	Three phase reference phase currents
$V_{as}, V_{bs}\ V_{cs}$	Three phase inverter voltages
$V_{as}^*, V_{bs}^*\ V_{cs}^*$	Three phase reference phase voltages
$i_{\alpha s}, i_{\beta s}$	Stator current components in α-β stator fixed frame
$i_{\alpha s}^*, i_{\beta s}^*$	Stator current components in α-β stator fixed frame
$V_{\alpha s}, V_{\beta s}$	Stator voltage components in α-β stator fixed frame
$V_{\alpha s}^*, V_{\beta s}^*$	Stator reference voltage components in α-β stator fixed frame
$\psi_{\alpha s}, \psi_{\beta s}$	Stator flux linkage components in α-β stator fixed frame
$\psi_{\alpha s}, \psi_{\beta s}$	Rotor flux linkage components in α-β stator fixed frame
ψ_r, ψ_r^*	Rotor actual and reference flux linkage magnitude
ω_r, ω_r^*	Rotor actual and reference speed in rpm
L_m	Magnetizing inductance
L_s, L_r	Stator and rotor inductances
R_s, R_r	Stator and rotor phase winding resistances
σ	$(1-\frac{L_m^2}{L_s L_r})$ Leakage coefficient
J, B	Moment of inertia and friction of motor
p	No. of pole pair
T_e, T_e^*, T_l	Electromagnetic, reference and load torque of motor
K_T	$\frac{3pL_m}{2L_r}$ Motor torque constant
$u1$, $u2$	Control outputs from the speed controller and the flux controller
K_{p1}, K_{i1}	Proportional integral (PI) constants of the mechanical subsystem
K_{p2}, K_{i3}	Proportional integral constants of the electrical subsystem
$\tau_{\psi r}$, $\tau_{\omega r}$	Flux and speed time constant
$G_1(s)$, $G_2(s)$	Transfer function of PI and electrical subsystem
$G_3(s)$, $G_4(s)$	Transfer function of PI and mechanical subsystem

$G_0(s)$, $G01(s)$	Open loop transfer function of the mechanical and the electrical subsystems including corresponding PI controller
ς, ω_n	Damping factor and natural frequency
μ	Degree of membership in a fuzzy set
s_1, s_2	the rotor speed sliding surface and the rotor flux sliding surface
λ_1, λ_2	Bandwidth of the rotor speed sliding surface and rotor flux sliding surface
η_1, η_1	Positive constant used in the sliding mode
$\text{sgn}(s_1), \text{sgn}(s_2)$	Rotor speed switching control signal and Rotor flux switching control signal
k_1, k_2	Discontinuous control gains of speed sliding mode and flux sliding mode controller
ϕ, Γ	Steady proportional and integral gains of iterative learning controller
$\Delta\phi, \Delta\Gamma$	Steady proportional and integral gains of TS fuzzy controller
$V_{sa}, V_{sb}\ V_{sc}$	Three phase supply voltages
$i_{sa}, i_{sb}\ i_{sc}$	Three phase supply currents
V_q , V_d	Direct and Quadrature axes components of stator voltage in the synchronously rotating (d-q) frame
i_q , i_d	Direct and Quadrature (d-q) axes components of stator current in the synchronously rotating (d-q) frame
V_s	Source (supply) voltage (Line to neutral)
I_s	Source (supply) current
V_l	Thevenin's equivalent load voltage (Line to neutral)
I_l	Thevenin's equivalent load current
f	Supply frequency
ω	Supply angular frequency
Z_s	Source Impedance
Z_{sh}	Impedance of the parallel passive filter
Z_{se}	Impedance of the series passive filter
Y_{se}	Admittance of the series passive filter

Z_l	Thevenin's equivalent impedance
h_n	Harmonic order of the filter
f_h	Resonant frequency for the h_n^{th} harmonic
h	Order of fundamental frequency
L_5, L_7, L_{11}	Inductance of passive filter tuned for 5^{th}, 7^{th} and 11^{th} harmonics
C_5, C_7, C_{11}	Capacitance of passive filter tuned for 5^{th}, 7^{th} and 11^{th} harmonics
R_5, R_7, R_{11}	Resistance of passive filter tuned for 5^{th}, 7^{th} and 11^{th} harmonics
R_{sh}, L_{sh}, C_{sh}	Resistance, inductance and capacitance of shunt passive filter
R_{se}, L_{se}, C_{se}	Resistance, inductance and capacitance of series passive filter
$Z_{5se}, Z_{7se}, Z_{11se}$	Impedances 5^{th},7^{th} and 11^{th} order series passive filters
R_{PF}, L_{PF}, C_{PF}	Resistance, inductance and capacitance of thyristor switched capacitor
γ	Positive constant used in the reference model adaptive controller
P, I	Positive symmetric definite constant matrix and positive symmetric unit matrix
X_{shc}, X_{shL}	Reactance of shunt capacitance C_{sh} and reactance of shunt inductance L_{sh} at fundamental frequency
X_{seC}, X_{seL}	Reactance of series capacitance C_{se} and reactance of series inductance L_{se} at fundamental frequency
L_{as}	Line Inductance
V_{dc}	DC-Link voltage
L_{dc}, C_{dc}	Inductance of DC link inductor and capacitor of DC link capacitor
P	Three phase active power
Q	Three phase reactive power
Q_{sh}	Reactive power of passive shunt filter
Q_{se}	Reactive power of passive series filter
Q_F	Quality factor

List of Figures

Fig.2.1 Stationary (α-β) equivalent circuit of three phase induction motor …12

Fig.2.2 Feedback linearizing controller …33

Fig.2.3 Block diagram of the open loop electrical system …34

Fig.2.4 Block diagram of the open loop mechanical system …34

Fig.2.5 Block diagram of the closed loop electrical subsystem with PI Controller …34

Fig.2.6 Block diagram of the closed loop mechanical subsystem with PI controller …37

Fig.2.7 Block diagram of speed controller with fuzzy torque compensator …39

Fig.2.8 Membership functions of fuzzy torque compensator : (a) error, (b) change in error, (e) change in control output …40

Fig.2.9 The dynamic behaviour of drive torque response …42

Fig. 3.1 Block diagram of sliding mode speed controller …51

Fig. 3.2 Block diagram of sliding mode flux controller …51

Fig.3.3 Membership functions of $\Delta e_k(t)$, $\Delta ce_k(t)$, $f_{(1,2,3,4)}$ and $\Delta u1^{kb}_{(k+1)}(t)$ …57

Fig.3.4 Block diagram of iterative learning speed controller for k^{th} trial …57

Fig.3.5 System configuration of the feedback linearized induction motor drive system with Lyapunov Function based controller …67

Fig.4.1 Schematic block diagram of a linearized induction motor drive system …70

Fig.4.2 Block diagram for proportional integral speed controller …72

Fig.4.3 Block diagram for proportional integral flux controller …75

Fig.4.4 Schematic diagram of current controlled VSI …79

Fig.4.5 Principle of hysteresis-band current control …80

Fig.4.6 MATLAB model of linearized induction motor drive using PI controller …81

Fig.4.7 MATLAB submodel of PI speed controller …82

Fig.4.8 MATLAB submodel of PI Flux controller …82

Fig.4.9 MATLAB submodel of fuzzy torque compensator …82

Fig.4.10 MATLAB submodel of sliding mode speed controller …83

Fig.4.11 MATLAB submodel of sliding mode flux controller …83

Fig.4.12 MATLAB submodel of TS fuzzy iterative learning controller …84

Fig.4.13 MATLAB model of the feedback linearizing decoupling controller …85

Fig.4.14 MATLAB submodel of rotor flux and torque estimator …86

Fig.4.15 MATLAB submodel of two phase to three phase converter …86

Fig.4.16 MATLAB submodel of current regulator

Fig.4.17 Simulation response of IM drive for step change and loading with PI controller showing: (a) reference and motor speed (b) load torque and electromagnetic torque (c) α-β stator current components (d) α-β rotor flux linkage component …90

Fig.4.18 Simulation response of IM drive for step change and loading using PI with fuzzy torque compensator showing: (a) reference and motor speed (b) load torque and electromagnetic torque (c) α-β stator current components (d) estimated α-β rotor flux linkage components …92

Fig.4.19 Simulation response of IM drive for starting, speed reversal and load perturbation with PI controller showing: (a) motor speed (b) load torque and electromagnetic torque (c) α-β stator current components (d) α-β rotor flux linkage components …93

Fig.4.20 Simulation response of IM drive for starting, speed reversal and load perturbation with SM showing: (a) motor speed (b) load torque and electromagnetic torque (c) α-β stator current components (d) α-β rotor flux linkage components …94

Fig.4.21 Simulation response of IM drive for starting, speed reversal and load perturbation with ILC showing: (a) motor speed (b) load torque and electromagnetic torque (c) α-β stator current components (d) α-β rotor flux linkage components …95

Fig.4.22. Simulation response of IM drive for periodic speed and periodic load perturbation with PI controller showing: (a) motor speed (b) motor speed error (c) load torque and electromagnetic torque (d) α-β stator current components (e) α-β rotor flux linkage components …97

Fig.4.23 Simulation response of IM drive for periodic speed and periodic load perturbation with SM controller showing: (a) motor speed (b) motor speed error (c) load torque and electromagnetic torque (d) α-β stator current components (e) α-β rotor flux linkage component …98

Fig.4.24. Simulation response of IM drive for periodic speed and periodic load perturbation with ILC showing: (a) motor speed (b) motor speed error (c) load torque and electromagnetic torque (d) α-β stator current components (e) α-β rotor flux linkage component …99

Fig.4.25 Simulation response of IM drive for 1000 rpm speed step change and heavy external load application with PI controller showing: (a) motor speed (b) load torque and electromagnetic torque (c) α-β stator current components (d) estimated α-β rotor flux linkage components …101

Fig.4.26 Simulation response of IM drive for 1000 rpm speed step change and heavy external load application with SM controller showing: (a) motor speed (b) load torque and electromagnetic torque (c) α-β stator current components (d) α-β rotor flux linkage components …102

Fig.4.27 Simulation response of IM drive for 1000 rpm speed step change and heavy external load application with Lyapunov function based controller showing: (a) motor speed (b) load torque and electromagnetic torque (c) α-β stator current components (d) estimated α-β rotor flux linkage components …103

Fig.5.1 RT-LAB Simulator Architecture …107

Fig.5.2 Building of a MATLAB /SIMULINK block model of a linearized induction motor using PI speed and flux controller …108

Fig.5.3 Grouping the induction motor MATLAB model into the subsystems namely sm_master, ss_slave and sc_console …110

Fig.5.4 Configuration of the sm_master subsystem …110

Fig.5.5 Configuration of the ss_slave subsystem …111

Fig.5.6 Configuration of the sc_console subsystem …111

Fig.5.7 Photographs of experimental setup with RT-LAB simulator interfaced to an oscilloscope and PC ...113

Fig.5.8 Photographs of experimental setup with RT-LAB simulator interfaced to an oscilloscope performance showing speed reversal tracking ...114

Fig.5.9 RTDS Hardware results for starting, and load perturbation of IM drive with PI controller illustrating; (a) 1. motor set speed (rpm), 2. motor actual speed (rpm), 3. electromagnetic and 4. load torque (N.m) ,(b) 1. α-β stator currents (A) and 2. α- β rotor flux linkages (V.s) ...119

Fig.5.10 RTDS Hardware results with PI controller for starting dynamics under no load illustrating: 1. α-β stator currents (A) and 2. α- β rotor flux linkages (V.s) ...119

Fig.5.11 RTDS Hardware results for starting, and load perturbation of 5 hp linearized induction motor with PI and fuzzy torque compensator illustrating; (a) 1. motor set speed (rpm), 2. motor actual speed (rpm), 3.

electromagnetic and 4. load torque (N.m) (b) 1. α-β stator currents (A) and 2. α- β rotor flux linkages (V.s) ...120

Fig.5.12 RTDS Hardware results for PI with fuzzy torque compensator for starting, dynamics under no load illustrating 1. α-β stator currents (A) and 2. α- β rotor flux linkages (V.s) ...120

Fig.5.13 RTDS Hardware results of IM drive with (a) P-I and (b) SM (c) ILC for speed step change ,10Nm external load and speed reversal; 1. motor speed (rpm) , 2. electromagnetic and 3. load torque (N.m) , 4. stator phase current (A) ...121

Fig.5.14 RTDS Hardware results of IM drive with PI controller for periodic speed and load torque illustrating; (a) 1. motor reference and actual speed (rpm) and 2. electromagnetic and load torque (N.m) (b) 1. α-β stator current (A) and 2. α- β rotor flux linkages (V.s) (c) 1. motor actual speed (rpm), 2. reference speed (rpm) and 3. speed error (rpm) ...122

Fig.5.15 RTDS Hardware results of IM drive with SM controller for periodic speed and load torque illustrating (a) 1.motor reference and actual speed (rpm) and 2. electromagnetic and load torque (Nm) (b) 1. α-β stator currents (A) and 2. α-β rotor flux linkages (V.s) (c) 1. motor actual speed (rpm) , 2. reference speed (rpm) and 3. speed error (rpm) ...123

Fig.5.16 RTDS Hardware results of IM drive with ILC for periodic speed and load torque illustrating; (a) 1. motor reference and actual speed (rpm) and 2. electromagnetic and load torque (N.m) (b) 1. α-β stator currents (A) and 2. α- β rotor flux linkages (V.s) (c) 1. motor actual speed (rpm) , 2. reference speed (rpm) and 3. speed error (rpm) ...124

Fig.5.17 RTDS Hardware results of IM drive with (a) PI and (b) SM and (c) Lyapunov function based controller for 1000 rpm speed step change and heavy external load application illustrating ; 1. motor speed (rpm), 2. electromagnetic and 3. load torque (N.m) , 4. stator phase current (A) ...125

Fig.6.1 Schematic diagram of a 3-phase uncontrolled ac-dc converter fed IM drive with passive shunt filter connected at point of common coupling ..129

Fig.6.2 Schematic diagram of a 3-phase uncontrolled ac-dc converter fed IM drive with passive series filter connected at point of common coupling ...130

Fig.6.3 Schematic diagram of a 3-phase uncontrolled ac-dc converter fed IM drive with passive hybrid filter connected at point of common coupling ...130

Fig.6.4 Thevenin's equivalent circuit of a shunt LC filter for harmonic voltage source ...132

Fig.6.5 Thevenin's equivalent circuit of a series LC filter for harmonic voltage source ...133

Fig.6.6 Thevenin's equivalent circuit of a hybride LC filter for harmonic voltage source ...133

Fig.6.7 Low pass Filter ...134

Fig.6.8 High pass Filter ...134

Fig.6.9 (a) Low block passive series filter and
(b) High block passive series filter ...137

Fig.6.10 Schematic diagram of a 3-phase uncontrolled ac-dc converter fed induction motor drive with TSC- hybrid filter ...138

Fig.6.11. a-b-c to d-q-0 transformation ...139

Fig.6.12 Model reference adaptive control scheme for the proposed TSC ...145

Fig.6.13 MATLAB model for three- phase uncontrolled ac-dc converter feeding induction motor drive ...151

Fig.6.14 MATLAB model for three- phase uncontrolled ac-dc converter feeding induction motor drive with passive shunt filter connected at PCC ...151

Fig.6.15 MATLAB model for three- phase uncontrolled ac-dc converter feeding induction motor drive with passive series filter connected at PCC ...152

Fig.6.16 MATLAB model for three- phase uncontrolled ac-dc converter feeding induction motor drive with passive hybrid filter connected at PCC ...152

Fig.6.17 MATLAB model for three- phase uncontrolled ac-dc converter feeding induction motor drive with TSC-Hybrid filter connected at PCC ...153

Fig.6.18 MATLAB model of the model adaptive reference controller design for thyristor switched capacitor ...153

Fig.6.19 Dynamic response of three-phase uncontrolled ac-dc converter feedinginduction motor drive system illustrating: (a) motor speed, (b) actual torque and electromagnética torque (c) active power and reactive power (d) dc link voltage (e) supply phase voltage (f) supply phase current full load, half load and no load …154

Fig.6.20 Supply voltage and current of three-phase uncontrolled rectifier feeding IM drive at (a) full load, (b) half load and (c) no load ...155

Fig.6.21 Supply current harmonic spectrum of three-phase uncontrolled converter feeding induction motor drive at (a) full load, (b) half load and (c) no load ...155

Fig.6.22 Dynamic response of three-phase uncontrolled ac-dc converter with passive shunt filter feeding induction motor illustrated for (a) motor speed, (b) actual torque and electromagnética torque (c) active power and reactive power (d) dc link voltage (e) supply phase voltage (f) supply phase current at full load, at half load and no load …156

Fig.6.23 5th , 7^{th} and 11^{th} harmonic currents ...157

Fig.6.24 Fig.6.24 Supply voltage and current of three-phase uncontrolled ac-dc converter with passive shunt filter at (a) full load, (b) half load and (c) no load ...157

Fig.6.25 Fig.6.25 Supply current harmonic spectrum of three-phase uncontrolled rectifier with passive shunt filter at (a) full load, (b) half load and (c) no load ...158

Fig.6.26 Dynamic response of three-phase uncontrolled ac-dc converter with passive series filter feeding induction motor illustrated for (a) motor speed, (b) actual torque and electromagnética torque (c) active power and reactive power (d) dc link voltage (e) supply phase voltage (f) supply phase current at full load, at half load and no load …159

Fig.6.27 Fig.6.27 Supply voltage and current of three-phase uncontrolled ac-dc converter with passive series filter at (a) full load, (b) half load and (c) no load ...160

Fig.6.28 Supply current harmonic spectrum of three-phase uncontrolled ac-dc converter with passive series filter feeding induction motor drive at (a) full load, (b) half load and (c) no load ...160

Fig.6.29 Dynamic response of three-phase uncontrolled ac-dc converter with passive hybrid filter with line inductor feeding induction motor illustrated for (a) motor speed, (b) actual torque and electromagnética torque (c) active power and reactive power (d) dc link voltage (e) supply phase voltage (f) supply phase current at full load, at half load and no load …161

Fig.6.30 Supply voltage and current of three-phase uncontrolled ac-dc converter with passive hybrid filter at full load, at half load and at no load ...162

Fig.6.31 Supply current harmonic spectrum of three-phase uncontrolled converter with passive hybrid filter feeding induction motor drive at full load, at half load and no load ..162

Fig. 6.32 Dynamic response of three- phase uncontrolled rectifier with TSC hybrid filter feeding induction motor illustrated for (a) motor speed, (b) actual torque and electromagnética torque (c) active power and reactive power (d) dc link voltage (e) supply phase voltage (f) supply phase current at full load, at half load and no load …163

Fig.6.33 Supply voltage and current of three-phase uncontrolled converter with TSC- hybrid filter at full load, at half load and at no load ...164

Fig.6.34 Supply current harmonic spectrum of three-phase uncontrolled ac-dc converter with TSC- hybrid filter feeding induction motor drive at full load, at half load and no load ...164

List of Tables

Table 2.1	Motor specifications and parameters	…12
Table 2.2	Stability test result for three cases	…30
Table 2.3	Evaluation of fuzzy inference rules	…43
Table 4.1	Switching states of inverter IGBT	…78
Table 4.2	Performance comparison between PI and PI with fuzzy torque compensator controllers	…89
Table 4.3	Performance comparison among PI, SM and IL controllers for starting, speed reversal, light load application	…96
Table 4.4	Performance comparison among PI, SM and Lyapunov Function based controllers for high speed and heavy load	…100
Table 6.1	Parameters of shunt filter	...146
Table 6.2	Parameters of series filter	...147
Table 6.3	Parameters of passive hybrid filter	...147
Table 6.4	Parameters of TSC-hybrid filter	...148
Table 6.5	Power quality comparison of three-phase uncontrolled converter with various passive filters and TSC-hybrid filter	...165

Chapter – 1

Introduction

1.1 General

Today the industrial demand is high performance drive for quality product at lesser cost and lower maintenance. DC motors with thyristor converter and simple control structure have been the traditional choice for most of the high performance industrial applications. The problems with this drive are its costly maintenance, low torque-to-weight ratio and reduced unity capacity. The rapid developments in power electronics and microprocessors technology, the field oriented control and feedback linearization technique have enhanced the potential of induction motor drive for high performance application. For field oriented control the decoupling of motor speed and rotor flux is obtained under the assumption that actual rotor flux is constant. Research and development activities for performance improvement of ac drives are going on continuously around the world. With availability of the technology and tools at low cost in the market, real time applications of modern control theory are being investigated for enhancing the performance of the ac drive system with various controller like neural network, gray feedback, model reference adaptive, fuzzy logic, fuzzy-neural, backsteping and sliding mode controllers. The present dissertation is an attempt to make a systematic study and design and development of some controllers for induction motor drive for comparative study of their performance with MATLAB modelling and simulation and finally implementation and testing with Real Time Digital simulator. The research work on drive system has been extended for investigation to improve the power quality to minimize the distortion/pollution due to converter based drive. Passive shunt, series and hybrid filters have been designed for harmonics mitigation. A thyristor swichted capacitor (TSC) based hybrid filter has also been designed with control law for variable reactive power compensation. The

designed filters have been tested in MATLAB /SIMULINK environment and the test results have been presented.

1.2 Literature Survey

The initial work on induction motor drive started long back [1] with the development of semiconductor power devices and microelectronics. As technology related to switching devices and processor pave the way for implementation of complex control theory [2] for ac motors in general and induction motor in particular. In the past two decade intensive research work has been taken-up for IM to improve the performance of the drive system particularly under transient condition. To set the aim and objective of the thesis the literature survey has been taken-up concerning various controllers for induction motor drive and also an effect of converter based drives on power utility and it's remedial measures.

The defacto industrial standard for high performance motion control applications necessitates four quadrant operation including field weakening, minimum torque ripple, rapid speed recovery under impact, load torque in addition to a fast dynamic speed response. To meet such requirements induction motor employing field oriented control scheme is the best option [3]-[4].

The field oriented control methods are complex to implement, because in field oriented control method, the decoupling relationship is obtained by means of proper selection of state coordinates, under the hypothesis that the rotor flux being kept constant. The torque is only asymptotically decoupled from the flux i.e., decoupling is obtained only in steady state, when the flux amplitude remains constant. Coupling is still present, when flux is weakened in order to operate the motor at higher speed within the input voltage saturation limit [5] or when flux is adjusted in order to maximize power efficiency [6][7].

This has further led to introduction of nonlinear differential geometric control theory, to develop the control techniques for linearization and decoupling control [8]-[11]. In last two decades many works on feedback linearization have been reported for decoupling [13]-[32]. In [13] an induction motor in field oriented coordinates. A hew multi-scalar model of the induction motor has been introduced to which nonlinear control system has been applied. Decoupling in the control of the speed and flux is

achieved by static state feedback controller. The use of dynamic state feedback for induction motor was first considered by De Luca, [14]-[15], where field linearization of the induction motor electrical dynamics were achieved under the assumption that the motor speed was constant, the outputs were chosen as the flux magnitude and torque. In [16], [18] the induction motor is controlled for high dynamic performance and maximum power efficiency by means of linear decoupling of motor flux and speed. The control algorithm based on flux estimates provided by an open loop flux simulator has proposed a nonlinear controller based on multiscalar motor model. R. Marino et al [19]-[25], it was shown that multi-input systems could become feedback linearizable from input to state after the addition of an integration to one of the input. In [23] a nonlinear adaptive state feedback input-output linearizing control is designed for a fifth order model of an induction motor which includes both electrical and mechanical dynamics under the assumption of linear magnetic circuits. The control algorithm contents a nonlinear identification scheme which asymptotically tracks the true values of the load torque and rotor resistance which are assumed to be constant but unknown. Further in [24] an output feedback control which guaranties global exponential tracking of speed and rotor flux modulus references signals is implemented on third order reduced model as the flux magnitude and torque, and simulation indicate the zero dynamics were stable. A fifth order state-space model of the induction motor in the (α-β) coordinate system was considered in which the input consisted of the two stator voltages and the state variable considered of the two stator currents, two rotor fluxes and the speed. Using this model, it was shown that the induction motor is dynamically feedback linearizable that is by adding integration to one of the two inputs of the induction motor [27]. However, this control structure had drawback. A non-singular feedback linearization transformation was shown to exist only as long as the electromagnetic torque produced by the motor was nonzero. The control structure required switching between two-different transformations to avoid the singularities in the transformation. These drawbacks make the dynamic feedback linearization approach is infeasible. A single dynamic feedback linearization transformation and controller are constructed whose singularity is exactly avoided and whose required computations are well within the limits of current microprocessor technology. The key to this alternative approach is to start with a model of the induction motor in the direct quadrature (d-q) [28]. Adaptive decoupling control of induction motor drive with flux magnitude and torque as output was obtained. It was

shown with fifth-order state-space model of the induction motor in the stationary (α-β) coordinate system that motor is dynamically feedback linearizable in [30]. In [32] input-output technique is used to linearize the model of induction motor and decouple the flux and torque loop. State feedback controllers are designed for linearization using pole placement technique to obtained desired dynamic and steady state response.

Parallel, the research work was going on for improving performance of classical controller approach like PID controller [33]. Amalgation of modern control approach like fuzzy logic, the use of sliding mode controller, neural network controller, grey feedback controller, adaptive fuzzy position controller, adaptive recurrent neural network controller, intelligent backstepping controller, robust petri fuzzy neural network controller for linear induction motor drive have been reported [32]-[68]. Lots of investigations have been reported on application by sliding mode controller for IM. Initially application of sliding mode control to IM was initiated by Sabanovic [34]. R. J. Wai et al [39] reported nonlinear decoupling control using sliding mode technique and in [42] adaptive fuzzy position control for induction servomotor drive using sliding mode controller techniques. Latter on sliding mode in combination of adaptive control found to be very effective and appeared in many papers [48]-[57]. The main problem with sliding mode control is chattering in control signal [42]. However, it may be noted that there are natural chattering and oscillation due to presence of PWM switching and limiter present in case of real implementation, leads to high stress for the system to be controlled.

Iterative learning control (ILC) is one of the recent emerging control methodologies which is based on the combination of knowledge and experience. Knowledge is concerned with information about the system model, it's environment, uncertainties, while experienced explores its repetitive behaviour, previous control efforts and some resulting error. Pioneer work on ILC has been initiated by Edwards [69] and Arimito et al [70]. With the understanding that the performance of repetitive task can be improved using information taken in the previous cycle and thus term learning was introduced [71]. The conventional ILC is essentially a feed-forward control strategy that rejects repeated uncertainties, but is useless against non-repetitive uncertainties. Due to environmental factors and changes in operating conditions, non-repeatability is inevitable. To guarantee the control performance in the presence of

both repeatable and non-repeatable disturbances, researchers [72], have combined ILC with feedback control strategies. The different configurations of ILC have been collected in a survey report on Iterative Learning Controller [73].Torque ripple minimization in PM synchronous motor using iterative learning controller has been reported in [74]. A stochastic iterative learning control algorithm for IM has been design and reported [75].

Most of the stability study of induction motor is based on conventional steady state torque-speed characteristics [76]-[77]. Stability study during transient conditions and rigorous stability analysis based on full nonlinear dynamical model are rather rare in literature. Stability analysis of the closed loop for feedback linearizing IM has not been noticed. Therefore, there is need of research and development activities for designing controller considering stability aspects of induction motor in the sense of Lyapunov.

The increasing usages of power electronic based appliances such as motor drives, switchgear applications and arc furnaces cause disturbance in the integrated electrical system. The brief description of the disturbances are given below [80]-[81].

- Voltage Sag: It is defined as rms voltage reduction that causes a short term power loss. In general it happens when load draws high current from the main supply such as a fault in a system that draws a high short circuit current from the source.

- Voltage Swell: Voltage swell can be stated as the opposite of voltage sag. It is an increase in voltage for a limited amount of time and occurs due to sudden decrease in load. This effect can be minimized by an efficient voltage regulator.

- Momentary interruptions: It is an instantaneous drop on supply voltage. It is differ from voltage sag. It happens for smaller amount of time with a higher voltage drop.

- Transients: It is defined as an increase in supply frequency for short time duration. The transient frequency can vary from several multiple of supply frequency to hundreds of kHz. Switching transients, capacitor energization

and lighting are dominating agent generating transients.

- Voltage unbalance: It occurs due to presence of negative and zero sequence components in supply voltage.

- Harmonics: It is a current or voltage waveform whose frequency is an integral multiple of the fundamental frequency. It deteriorates the pure sinusoidal waveform, and causes extra current flowing through the transmission lines that does not contributes any work. It arises from connecting nonlinear load to the ac mains supply such as variable frequency drive, power ac-dc converter, etc. This is the most common threat for power quality issues.

- Voltage Fluctuations: This occurs due to small variation in rms line voltage.

Due to above reasons, the power quality has become a prudent issues. Therefore, various reputed international electricity authorities such as the Institute of Electrical and Electronics Engineering (IEEE) and International Electrotechnical Commission (IEC) published some standards as IEEE-519 [82], IEEE-1531[83], IEEE-1150 [84] and IEC-61000-3-2 [85]. They have given guidelines to impose strict limit to the pollution ratio of the electricity to prevent further drawbacks of the disturbances. This has opened a vital issue for research for finding the way, which assures to meet the standard limit and enhance the power quality.

The induction motor drive system generally uses an ac-dc converter for rectification of ac mains voltage, an energy storage capacitor, and a voltage source inverter feeding to the motor for variable frequency application. Such type of arrangement suffers from operating problems such as poor power factor, injection of harmonics into the ac mains, equipment overheating due to harmonic current absorption and variation in dc link, which creates fluctuations in the voltage of input supply system. The uncontrolled ac-dc converter along with series and shunt passive (LC) filters are the engineer's preferable choice that is popularly used to compensate harmonic currents and improve input power factor, because of low cost, simplicity, reliability and control less operation. Many authors [86-91] have reported about design procedure for the passive shunt, series and hybrid filter for improvement the THD of supply current. Peng et. al. [88] designed series filter and compared the performance with passive filter for variable frequency drive application. Phipps [89]

has given the procedure to use transfer function approach for passive filter design. It gives inside dynamic behavior of the individual filter. In 2004 J C Das [90] has reported various constraints and limitation in designing and implementation of passive filters. In 2005 B. Singh et. al. [91] reported the design of hybrid filter, which is a combination of passive series filter and high order passive shunt filter. This configuration meets the IEEE 519 standard even for variable load.

However, the passive filters have many disadvantages, such as resonance, fixed compensation characteristics, large size, tuning problems, and inability to compensate changing harmonic current content and reactive power. Therefore, the control strategies based on the technique of power electronics have become an important issue recently. The active filters are mostly used active filter for variable load because of its excellent, flexible and smooth performance characteristics and simplicity in implementation, both in single-phase and three-phase configurations [92]-[109]. But the cost of active filter is high and they are not recommended for a large-scale system because the power rating, as the shunt active filter cost is directly proportional to the load current. There many work reported to use hybrid power filter comprises of a rated small active filter and a passive filter tuned for special harmonic mitigation [110]-[118]. The drawback still exists with hybrid power filters. It's performance is not found satisfactory for variable-load reactive power compensation.

Flexible AC Transmission systems (FACTS) devices plays an important role in improving the stability of a power system. FACTS devices also provide reactive power compensation [119]-[129]. The structure of two FACTS devices are similar i.e. these are thyristor switched reactor with fixed capacitors (TSR/FC) and thyristor switched capacitor (TSC). It is studied that in most of the cases parameters of FACT devices are tuned for specific harmonic frequencies and designed for variable reactive power compensation [124], [125].

Thyristor-switched capacitor (TSC) consists of a series RLC circuit similar to passive shunt low pass filter, and a bidirectional thyristor switch. In comparison to active and hybrid filter, TSC offers countless benefits including simple design and installation. Beside this, TSC can be used for many application areas. Some of them are supply voltage support, reactive power compensation, harmonics filtration, etc.

Among these, the most common one is the reactive power compensation [123][125][128][129].

1.3 Aims and Objectives of the Thesis

The availability of fast switching devices, new converter topology and high speed processor have increased the interest in designing and developing high performance ac drive in general and induction motor drive in particular. Further there is demand from industries for maintenance free, low cost drive system. Their quality product is opening up new opportunity and vistas for electrical engineers to go for research and development work in this area. Various issues related to modern control theory for real applications are being investigated in laboratories of academic institutions and research worldwide. In course of literature survey it has been noted the investigation of drive system is not much concerned with side effect of converter based drive on power utility. The author is of the view that while carrying out research related to drive system some contribution must be made toward power conditioning. The present research work which aims at studies on various aspects of different controller for induction motor drive for performance improvement and comparative study fulfils the following objectives:

- Study of various controllers for high performance induction motor drive
- Stability study in the light of Lyapunov theorem
- Design and development of P-I controller with fuzzy torque compensator for linearzing control of induction motor drive.
- Design and development of sliding mode, iterative learning and Lyapunov theory based controllers to achieve improved performance of linearized induction motor drive system.
- MATLAB /SIMULINK modelling and simulation of the induction motor drive using proposed controller for performance analysis and comparison.
- Implementation and testing of the drive system with typical controllers on RT-LAB simulator in the laboratory.
- Study on impact of modern drive system on power utility and to design and develop Active Hybrid Filter for power conditioning.

1.4 Scope of the Thesis

As mentioned, the work presented in the thesis is related to the study and design and development of various controllers for induction motor drive for performance improvement and power conditioning. Initially stability study has been carried out. In the course of investigation various aspect of the controllers like P-I, sliding mode, iterative learning and Lyapunov have been taken-up. MATLAB/SIMULINK model of the drive system has been developed with various controllers for simulation study. Subsequently the implementation of the controller has been developed in the laboratory for testing on RTDS. The following section presents the outline of the work as reported in the thesis in **seven** chapters.

Chapter 1 reviews the available literatures on various types of control schemes for induction motor drive and it also describes simple measures for power conditioning to reduced the side effects of converter based modern drive system. Finally the objective of the thesis is set and organization of the thesis is outlined.

The mathematical model of the induction motor is presented in a stationary (α-β) reference frame with stator current and rotor flux as state variables. A stability analysis of induction motor drive in the light of Lyapunov Global Stability theorem is discussed. Feedback linearization is taken up for developing simple induction motor model. In this way drive system splited in two linear and decoupled system: Electrical and Mechanical. A systematic design procedure is outlined to determined the P-I controller gains for electrical and mechanical subsystems. A fuzzy torque compensator is created to be added with speed controller to improve the performance of drive system in **Chapter 2**.

Chapter 3 presents sliding mode control laws for flux and speed control loop. A case study is presented to find the controller gains and bandwidths considering motor parameter variation and load torque disturbance. P-I type iterative control strategy for performance improvement and reduction of chattering is outlined. Procedure for controller design based on Lyapunov theorem is also presented.

MATLAB simulation study of the decoupled and feedback linearized drive system under various operating condition using different designed controllers are carried out. The simulation results are analysed and compared in **Chapter 4**. **Chapter 5** initially describe a real-time digital simulator (RTDS). The testing and performance comparison of the feedback linearized induction motor using different controllers

designed Chapter 2 and Chapter 3 are taken up. The test results are presented to validate the simulation results. **Chapter 6** deals with the power quality improvement techniques. Passive shunt, series and hybrid filters are designed for harmonic mitigation. Model reference adaptive controller strategy is described for variable reactive power compensation using thyristor switch capacitor. MATLAB/SIMULINK models are developed to study power quality indices. Finally general conclusions are presented in **Chapter 7**. This Chapter also includes certain suggestions for future research work that may be carried-out to further simplify the design procedures and performance improvement of the drive system and power quality.

The salient points of the thesis may be detailed as follows:

a. Design of P-I controllers and fuzzy torque compensator for the electrical and mechanical subsystems using decoupling control scheme.

b. Simplified designed approach for developing controllers like sliding mode controller, iterative learning controller and Lyapunov based controller.

c. Simulation of the induction motor drive with designed controllers and analysis for performance comparison.

d. Stability study of induction motor drive using Lyapunov theorem.

e. Implementation and testing of the various designed controllers in RT-LAB simulator, and validation of simulation results.

f. Systematic design of passive shunt, series and hybrid filter for harmonic mitigation.

g. Design of active power filter with thyristor switch capacitor based on model reference adaptive control principle for variable reactive power compensation.

h. Simulation in MATLAB/SIMULINK environment for performance evaluation.

Chapter – 2

Stability Study and Feedback Linearization of Induction Motor Drive with PI Controller and PI with Fuzzy Torque Compensator

2.1 General

This chapter presents mathematical model of induction motor in stationary reference frame with stator current, rotor flux, rotor speed as state variable as required for the controller design. Initially a study of Lyapunov stability of an open loop induction motor has been taken-up with no load and with load and sufficient conditions for the global asymptotic stability has been derived using induction motor model developed in the section 2.2. Further the feedback linearization for decoupling control as needed in case of the induction motor drive is presented. With this control, it becomes possible to split the IM into two linear subsystems: electrical and mechanical. Comprehensive and systematic procedures are developed to determine the gains of the proportional integral (PI) controllers for electrical and mechanical subsystems. Finally fuzzy torque compensator is added to the system to improve the speed response.

2.2. Induction Motor Modeling

A proper model for the three phase induction motor is essential to simulate and study the complete drive system. The model of induction motor in the stationary (α-β) reference frame is derived in [12]. The following assumptions are made:

a. Each stator winding is distributed so as to produce a sinusoidal mmf along the air gap, i.e., space harmonics are negligible.

b. The slotting in stator and rotor produces negligible variation in respective inductances.
c. Mutual inductances are equal.
d. The harmonics in voltages and currents are neglected.
e. The saturation of the magnetic circuit is neglected.
f. Hysteresis and eddy current losses and skin effect are neglected.

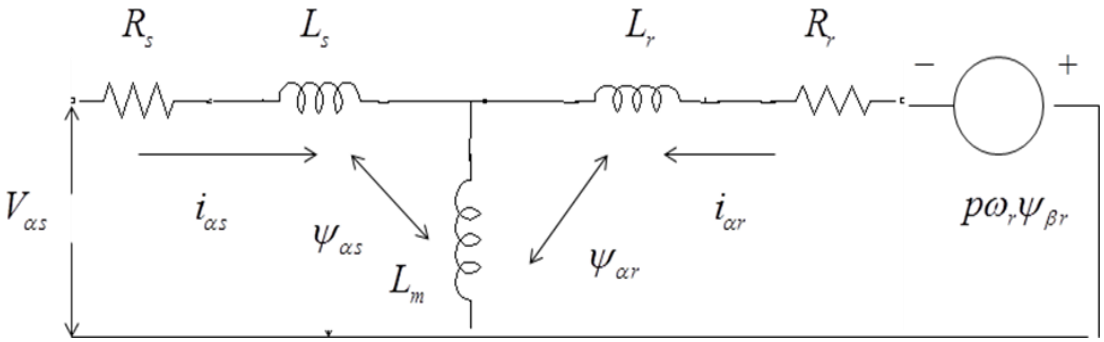

(a) α-axis circuit

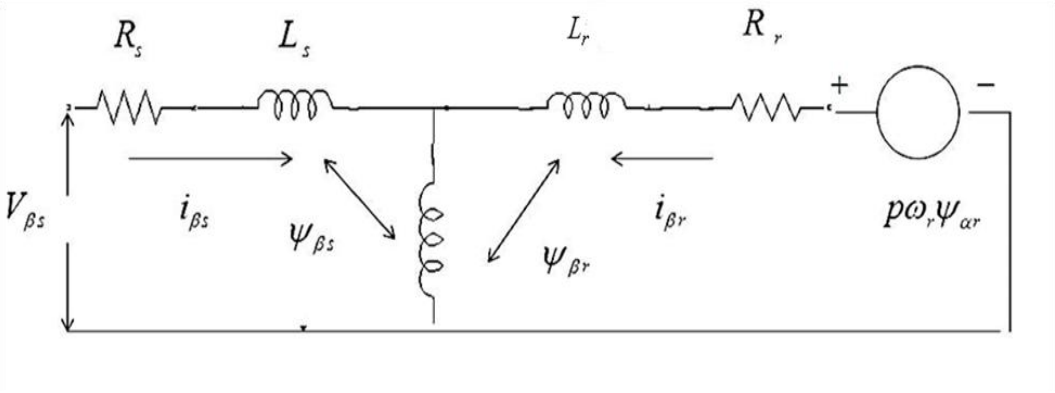

(b) β-axis circuit

Fig.2.1 Stationary (α-β) equivalent circuit of three phase induction motor

The voltage equations for the three phase induction motor in stationary (α-β) reference frame with equivalent circuits shown in Fig.2.1 can be written as [12]

$$V_{\alpha s} = i_{\alpha s} R_s + \frac{d\psi_{\alpha s}}{dt} \tag{2.1}$$

$$V_{\beta s} = i_{\beta s} R_s + \frac{d\psi_{\beta s}}{dt} \tag{2.2}$$

$$\frac{d\psi_{\alpha r}}{dt} + i_{\alpha r} R_r + p\omega_r \psi_{\beta r} = 0 \tag{2.3}$$

$$\frac{d\psi_{\beta r}}{dt} + i_{\beta r} R_r - p\omega_r \psi_{\alpha r} = 0 \tag{2.4}$$

The torque balance equation is:

$$\frac{d\omega_r}{dt} = -\frac{B}{J}\omega_r + \frac{1}{J}(T_e - T_l) \tag{2.5}$$

The developed electromagnetic torque, T_e is:

$$T_e = \frac{3}{2} p \frac{L_m}{L_r}\left(\psi_{\alpha r} i_{\beta s} - \psi_{\beta r} i_{\alpha s}\right) = K_T\left(\psi_{\alpha r} i_{\beta s} - \psi_{\beta r} i_{\alpha s}\right) \tag{2.6}$$

where, in the above equations, all voltages (V) and currents (A) refer to the stationary reference frame. The subscripts, *αs, βs, αr*, and *βr* correspond to *α*- and *β*- axis quantities for the stator (*s*) and rotor (*r*) in all combinations. ψ denotes flux linkage, ω_r represents the mechanical speed of the rotor in rad/s. R_s and R_r are stator and rotor resistances per phase respectively. p is the number of pole pairs. J is the moment of inertia and B is the coefficient of viscous friction. T_e is the developed electromagnetic torque and T_l is load.

Derivation of the dynamic model of induction motor in the stationary (*α-β*) reference frame, with stator current component and rotor flux components variables is given below.

The expression for stator flux linkages given by:

$$\psi_{\alpha s} = i_{\alpha s} L_s + i_{\alpha r} L_m \tag{2.7}$$

$$\psi_{\beta s} = i_{\beta s} L_s + i_{\beta r} L_m \tag{2.8}$$

Similarly, the expression for rotor flux linkages given by:

$$\psi_{\alpha r} = i_{\alpha r} L_r + i_{\alpha s} L_m \tag{2.9}$$

$$\psi_{\beta r} = i_{\beta r}L_r + i_{\beta s}L_m \tag{2.10}$$

where L_s ,L_r and L_m represent stator self inductance, rotor self inductance and mutual inductance, respectively. From (2.9) and (2.10) we obtains $i_{\alpha r}$ and $i_{\beta r}$ in terms of stator current ($i_{\alpha s}$ and $i_{\beta s}$) and rotor flux linkage ($\psi_{\alpha r}$ and $\psi_{\beta r}$) as follows:

$$i_{\alpha r} = -\frac{L_m}{L_r} i_{\alpha s} + \frac{\psi_{\alpha r}}{L_r} \tag{2.11}$$

$$i_{\beta r} = -\frac{L_m}{L_r} i_{\beta s} + \frac{\psi_{\beta r}}{L_r} \tag{2.12}$$

Substituting $i_{\alpha r}$ from (2.11) and $i_{\beta r}$ from (2.12) into (2.3) and (2.4), and solving for the time derivatives of rotor flux linkages.

$$\frac{d\psi_{\alpha r}}{dt} = \frac{-R_r}{L_r}\psi_{\alpha r} + \frac{R_r L_m}{L_r} i_{\alpha s} - p\omega_r \psi_{\beta r} \tag{2.13}$$

$$\frac{d\psi_{\beta r}}{dt} = \frac{-R_r}{L_r}\psi_{\beta r} + \frac{R_r L_m}{L_r} i_{\beta s} + p\omega_r \psi_{\alpha r} \tag{2.14}$$

Substituting the $i_{\alpha r}$ from (2.11) and $i_{\beta r}$ from (2.12) into (2.7) and (2.8)

$$\psi_{\alpha s} = L_s i_{\alpha s} + L_m \left[\frac{\psi_{\alpha r}}{L_r} - \frac{L_m}{L_r} i_{\alpha s} \right] = \left[L_s - \frac{L_m^{\,2}}{L_r} \right] i_{\alpha s} + \frac{L_m}{L_r}\psi_{\alpha r} \tag{2.15}$$

$$\psi_{\beta s} = L_s i_{\beta s} + L_m \left[\frac{\psi_{\beta r}}{L_r} - \frac{L_m}{L_r} i_{\beta s} \right] = \left[L_s - \frac{L_m^{\,2}}{L_r} \right] i_{\beta s} + \frac{L_m}{L_r}\psi_{\beta r} \tag{2.16}$$

Taking derivative of (2.15) and (2.16)

$$\frac{d\psi_{\alpha s}}{dt} = \left[L_s - \frac{L_m^{\,2}}{L_r} \right] \dot{i}_{\alpha s} + \frac{L_m}{L_r}\dot{\psi}_{\alpha r} \tag{2.17}$$

$$\frac{d\psi_{\beta s}}{dt} = \left[L_s - \frac{L_m^{\,2}}{L_r} \right] \dot{i}_{\beta s} + \frac{L_m}{L_r}\dot{\psi}_{\beta r} \tag{2.18}$$

Substituting $\dot{\psi}_{\alpha r}$ and from $\dot{\psi}_{\beta r}$ from (2.13) and (2.14) into (2.17) and (2.18) respectively.

$$\frac{d\psi_{\alpha s}}{dt} = \sigma L_s \dot{i}_{\alpha s} + \frac{L_m}{L_r}\left[-\frac{R_r}{L_r}\psi_{\alpha r} - p\omega_r \psi_{\beta r} + \frac{R_r}{L_r} L_m i_{\alpha s} \right] \tag{2.19}$$

$$\frac{d\psi_{\beta s}}{dt} = \sigma L_s \dot{i}_{\beta s} + \frac{L_m}{L_r}\left[-\frac{R_r}{L_r}\psi_{\beta r} + p\omega_r \psi_{\alpha r} + \frac{R_r}{L_r} L_m i_{\beta s} \right] \tag{2.20}$$

where, $\sigma = (1 - \frac{L_m^2}{L_s L_r})$ is the leakage coefficient .

Further substituting $\frac{d\psi_{\alpha s}}{dt}$ and $\frac{d\psi_{\beta s}}{dt}$ from (2.17) and (2.18) into (2.1) and (2.2).

$$V_{\alpha s} = i_{\alpha s} R_s + \sigma L_{s\sigma} \dot{i}_{\alpha s} + \frac{L_m}{L_r}\left[-\frac{R_r}{L_r}\psi_{\alpha r} - p\omega_r \psi_{\beta r} + \frac{R_r}{L_r} L_m i_{\alpha s} \right] \tag{2.21}$$

$$V_{\beta s} = i_{\beta s} R_s + \sigma L_{s\sigma} \dot{i}_{\beta s} + \frac{L_m}{L_r}\left[-\frac{R_r}{L_r}\psi_{\beta r} + p\omega_r \psi_{\alpha r} + \frac{R_r}{L_r} L_m i_{\beta s} \right] \tag{2.22}$$

Solving (2.21) and (2.22) to get expressions in terms of the time derivatives of stator current components $i_{\alpha s}$ and $i_{\beta s}$:

$$\frac{di_{\alpha s}}{dt} = -\frac{1}{\sigma L_{s\sigma}}\left[R_s + \frac{R_r}{L_r^{\,2}} L_m^{\,2} \right] i_{\alpha s} + \frac{L_m R_r}{\sigma L_{s\sigma} L_r^{\,2}} \psi_{\alpha r} + \frac{L_m}{\sigma L_s L_r} p\omega_r \psi_{\beta r} + \frac{V_{\alpha s}}{\sigma L_s} \tag{2.23}$$

$$\frac{di_{\beta s}}{dt} = -\frac{1}{\sigma L_s}\left[R_s + \frac{R_r}{L_r^{\,2}} L_m^{\,2} \right] i_{\beta s} + \frac{L_m R_r}{\sigma L_s L_r^{\,2}} \psi_{\beta r} - \frac{L_m}{\sigma L_s L_r} p\omega_r \psi_{\alpha r} + \frac{V_{\beta s}}{\sigma L_s} \tag{2.24}$$

Rewriting (2.23), (2.24), (2.13) and (2.14) together with speed dynamic equation for representing induction motor dynamic model in the stationary (α-β) reference frame is obtained as follows:

$$\dot{i}_{\alpha s} = -\frac{1}{\sigma L_s}\left(R_s + \frac{L_m^2}{L_r^2} R_r \right) i_{\alpha s} + \frac{1}{\sigma L_s} \frac{L_m R_r}{L_r^{\,2}} \psi_{\alpha r} + \frac{pL_m}{\sigma L_s L_r} \omega_r \psi_{\beta r} + \frac{V_{\alpha s}}{\sigma L_s} \tag{2.25}$$

$$\dot{i}_{\beta s} = -\frac{1}{\sigma L_s}\left(R_s + \frac{L_m^2}{L_r^2} R_r \right) i_{\beta s} + \frac{1}{\sigma L_s} \frac{L_m R_r}{L_r^{\,2}} \psi_{\beta r} - \frac{pL_m}{\sigma L_s L_r} \omega_r \psi_{\alpha r} + \frac{V_{\beta s}}{\sigma L_s} \tag{2.26}$$

$$\dot{\psi}_{\alpha r} = -\frac{R_r}{L_r}\psi_{\alpha r} - p\omega_r \psi_{\beta r} + \frac{L_m R_r}{L_r} i_{\alpha s} \tag{2.27}$$

$$\dot{\psi}_{\beta r} = -\frac{R_r}{L_r}\psi_{\beta r} + p\omega_r\psi_{\alpha r} + \frac{L_m R_r}{L_r} i_{\beta s} \tag{2.28}$$

$$\dot{\omega}_r = -\frac{B}{J}\omega_r + \frac{1}{J}(T_e - T_l) \tag{2.29}$$

$$T_e = \frac{3}{2} p \frac{L_m}{L_r}\left(\psi_{\alpha r} i_{\beta s} - \psi_{\beta r} i_{\alpha s}\right) = K_T\left(\psi_{\alpha r} i_{\beta s} - \psi_{\beta r} i_{\alpha s}\right) \tag{2.30}$$

2.3 Study of Induction Motor Stability in Lyapunov Sense

Stability study of IM drive is ignoned while investigating performance of the IM drive system. But the control principles are sensitive to speed changes, parameter variations and load disturbances. Under these situations, it is necessary to understand motor sustaining capability during steady state as well as transient periods. With this objective, stability analysis using the Lyapunov's criteria [2] is pertinent. Stability study is available in literature. The analysis and particularly, study of global asymptotic stability in the sense of Lyapunov for induction motor considering the full nonlinear dynamical model in stationary (α-β) reference frame are presented in this section which is different from reported in [77]. Conditions of stability are derived in terms of operating speed, load, frequency and motor parameters.

2.3.1 Perturbation Model about Equilibrium Point

Many control schemes have been implemented considering the induction motor state space representation in stationary (α-β) reference frame with two stator current components ($i_{\alpha s}$, $i_{\beta s}$), two rotor flux components ($\psi_{\alpha r}$, $\psi_{\beta r}$) and speed (ω_r) as variables [6]. The state space represented of IM as obtained in previous section in stationary reference can be written as:

$$\dot{x} = f(x) + bu \tag{2.31}$$

where,

$$x = [i_{\alpha s}, i_{\beta s}, \psi_{\alpha r}, \psi_{\beta r}, \omega_r]^T \qquad u = [u_{\alpha s}, u_{\beta s}, T_l]^T$$

$$f(x)=\begin{bmatrix} -\frac{1}{\sigma L_s}\left(R_s+\frac{L_m^2}{L_r^2}R_r\right)i_{\alpha s}+\frac{1}{\sigma L_s}\frac{L_m}{L_r^2}\psi_{\alpha r}+\frac{pL_m}{\sigma L_s L_r}\omega_r\psi_{\beta r} \\ -\frac{1}{\sigma L_s}\left(R_s+\frac{L_m^2}{L_r^2}R_r\right)i_{\beta s}+\frac{1}{\sigma L_s}\frac{L_m}{L_r^2}\psi_{\beta r}-\frac{pL_m}{\sigma L_s L_r}\omega_r\psi_{\alpha r} \\ -\frac{R_r}{L_r}\psi_{\alpha r}-p\omega_r\psi_{\beta r}+\frac{L_m R_r}{L_r}i_{\alpha s} \\ -\frac{R_r}{L_r}\psi_{\alpha r}+p\omega_r\psi_{\beta r}+\frac{L_m R_r}{L_r}i_{\alpha s} \\ -\frac{B}{J}\omega_r+\frac{K_T}{J}\left(i_{\beta s}\psi_{\alpha r}-i_{\alpha s}\psi_{\beta r}\right) \end{bmatrix} \tag{2.32}$$

$$b=\begin{bmatrix} \frac{1}{\sigma L_s} & 0 & 0 \\ 0 & \frac{1}{\sigma L_s} & 0 \\ 0 & 0 & 0 \\ 0 & 0 & 0 \\ 0 & 0 & -\frac{1}{J} \end{bmatrix} \tag{2.33}$$

where, suffixes (α, β) denote the equivalent direct and quadrature axis components on the stator fixed frame. (L_s, R_s) and (L_r, R_r) are the stator and the rotor parameters (inductance and resistance). L_m is the mutual inductance. p is the number of pole pair. J and B represent the moment of inertia and viscous frictional coefficient. T_l is the load torque. Inputs $u_{\alpha s}$ and $u_{\beta s}$ are two stator voltage components. σ is the leakage coefficient, defined as $\sigma=\left(1-L_m^2/L_rL_s\right)$. K_T is the torque constant, defined as $K_T = p\,L_m/L_r$. ω_r is the motor mechanical speed.

Induction motor exhibits stable performance at its rated slip speed under steady state condition. The field oriented control and feedback linearization control also force the motor to run near stable slip region. In this work, we assume an arbitrary machine operating equilibrium point near steady state condition (around the stable slip region).

Let the equilibrium point variable be x_o,

where, $x_0=[i_{\alpha so}, i_{\beta so}, \psi_{\alpha ro}, \psi_{\beta ro}, \omega_{ro}]^T$

The equilibrium point is a fixed point. Hence, the system response at equilibrium point will be:

$$\left(R_s+\frac{L_m^2}{L_r^2}R_r\right)i_{\alpha so}-\frac{L_mR_r}{L_r^2}\psi_{\alpha ro}-\frac{pL_m}{L_r}\omega_{ro}\psi_{\beta ro}=u_{\alpha s}$$

$$\left(R_s+\frac{L_m^2}{L_r^2}R_r\right)i_{\beta so}-\frac{L_mR_r}{L_r^2}\psi_{\beta ro}+\frac{pL_m}{L_r}\omega_{ro}\psi_{\alpha ro}=u_{\beta s}$$

$$\frac{R_r}{L_r}\psi_{\alpha ro}+p\omega_{ro}\psi_{\beta ro}-\frac{L_mR_r}{L_r}i_{\alpha so}=0$$

$$\frac{R_r}{L_r}\psi_{\beta ro}-p\omega_{ro}\psi_{\alpha ro}-\frac{L_mR_r}{L_r}i_{\beta so}=0$$

$$\frac{B}{J}\omega_{ro}-\frac{K_T}{J}(i_{\beta so}\psi_{\alpha ro}-i_{\alpha so}\psi_{\beta ro})+\frac{T_l}{J}=0 \tag{2.34}$$

When the operating point of the motor drive system is subjected to any change due to the change in motor speed, load torque or parameter, it deviates from its steady state position, i.e., the current equilibrium point. If the nature of error is converging, then after sometime motor acquires another stable position and gets new equilibrium points. In this section theoretical analysis of the system error is done to explore the natural stability of the motor drive system.

The set of system error variables is defined as

$$e=(e_1,e_2,e_3,e_4,e_5)=(i_{\alpha s}-i_{\alpha so},i_{\beta s}-i_{\beta so},\psi_{\alpha r}-\psi_{\alpha ro},\psi_{\beta r}-\psi_{\beta ro},\omega_r-\omega_{ro}) \tag{2.35}$$

Next, representing (2.31) in state space model with the errors as variables:

$$\dot{e}=A(x_o)e+g(e) \tag{2.36}$$

where,

$$A(x_o)=\begin{bmatrix} -\left[\frac{1}{\sigma L_s}\left(R_s+\frac{L_m^2}{L_r^2}R_r\right)\right] & 0 & \left(\frac{1}{\sigma L_s}\frac{L_mR_r}{L_r^2}\right) & \left(\frac{pL_m}{\sigma L_sL_r}\omega_{ro}\right) & \left(\frac{pL_m}{\sigma L_sL_r}\psi_{\beta ro}\right) \\ 0 & -\left[\frac{1}{\sigma L_s}\left(R_s+\frac{L_m^2}{L_r^2}R_r\right)\right] & -\left(\frac{pL_m}{\sigma L_sL_r}\omega_{ro}\right) & \left(\frac{1}{\sigma L_s}\frac{L_mR_r}{L_r^2}\right) & -\left(\frac{pL_m}{\sigma L_sL_r}\psi_{\alpha ro}\right) \\ \frac{L_mR_r}{L_r} & 0 & -\frac{R_r}{L_r} & -p\omega_{ro} & -p\psi_{\beta ro} \\ 0 & \frac{L_mR_r}{L_r} & p\omega_{ro} & -\frac{R_r}{L_r} & p\psi_{\alpha ro} \\ -\left(\frac{K_T}{J}\psi_{\beta ro}\right) & \left(\frac{K_T}{J}\psi_{\alpha ro}\right) & \left(\frac{K_T}{J}i_{\beta so}\right) & -\left(\frac{K_T}{J}i_{\alpha so}\right) & -\left(\frac{B}{J}\right) \end{bmatrix}$$

$$g(e)=\begin{bmatrix} \frac{pL_m}{\sigma L_sL_r}e_4e_5 \\ -\frac{pL_m}{\sigma L_sL_r}e_3e_5 \\ -pe_4e_5 \\ pe_3e_5 \\ \frac{K_T}{J}(e_2e_3-e_1e_4) \end{bmatrix}$$

2.3.2 Energy and Power Balance Equations

The expressions of magnetic energy (w_f) and the mechanical energy (w_J) of the induction motor in the stationary (α-β) reference frame with stator and rotor current components as variables can be written as [77]:

$$w_f = \frac{1}{2}L_s\left(i_{\alpha s}^2 + i_{\beta s}^2\right) + \frac{1}{2}L_r\left(i_{\alpha r}^2 + i_{\beta r}^2\right) + L_m\left(i_{\alpha s}i_{\alpha r} + i_{\beta s}i_{\beta r}\right) \tag{2.37}$$

$$w_J = \frac{1}{2}J\omega_r^2 \tag{2.38}$$

Let the total motor energy be defined as w_p , such that

$$w_p = w_f + w_J \tag{2.39}$$

The total motor energy in terms of two stator current components ($i_{\alpha s,}\ i_{\beta s}$), two rotor flux components ($\psi_{\alpha r,}\ \psi_{\beta r}$) and rotor speed ($\omega_r$) can be expressed as:

$$w_p = \frac{1}{2}\sigma L_s\left(i_{\alpha s}^2 + i_{\beta s}^2\right) + \frac{1}{2L_r}\left(\psi_{\alpha r}^2 + \psi_{\beta r}^2\right) + \frac{1}{2}J\omega_r^2 \tag{2.40}$$

Taking the derivatives of (2.40) and from (2.31), equation (2.40) can be written as:

$$\frac{dw_p}{dt} = \sigma L_s\left(i_{\alpha s}\dot{i}_{\alpha s} + i_{\beta s}\dot{i}_{\beta s}\right) + \frac{1}{L_r}\left(\psi_{\alpha r}\dot{\psi}_{\alpha r} + \psi_{\beta r}\dot{\psi}_{\beta r}\right) + J\omega_r\dot{\omega}_r$$

$$= \sigma L_s i_{\alpha s}\left(-\frac{1}{\sigma L_s}\left(R_s + \frac{L_m^2}{L_r^2}R_r\right)i_{\alpha s} + \frac{1}{\sigma L_s}\frac{L_m R_r}{L_r^2}\psi_{\alpha r} + \frac{pL_m}{\sigma L_s L_r}\omega_r\psi_{\beta r} - \frac{u_{\alpha s}}{\sigma L_s}\right) + \sigma L_s i_{\beta s}\left(-\frac{1}{\sigma L_s}\left(R_s + \frac{L_m^2}{L_r^2}R_r\right)i_{\beta s} + \frac{1}{\sigma L_s}\frac{L_m R_r}{L_r^2}\psi_{\beta r} - \frac{pL_m}{\sigma L_s L_r}\omega_r\psi_{\alpha r} - \frac{u_{\beta s}}{\sigma L_s}\right)$$

$$+\frac{1}{L_r}\left(\psi_{\alpha r}\left(-\frac{R_r}{L_r}\psi_{\alpha r} - p\omega_r\psi_{\beta r} + \frac{L_m R_r}{L_r}i_{\alpha s}\right) + \psi_{\beta r}\left(-\frac{R_r}{L_r}\psi_{\beta r} + p\omega_r\psi_{\alpha r} + \frac{L_m R_r}{L_r}i_{\beta s}\right)\right) + J\omega_r\left(-\frac{B}{J}\omega_r + \frac{K_T}{J}(i_{\beta s}\psi_{\alpha r} - i_{\alpha s}\psi_{\beta r}) - \frac{T_l}{J}\right)$$

$$= \left(-\left(R_s + \frac{L_m^2}{L_r^2}R_r\right)\left(i_{\alpha s}^2 + i_{\beta s}^2\right) + \frac{L_m R_r}{L_r^2}\left(i_{\alpha s}\psi_{\alpha r} + i_{\beta s}\psi_{\beta r}\right) + \frac{pL_m}{L_r}\omega_r\left(i_{\alpha s}\psi_{\beta r} - i_{\beta s}\psi_{\alpha r}\right) + u_{\alpha s}i_{\alpha s} + u_{\beta s}i_{\beta s}\right)$$

$$+\left(\left(-\frac{R_r}{L_r^2}\psi_{\alpha r}^2 - \frac{p\omega_r\psi_{\alpha r}\psi_{\beta r}}{L_r} + \frac{L_m R_r\psi_{\alpha r}i_{\alpha s}}{L_r^2}\right) + \left(-\frac{R_r}{L_r^2}\psi_{\beta r}^2 + \frac{p\omega_r\psi_{\alpha r}\psi_{\beta r}}{L_r} + \frac{L_m R_r\psi_{\beta r}i_{\beta s}}{L_r^2}\right)\right)$$

$$+\left(-B\omega_r^2 + \frac{pL_m\omega_r}{L_r}(i_{\beta s}\psi_{\alpha r} - i_{\alpha s}\psi_{\beta r}) - T_l\omega_r\right)$$

Further simplification of the above leads to (2.41).

$$\frac{dw_p}{dt} = u_{\alpha s} i_{\alpha s} + u_{\beta s} i_{\beta s} - B\omega_r^2 - T_l \omega_r - \left(R_s + \frac{L_m^2}{L_r^2} R_r \right) \left(i_{\alpha s}^2 + i_{\beta s}^2 \right) + \frac{2 L_m R_r}{L_r^2} \left(i_{\alpha s} \psi_{\alpha r} + i_{\beta s} \psi_{\beta r} \right) - \frac{R_r}{L_r^2} \left(\psi_{\alpha r}^2 + \psi_{\beta r}^2 \right) \tag{2.41}$$

Eqn. (2.41) is the expression for induction motor power balance as given in [77]. Equation (2.41) confirms the known fact that the rate of change of stored energy is equal to input power minus sum of mechanical power output and power loss.

The power loss in the windings is given by [77]

$$P_{loss} = \left(i_{\alpha s}^2 + i_{\beta s}^2 \right) R_s + \left(i_{\alpha r}^2 + i_{\beta r}^2 \right) R_r \tag{2.42}$$

The expression of power loss in terms of the stator current and the rotor flux (α-β) component is obtained by substituting (2.11) and (2.12), which are repeated in (2.43) and (2.44) , into (2.42).

$$i_{\alpha r} = -\frac{L_m}{L_r} i_{\alpha s} + \frac{\psi_{\alpha r}}{L_r} \tag{2.43}$$

$$i_{\beta r} = -\frac{L_m}{L_r} i_{\beta s} + \frac{\psi_{\beta r}}{L_r} \tag{2.44}$$

The expression for power loss is thus obtained as (2.45).

$$P_{loss} = \left(R_s + \frac{R_r L_m^2}{L_r^2} \right) \left(i_{\alpha s}^2 + i_{\beta s}^2 \right) + \frac{R_r}{L_r^2} \left(i_{\alpha r}^2 + i_{\beta r}^2 \right) - \frac{2 L_m R_r}{L_r^2} \left(i_{\alpha s} \psi_{\alpha r} + i_{\beta s} \psi_{\beta r} \right) \tag{2.45}$$

The energy and power balance relationship is used for the Lyapunov stability analysis. For this, starting with the equilibrium point expression in terms of error variable for the total stored energy w_p is given by (2.40).

$$\begin{aligned} w_p(i_{\alpha so} + e_1, i_{\beta so} + e_2, \psi_{\alpha ro} + e_3, \psi_{\beta ro} + e_4, \omega_{ro} + e_5) &= \frac{\sigma L_s}{2} \left(\left(i_{\alpha so} + e_1 \right)^2 + \left(i_{\beta so} + e_2 \right)^2 \right) \\ + \left(\frac{1}{2} \frac{\left(\psi_{\alpha ro} + e_3 \right)^2 + \left(\psi_{\beta ro} + e_4 \right)^2}{L_r} \right) &+ \left(\frac{1}{2} J (\omega_{ro} + e_5)^2 \right) \end{aligned} \tag{2.46}$$

The total stored energy at the equilibrium point, w_p in terms of the equilibrium point variable is given by (2.47).

$$w_p(i_{\alpha so}, i_{\beta so}, \psi_{\alpha ro}, \psi_{\beta ro}, \omega_{ro}) = \frac{\sigma L_s}{2}\left(\left(i_{\alpha so}\right)^2 + \left(i_{\beta so}\right)^2\right) + \left(\frac{1}{2}\frac{\left(\psi_{\alpha ro}\right)^2 + \left(\psi_{\beta ro}\right)^2}{L_r}\right) + \left(\frac{1}{2}J(\omega_{ro})^2\right) \tag{2.47}$$

Difference of (2.46) and (2.47) gives, the change in energy, $w_p(e)$ in terms of the error variables,

$$w_p(e) = w_p - w_p(0)$$

$$w_p(e) = \frac{\sigma L_s}{2}\left(e_1^2 + 2e_1 i_{\alpha so} + e_2^2 + 2e_2 i_{\beta so}\right) + \left(\frac{1}{2}\frac{e_3^2 + 2e_3\psi_{\alpha ro} + e_4^2 + 2e_4\psi_{\beta ro}}{L_r}\right) + \left(\frac{1}{2}J\left({e_5}^2 + 2e_5\omega_{ro}\right)\right) \tag{2.48}$$

Arranging (2.48) in the error product form as in (2.49):

$$w_p(e) = e^T K e + d^T e \tag{2.49}$$

where,

$$K = \frac{1}{2}\begin{bmatrix} \sigma L_s & 0 & 0 & 0 & 0 \\ 0 & \sigma L_s & 0 & 0 & 0 \\ 0 & 0 & \frac{1}{L_r} & 0 & 0 \\ 0 & 0 & 0 & \frac{1}{L_r} & 0 \\ 0 & 0 & 0 & 0 & J \end{bmatrix}, d = \begin{bmatrix} \sigma L_s i_{\alpha so} \\ \sigma L_s i_{\beta so} \\ \frac{\psi_{\alpha ro}}{L_r} \\ \frac{\psi_{\beta ro}}{L_r} \\ J\omega_{ro} \end{bmatrix}$$

The derivative of w_p is the power balance equation (2.41), as rewritten in terms of deviation from equilibrium point. This is expressed in (2.50) below.

$$\frac{dw_p(e)}{dt} = u_{\alpha s}e_1 + u_{\beta s}e_2 - B(e_5^2 + 2e_5\omega_{ro}) - T_l e_5 - \left(R_s + \frac{R_r L_m^2}{L_r^2}\right)\left(e_1^2 + 2e_1 i_{\alpha so} + e_2^2 + 2e_2 i_{\beta so}\right)$$

$$+\frac{2L_m R_r}{L_r^2}\left(i_{\alpha so}e_3 + \psi_{\alpha ro}e_1 + e_1e_3 + i_{\beta so}e_4 + \psi_{\beta ro}e_2 + e_2e_4\right) - \frac{R_r}{L_r^2}\left(e_3^2 + 2e_3\psi_{\alpha ro} + e_4^2 + 2e_4\psi_{\beta ro}\right) \tag{2.50}$$

Equation (2.50) is rewritten in error vector product form as in (2.51),

$$\frac{dw_p(e)}{dt} = -e^T M_w e - s^T e \tag{2.51}$$

where,

$$M_w = \begin{bmatrix} \left(R_s + \frac{R_r L_m^2}{L_r^2}\right) & 0 & -\left(\frac{L_m R_r}{L_r^2}\right) & 0 & 0 \\ 0 & \left(R_s + \frac{R_r L_m^2}{L_r^2}\right) & 0 & -\left(\frac{L_m R_r}{L_r^2}\right) & 0 \\ -\left(\frac{L_m R_r}{L_r^2}\right) & 0 & \frac{R_r}{L_r^2} & 0 & 0 \\ 0 & -\left(\frac{L_m R_r}{L_r^2}\right) & 0 & \frac{R_r}{L_r^2} & 0 \\ 0 & 0 & 0 & 0 & B \end{bmatrix}$$

$$s = \begin{bmatrix} 2\left(R_s + \frac{R_r L_m^2}{L_r^2}\right) i_{\alpha so} - \frac{2L_m R_r}{L_r^2}\psi_{\alpha ro} - u_{\alpha s} \\ 2\left(R_s + \frac{R_r L_m^2}{L_r^2}\right) i_{\beta so} - \frac{2L_m R_r}{L_r^2}\psi_{\beta ro} - u_{\beta s} \\ \frac{2R_r}{L_r^2}\psi_{\alpha ro} - \frac{2L_m R_r}{L_r^2} i_{\alpha so} \\ \frac{2R_r}{L_r^2}\psi_{\beta ro} - \frac{2L_m R_r}{L_r^2} i_{\beta so} \\ 2B\omega_{ro} + T_l \end{bmatrix}$$

2.3.3 Stability Analysis of the Induction Motor in the Sense of Lyapunov

A. Selection of the Lyapunov Function

Let first term from (2.49) be taken as a Lyapunov fuction candidate, V:

$$V = e^T K e \tag{2.52}$$

Taking the time derivative of (2.49) and equating it with (2.51), the time derivative of the Lyapunov function is obtained as:

$$\dot{V} = \frac{dw_p(e)}{dt} - d^T \dot{e} = -e^T M_w e - s^T e - d^T \left(A(x_o) + g(e)\right)$$

As the second and third terms in above equation cancel out

$$\dot{V} = -e^T Me \tag{2.53}$$

where,

$$M = \begin{bmatrix} \left(R_s + \frac{R_r L_m^2}{L_r^2}\right) & 0 & -\left(\frac{L_m R_r}{L_r^2}\right) & -\left(\frac{pL_m\omega_{ro}}{2\times L_r}\right) & 0 \\ 0 & \left(R_s + \frac{R_r L_m^2}{L_r^2}\right) & \left(\frac{pL_m}{2\times L_r}\omega_{ro}\right) & \left(-\frac{L_m R_r}{L_r^2}\right) & 0 \\ -\left(\frac{L_m R_r}{L_r^2}\right) & \left(\frac{pL_m}{2\times L_r}\omega_{ro}\right) & \left(\frac{R_r}{L_r^2}\right) & 0 & \frac{p}{2L_r}\left(\psi_{\beta ro} - L_m i_{\beta so}\right) \\ -\left(\frac{pL_m\omega_{ro}}{2\times L_r}\right) & -\left(\frac{L_m R_r}{L_r^2}\right) & 0 & \left(\frac{R_r}{L_r^2}\right) & \frac{p}{2L_r}\left(L_m i_{\alpha so} - \psi_{\alpha ro}\right) \\ 0 & 0 & \frac{p}{2L_r}\left(\psi_{\beta ro} - L_m i_{\beta so}\right) & \frac{p}{2L_r}\left(L_m i_{\alpha so} - \psi_{\alpha ro}\right) & B \end{bmatrix}$$

2.3.4 Global Stability of Induction Motor

According to the theorem 3.3 for the Global stability [2] of a scalar function *V* of the state error, *e* with continuous first order derivatives, conditions of stability are

(a) *V(e)* is positive definite $\forall e \neq 0$, and $V(0) = 0$

(b) $\frac{dV(e)}{dt} \leq 0 \forall e \neq 0$

(c) $\frac{dV(e)}{dt} \equiv 0 \Rightarrow e = 0$

(d) $V(e) \to \infty as \|e\| \to \infty$ (2.54)

For verification of the first condition, the leading principal minors of the *K* should be positive definite. These are given below and verified.

$$K_1 = \frac{\sigma L_s}{2} > 0, K_2 = \frac{(\sigma L_s)^2}{4} > 0, K_3 = \frac{(\sigma L_s)^2}{8L_r} > 0 \text{ , } K_4 = \frac{(\sigma L_s)^2}{16L_r^2} > 0$$

$$K_5 = \frac{(\sigma L_s)^2 J}{32L_r^2} > 0, \tag{2.55}$$

All principal minors of *K* are positive definite. Apart from these, all principal minors are also positive. This is verified. Conditions (a) and (d) hold good for the Lypunov function defined in (2.52). To check conditions (b) and (c) we proceed as follows.

2.3.5 Global Asymptotic Stability of the Unloaded Induction Motor

Under no load condition motor load torque is zero. If $B=0$, the electromagnetic torque, $T_e=0$ and $i_{\alpha ro}$ and $i_{\beta ro}$ become zero. Therefore, (2.43) and (2.44) become

$$i_{\alpha ro} = -\frac{L_m}{L_r} i_{\alpha so} + \frac{\psi_{\alpha ro}}{L_r} = 0 \tag{2.56}$$

$$i_{\beta ro} = -\frac{L_m}{L_r} i_{\beta so} + \frac{\psi_{\beta ro}}{L_r} = 0 \tag{2.57}$$

Substituting (2.56) and (2.57) in (2.53), matrix M reduces to M_o, where,

$$M_0 = \begin{bmatrix} \left(R_s + \frac{R_r L_m^2}{L_r^2}\right) & 0 & -\left(\frac{L_m R_r}{L_r^2}\right) & -\left(\frac{pL_m\omega_{ro}}{2\times L_r}\right) & 0 \\ 0 & \left(R_s + \frac{R_r L_m^2}{L_r^2}\right) & \left(\frac{pL_m}{2\times L_r}\omega_{ro}\right) & \left(-\frac{L_m R_r}{L_r^2}\right) & 0 \\ -\left(\frac{L_m R_r}{L_r^2}\right) & \left(\frac{pL_m}{2\times L_r}\omega_{ro}\right) & \left(\frac{R_r}{L_r^2}\right) & 0 & 0 \\ -\left(\frac{pL_m\omega_{ro}}{2\times L_r}\right) & -\left(\frac{L_m R_r}{L_r^2}\right) & 0 & \left(\frac{R_r}{L_r^2}\right) & 0 \\ 0 & 0 & 0 & 0 & B \end{bmatrix} \tag{2.58}$$

This matrix M_o should be positive semidefinite. For this all the possible principal minors of M_0 are obtained and given below.

$$M_{0(1\times1)} = \left(R_s + \frac{R_r L_m^2}{L_r^2}\right), \left(\frac{R_r}{L_r^2}\right), B \tag{2.59}$$

$$M_{0(2\times2)} = \left(R_s + \frac{R_r L_m^2}{L_r^2}\right)^2, \left(R_s + \frac{R_r L_m^2}{L_r^2}\right)\left(\frac{R_r}{L_r^2}\right) - \left(\frac{pL_m\omega_{ro}}{2L_r}\right)^2,$$

$$\left(\frac{R_r}{L_r^2}\right)^2, B\left(\frac{R_r}{L_r^2}\right), B\left(R_s + \frac{R_r L_m^2}{L_r^2}\right) \tag{2.60}$$

$$M_{0(3\times3)} = \left(R_s + \frac{R_r L_m^2}{L_r^2}\right)\left(\left(\left(R_s + \frac{R_r L_m^2}{L_r^2}\right)\left(\frac{R_r}{L_r^2}\right) - \left(\frac{pL_m\omega_{ro}}{2L_r}\right)^2\right) - \left(\frac{L_m R_r}{L_r^2}\right)^2\right),$$

$$\left(\frac{R_r}{L_r^2}\right)\left(\left(R_s + \frac{R_r L_m^2}{L_r^2}\right)\left(\frac{R_r}{L_r^2}\right) - \left(\frac{pL_m\omega_{ro}}{2L_r}\right)^2 - \left(\frac{L_m R_r}{L_r^2}\right)^2\right)$$

$$B\left(\frac{R_r}{L_r^2}\right)^2, B\left(R_s+\frac{R_r L_m^2}{L_r^2}\right)^2 \tag{2.61}$$

$$M_{0(4\times4)}=\begin{pmatrix}\left(\left(\frac{L_m R_r}{L_r^2}\right)^2-\left(R_s+\frac{R_r L_m^2}{L_r^2}\right)\left(\frac{R_r}{L_r^2}\right)\right)^2+\left(\left(\frac{pL_m\omega_{ro}}{2L_r}\right)^2-\left(R_s+\frac{R_r L_m^2}{L_r^2}\right)\left(\frac{R_r}{L_r^2}\right)\right)^2\\ +2\left(\frac{L_m R_r}{L_r^2}\right)^2\left(\frac{pL_m\omega_{ro}}{2L_r}\right)^2-\left(R_s+\frac{R_r L_m^2}{L_r^2}\right)\left(\frac{L_m R_r}{L_r^2}\right)\end{pmatrix}$$

$$,B\left(\frac{R_r}{L_r^2}\right)\left(\left(R_s+\frac{R_r L_m^2}{L_r^2}\right)\left(\frac{R_r}{L_r^2}\right)-\left(\frac{pL_m\omega_{ro}}{2L_r}\right)^2-\left(\frac{L_m R_r}{L_r^2}\right)^2\right) \tag{2.62}$$

and

$$M_{0(5\times5)}=B\begin{pmatrix}\left(\left(\frac{L_m R_r}{L_r^2}\right)^2-\left(R_s+\frac{R_r L_m^2}{L_r^2}\right)\left(\frac{R_r}{L_r^2}\right)\right)^2\\ +\left(\left(\frac{pL_m\omega_{ro}}{2L_r}\right)^2-\left(R_s+\frac{R_r L_m^2}{L_r^2}\right)\left(\frac{R_r}{L_r^2}\right)\right)^2\\ +\left(2\left(\frac{L_m R_r}{L_r^2}\right)^2\left(\frac{pL_m\omega_{ro}}{2L_r}\right)^2-\left(R_s+\frac{R_r L_m^2}{L_r^2}\right)^2\left(\frac{R_r}{L_r^2}\right)^2\right)\end{pmatrix} \tag{2.63}$$

Here we conclude that M_0 is positive semidefinite if and only if it fulfils following condition obtained from (2.61) and (2.62).

$$\left(\left(R_s+\frac{R_r L_m^2}{L_r^2}\right)\left(\frac{R_r}{L_r^2}\right)-\left(\frac{pL_m\omega_{ro}}{2L_r}\right)^2-\left(\frac{L_m R_r}{L_r^2}\right)^2\right)\geq 0 \tag{2.64}$$

The above condition is influenced by the machine parameter. Equation (3.64) gives positive definite value in case of low rating motors [77] and at low speeds applicable to all induction motors. In case of the large induction motor (2.64) becomes negative. Hence, for starting the large induction motor under loaded condition it is required to increase the rotor resistance as well as stator resistance. This confirms the known fact that, small rating induction motors and some medium power rating motors at no load can be started directly on line without losing stability. To achieve the same in large motors, rotor resistance needs to be increased, to increase the starting torque, so that motor is stable during starting and acceleration.

To check the condition(c) $\frac{dV(e)}{dt}\equiv -e^T Me\equiv 0\forall e=0$

.

From (2.53) and (2.58)

$$\frac{dV(e)}{dt}=\left(R_s+\frac{R_rL_m^2}{L_r^2}\right)\left(e_1^2+e_2^2\right)+\frac{R_r}{L_r^2}\left(e_3^2+e_4^2\right)-\frac{2L_mR_r}{L_r^2}\left(e_1e_3+e_2e_4\right)-\frac{n_p\omega_{ro}L_m}{L_r}\left(e_1e_4-e_2e_3\right)+Be_5 \equiv 0 \tag{2.65}$$

Here, an arbitrary positive expression in terms machine parameters and error variables are taken as follows

$$\left(\sqrt{\left(R_s+\frac{R_rL_m^2}{L_r^2}\right)}e_1\pm\sqrt{\frac{R_r}{L_r^2}}e_3\right)^2+\left(\sqrt{\left(R_s+\frac{R_rL_m^2}{L_r^2}\right)}e_2\pm\sqrt{\frac{R_r}{L_r^2}}e_4\right)^2\geq 0 \tag{2.66}$$

On expanding one can get

$$\left(R_s+\frac{R_rL_m^2}{L_r^2}\right)e_1^2+\left(R_s+\frac{R_rL_m^2}{L_r^2}\right)e_2^2+\frac{R_r}{L_r^2}e_3^2+\frac{R_r}{L_r^2}e_4^2\pm 2\sqrt{\left(R_s+\frac{R_rL_m^2}{L_r^2}\right)}\sqrt{\frac{R_r}{L_r^2}}\left(e_1e_3+e_2e_4\right)\geq 0 \tag{2.67}$$

Subtracting (2.65) from (2.67)

$$\frac{2L_mR_r}{L_r^2}\left(e_2e_4+e_1e_3\right)\pm 2\sqrt{\left(R_s+\frac{R_rL_m^2}{L_r^2}\right)}\sqrt{\frac{R_r}{L_r^2}}\left(e_1e_3+e_2e_4\right)+\frac{p\omega_{ro}L_m}{L_r}\left(e_2e_3-e_1e_4\right)-Be_5\geq 0 \tag{2.68}$$

Finally equation (2.68) becomes:

$$\left(\pm 2\sqrt{\left(R_s+\frac{R_rL_m^2}{L_r^2}\right)}\sqrt{\frac{R_r}{L_r^2}}+\frac{2L_mR_r}{L_r^2}\right)\left(e_1e_3+e_2e_4\right)+\frac{p\omega_{ro}L_m}{L_r}\left(e_2e_3-e_1e_4\right)-Be_5\geq 0 \tag{2.69}$$

The first, second and third coefficient in (2.69) are positive, left side of (2.68) will be equal to zero, only when *e=0*.

2.3.6 Global Stability of Loaded Induction Motor

Next, the positive definite condition of matrix *M* is investigated, when induction motor is subjected to the load. This condition will be fulfilled if and only if it's leading principal minors are positive. The leading principal minors are as following

$$M_1 = \left(R_s + \left(\frac{L_m}{L_r} \right)^2 R_r \right) \tag{2.70}$$

$$M_2 = \left(R_s + \left(\frac{L_m}{L_r} \right)^2 R_r \right)^2 \tag{2.71}$$

$$M_3 = \left(R_s + \frac{R_r L_m^2}{L_r^2} \right) \left(\left(R_s + \frac{R_r L_m^2}{L_r^2} \right) \left(\frac{R_r}{L_r^2} \right) - \left(\frac{pL_m \omega_{ro}}{L_r} \right)^2 - \left(\frac{L_m R_r}{L_r^2} \right)^2 \right), \tag{2.72}$$

$$M_4 = \left(\left(R_s + \frac{R_r L_m^2}{L_r^2} \right) \left(\frac{R_r}{L_r^2} \right) - \left(\left(\frac{L_m R_r}{L_r^2} \right)^2 + \left(\frac{pL_m \omega_{ro}}{L_r} \right)^2 \right) \right)^2 \tag{2.73}$$

$$M_5 = \left(\left(\frac{pL_m \omega_{ro}}{2L_r} \right)^2 - \left(R_s + \frac{R_r L_m^2}{L_r^2} \right) \left(\frac{R_r}{L_r^2} \right) \right) \left(\left(\frac{p}{2L_r} \left(\psi_{\beta ro} - L_m i_{\beta so} \right) \right)^2 + \left(\frac{p}{2L_r} \left(L_m i_{\alpha so} - \psi_{\alpha ro} \right) \right)^2 - B \frac{R_r}{L_r^2} \right) - B \frac{R_r}{L_m^2} \left(\left(\frac{L_m R_r}{L_r^2} \right)^2 + \left(\frac{pL_m \omega_m}{2L_r} \right)^2 \right)$$

$$+ \left(\frac{L_m R_r}{L_r^2} \right) \left(\frac{p}{2L_r} \left(\psi_{\beta ro} - L_m i_{\beta so} \right) \right) \left(\left(\frac{L_m R_r}{L_r^2} \right) \left(\frac{p}{2L_r} \left(\psi_{\beta ro} - L_m i_{\beta so} \right) \right) + \left(\frac{pL_m \omega_m}{2L_r} \right) \left(\frac{p}{2L_r} \left(L_m i_{\alpha so} - \psi_{\alpha ro} \right) \right) \right) \tag{2.74}$$

2.3.7 A Case Study

In this section , the global asymptotic stability condition is verified by considering an induction motor with the following specifications and parameters given in Table 2.1.

Table-2.1

Motor Specifications and Parameters

Parameters	Symbol	Value
Rated Power	P	3.7 KW
Rated Voltage (Line)	V_L	415 V
Rated speed	ω_m	1445 rpm
Stator resistance	R_s	7.34 Ω

Stator Inductance	L_{ls}	0.021 H
Rotor Resistance	R_r	5.64 Ω
RotorLeakage Inductance	L_{lr}	0.021 H
Rotor Self Inductance	L_r	0.521 H
Mutual Inductance	L_m	0.5 H
Number of Pole pair	p	2
Moment of Inertia	J	0.16 kg-m^2
Frictional Constant	B	0.035 kg-m^2/s

the Induction motor parameters value are substituted in the matrix *M* and solved for leading positive minors.

$$M=\begin{bmatrix} (12.5) & 0 & (-9.95) & -(0.4\omega_r) & 0 \\ 0 & (12.5) & (0.4\omega_r) & (-9.95) & 0 \\ (-9.95) & (0.4\omega_r) & (19.89) & 0 & (1.9\psi_{\beta ro}-0.95i_{\beta so}) \\ -(0.4\omega_r) & (-9.95) & 0 & (19.89) & (0.95i_{\alpha so}-1.9\psi_{\alpha ro}) \\ 0 & 0 & (1.9\psi_{\beta ro}-0.95i_{\beta so}) & (0.95i_{\alpha so}-1.9\psi_{\alpha ro}) & 0.035 \end{bmatrix} \tag{2.75}$$

The leading positive minors of *M* are

$$M_1=\left(R_s+\left(\frac{L_m}{L_r}\right)^2 R_r\right)=12.5 \tag{2.76}$$

$$M_2=\left(R_s+\left(\frac{L_m}{L_r}\right)^2 R_r\right)^2=156.3 \tag{2.77}$$

$$M_3=\left(R_s+\frac{R_r L_m^2}{L_r^2}\right)\left(\left(R_s+\frac{R_r L_m^2}{L_r^2}\right)\left(\frac{R_r}{L_r^2}\right)-\left(\frac{pL_m\omega_{ro}}{L_r}\right)^2-\left(\frac{L_m R_r}{L_r^2}\right)^2\right) \tag{2.78}$$

The forth principal minor is solved as follows:

$$M_4=\begin{bmatrix} (12.5) & 0 & (-9.95) & (-0.4v\omega_s) \\ 0 & (12.5) & (0.4v\omega_s) & (-9.95) \\ (-9.95) & (0.4v\omega_s) & (19.89) & 0 \\ (-0.4v\omega_s) & (-9.95) & 0 & (19.89) \end{bmatrix}$$

here ω_r is replace by the product of a variable ν and synchronous speed ω_s (314.16) i.e., $\nu\omega_s$ where $\nu = 1 - s$, *s* is defined as motor slip.

$$M_{41} = 12.5\begin{bmatrix} 12.5 & (0.4\nu\omega_s) & (-9.95) \\ (0.4\nu\omega_s) & 19.89 & 0 \\ (-9.95) & 0 & 19.89 \end{bmatrix}$$

$$M_{41} = 12.5\left(12.5(19.89)^2 - 19.89(0.4\nu\omega_s)^2 - 19.8(9.95)^2\right)$$

$$M_{41} = 35711.88 - 980537.125\nu^2$$

$$M_{43} = -9.95\begin{bmatrix} 0 & (12.5) & (-9.95) \\ (-9.95) & (0.4\nu\omega_s) & 0 \\ ((-0.4\nu\omega_s)) & -9.95 & 19.89 \end{bmatrix}$$

$$M_{43} = -9.95\left(-12.5(-9.95\times 19.89) - 9.95\left((9.95)^2 + (0.4\nu\omega_s)^2\right)\right)$$

$$M_{43} = -14812.5 + 390449.94\nu^2$$

$$M_{44} = -0.4\nu\omega_s\begin{bmatrix} 0 & (12.5) & (0.4\nu\omega_s) \\ (-9.95) & (0.4\nu\omega_s) & 19.89 \\ (-0.4\nu\omega_s) & -9.95 & 0 \end{bmatrix}$$

$$M_{44} = 0.4\nu\omega_s\left(-12.5(0.4\nu\omega_s \times 19.89) + 0.4\nu\omega_s\left((9.95)^2 + (0.4\nu\omega_s)^2\right)\right)$$

$$M_{44} = -590090.78\nu^2 + 15553873.82\nu^4$$

$$M_4 = M_{41} + M_{43} + M_{44}$$

$$M_4 = 35711.88 - 980537.125\nu^2 - 14812.5 + 390449.94\nu^2 - 590090.78\nu^2 + 15553873.82\nu^4$$

$$M_4 = 15553873.82\nu^4 - 2\times 590090.78\nu^2 + 20899.38$$

Let $\nu^2 = x$

Then

$$M_4 = 15553873.82x^2 - 2\times 590090.78x - 109843.12 = 0$$

The above equation is solved for real roots,

$$x = \pm 0.13, \Rightarrow x = \nu^2 > 0.13$$

$$-0.36 < \nu > 0.36 \Rightarrow -0.36 < 1 - s > 0.36$$

$$s < 0.64$$

$$s < 1.36$$

The fifth minor of the M_5 matrix contains motor current and flux equilibrium point values Therefore for testing the positive definiteness of the fourth minor and the fifth minor the following three sets of observations have been considered for open loop operating condition.

(a) Induction Motor running at 52.19rad/s (500rpm) under no load.

(b) Induction Motor running at 52.19rad/s (500rpm) subjected to 10 N.m load torque.

(c) Induction Motor running at 104.7rad/s (1000rpm) under no load.

Testing the validity of the test result for stability are obtained from solving determinant of the matrix M_4 and M_5 and results are given in Table-2.2, respectively.

Table 2.2

Stability Test Result for three Cases

ω_{ro} (rad/s)	T_l (N.m)	$i_{\alpha so}$(A) $i_{\beta so}$(A)	$\psi_{\alpha r0}$ (V.s) $\psi_{\beta r0}$ (V.s)	Principal Minor
52.1	0.575	2.17 1.947	0.45 -0.48	M_4=8.1e4 M_5=2.12e4
52.02	10.1	-5.415 -8.468	0.220 -0.427	M_4=8.1e4 M_5=2.72e5
104.7	0.4	-1.78 -3.965	-3.965 -0.48	M_4=1.16e8 M_5=5.9e6

Sufficient condition for the global asymptotic stability in the sense of Lyapunov for an induction motor has been derived. It has been found that, for steady state stability, slip of the induction motor depends on its parameters, i.e., stator resistance, rotor resistance, mutual and rotor self inductance. But, the rotor resistance is more prominent in comparison to other parameters. Though such results were empirically

known earlier, the mathematical analysis for Lyapunov's stability is of great relevance. It is well known that addition of rotor resistance increases the starting torque and hence motor can accelerate stably. The slip condition for stability is also derived. Although it gives limited information, this analysis helps to understand the basic inherent stability characteristics of the induction motor. It is very convincing and natural way to test the validity of induction motor stability in any open loop or closed loop control scheme.

2.4 Feedback Linearization Control

Feedback linearization is an approach to nonlinear control design which has attracted great deal of research interest in recent years. The central idea of the approach is to algebraically transform a nonlinear system dynamics into a fully or partially linear one so that linear control technique can be applied. This differs entirely from conventional linearization techniques like perturbation about an equilibrium point. Feedback linearization is achieved by exact state transformation. It uses a nonlinear transformation on system variables expressing them in a new suitable coordinate system which enables the introduction of a feedback, so that an input-output or state linearization in new coordinates is achieved. The theoretical foundation and a systematic approach can be found in [2].

In order to control the induction motor in field orientation schemes to get a dc motor like performance, the rotor speed and rotor flux must be decoupled. Therefore, output to be controlled is chosen as

$$[y] = [\omega_r, \psi_r] \tag{2.79}$$

Where, ω_r is rotor speed and ψ_r is the rotor flux. The rotor flux is calculated as follows.

$$\psi_r^2 = \psi_{\alpha r}^2 + \psi_{\beta r}^2 \tag{2.80}$$

The time derivative of ψ_r given by (2.80) is:

$$\dot{\psi}_r = \frac{1}{\psi_r}\left[\psi_{\alpha r}\dot{\psi}_{\alpha r} + \psi_{\beta r}\dot{\psi}_{\beta r}\right] \tag{2.81}$$

Substituting $\dot{\psi}_{\alpha r}$ and $\dot{\psi}_{\beta r}$ from (2.27) and (2.28) into (2.81), we have:

$$\dot{\psi}_r = \frac{1}{\psi_r}\left[\psi_{\alpha r}\left(-\frac{R_r}{L_r}\psi_{\alpha r} - p\omega_r\psi_{\beta r} + \frac{L_m R_r}{L_r} i_{\alpha s}\right) + \psi_{\beta r}\left(-\frac{R_r}{L_r}\psi_{\beta r} + p\omega_r\psi_{\alpha r} + \frac{L_m R_r}{L_r} i_{\beta s}\right)\right] \tag{2.82}$$

$$= \frac{1}{\psi_r}\left[-\frac{R_r}{L_r}\psi_{\alpha r}^2 - p\omega_r\psi_{\alpha r}\psi_{\beta r} + \frac{L_m}{L_r}R_r\psi_{\alpha r}i_{\alpha s} + \frac{R_r}{L_r}\psi_{\beta r}^2 + p\omega_r\psi_{\alpha r}\psi_{\beta r} + \frac{L_m}{L_r}R_r\psi_{\beta r}i_{\beta s}\right] \tag{2.83}$$

$$= \frac{1}{\psi_r}\left[-\frac{R_r}{L_r}\psi_r^{\,2} + \frac{L_m R_r}{L_r}\left(i_{\alpha s}\psi_{\alpha r} + i_{\beta s}\psi_{\beta r}\right)\right] \tag{2.84}$$

Hence, the final expression of (2.81) can written as follows:

$$\dot{\psi}_r = -\frac{R_r}{L_r}\psi_r + \frac{L_m R_r}{L_r\psi_r}(i_{\alpha s}\psi_{\alpha r} + i_{\beta s}\psi_{\beta r}) \tag{2.85}$$

From (2.5) and (2.6) the dynamic equation of rotor speed can be rewritten as:

$$\dot{\omega}_r = -\frac{B}{J}\omega_r + \frac{1}{J}K_T(\psi_{\alpha r}i_{\beta s} - \psi_{\beta r}i_{\alpha s}) - \frac{1}{J}T_l \tag{2.86}$$

Equations (2.85) and (2.86) represent separate electrical and mechanical subsystem with iαs, and $i_{\beta s}$ as two control inputs, ψr and ω_r as the two outputs. But, each of them represents a coupled system. Since, there are no direct relation between the outputs and inputs. Therefore, the nonlinear feedback theory [2] is used to eliminate this coupling relationship between the control inputs $i_{\alpha s}$, $i_{\beta s}$ and the system outputs ψ_r and ω_r. Let $u1$ and $u2$ be taken as two new intermediate control inputs which convert coupled system into decoupled one [17]. Equations (2.85) and (2.86) with two new control inputs $u1$ and $u2$ can be written as

$$\dot{\omega}_r = -\frac{B}{J}\omega_r + \frac{1}{J}K_T u1 - \frac{T_l}{J} \tag{2.87}$$

$$\dot{\psi}_r = -\frac{R_r}{L_r}\psi_r + \frac{L_m R_r}{L_r}u2 \tag{2.88}$$

From equations (2.85). (2.86), (2.87) and (2.88) the expression of the new control inputs can be expressed as

$$u1 = \left(\psi_{\alpha r} i_{\beta s} - \psi_{\beta r} i_{\alpha s}\right) \tag{2.89}$$

$$u2 = \frac{1}{\psi_r}\left(\psi_{\alpha r} i_{\alpha s} + \psi_{\beta r} i_{\beta s}\right) \tag{2.90}$$

The inverse of (2.89) and (2.90) gives the expression of $i_{\alpha s}$ and $i_{\beta s}$ in terms of $u1, u2$, $\psi_{\alpha r}$ and $\psi_{\beta r}$

$$i_{\alpha s} = \frac{\psi_{\alpha r}}{\psi_r} u2 - \frac{\psi_{\beta r}}{\psi_r^2} u1 \tag{2.91}$$

$$i_{\beta s} = \frac{\psi_{\beta r}}{\psi_r} u2 + \frac{\psi_{\alpha r}}{\psi_r^2} u1 \tag{2.92}$$

The above equations (2.91) and (2.92) represent a feedback linearization decoupling controller. The block diagram of feedback linearizing controller is shown in Fig.2.2.

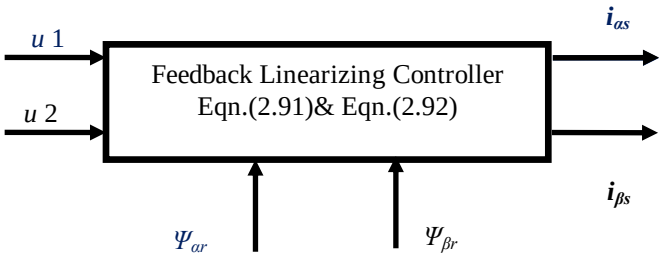

Fig. 2.2. Feedback linearizing controller

2.5 Design of PI Controllers

The transformed model of induction motor is given in (2.87) and (2.89) along with feedback linearizing controller decouples the developed torque and the rotor flux path completely. The simplified open loop block diagrams of the electrical and mechanical subsystems are shown in Fig. 2.3 and Fig. 2.4 respectively. The intermediate control inputs $u1$ and $u2$ can be obtained using PI controllers as follows:

$$u1 = K_{p1}(\omega_r^* - \omega_r) + K_{i1}\int_0^t (\omega_r^* - \omega_r)dt \tag{2.93}$$

$$u2 = K_{p2}(\psi_r^* - \psi_r) + K_{i2}\int_0^t (\psi_r^* - \psi)dt \tag{2.94}$$

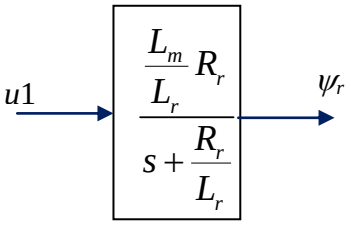

Fig.2.3 Block diagram of the open loop electrical system

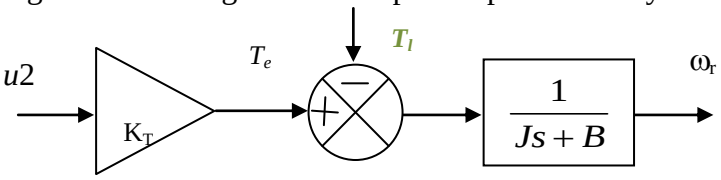

Fig.2.4. Block diagram of the open loop mechanical system

The choice of gains of these PI controllers is crucial for the design of the controller drive system. A wrong choice of such gains may result in unstable response and/or undesirable performance. To have a feel of the influence of controller gains on the characteristic of the drive system in general and the factors affecting the gains of the PI controllers in particular, the transfer function of the electrical and mechanical subsystem are analyzed. Electrical subsystem with it's controller is simulated and it is verified that simulation response with the designed controller is satisfactory. Mechanical subsystem with one PI controller is also simulated.

2.5.1 PI Controller for Electrical Subsystem

The block diagram of unity feedback closed loop electrical subsystem with one proportional integral (PI) controller is shown in Fig.2.5.

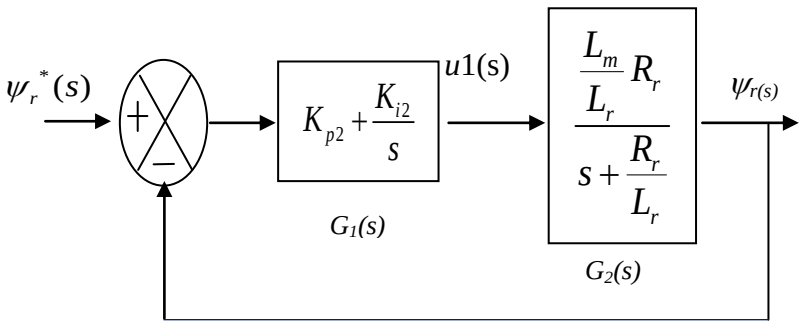

Fig. 2.5 Block diagram of the closed loop electrical subsystem with PI controller

Using the induction motor parameters given in Table 2.1, L_r=0.52H, L_m=0.5H and R_r=5.64Ω , the open loop transfer function for the electrical subsystem (Fig.2.3) can be express as

$$\frac{\psi_r(s)}{u1(s)} = \frac{\frac{L_m R_r}{L_r}}{s + \frac{R_r}{L_r}} = \frac{5.42}{s + 10.846} \tag{2.95}$$

This is a first order transfer function and time constant of flux is:

$$\tau_{\psi r} = \frac{1}{10.846} = 0.092 \sec. \tag{2.96}$$

The time constant of the open system response is 0.092sec. For a unit step input, 90% rise time of flux is 2.3 times electrical time constant, i.e.,2.3x0.092= 0.216 s. As it has a pole at -10.84, it gives sluggish response. In order to track the reference flux ψ_r^* and to improve the system response one PI controller is connected and designed for closed loop electrical subsystem, which block diagram is shown in Fig. 2.5.

The transfer function $G_0(s)$ the forward path including that of the controller is

$$G_0(s) = G_1(s) \,.\, G_2(s) = \frac{K_{p2}s + K_{i2}}{s} . \frac{5.42}{s + 10.846} = \frac{5.42(K_{p1}s + K_{i1})}{s(s + 10.846)} \tag{2.97}$$

Next, the overall closed loop transfer function of the unity feedback flux control loop

$$\frac{\psi_r(s)}{\psi_r^*(s)} = \frac{G_0(s)}{1 + G_0(s)} = \frac{\frac{5.42(K_{p2}s + K_{i2})}{s(s + 10.846)}}{1 + \frac{5.42(K_{p2}s + K_{i2})}{s(s + 10.846)}}$$

$$= \frac{5.42(K_{p2}s + K_{i2})}{s^2 + (10.846 + 5.42K_{p2})s + 5.42K_{i2}} \tag{2.98}$$

The characteristic polynomial of the closed loop transfer function is of second order

$s^2 + (10.846 + 5.42K_{p2})s + 5.42K_{i2}$,

This is compared with the standard form $(s^2 + 2\xi\omega_n s + \omega_n^2)$, where, ω_n is the natural frequency of oscillation and ζ is the damping factor. Assuming the natural frequency of oscillation, ω_n is taken 75.

$$5.42K_{i2} = \omega_n^{\ 2} = 5625$$

$$K_{i2} = \frac{5625}{5.42} = 1037.8$$

Designing the system to be critically damped (i.e.,ξ=1), the proportional gain $K_{p2,}$ is obtained as follows.

$$10.846 + 5.42K_{p2} = 2\xi\omega_n$$

$$10.846 + 5.42K_{p2} = 150$$

$$K_{p2} = \frac{139.154}{5.42} = 25.67$$

With these values of K_{p1} and $K_{i1,}$ the control law for the electrical subsystem is:

$$u2 = 25.67(\psi_r^* - \psi_r) + 1037.8\int_0^t (\psi_r^* - \psi_r)dt \qquad (2.99)$$

With K_{p2} = 25.67 and K_{i2} = 1037.8, the characteristic polynomial of the closed loop transfer function becomes as follows

$$s^2 + 150s + 5625 \qquad (2.100)$$

Solving for getting poles of the characteristics polynomial in (2.101)

$$S_1, S_2 = \frac{-150 \pm \sqrt{(150)^2 - 4\times 5625}}{2} = -75, -75$$

(2.101)

Here the roots of the characteristic polynomial are equal and in the left half plane. The poles are at -75, are more far away from the of complex plane imaginary axis than the open loop pole at -10.5.The rise time for unit step speed input is $2.3\times\frac{1}{75} = 0.03$ s. This makes the close loop system's dynamic response more faster and stable. The

drive system is simulated, for different value of ω_n and it is observed from the simulation studies that ω_n = 75 rad/sec is acceptable.

2.5.2 PI Controller for Mechanical Subsystem

State feedback linearization scheme require one loop controller for mechanical subsystem The block diagram of unity feedback close loop mechanical subsystem with one proportional integral (PI) controller is shown in Fig.2.6.

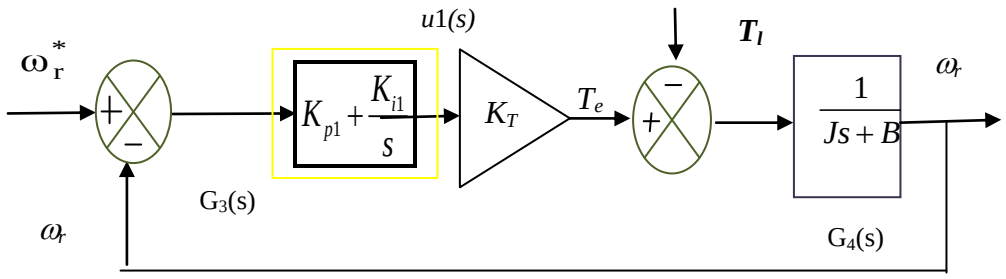

Fig.2.6 Block diagram of the closed loop mechanical subsystem with PI controller

The open loop speed transfer function is

$$\frac{\omega_r(s)}{u1(s)} = \frac{K_T}{Js+B}$$

(2.102)

using the induction motor parameters given in Table. 2.1, L_r=0.52H, L_m=0.5H and R_r=5.64Ω , J=0.16kg.m^2 and B=0.035kg.m$^{2/}$ /s substituting these values in (2.102).

$$\frac{\omega_r(s)}{u1(s)} = \frac{K_T}{Js+B} = \frac{18}{s+0.22} \qquad (2.103)$$

This is a first order transfer function and time constant of speed is

$$\tau_{\omega_r} = \frac{1}{0.22} = 4.55\text{sec} \qquad (2.104)$$

The rise time is obtained as $2.3\times4.55=10.465$ sec. It has a pole at -0.22, being a slow one, gives very sluggish speed response. In order to track the reference

speed ω_r^* and to improve the transient performance a PI controller is connect in the forward path as shown in Fig. 2.6.

The transfer function of the forward path including that of the controller is

$$G_{01}(s) = G_3(s).G_4(s) = \frac{K_{p1}s + K_{i1}}{s}.\frac{K_T}{(Js + B)} = \frac{18(K_{p1}s + K_{i1})}{s(s + 0.22)} \quad (2.105)$$

Then, the overall close loop transfer of the mechanical subsystem can be expressed as

$$\frac{\omega_r(s)}{\omega_r^*(s)} = \frac{18(K_{p1}s + K_{i1})}{s^2 + (0.22 + 18K_{p1})s + 18K_{i1}} \quad (2.106)$$

The close loop $\frac{\omega_r(s)}{\omega_r^*(s)}$ is of second order. The characteristic polynomial is in the form $s^2 + 2\xi\omega_n s + \omega_n^2$. Assuming ω_n to be 4 rad/sec.

18 K_{i1} = 16 $K_{i1} = \frac{16}{18} = 0.88$

Assuming the system to critically damped (i.e., ξ=1)

0.22 + 18 K_{p1} = $2\xi\omega_n$ = 2 x4

$$K_{p1} = \frac{8 - 0.22}{18} = 0.432$$

With these gain values the speed control law is given by:

$$u1 = 0.432(\omega_r^* - \omega_r) + 0.88\int(\omega_r^* - \omega_r) \quad (2.107)$$

The characteristic polynomial of the closed loop transfer function now becomes

s^2 + (0.22 + 18 x0.432)s + 16 = $s^2 + 8.00s + 16$ (2.108)

and solving it for getting poles of the characteristics polynomial (2.108)

$$s_1, s_2 = \quad = \frac{-8.00 \pm \sqrt{(8.00)^2 - 4 \times 1 \times 16}}{2} \quad = (s + 4)(s + 4) \quad (2.109)$$

The roots of the characteristic polynomial are in the left half plane. The pole is at -4, farther from the imaginary axis than the pole -0.22. The Rise time for unit step speed input is $= 2.3 \times \frac{1}{4} = 0.575 \sec$. The dynamic response is faster and stable. Therefore, the above gains are acceptable. The drive system is simulated, for different value of ω_n and it is observed from the simulation studies that ω_n = 4rad/sec is acceptable. From the simulation results it is observed that the assumption of K_{p1} and K_{i1} are acceptable.

2.6 Fuzzy Torque Compensator for Speed Response Improvement

In an improved scheme a fuzzy torque compensator is designed and connected in cascade to the PI speed controller. Reference torque, which is the output of the speed controller and the actual estimated torque are input signals to the fuzzy torque compensator,which would eliminate undesired features appearing in the response with conventional PI controller, such, as torque ripple, overshoot, and steady state error. The schematic block diagram of the speed controller with fuzzy torque compensator is shown in Fig 2.7.

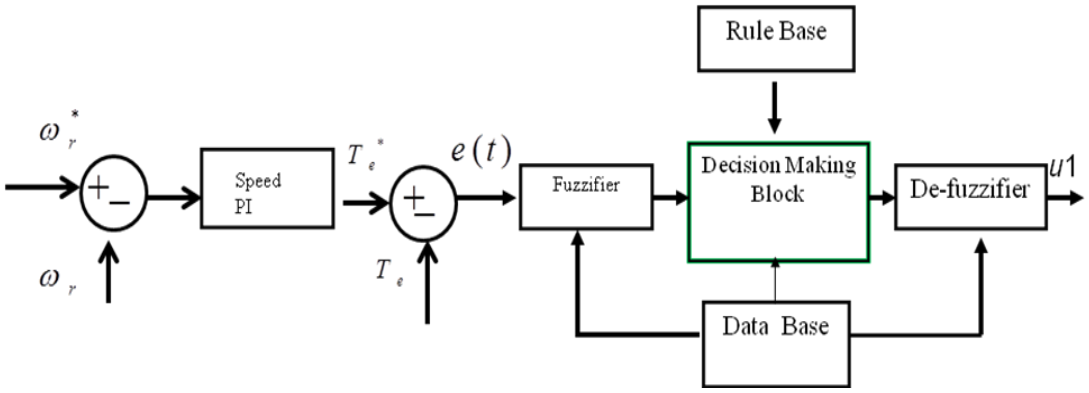

Fig.2.7 Block diagram of speed controller with fuzzy torque compensator

According to the fuzzy logic (FL) principle the controller action proceeds as follows.

(i) Computation of the value of the two inputs

- Reference torque T^*_e and estimated torque T_e are sampled.

- Torque error (e(t)) and change of torque is error (Δe(t)) pu is computed in per unit and fed to the fuzzifier.

e(t) in per unit = $(T^*_e - T_e)/T^*_e$ (2.110)

Rate of change of error in per unit = $(e(t)_n\text{-}e(t)_{n-1})/ce_{max}$ (2.111)

The membership functions for torque error, change in torque error and control output are shown in Fig. 2.8

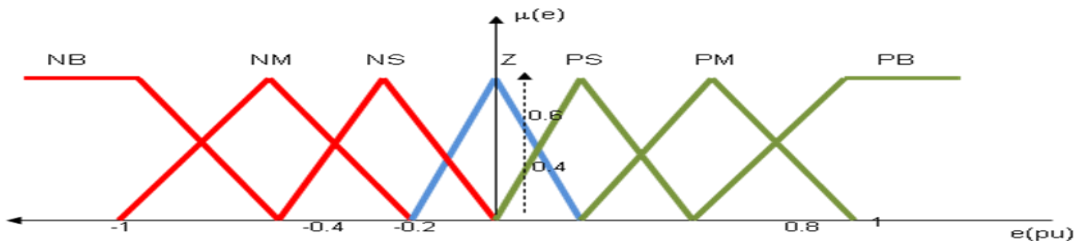

(a) Error(e (pu))

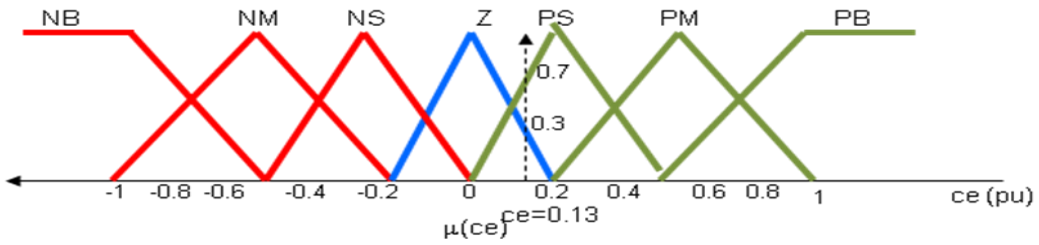

(b) Change in error (ce(pu))

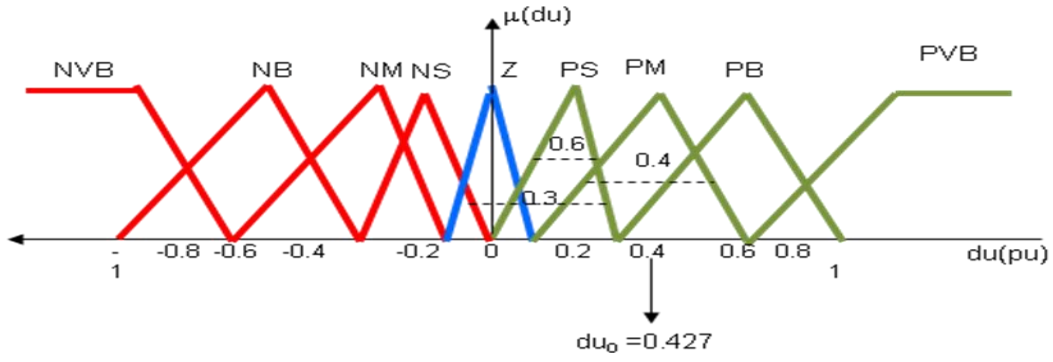

(c) Change in control output du(pu)

Fig. 2.8 Membership functions of fuzzy torque compensator : (a) error, (b) change in error, (c) change in control output

On the basis of the magnitude of e and the sign of ce as shown in Fig2.9 (a), the response plane is roughly divided into four areas *a1, a2, a3, a4* where

a1: e > 0 and ce < 0, a2: e < 0 and ce < 0

a3 : e < 0 and ce > 0, a4 : e > 0and ce > 0.

To increase in the resolution of the behavior representation, the response around the set point, the extremes are emphasized in Fig. 2.9 (b) and Fig.2.9 (c). The crossover index c for identifying the slope of the response across the set point can be defined as

c1: e = 0 and ce < < < 0 (NB)

c2: e = 0 and ce << 0 (NM)

c3: e = 0 and ce < 0 (NS)

c4: e = 0 and ce > 0 (PS)

c5: e = 0 and ce > > 0 (PM)

c6: e = 0 and ce > > > 0 (PB)

Also, the magnitude index for representing the extent of overshoot and undershoot can be defined as

m1: ce = 0 and e < < < 0 (NB)

m2: ce = 0 and e < < 0(NM)

m3: ce = 0 and e < 0 (NS)

m4 : ce = 0 and e > 0 (PS)

m5: ce = 0 and e > > 0 (PM)

m6: ce = 0 and e > > > 0 (PB)

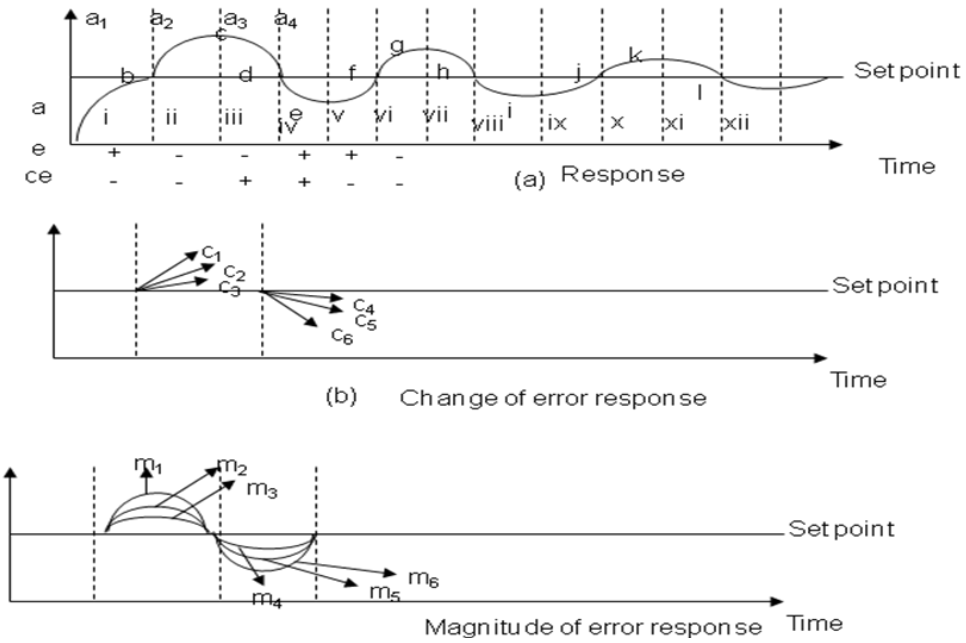

(c)

Fig . 2.9 The dynamic behavior of drive torque response

ii) Fuzzification

- Scaling of input signal by suitable scaling factors.
- Limiting the input data between +1.0 and -1.0 boundaries.

If input is greater than +1.0, then input equal to +1.0

If input is less than -1.0, then input equal to -1.0

If input is greater than -1.0 and less than +1.0, then it remains same.

Input data is converted into linguistic format in accordance with the defined fuzzy sets in accordance to Fig.2.8.

(iii) Inference

The linguistic value of the output signal is determined according to the linguistic rule. The fuzzy rules are stated in Table 2.3. As objective of the compensator is to compensate the chattering signal around reference torque, there only 16 rules are sufficient to achieve the objective.

Table 2.3

Evaluation of Fuzzy Inference Rules

Rules	e(t)p.u	ce(t)p.u	u2p.u	Reference
1	PB	Z	PB	a
2	PM	Z	PM	e
3	PS	Z	PS	i
4	Z	Z	Z	Set point
5	NS	Z	NS	k m3
6	NM	Z	NM	g m2
7	NB	Z	NB	c m1
8	Z	NB	NB	b c1
9	Z	NM	NM	f c2
10	Z	NS	NS	J c3
11	Z	PB	PB	d c6
12	Z	PM	PM	h c6
13	Z	PS	PS	l c6
14	PB	NB	Z	Rise time region
15	PB	NM	PS	Rise time region
16	PB	NS	PM	Rise time region

(iv) De-fuzzification

- It is the process of determining the numerical value to represent a given fuzzy set. It involves following steps
- $\alpha = \min[\mu(e(t),\mu(\Delta e(t)]$,where α, represents degree of fulfillment (DOF) and μ represents "membership of".
- Latest instant α should be maximum of represents instant values.

Crisp value = $c_e[\sum p(m).\ \alpha / \sum \alpha]$, where p(m) is the location of the peak membership function and c_e is the scaling factor

2.7 Summary of the Chapter

The model of the induction motor in stationary reference frame, with stator current and rotor flux component and motor speed as state variables, is briefly reviewed. Study of the Lyapunov stability of an open loop IM without load and with load has been taken-up and sufficient condition for the global asymptotic stability are derived for better understanding of characteristic of IM. Stability study reveals that pull-out slip depends on motor parameters like stator resistance, rotor resistance, mutual and self inductance. But, the rotor resistance is more prominent. Though such results were well known, more over the mathematical analysis based Lyapunov's stability is of great relevance. The feedback linearization control as applied to the induction motor drive has been presented. It has been become possible to split the induction motor drive into two linear subsystems: the electrical and mechanical subsystem. Further systematic procedure has been developed to determine the gains of the PI controllers for the electrical and mechanical subsystems. For overall performance improvement a 16 rule based fuzzy torque compensator is added in forward path of the speed control loop. With fuzzy torque compensator, improvement in the speed response is obvious but at the cost of complex system. Therefore, scope of study on other closed loop controllers are necessary to find the scope of performance improvement which is taken-up in the next Chapter.

Chapter – 3

Design of SM, ILC and Lyapunov Function Based Controller for Induction Motor Drive

3.1 General

The present chapter is devoted to report various aspects related to the design of sliding mode, iterative learning and Lyapunov function controller. Sliding mode controller is robust over modelling inaccuracy and system parameter. In first part a comprehensive procedure for the design of sliding mode controller for enhancing performance of the drive is presented.

Next iterative learning controller for induction motor drive is taken-up which is of the recent emerging control methodology based on combination of knowledge and experience. Particularly this type of controller has been found to be very suitable for periodic nature of disturbances. During practical operation in speed tracking application induction motor exhibits repetitive oscillation and chattering of stator variables due to PWM switching and limiter with conventional speed controller. It has adverse effects on the performance of the whole drive systems. Here iterative learning controller is designed and developed to demonstrate the enhanced performance of the drive system under worse type of the loading of induction motor.

The third part of this chapter presents analysis of global asymptotic stability of induction motor in the sense of Lyapunov. The full nonlinear dynamic model in stationary (α-β) is considered. This is found to be more convenient from synchronously reference frame implementation point of view. Conditions of stability are derived in

terms of operating speed, load frequency and stability of closed loop system with this controller is investigated.

3.2 Sliding Mode Controller

Sliding Mode Control is one of the effective nonlinear robust control approaches since it provides system dynamics with an invariance property to uncertainties. The first step of SMC design is to select a sliding surface that models the desired closed –loop performance in state variable space. In the second step, a control law such that the system state trajectories are forced toward the sliding surface and stay on it. The system state trajectory in the period of time before reaching the sliding surface is called the reaching phase. Once the system trajectory reaches the sliding surface, it stays on it and slides along it to the origin. The system trajectory sliding along the sliding surface to the origin is called the sliding mode. Under certain conditions, the SMC is robust with respect to system perturbation and external disturbance [34]-[39]. However, this control strategy produces some drawbacks associated with large control chattering that may wear coupled mechanisms and excite unstable system dynamics. Though introducing a boundary layer may reduce the chatter amplitude [2], the stability inside the boundary layer cannot be guaranteed and poor selection of boundary layer will result in unstable tracking responses.

To design sliding mode controller for rotor speed and rotor flux control, the induction motor model is first linearized using feedback linearization technique as described in Chapter- 2.

The control problem is to make the system state, for mechanical and electrical subsystems to track along the sliding line. The system states:

rotor speed: $X_1 = [\omega_r \dot{\omega}_r]^T$ and rotor flux $X_2 = [\psi_r \dot{\psi}_r]^T$

have to track the specific time-varying state, $X_1^* = \left[\omega_r^* \dot{\omega}_r^*\right]^T$ and $X_2^* = \left[\psi_r^* \dot{\psi}_r^*\right]^T$

In presence of modeling imperfections and disturbances. Let, $e_1(t)$ and $e_2(t)$ be speed and flux error such as

$$e_1(t) = \omega_r - \omega_r^* \tag{3.1}$$

$$e_2(t) = \psi_r - \psi_r^* \tag{3.2}$$

Next defining two time varying classical sliding surfaces $s_1(t)$ and $s_2(t)$ each for rotor speed and rotor flux dynamics of the linearized induction motor, as described in [2].

$$s_1(t) = e_1(t) + \lambda_1 \int e_1(t)dt \tag{3.3}$$

$$s_2(t) = e_2(t) + \lambda_2 \int e_2(t)dt \tag{3.4}$$

where, λ_1 and λ_2 represent the bandwidths of the above sliding surfaces. These can be calculated on the basis of the range of the universe of discourse of the input variables. The reciprocal of the bandwidths give the respective time constants.

The derivative of $s_1(t)$ *and* $s_2(t)$ are

$$\dot{s}_1(t) = \dot{e}_1(t) + \lambda_1 e_1(t) \tag{3.5}$$

$$\dot{s}_2(t) = \dot{e}_2(t) + \lambda_2 e_2(t) \tag{3.6}$$

Taking the derivative of errors

$$\dot{e}_1(t) = \dot{\omega}_r - \dot{\omega}_r^* \tag{3.7}$$

$$\dot{e}_2(t) = \dot{\psi}_r - \dot{\psi}_r^* \tag{3.8}$$

Substituting (2.85) and (2.86) into (3.7) and (3.8), the derivatives of errors can be written as

$$\dot{e}_1(t) = -\frac{B}{J}\omega_r + \frac{K_T}{J}u1 - \frac{T_L}{J} - \dot{\omega}_r^* \tag{3.9}$$

$$\dot{e}_2(t) = -\frac{R_r}{L_r}\psi_r + \frac{L_m}{L_r}R_r u2 - \dot{\psi}_r^* \tag{3.10}$$

Substituting $\dot{e}_1(t)$ and $\dot{e}_2(t)$ from (3.9) and (3.10) into (3.5) and (3.6), $\dot{s}_1(t)$ and $\dot{s}_2(t)$ become

$$\dot{s}_1(t) = -\frac{B}{J}\omega_r + \frac{K_T}{J}u1 - \frac{T_L}{J} - \dot{\omega}_r^* + \lambda_1 e_1 \tag{3.12}$$

$$\dot{s}_2(t) = -\frac{R_r}{L_r}\psi_r + \frac{L_m}{L_r}R_r u2 - \dot{\psi}_r^* + \lambda_2 e_2 \tag{3.13}$$

These are rewritten as follows:

$$\dot{s}_1(t) = f_1 + u_1 - \dot{\omega}_r^* + \lambda_1 e_1 \tag{3.14}$$

$$\dot{s}_2(t) = f_2 + u_2 - \dot{\psi}_r^* + \lambda_2 e_2 \tag{3.15}$$

where, f_1 and f_2 are the functions for mechanical and the electrical subsystems (parameter dependent, nonlinear or time varying), which can be estimated; u_1 and u_2 are the control inputs. These are represented as follows:

$$f_1 = -\frac{B}{J}\omega_r - \frac{T_l}{J} = -\left(a_1\omega_r + c_1 T_l\right) rad/s^2, \quad a_1 = \frac{B}{J}s^{-1}, \quad c_1 = \frac{1}{J} \quad \left(kg.m^2\right)^{-1},$$

$$u_1 = \frac{K_T}{J}u1 = b_1 u1 \ \ rad/s^2$$

$$f_2 = -\frac{R_r}{L_r}\psi_r = -a_2\psi_r \ \ V, \quad a_2 = \frac{R_r}{L_r}s^{-1}, \qquad u_2 = \frac{L_m R_r}{L_r}u2 = b_2 u2 \ V \tag{3.16}$$

Here a_1 , a_2, b_1, b_2, c_1 and c_2 are parameter gains, which are uncertain and but bounded within certain limits as given below [2].

$$a_{\min 1} \le a_1 \le a_{\max 1} \quad a_{\min 2} \le a_2 \le a_{\max 2} \qquad b_{\min 1} \le b_1 \le b_{\max 1}$$

$$b_{\min 2} \le b_2 \le b_{\max 2} \quad c_{\min 1} \le c_1 \le c_{\max 1} \tag{3.17}$$

The geometric mean of the above bounds gives the estimated gain value for the mechanical system and the electrical system:

$$\hat{a}_1 = (a_{\min 1} a_{\max 1})^{1/2}, \hat{b}_1 = (b_{\min 1} b_{\max 1})^{1/2}, \hat{c}_1 = (c_{\min 1} c_{\max 1})^{1/2}$$

$$\hat{a}_2 = (a_{\min 2} a_{\max 2})^{1/2}, \hat{b}_2 = (b_{\min 2} b_{\max 2})^{1/2} \tag{3.18}$$

Let, $\hat{f}_1$, $\hat{f}_2$, $\hat{u}_1$ and $\hat{\boldsymbol{u}}_2$ be the best approximate estimated states and control inputs for the individual system. Now substituting these values in (3.14), (3.15), and from equations: $\dot{s}_1 = 0$ and $\dot{s}_2 = 0$, the approximate continuous control laws for the electrical subsystem as well as the mechanical subsystem are obtained in (3.19) and (3.20) in terms of $\hat{f}_1$, $\hat{f}_2$, $\hat{u}_1$ and $\hat{\boldsymbol{u}}_2$.

$$\hat{u}_1 = -\hat{f}_1 + \dot{\omega}_r^* - \lambda_1 e_1 \tag{3.19}$$

$$\hat{u}_2 = -\hat{f}_2 + \dot{\psi}_r^* - \lambda_2 e_2 \tag{3.20}$$

where ,

$$\hat{f}_1 = -\left(\hat{a}_1 \omega_r + \hat{c}_1 T_l\right) \qquad \hat{f}_2 = -\hat{a}_2 \psi_r$$

$$\hat{u}_1 = \hat{b}_1 u1 \qquad \hat{u}_2 = \hat{b}_2 u2 \tag{3.21}$$

In order to satisfy sufficient sliding condition [2], $\frac{1}{2}\frac{d}{dt}(s^2) \le -\eta |s|$ despite uncertainty on the system, a discontinuous term is added to respective $\hat{u}_1$ and $\hat{u}_2$ across the surface $\dot{s}_1 = 0$ and $\dot{s}_2 = 0$.

$$u1 = \hat{b}_1^{-1}\left[-\hat{f}_1 + \dot{\omega}_r^* - \lambda_1 e_1 - k_1 \operatorname{sgn}(s_1)\right] \tag{3.22}$$

$$u2 = \hat{b}_2^{-1}\left[-\hat{f}_2 + \dot{\psi}_r^* - \lambda_2 e_2 - k_2 \operatorname{sgn}(s_2)\right] \tag{3.23}$$

where,

$\operatorname{sgn}(s_1) = +1$ if $s_1 > 0$

$\operatorname{sgn}(s_1) = -1$ if $s_1 < 0$

and

$\operatorname{sgn}(s_2) = +1$ if $s_2 > 0$

$\text{sgn}(s_2) = -1 \quad \text{if} \quad s_2 < 0$

The switching gains k_1 and k_2 should be of enough value, so that the stability is guaranteed. This is obtained from the Lyapunov stability analysis as follows. Let V_1 be the Lyapunov function taken for the mechanical system as

$$V_1 = \frac{1}{2} s_1^{\,2} \tag{3.24}$$

For the stability of the system the derivative of the Lyaponov function should be negative definite. Let

$$\dot{V} = \frac{1}{2}\frac{d}{dt}(s_1^{\,2}) = \dot{s}_1 s_1 = -\eta_1 |s_1| \tag{3.25}$$

where, η_1 is a strictly positive definite constant and (3.25) states that the squared distance to the surface, as measured by $s_1^{\,2}$, decreases along all system trajectories[1].

From (3.25), (3.14) and (3.22), $\dot{V}_1$ can be rewritten as follows:

$$\dot{V}_1 = \left[f_1 + b_1 \left[\hat{b}_1^{-1} \left(\hat{u}_1 - k_1 \,\text{sgn}(s_1) \right) \right] - \dot{\omega}_r^* + \lambda_1 e_1 \right] s_1 = -\eta_1 |s_1| \tag{3.26}$$

Substituting (3.19) in (3.26) and simplifying, we get

$$k_1 \geq \hat{b}_1 b_1^{-1} f_1 - \hat{f}_1 + \left(\hat{b}_1 b_1^{-1} - 1 \right) \left(-\dot{\omega}_r^* + \lambda_1 e_1 \right) + \eta_1 \hat{b}_1 b_1^{-1} \tag{3.27}$$

When the controller gain k_1 is set as (3.27), we get

$$\frac{1}{2}\frac{d}{dt}(s_1^{\,2}) \leq -\eta_1 |s_1| \cdot \tag{3.28}$$

In the same way k_2 is obtained for the electrical subsystem to ensure stability, as

$$k_2 \geq \hat{b}_2 b_2^{-1} f_2 - \hat{f}_2 + \left(\hat{b}_2 b_2^{-1} - 1 \right) \left(-\dot{\psi}_r^* + \lambda_2 e_2 \right) + \eta_2 \hat{b}_2 b_2^{-1} \tag{3.29}$$

This way the discontinuous controller gains k_1 and k_2, across the surface are obtained to accommodate the extent of parameter uncertainty.

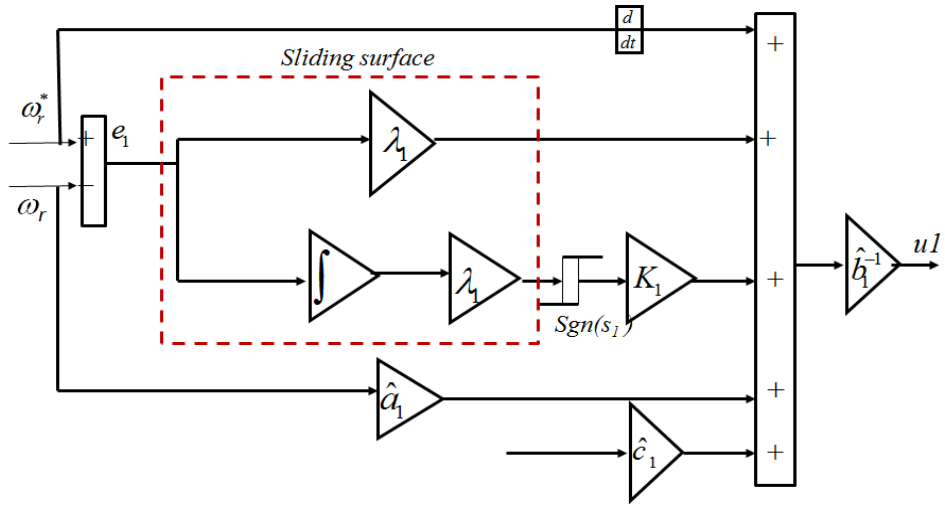

Fig. 3.1 Block diagram of sliding mode speed controller

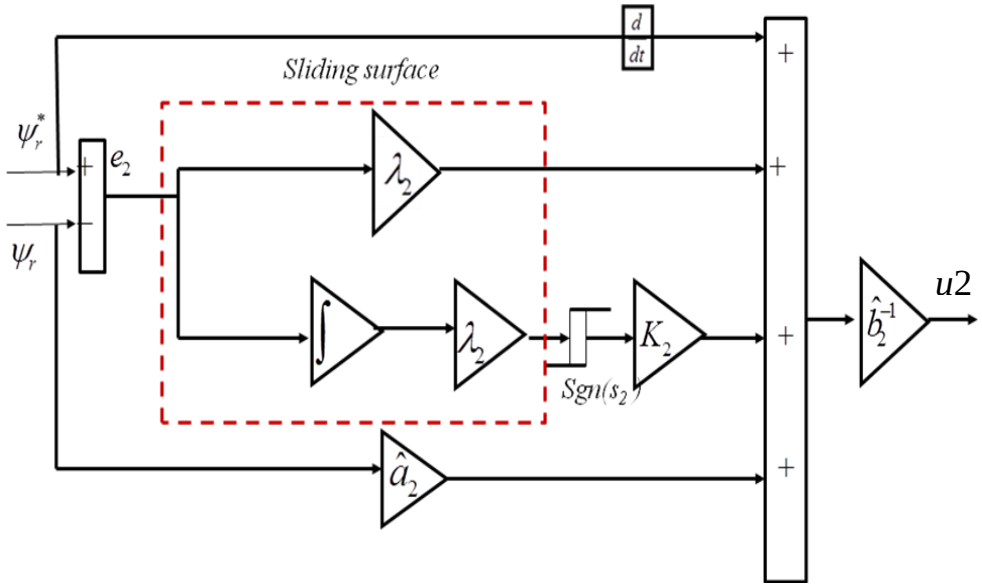

Fig. 3.2 Block diagram of sliding mode flux controller

3.2.1 A Case Study

An illustrative procedure to obtained the controller gains k_1 , k_2 λ_1 and λ_2 are presented for a typical induction motor whose specifications and parameters are given in Table 2.1. The induction motor is initially running at 1000 r.p.m., the rotor flux is set to 0.5 V.s. The disturbance and parameter variations of the induction motor drive system are assumed as follows.

a. The reference speed is increased by 50%, to 1500rpm in 0.4sec. The rotor flux magnitude 0.5 V.s is decreased from 0.5 V.s to 0.4V.s.

b. The load torque is increased from 0 to 20Nm, 80% of full load.

c. The stator and rotor resistance increase by 50% due to temperature rise.

d. The motor inertia constant is doubled to 0.32 kg-m^2

Solution:

Rotor angular speed: $\omega_r = \frac{2\pi \times 1000}{60} = 104.72 \ \ rad/s$

Rotor set angular speed: $\omega_r^* = \frac{2\pi \times 1500}{60} = 157.08 \ \ rad/s$

Rate of reference speed: $\dot{\omega}_r^* = \frac{157.08 - 104.72}{0.4} = 130.9 \ \ rad/s^2$

Rate of rotor flux : $\dot{\psi}_r^* = \frac{0.4 - 0.5}{0.4} = -0.25 \ \ V$

Motor parameter gains:

$$a_1 = \frac{B}{J} = \frac{0.035}{0.16} = 0.22 \ \ s^{-1}$$

$$b_1 = \frac{K_T}{J} = \frac{3 \times p \times L_m}{2 \times L_r \times J} = 18 \left(kg.m^2\right)^{-1}$$

$$c_1 = \frac{1}{J} = 6.25 \ \left(kg.m^2\right)^{-1}$$

$$a_2 = \frac{R_r}{L_r} = \frac{5.4}{0.521} = 10.38 \ s^{-1}$$

$$b_2 = \frac{L_m R_r}{L_r} = \frac{0.5 \times 5.4}{0.52} = 5.2 \ \ \Omega$$

Estimated parameter gains:

$$\hat{a}_1 = \frac{B}{\sqrt{2}J} = 0.155 s^{-1}$$

$$\hat{b}_1 = \frac{K_T}{\sqrt{2}J} = 12.73 \ \left(kg.m^2\right)^{-1}$$

$$\hat{c}_1 = \frac{1}{\sqrt{2}J} = 4.42 \ \left(kg.m^2\right)^{-1}$$

$$\hat{a}_2 = \frac{\sqrt{1.5}R_r}{L_r} = 12.71 \ \ s^{-1}$$

$$\hat{b}_2 = \frac{\sqrt{1.5}L_m R_r}{L_r} = 6.37 \ \ \Omega$$

Motor actual states values:

$$f_1 = -\left(a_1\omega_r + c_1 T_l\right) = -\left(0.22 \times 104.72 + 6.25 \times 20\right) = -148.04 \ \ rad/s^2$$

$$f_2 = -a_2\psi_r = -10.36 \times 0.5 = -5.19 \ \ V$$

Motor estimated state values:

$$\hat{f}_1 = -\left(\hat{a}_1\omega_r + \hat{c}_1 T_l\right) = -\left(0.155 \times 104.72 + 4.42 \times 20\right) = -104.63 rad/s^2$$

$$\hat{f}_2 = -\hat{a}_2\psi_r = -12.71 \times 0.5 = -6.36 \ \ V$$

Determination of λ_1 using (3.19) and (3.21)

$$u1 = \hat{b}^{-1}\left(-\hat{f}_1 + \dot{\omega}_r^* - \lambda_1 e_1\right) = \left(12.73\right)^{-1}\left(104.63 + 130.9 - \lambda_1\left(104.72 - 157.08\right)\right) \ \ \text{N}\cdot\text{m}$$

$$= \frac{235.53 + 52.36\lambda_1}{12.73} = 18.50 + 4.1\lambda_1 \ \ \text{N}\cdot\text{m}$$

Taking *u1* equal to 24 N·m which is the motor rated torque, we get $\lambda_1 = 1.34 \ \ s^{-1}$

Determination of λ_2 using (3.20) and (3.21)

$$u2 = \hat{b}_2^{-1}\left(-\hat{f}_2 + \dot{\psi}_r^* - \lambda_2 e_2\right) = \left(6.37\right)^{-1}\left(6.36 - 0.25 - \lambda_2\left(0.5 - 0.4\right)\right) \ = 0.96 - 0.016\lambda_2 \ \ A$$

Taking *u2* equal to 0.8 A, we get $\lambda_2 = 10 s^{-1}$

Determination of switching gains k_1 using (3.27): For getting k_1, we take $\eta_1 = 1$

$$k_1 \geq \hat{b}_1 b_1^{-1} f_1 - \hat{f}_1 + \left(\hat{b}_1 b_1^{-1} - 1\right)\left(-\dot{\omega}_r^* + \lambda_1 e_1\right) + \eta_1 \hat{b}_1 b_1^{-1}$$

$$k_1 \geq \frac{12.73}{18}(-148.04) - (-104.63) + \left(\frac{12.73}{18} - 1\right)(-130.9 - 1.34 \times 52.36) + \frac{12.73}{18} \times 1$$

$$k_1 \geq -104.7 + 104.63 + 58.87 + 0.7\eta_1 = 58.8 + 0.7 \times 1 = 59.5$$

Next, solving (3.29) for getting k_2, and taking η_2 =1

$$k_2 \geq \hat{b}_2 b_2^{-1} f_2 - \hat{f}_2 + \left(\hat{b}_2 b_2^{-1} - 1\right)\left(-\dot{\psi}_r^* + \lambda_2 e_2\right) + \eta_2 \hat{b}_2 b_2^{-1}$$

$$k_2 \geq \frac{6.37}{5.2}(-5.19) + 6.36 + \left(\frac{6.37}{5.2} - 1\right)(0.25 + 10 \times 0.1) + \eta_2 \frac{6.37}{5.2}$$

$$k_2 \geq -6.36 + 6.36 + 0.28 + 1.23\eta_2$$

$$k_2 \geq 1.51$$

With these gains, the control law (3.22) and (3.33) can be written as

$$u1 = \hat{b}^{-1}\left[\hat{u}_1 - k_1 \operatorname{sgn}(s_1)\right] = \hat{b}^{-1}\left(-\hat{f}_1 + \dot{\omega}_r^* - \lambda_1 e_1 - k_1 \operatorname{sgn}(s_1)\right)$$

$$= \hat{b}^{-1}\left(-\hat{f}_1 + \dot{\omega}_r^* - 1.34 e_1 - 59.5 \operatorname{sgn}(s_1)\right)$$

and $u2 = \hat{b}_2^{-1}\left[\hat{u}_2 - k_2 \operatorname{sgn}(s_2)\right] = \hat{b}_2^{-1}\left(-\hat{f}_2 + \psi_r^* - \lambda_2 e_2 - k_2 \operatorname{sgn}(s_2)\right)$

$$= \hat{b}_2^{-1}\left(-\hat{f}_2 + \psi_r^* - 10 e_2 - 1.51 \operatorname{sgn}(s_2)\right)$$

3.3 Iterative Learning Controller

In recent years, many research works have been reported on application of iterative learning controller (ILC) to servomechanism [71]-[73]. ILC is basically an error correction algorithm and it has a memory that stores previous controller output data. It removes error by using the previous information for the present trial [70].

Here, we consider a discrete, linear time-invariant, SISO repetitive system:

$$x_k(t+1) = Ax_k(t) + Bu_k(t) \qquad (3.30)$$

$$y_k(t) = Cx_k(t) \tag{3.31}$$

where k is the iterative index, repetitive operation of the system; $x_k(t)$, $u_k(t)$, and $y_k(t)$ are the repetitive system state, control input, and output of the system; A, B, and C are matrices with appropriate dimensions.

The output signal of the PI –Type iterative learning controller can be written as

$$u_{k+1}(t) = u_k(t) + \phi_k e_k(t) + \Gamma_k \int e_k(t) d\tau \tag{3.32}$$

where, $u_k(t)$ is system input and, $e_k(t) = y_d(t) - y_k(t)$ is the error on trial k^{th}, with $y_k(t)$ as the system output and $y_d(t)$ as the desired response. The proportional gain ϕ and the integral gain Γ are the learning gains and ensure convergence of the system dynamics such that as $k \to \infty$ we have $y_k(t) \to y_d(t)$ for all $t \in [0, T]$.

Using (2.86), a repetitive IM dynamic equation for speed control loop can be represented as:

$$\dot{\omega}_{rk}(t) = -\frac{B}{J}\omega_{rk}(t) + \frac{1}{J}K_T u1_k(t) - \frac{T_l}{J} \tag{3.33}$$

The P-I-type feedback control law for updating control in each iteration can be written as:

$$u1^{fb}_{(k+1)}(t) = u1_k(t) + \phi_k e_{1k}(t) + \Gamma_k \int e_{1k}(t) d\tau \tag{3.34}$$

where, $e_{1k}(t) = \omega_r^*(t) - \omega_{rk}(t)$.

where, ϕ and Γ are steady gains. In order to reduce the initial offset, an initial correction term $u_0(t)$ is included in (3.34) as in (3.35). The final expression for the feedback control loop can be written as:

$$u1^{fb}_{(k+1)}(t) = (1-\lambda)u1^{fb}_k(t) + \lambda u_0(t) + \phi e_{1k}(t) + \Gamma \int e_{1k}(t) d\tau \tag{3.35}$$

where, λ is the forgetting factor. Here, λ is introduced to ensure the convergence of the iterative learning.

In case of uncertain external disturbances and parameter variations the gain constant needs to be modified. Modifying (3.35) to get system control dynamics including a feedback $u1_{(k+1)}^{fb}(t)$ and a feedback compensator $\Delta u1_{(k+1)}^{fb}(t)$ control signal such as:

$$u1_{(k+1)}^{fb}(t)+\Delta u1_{(k+1)}^{fb}(t)=(1-\lambda)u1_{k}^{fb}(t)+\lambda u_0(t)+\phi_k e_{1k}+\Gamma_k\int e_{1k}(t)d\tau+\Delta\phi_k(t)\Delta e_{1k}(t)+\Delta\Gamma_k\int\Delta e_{1k}(t)d\tau \quad (3.36)$$

$$\Delta u1_{(k+1)}^{bf}(t)=\Delta\phi_k\Delta e_{1k}(t)+\Delta\Gamma_k\int\Delta e_{1k}(t)d\tau \quad (3.37)$$

For the feedback compensating iterative controller, TS Fuzzy based ILC, is proposed to compensate and adjust the control signal accordingly. The fuzzy inference mechanism has been used obtain real time gain value for each trial. For this we calculate $\Delta e_k(t)=u1_{(k+1)}(t)-u1_k(t)$ and it's change rate $ce_{1k}(t)=\left[\Delta e_k(t)-\Delta e_{k-1}(t)\right]$. Here we take only two states: positive (P) and negative (N) for $\Delta e_k(t)$ and $\Delta ce_k(t)$.Two triangular membership functions namely P and N have been taken for each trial *k*. In case of parameter change and external disturbance, fuzzy feedback control signal will activate and generate positive or negative compensating signal accordingly. The outputs signals scaled on per unit bounded range $\left(r_{1(1)}, r_{2(-1)}\right)$. The Fig.3.3 shows membership functions. The algebraic expressions of P(e_{1k}), N(e_{1k}), P(ce_{1k})and N(ce_{1k}) are taken as:

$$P(\Delta e_{1k}(t))=\frac{\Delta e_{1k}(t)+1}{2},\ N(\Delta e_{1k}(t))=\frac{1-\Delta e_{1k}(t)}{2},\ P(\Delta ce_{1k}(t))=\frac{\Delta ce_{1k}(t)+1}{2},$$

$$N(\Delta ce_{1k}(t))=\frac{1-\Delta ce_{1k}(t)}{2} \quad (3.38)$$

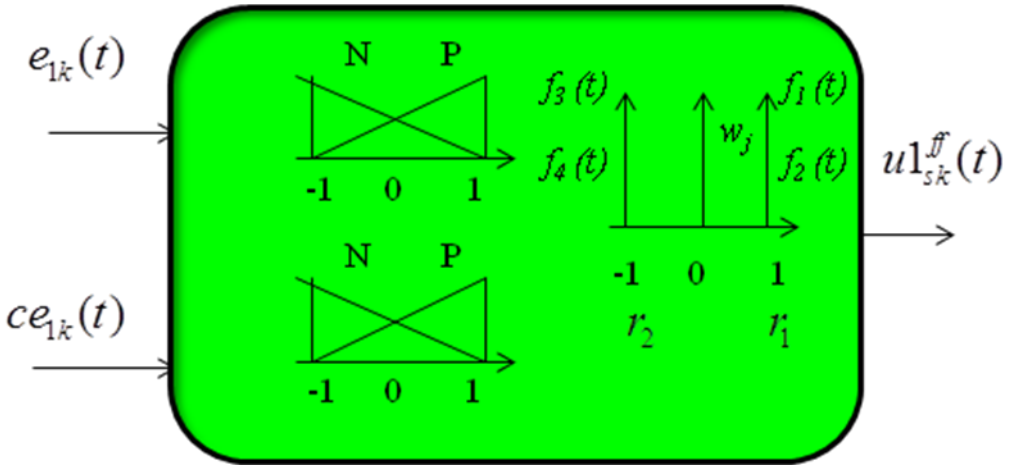

Fig.3.3 Membership functions of $\Delta e_k(t)$, $\Delta ce_k(t)$, $f_{(1,2,3,4)}$ and $\Delta u1^{kb}_{(k+1)}(t)$

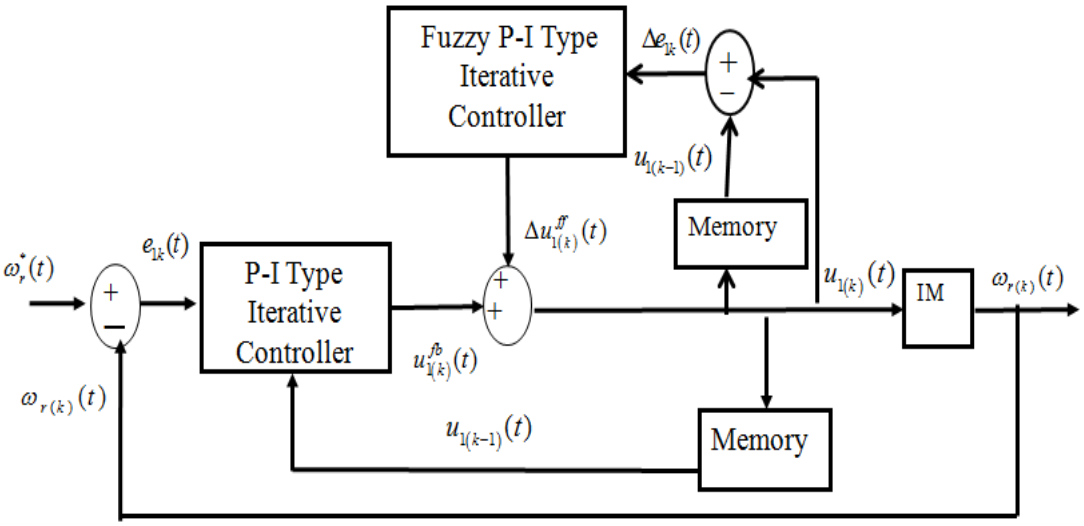

Fig.3.4 Block diagram of iterative learning speed controller for k[th] trial

The four possible inference rules are formulated as follows:

Rule1: If $\Delta e_{1k}(t)$ is P and $\Delta ce_{1k}(t)$ is P then $f_{k1}(t) = w_{k1} r_1$

Rule2: If $e_{1k}(t)$ is P and $ce_{1k}(t)$ is N then $f_{k2}(t) = w_{k2} r_2$

Rule 3: If $e_{1k}(t)$ is N and $ce_{1k}(t)$ is P then $f_{k3}(t) = w_{k3} r_3$

Rule 4: If $e_{1k}(t)$ is N and $ce_{1k}(t)$ is N then $f_{k4}(t) = w_{k4} r_4$ (3.39)

The result of the fuzzy inference is obtained from (3.40)

$$u_{1sk}(t) = \frac{\sum_{j=1}^{4} w_{kj} r_{kj}}{\sum_{j=1}^{4} w_{kj}} = \frac{w_{k1} r_{k1} + w_{k2} r_{k1} + w_{k3} r_{k2} + w_{k4} r_{k2}}{w_{k1} + w_{k2} + w_{k3} + w_{k4}} \tag{3.40}$$

where, suffix j represents rule, and w_j represents the firing strength of the corresponding rule.

The block diagram of iterative learning speed controller is shown in the Fig. 3.3.

3.4 Lyapunov Function Based Controller

The literature related to IM drive based on different type of controllers like PI, SM Fuzzy logic and Fuzzy- Neural-Network etc has seen in good volume [39, 47,64] but controller design based on Lyapunov theorem and Energy balance equation are rare. In this section Global asymptotic stability of induction motor in the sense of Lyapunov is analyzed and the control strategy are developed. Controller is designed based on Lyapunov criteria [2] and stability of the closed loop system is investigated. Finally the closed loop system along with the Lyapunov controller is simulated in MATLAB/SIMULINK environment and also implemented in real time digital simulator under various operating conditions. The results obtained are compared with PI and Sliding mode controllers.

3.4.1 State-Space Model of induction motor

Many control schemes have been implemented considering the induction motor state space representation in stationary (α-β) reference frame with two stator current components ($i_{\alpha s}$, $i_{\beta s}$), two rotor flux components ($\psi_{\alpha r}$, $\psi_{\beta r}$) and speed (ω_r) as variables [19]. The mathematical model is as follows.

$$\dot{x} = f(x) + bu \tag{3.41}$$

where

$$x = [i_{\alpha s}, i_{\beta s}, \psi_{\alpha r}, \psi_{\beta r}, \omega_r]^T$$

$$u = [u_{\alpha s}, u_{\beta s}, T_l]^T$$

$$f(x) = \begin{bmatrix} -\frac{1}{\sigma L_s}\left(R_s + \frac{L_m^2}{L_r^2}R_r\right) i_{\alpha s} + \frac{1}{\sigma L_s}\frac{L_m R_r}{L_r^2}\psi_{\alpha r} + \frac{pL_m}{\sigma L_s L_r}\omega_r \psi_{\beta r} \\ -\frac{1}{\sigma L_s}\left(R_s + \frac{L_m^2}{L_r^2}R_r\right) i_{\beta s} + \frac{1}{\sigma L_s}\frac{L_m R_r}{L_r^2}\psi_{\beta r} - \frac{pL_m}{\sigma L_s L_r}\omega_r \psi_{\alpha r} \\ -\frac{R_r}{L_r}\psi_{\alpha r} - p\omega_r \psi_{\beta r} + \frac{L_m R_r}{L_r} i_{\alpha s} \\ -\frac{R_r}{L_r}\psi_{\beta r} + p\omega_r \psi_{\alpha r} + \frac{L_m R_r}{L_r} i_{\beta s} \\ -\frac{B}{J}\omega_r + \frac{K_T}{J}(i_{\beta s}\psi_{\alpha r} - i_{\alpha s}\psi_{\beta r}) \end{bmatrix} \qquad b = \begin{bmatrix} \frac{1}{\sigma L_s} & 0 & 0 \\ 0 & \frac{1}{\sigma L_s} & 0 \\ 0 & 0 & 0 \\ 0 & 0 & 0 \\ 0 & 0 & -\frac{1}{J} \end{bmatrix}$$

where, suffixes (α, β) denote the equivalent direct and quadrature axis components on the stator fixed frame. (L_s, R_s) and (L_r, R_r) are the stator and the rotor parameters (inductance and resistance). L_m is the mutual inductance. p is the number of pole pair. J and B represent the moment of inertia and viscous friction coefficient. T_l is the load torque. Inputs $u_{\alpha s}$ and $u_{\beta s}$ are two stator voltage components. σ is the leakage coefficient, defined as $\sigma = \left(1 - L_m^2 / L_r L_s\right)$. K_T is the torque constant, defined as $K_T = \frac{3}{2} p L_m / L_r$ and ω_r is the motor mechanical speed.

The state decoupling feedback linearization control algorithm for separate rotor speed and rotor flux is expressed as:

$$\dot{\omega}_r = -\frac{B}{J}\omega_r + \frac{K_T}{J}u1 - \frac{T_l}{J} \tag{3.42}$$

$$\dot{\psi}_r = -\frac{R_r}{L_r}\psi_r + \frac{L_m}{L_r}u2 \tag{3.43}$$

where, $u1$ and $u2$ are nonlinear control signals,

$$u1 = \left(\psi_{\alpha r} i_{\beta s} - \psi_{\beta r} i_{\alpha s}\right) \tag{3.44}$$

$$u2 = \frac{1}{\psi_r}\left(i_{\alpha s}\psi_{\alpha r} + i_{\beta s}\psi_{\beta r}\right) \tag{3.45}$$

and ψ_r is rotor flux magnitude is obtained from (3.46).

$$\psi_r = \sqrt{\psi_{\alpha r}^2 + \psi_{\beta r}^2} \tag{3.46}$$

The inverse of (3.44) and (3.45) give the expression of the feedback linearizing controller as follows:

$$i_{\alpha s} = \frac{\psi_{\alpha r}}{\psi_r} u2 - \frac{\psi_{\beta r}}{\psi_r^2} u1 \tag{3.47}$$

$$i_{\beta s} = \frac{\psi_{\alpha r}}{\psi_r} u2 + \frac{\psi_{\beta r}}{\psi_r^2} u1 \tag{3.48}$$

Thus, two nonlinear inputs $u1$ and $u2$ along with feedback linearizing controller are used to control motor speed and rotor flux independently. The nonlinear control signals $u1$ and $u2$ are obtained from speed and flux controller. In this work, the decoupling and linearizing control of the induction motor are proposed, with a new control law, which is based on induction motor energy and power balance equation using Lyapunov stability theory.

3.4.2 Energy and Power Balance Equations

The total energy (w_p) of the induction motor is the sum of the magnetic energy (w_f) and the mechanical energy (w_J), and can be written in terms of the stator currents ($i_{\alpha s}, i_{\beta s}$), rotor currents ($i_{\alpha r}, i_{\beta r}$) and rotor speed ($\omega_r$) variables as given in [76]:

$$w_p = w_f + w_J \tag{3.49}$$

where,

$$w_f = \frac{1}{2} L_s \left(i_{\alpha s}^2 + i_{\beta s}^2 \right) + \frac{1}{2} L_r \left(i_{\alpha r}^2 + i_{\beta r}^2 \right) + L_m \left(i_{\alpha s} i_{\alpha r} + i_{\beta s} i_{\beta r} \right) \tag{3.50}$$

$$w_J = \frac{1}{2} J \omega_r^2 \tag{3.51}$$

The feedback lineazation scheme discussed in section-II does not involve the rotor currents ($i_{\alpha r}$ and $i_{\beta r}$). Therefore, the expression of motor total energy in terms of stator currents ($i_{\alpha s}$ and $i_{\beta s}$) and rotor flux ($\psi_{\alpha r}$ and $\psi_{\beta r}$) is obtained by substituting ($i_{\alpha r}$ and $i_{\beta r}$) from (3.52) and (3.53), into (3.50).

$$i_{\alpha r} = -\frac{L_m}{L_r} i_{\alpha s} + \frac{\psi_{\alpha r}}{L_r} \tag{3.52}$$

$$i_{\beta r} = -\frac{L_m}{L_r} i_{\beta s} + \frac{\psi_{\beta r}}{L_r} \tag{3.53}$$

Thus, the expression of the total energy of induction motor is obtained as follows:

$$w_p = \frac{1}{2}\sigma L_s \left(i_{\alpha s}^2 + i_{\beta s}^2\right) + \frac{1}{2L_r}\psi_r^2 + \frac{1}{2} J \omega_r^2 \tag{3.54}$$

The time derivative of the total energy of induction motor energy (w_p) gives the induction motor total power (P_e), which is obtained as follows:

$$P_e = \frac{dw_p}{dt} = \sigma L_s \left(i_{\alpha s}\dot{i}_{\alpha s} + i_{\beta s}\dot{i}_{\beta s}\right) + \frac{1}{L_r}\left(\psi_{\alpha r}\dot{\psi}_{\alpha r} + \psi_{\beta r}\dot{\psi}_{\beta r}\right) + J\omega_r\dot{\omega}_r \tag{3.55}$$

Substituting current derivatives, flux derivatives and speed derivative from (3.41), into (3.55) we have:

$$P_e = \sigma L_s i_{\alpha s}\left(-\frac{1}{\sigma L_s}\left(R_s + \frac{L_m^2}{L_r^2}R_r\right)i_{\alpha s} + \frac{1}{\sigma L_s}\frac{L_m R_r}{L_r^2}\psi_{\alpha r} + \frac{pL_m}{\sigma L_s L_r}\omega_r\psi_{\beta r} - \frac{u_{\alpha s}}{\sigma L_s}\right) + \sigma L_s i_{\beta s}\left(-\frac{1}{\sigma L_s}\left(R_s + \frac{L_m^2}{L_r^2}R_r\right)i_{\beta s} + \frac{1}{\sigma L_s}\frac{L_m R_r}{L_r^2}\psi_{\beta r} - \frac{pL_m}{\sigma L_s L_r}\omega_r\psi_{\alpha r} - \frac{u_{\beta s}}{\sigma L_s}\right)$$
$$+\frac{1}{L_r}\left(\psi_{\alpha r}\left(-\frac{R_r}{L_r}\psi_{\alpha r} - p\omega_r\psi_{\beta r} + \frac{L_m R_r}{L_r}i_{\alpha s}\right) + \psi_{\beta r}\left(-\frac{R_r}{L_r}\psi_{\beta r} + p\omega_r\psi_{\alpha r} + \frac{L_m R_r}{L_r}i_{\beta s}\right)\right) + J\omega_r\left(-\frac{B}{J}\omega_r + \frac{K_T}{J}(i_{\beta s}\psi_{\alpha r} - i_{\alpha s}\psi_{\beta r}) - \frac{T_l}{J}\right)$$
$$= \left(-\left(R_s + \frac{L_m^2}{L_r^2}R_r\right)\left(i_{\alpha s}^2 + i_{\beta s}^2\right) + \frac{L_m R_r}{L_r^2}\left(i_{\alpha s}\psi_{\alpha r} + i_{\beta s}\psi_{\beta r}\right) + \frac{pL_m}{L_r}\omega_r\left(i_{\alpha s}\psi_{\beta r} - i_{\beta s}\psi_{\alpha r}\right) + u_{\alpha s}i_{\alpha s} + u_{\beta s}i_{\beta s}\right)$$

$$+\left(\left(-\frac{R_r}{L_r^2}\psi_{\alpha r}^2 - \frac{p\omega_r\psi_{\alpha r}\psi_{\beta r}}{L_r} + \frac{L_m R_r\psi_{\alpha r}i_{\alpha s}}{L_r^2}\right) + \left(-\frac{R_r}{L_r^2}\psi_{\beta r}^2 + \frac{p\omega_r\psi_{\alpha r}\psi_{\beta r}}{L_r} + \frac{L_m R_r\psi_{\beta r}i_{\beta s}}{L_r^2}\right)\right)$$

$$+\left(-B\omega_r^2 + \frac{3pL_m\omega_r}{2L_r}(i_{\beta s}\psi_{\alpha r} - i_{\alpha s}\psi_{\beta r}) - T_l\omega_r\right)$$

Further simplification of the above leads to (3.56).

$$P_e = u_{\alpha s}i_{\alpha s} + u_{\beta s}i_{\beta s} - B\omega_r^2 - T_l\omega_r + \frac{pL_m\omega_r}{2L_r}\left(i_{\beta s}\psi_{\alpha r} - i_{\alpha s}\psi_{\beta r}\right) - \left(R_s + \frac{L_m^2}{L_r^2}R_r\right)\left(i_{\alpha s}^2 + i_{\beta s}^2\right) + \frac{2L_m R_r}{L_r^2}\left(i_{\alpha s}\psi_{\alpha r} + i_{\beta s}\psi_{\beta r}\right) - \frac{R_r}{L_r^2}\left(\psi_r^2\right)$$

(3.56)

Substituting (3.44) and (3.45) in (3.46), we have,

$$P_e = u_{\alpha s} i_{\alpha s} + u_{\beta s} i_{\beta s} - B\omega_r^2 - T_l \omega_r + \frac{pL_m \omega_r}{2L_r} u1 - \left(R_s + \frac{L_m^2}{L_r^2} R_r \right) \left(i_{\alpha s}^2 + i_{\beta s}^2 \right) + \frac{2L_m R_r \psi_r}{L_r^2} u2 - \frac{R_r}{L_r^2} \left(\psi_r^2 \right)$$

(3.57)

The above expression will be valid for the induction motor power balance relationship for open loop as well as closed loop control system. We will develop a stable control strategy for a feedback linearized induction motor drive using energy-power balance relationship and Lyapunov stability theory. For this, initially it has been assumed that the induction motor is running under steady state condition with motor speed (ω_r) and (3.54) and (3.57) representing energy and power equations at this state. When, induction motor is subjected to tracking reference speed (ω_r^*) and reference flux ψ_r^* let $u_{\alpha s}^*$, $u_{\beta s}^*$, $i_{\alpha s}^*$, $i_{\beta s}^*$, $\psi_{\alpha r}^*$, $\psi_{\beta r}^*$, $u1^*$ and $u2^*$ are the corresponding voltage, current, flux and nonlinear control signal variable and $e_1 = i_{\alpha s} - i_{\alpha s}^*$, $e_2 = i_{\beta s} - i_{\beta s}^*$, $e_3 = \psi_r - \psi_r^*$ and $e_4 = \omega_r - \omega_r^*$ are stator current error, rotor flux magnitude error and speed error.

Further the total energy equation in terms of the reference as well as the error variables can be written as:

$$w_p(i_{\alpha s}^* + e_1, i_{\beta s}^* + e_2, \psi_r^* + e_3, \omega_r^* + e_4) = \frac{\sigma L_s}{2} \left(\left(i_{\alpha s}^* + e_1 \right)^2 + \left(i_{\beta s}^* + e_2 \right)^2 \right) + \left(\frac{1}{2} \frac{\left(\psi_r^2 + e_3 \right)}{L_r} \right) + \left(\frac{1}{2} J (\omega_r^* + e_4)^2 \right)$$

(3.58)

In the same way the total stored energy (w_p) about reference point, can be written as (3.59).

$$w_p(i_{\alpha s}^*, i_{\beta s}^*, \psi_r^*, \omega_r^*) = \frac{\sigma L_s}{2} \left(\left(i_{\alpha s}^* \right)^2 + \left(i_{\beta s}^* \right)^2 \right) + \left(\frac{1}{2} \frac{\left(\psi_r^* \right)^2}{L_r} \right) + \left(\frac{1}{2} J (\omega_r^*)^2 \right)$$

(3.59)

Difference of (3.58) and (3.59) gives, the differential stored energy w_p *(e)* expression as:

$$w_p(e) = \frac{\sigma L_s}{2} \left(e_1^2 + 2e_1 i_{\alpha s}^* + e_2^2 + 2e_2 i_{\beta s}^* \right) + \left(\frac{1}{2} \frac{e_3^2 + 2e_3 \psi_r^*}{L_r} \right) + \left(\frac{1}{2} J \left(e_4{}^2 + 2e_4 \omega_r^* \right) \right)$$

(3.60)

or,

$$w_p(e) = e^T K e + \sigma L_s \left(e_1 i_{\alpha s}^* + e_2 i_{\beta s}^* \right) + \frac{e_3 \psi_r^*}{L_r} + J e_4 \omega_r^* \tag{3.61}$$

where,

$$K = \frac{1}{2} \begin{bmatrix} \sigma L_s & 0 & 0 & 0 \\ 0 & \sigma L_s & 0 & 0 \\ 0 & 0 & \frac{1}{L_r} & 0 \\ 0 & 0 & 0 & J \end{bmatrix}$$

Next, the motor power equation (3.57) in terms of the reference as well as the error variables is obtained as:

$$P_e(i_{\alpha s}^* + e_1, i_{\beta s}^* + e_2, \psi_r^* + e_3, \omega_r^* + e_4) = u_{\alpha s}\left(i_{\alpha s}^* + e_1\right) + u_{\beta s}\left(i_{\beta s}^* + e_2\right) - B\left(\omega_r^* + e_4\right)^2 - T_l\left(\omega_r^* + e_4\right)$$
$$+ \frac{pL_m\left(\omega_r^* + e_4\right)}{2L_r} u1 - \left(R_s + \frac{L_m^2}{L_r^2} R_r \right)\left(\left(i_{\alpha s}^* + e_1\right)^2 + \left(i_{\beta s}^* + e_2\right)^2\right) + \frac{2L_m R_r\left(\psi_r^* + e_3\right)}{L_r^2} u2 - \frac{R_r}{L_r^2}\left(\psi_r^* + e_3\right)^2 \tag{3.62}$$

Further, the motor total power at the reference point, is written as (3.63).

$$P_e^* = u_{\alpha s}^* i_{\alpha s}^* + u_{\beta s}^* i_{\beta s}^* - B\omega_r^{*2} - T_l\omega_r^* + \frac{pL_m\omega_r^*}{2L_r} u1^* - \left(R_s + \frac{L_m^2}{L_r^2} R_r \right)\left(i_{\alpha s}^{*2} + i_{\beta s}^{*2}\right) + \frac{2L_m R_r \psi_r^*}{L_r^2} u2^* - \frac{R_r}{L_r^2}\left(\psi_r^{*2}\right) \tag{3.63}$$

Subtracting (3.63) from (3.62), the motor total power error, $P_e(e)$ expression is obtained as follows.

$$P_e(e) = \frac{dw_p(e)}{dt} = \left(u_{\alpha s} - u_{\alpha s}^*\right) i_{\alpha s}^* + \left(u_{\beta s} - u_{\beta s}^*\right) i_{\beta s}^* + u_{\alpha s} e_1 + u_{\beta s} e_2 - B(e_4^2 + 2e_4\omega_r^*) - T_l e_4$$

$$- \left(R_s + \frac{R_r L_m^2}{L_r^2} \right)\left(e_1^2 + 2e_1 i_{\alpha s}^* + e_2^2 + 2e_2 i_{\beta s}^*\right) + \frac{pL_m}{2L_r}\left(\omega_r^*(u1 - u1^*) + e_4 u1\right) - \frac{R_r}{L_r^2}(e_3^2 + 2e_3\psi_r^*)$$

$$+ \frac{2L_m R_r}{L_r^2}\left(\psi_r^*(u2 - u2^*) + e_3 u2\right) \tag{3.64}$$

3.4.3 Controller Design and Stability Analysis of the Induction Motor

3.4.3.1 *Selection of the Lyapunov Function*

Let, a Lyapunov function candidate, V be taken as

$$V = e^T Ke + \frac{1}{2}\left(\frac{1}{\lambda_1}(e_1)^2 + \frac{1}{\lambda_2}(e_2)^2 + \frac{1}{\lambda_3}(e_3)^2 + \frac{1}{\lambda_4}(e_4)^2 \right) \tag{3.65}$$

where, $e^T Ke$ is the first term of the equation (3.61) and λ_1-λ_4 are positive constants representing gains. The derivative of the Lyapunov function V is taken from (3.65) and using (3.61) and (3.64), the following expression is obtained:

$$\dot{V} = \frac{dw_p(e)}{dt} - \frac{d}{dt}\left(\sigma L_s \left(e_1 i_{\alpha s}^* + e_2 i_{\beta s}^* \right) + \frac{e_3 \psi_r^*}{L_r} + J e_4 \omega_r^* \right)$$

$$+ \frac{1}{\lambda_1} e_1 \dot{e}_1 + \frac{1}{\lambda_2} e_2 \dot{e}_2 + \frac{1}{\lambda_3} e_3 \dot{e}_3 + \frac{1}{\lambda_4} e_4 \dot{e}_4$$

$$= \left(u_{\alpha s} - u_{\alpha s}^* \right) i_{\alpha s}^* + \left(u_{\beta s} - u_{\beta s}^* \right) i_{\beta s}^* + u_{\alpha s} e_1 + u_{\beta s} e_2 - B(e_4^2 + 2e_4 \omega_r^*) - T_l e_4$$

$$- \left(R_s + \frac{R_r L_m^2}{L_r^2} \right) \left(e_1^2 + 2e_1 i_{\alpha s}^* + e_2^2 + 2e_2 i_{\beta s}^* \right) + \frac{pL_m}{2L_r} \left(\omega_r^* (u1 - u1^*) + e_4 u1 \right)$$

$$+ \frac{2L_m R_r}{L_r^2} \left(\psi_r^* (u2 - u2^*) + e_3 u2 \right) - \frac{R_r}{L_r^2} (e_3^2 + 2e_3 \psi_r^*) - \sigma L_s \left(\dot{e}_1 i_{\alpha s}^* + \dot{e}_2 i_{\beta s}^* \right) - \frac{\dot{e}_3 \psi_r^*}{L_r}$$

$$- J \dot{e}_4 \omega_r^* + \frac{1}{\lambda_1} e_1 \dot{i}_{\alpha s} + \frac{1}{\lambda_2} e_2 \dot{i}_{\alpha s} + \frac{1}{\lambda_3} e_3 \dot{\psi}_r + \frac{1}{\lambda_4} e_4 \dot{\omega}_r \tag{3.66}$$

The above equation further simplified and rewritten into shorted form as

$$\dot{V} = -e^T Me + a + b + c + d \tag{3.67}$$

where,

$$M = -\begin{bmatrix} \left(R_s + \frac{R_r L_m^2}{L_r^2}\right) & 0 & 0 & 0 \\ 0 & \left(R_s + \frac{R_r L_m^2}{L_r^2}\right) & 0 & 0 \\ 0 & 0 & \frac{R_r}{L_r^2} & 0 \\ 0 & 0 & 0 & B \end{bmatrix} \tag{3.68}$$

$$a = \left(u_{\alpha s} - u_{\alpha s}^*\right) i_{\alpha s}^* + u_{\alpha s} e_1 - 2 e_1 i_{\alpha s}^* \left(R_s + \frac{R_r L_m^2}{L_r^2}\right) - \sigma L_s i_{\alpha s}^* \dot{i}_{\alpha s} + \frac{1}{\lambda_1} e_1 \dot{i}_{\alpha s} \tag{3.69}$$

$$b = \left(u_{\beta s} - u_{\beta s}^*\right) i_{\beta s}^* + u_{\beta s} e_2 - 2 e_2 i_{\beta s}^* \left(R_s + \frac{R_r L_m^2}{L_r^2}\right) - \sigma L_s i_{\beta s}^* \dot{i}_{\beta s} + \frac{1}{\lambda_2} e_2 \dot{i}_{\beta s} \tag{3.70}$$

$$c = \frac{2 L_m R_r}{L_r^2}\left(u2 - u2^*\right)\psi_r^* + u2 e_3 - \frac{2 R_r}{L_r^2} e_3 \psi_r^* - \frac{1}{L_r} \dot{\psi}_r \psi_r^* + \frac{1}{\lambda_3} e_3 \dot{\psi}_r \tag{3.71}$$

$$d = \frac{p L_m}{2 L_r}\left(u1 - u1^*\right)\omega_r^* + u1 e_4 - 2 B e_4 \omega_r^* - T_l e_4 - J \dot{\omega}_r \omega_r^* + \frac{1}{\lambda_4} e_4 \dot{\omega}_r \tag{3.72}$$

The second, third, fourth and fifth terms of equation (3.68), as given in (3.69), (3.70), (3.871) and (3.72) represents uncoupled equations, and if these are equated to zero, equation (3.78) reduces to (3.73).

$$\dot{V} = -e^T M e \tag{3.73}$$

For the fulfillment of above condition the following four control laws are derived.

$$u_{\alpha s}^* = u_{\alpha s} + \left(\frac{u_{\alpha s}}{i_{\alpha s}^*} - 2\left(R_s + \frac{R_r L_m^2}{L_r^2}\right) + \frac{\dot{i}_{\alpha s}}{\lambda_1 i_{\alpha s}^*}\right) e_1 - \sigma L_s \dot{i}_{\alpha s} \tag{3.74}$$

$$u_{\beta s}^* = u_{\beta s} + \left(\frac{u_{\beta s}}{i_{\beta s}^*} - 2\left(R_s + \frac{R_r L_m^2}{L_r^2}\right) + \frac{\dot{i}_{\beta s}}{\lambda_2 i_{\beta s}^*}\right) e_2 - \sigma L_s \dot{i}_{\beta s} \tag{3.75}$$

$$u2^* = u2 + \frac{L_r^2}{2 L_m R}\left(\frac{u2}{\psi_r^*} - \frac{2 R_r}{L_r^2} + \frac{\dot{\psi}_r}{\lambda_3 \psi_r^*}\right) e_3 - \frac{1}{L_r} \frac{L_r^2}{2 L_m R} \dot{\psi}_r \tag{3.76}$$

$$u1^* = u1 + \frac{2 L_r}{p L_m}\left(\frac{u1}{\omega_r^*} - 2B - \frac{T_l}{\omega_r^*} + \frac{\dot{\omega}_r}{\lambda_4 \omega_r^*}\right) e_4 - \frac{2 L_r}{p L_m} J \dot{\omega}_r \tag{3.77}$$

The control laws (3.74) and (3.75) generate reference voltages by proper tuning of the gain constants. The control law (3.76) defines flux controller, which generates nonlinear $u2^*$ control signal. It utilizes actual nonlinear control signal, therefore, minimizes control effort. The control law (3.77) defines speed controller, which generates speed nonlinear control signal. This controller also uses the history of nonlinear speed control signal ($u1$). It also reduces the control stress.

3.4.3.2 Global Stability analysis of the Induction Motor drive

According to the theorem 3.3 for Global stability [2], a scalar function *V* of the state error, *e* with continuous first order derivatives, is stable when,

(a) *V(e)* is positive definite $\forall e \neq 0$, and $V(0) = 0$

(b) $\frac{dV(e)}{dt} \leq 0 \forall e \neq 0$

(c) $\frac{dV(e)}{dt} \equiv 0 \Rightarrow e = 0$

(d) $V(e) \to \infty as \|e\| \to \infty$ (3.78)

For verification of the first condition, the leading principal minors of the matrix *K* should be positive definite. These are given below and verified.

$$K_1 = \frac{\sigma L_s}{2} > 0 , K_2 = \frac{(\sigma L_s)^2}{4} > 0 , K_3 = \frac{(\sigma L_s)^2}{8L_r} > 0 \ , \ K_4 = \frac{J(\sigma L_s)^2}{16L_r^2} > 0 \quad (3.79)$$

All principal minors of *K* are positive definite. Apart from these, all other minors are also positive, because of square terms. This way conditions (a) and (d) hold good for the Lyapunov function defined in (3.78). To check conditions (b) and (c) we proceed as follows

Next, the positive definite condition of matrix *M* in (3.73) is investigated, when induction motor is subjected to speed change and the load. This condition will be fulfilled if and only if it's leading principal minors are positive. The leading principal minors are as following

$$M_1 = \left(R_s + \left(\frac{L_m}{L_r} \right)^2 R_r \right) \; M_2 = \left(R_s + \left(\frac{L_m}{L_r} \right)^2 R_r \right)^2 \; M_3 = \left(\left(R_s + \frac{R_r L_m^2}{L_r^2} \right)^2 \left(\frac{R_r}{L_r^2} \right) \right), \; M_4 = \left(\left(R_s + \frac{R_r L_m^2}{L_r^2} \right)^2 \left(\frac{R_r}{L_r^2} \right) B \right)$$

(3.80)

Clearly, leading principle minors of (3.73) are positive, and (b) and (c) conditions hold good.

3.4.4 System Description

The block diagram for feedback linearizing control using Lyapunov Function based controller is shown in Fig. 3.5. Two Lyapunov controllers are regulating the flux and speed. Voltage model [12] is used for flux estimation. Output of flux and speed regulator, and estimated flux are the inputs to the feedback linearizing block and its output goes to the Lyapunov voltage controller, which generates reference voltages by proper tuning of the gain constant. Output of voltage controller is quadrature voltages, which then transformed into three phase reference voltages. These are compared with ramp signal to generate gate drive signals for voltage source inverter (VSI) switches, which regulates required voltage and frequency of the power supply feeding to induction motor.

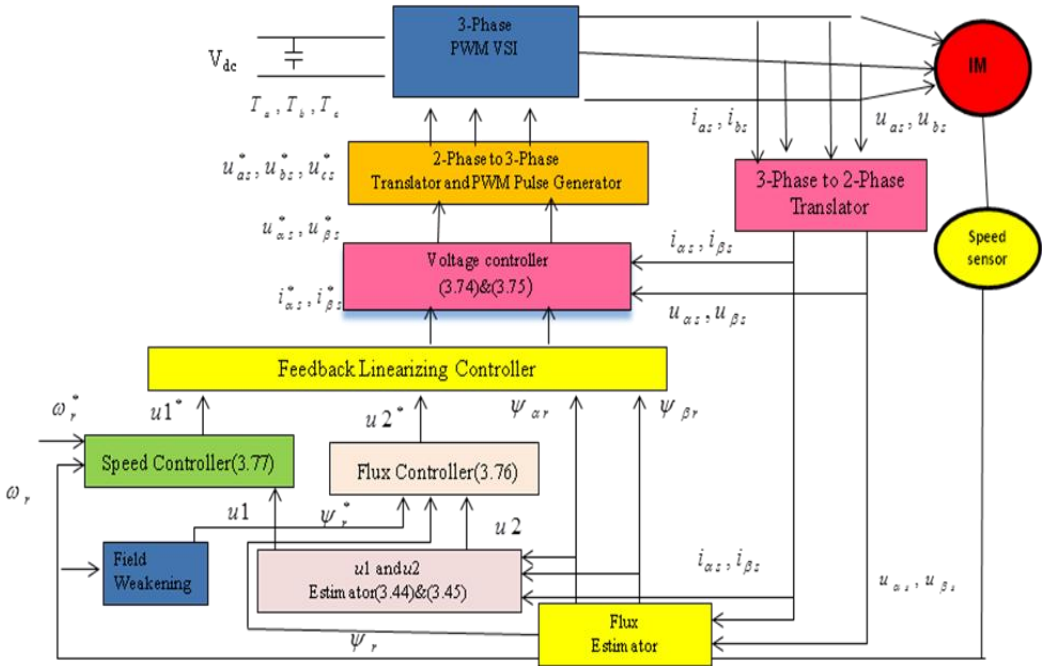

Fig. 3.5 System configuration of the feedback linearized induction motor drive system with Lyapunov Function based controller

3.5 Summary of the Chapter

In this chapter various aspects of controller design based on theory of sliding mode, iterative learning and Lyapunov criteria have been thoroughly discussed and comprehensive design procedure are presented. The equation in the induction motor model is reorganized so as to apply the sliding mode control algorithm. The controller gain and bandwidth are designed, considering various factors such as rotor resistance variation, model inaccuracies, load torque disturbance, and also to have ideal speed and flux tracking. The stability analysis is also presented for the closed loop system based on Lyapunov theorem. The controller developed here would be used in the next chapter to develop model in MATLAB/SIMULINK environment for simulation study and performance analysis.

Chapter – 4

Simulation and Performance Comparison of the Induction Motor Drive with PI, Sliding Mode, Iterative Learning and Lyapunov Function Based Controller

4.1 General

A good performance of the drive system will required a suitable controller. The performance of the induction motor drive system has been investigated with controllers based on modern control theory. It has been claimed by the authors that the controller used gives enhanced performance in terms of fast speed response and negligible effect of impact torque. It is interesting and may be useful to compare the performance of the drive system operating under various controller. Such type of study would be useful in selection of a particular controller for particular application for optimum performance.

The present chapter deals with the simulation study of induction motor drive system with closed some of the controller designed and developed in previous Chapters. The MATLAB/SIMULINK model using power system blockset of the drive system with one controller at a time is developed. The simulation study under various operating condition like step change of speed, step change of load torque, periodic change of speed and torque are investigated. Controller performances are compared analysed and observations are recorded.

4.2 Description of the Proposed Induction Motor Drive System

Generally, the requirements for a high performance motor drive system are [5]:

- Fast tracking of set point changes without overshoot.
- Minimum speed change and small-resting time in case of step load change.
- Zero steady state error.
- The response rise time, which is designated as the time that the unit-step tracking speed response rises from 0% to 90% of its steady state value.

These are only possible with closed loop control. Objective of the proposed scheme is to have above features in the drive system.

The schematic block diagram of the proposed system is shown in Fig 4.1. The scheme consists of three controllers, one flux estimator, one current controlled PWM voltage source inverter, and an induction motor. Two controllers are regulating flux and speed loop. Voltage model [12] is used for flux estimation.

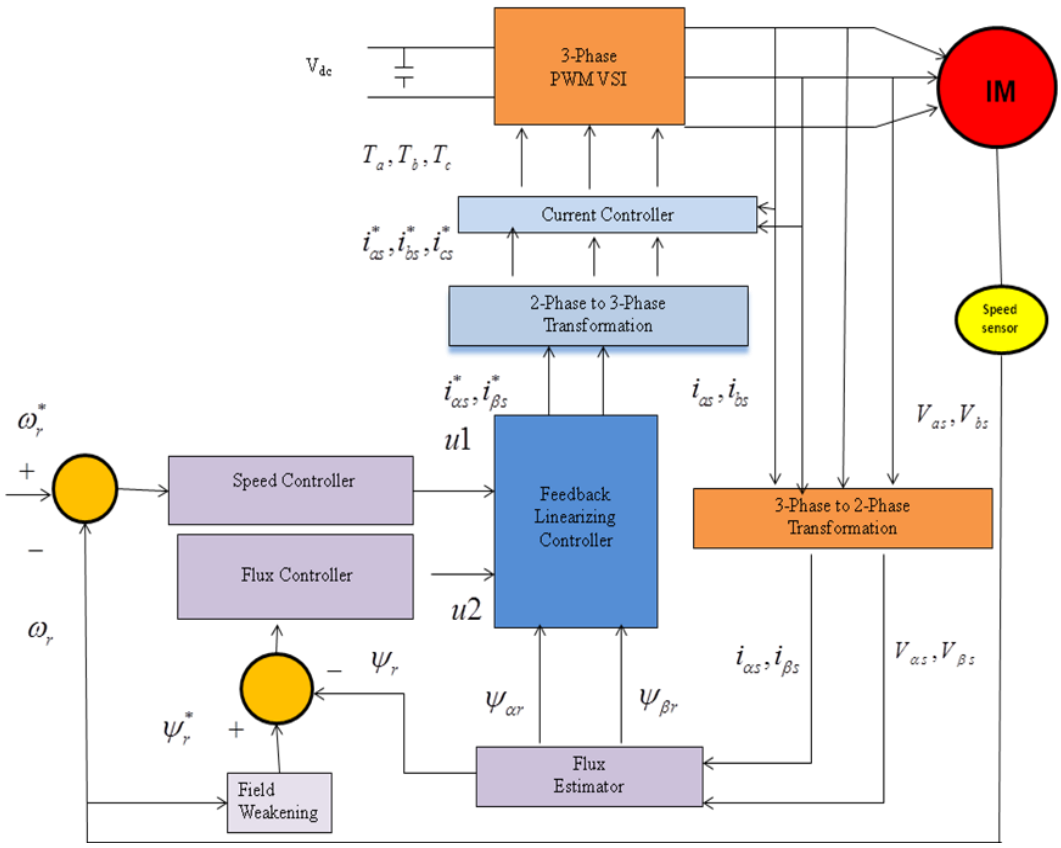

Fig. 4.1 Schematic block diagram of a linearized induction motor drive system

The output of the flux and the speed regulator and also estimated flux are the inputs to the decoupling controller and its output goes to the current controller. The output of the current controller is utilized to generate gate drive signal for IGBT of the PWM voltage source inverter (VSI), which forces reference current in the motor to develop required torque.

Initially the functions of the different blocks of the drive system are outlined separately and later modeled using set of equations and then integrated to get the complete model of the system. The descriptions of these blocks are given in the following sections.

4.2.1 Speed Controller

The reference speed (ω_r^*) is compared with the feedback speed (ω_r) and the speed error is processed in the speed controller. The different speed controllers namely, the proportional integral controller, proportional integral (PI) controller with fuzzy torque controller, the sliding mode controller and the iterative learning controller are used. The speed controller output is the input to the limiter, which is discussed in next section.

4.2.1.1 Proportional Integral Speed Controller

The computed value of the speed error is fed to the speed controller. Which output is fed to the limiter and output of the limiter is taken as a new state variable $u1$. This is the input of the feedback linearized controller. The speed error is given as:

$$e_1(t) = \omega_r^* - \omega_r \tag{4.1}$$

The general equation of PI controller for speed in time domain is

$$u1(t) = k_{p1} e_1(t) + k_{i1} \int_0^t e_1(t)dt \tag{4.2}$$

where $u1\ (t)$ is the respective controllers output. k_{p1} and k_{i1} are the proportional and integral gain of the speed PI controller. Numerical values of the gains are calculated in Chapter -2.

For simulation purpose this equation needs to be discredited. The discrete input to the PI controller requires a discrete form of PI controller and is given by

$$u1(k) = u1(k-1) + k_{p1}(e_1(k) - e_1(k-1)) + k_{i1}e_1(k) \tag{4.3}$$

The general block diagram of the PI controller is shown in Fig. 4.2.

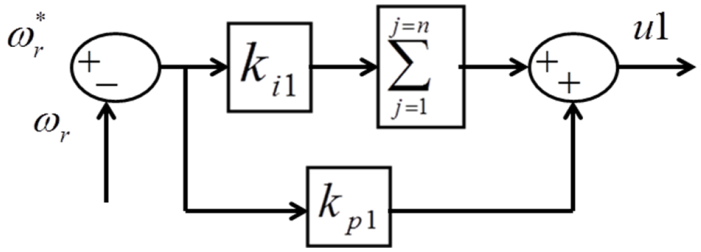

Fig.4.2 Block diagram for proportional integral speed controller

4.2.1.2 Fuzzy Torque Compensator

In this scheme a fuzzy torque compensator is designed and connected in cascade to the PI speed controller. Reference torque, which is the output of the speed controller and the actual estimated torque are compared and error and change in error are input signals to the fuzzy torque compensator, which eliminate undesired features appearing in the response with conventional PI controller, such, as torque ripple, overshoot, and steady state error. The processing is shown in Fig 2.7.

4.2.1.3 Sliding Mode Speed Controller

The algorithm and calculation of controller constants required for designing the sliding mode speed controller for the feedback linearized induction motor system described in chapter- 3. The sliding mode control law is given below.

$$u1 = \hat{b}_1^{-1}\left[-\hat{f}_1 + \dot{\omega}_r^* - \lambda_1 e_1 - k_1 \operatorname{sgn}(s_1)\right] \tag{4.4}$$

where, $u1$ is the output of the SM controller and the new state variable of the speed control loop, $e_1 = \omega_r - \omega_r^*$ is speed error, k_1 sliding mode switching constants, s_1 is sliding surfaces , $\hat{f}_1$ is approximate estimated obtained from (3.21), $\hat{b}_1$ is estimated gain (3.18), ω_r^* is the reference speed and ω_r is the actual values. The block diagram of this controller is given in Fig. 3.1.

4.2.1.4 Iterative Learning Controller

In recent years so many works have been reported on application of iterative learning controller (ILC) for servomechanism. ILC is basically an error correction algorithm and it has a memory that stores previous controller output data. It removes periodic error by using the previous information for the present trial [72]. In this work an ILC controller is designed for speed tracking. It is connected in the path of speed control loop. It consists of two controllers. One is PI type conventional feedback ILC controller and another one is TS fuzzy feedforward controller.

The PI type feedback control law , which updating control signal in each iteration is represented as:

$$u_{1(k+1)}^{fb}(t) = u_{1k}(t) + \phi_k e_{1k}(t) + \Gamma_k \int e_{1k}(t) d\tau \tag{4.5}$$

where, where *k* is the iterative index, $u_{1k}(t)$, and $u_{1(k+1)}(t)$ are control input and output of the system; and $e_{1k}(t) = \omega_r^*(t) - \omega_{rk}(t)$ is speed error; ϕ and Γ are steady gains. In order to reduce the initial offset, an initial correction term $u_0(t)$ is included. The final expression for the feedback control loop can be written as:

$$u_{1(k+1)}^{fb}(t) = (1-\lambda) u_{1k}^{fb}(t) + \lambda u_0(t) + \phi e_{1k}(t) + \Gamma \int e_{1k}(t) d\tau \tag{4.6}$$

where λ is the forgetting factor. Here λ is introduced to ensure the convergence of the iterative learning. In case of uncertain external disturbances and parameter variations the gain constant needs to be modified. Modifying (4.6) to get system output control dynamics including a feedback $u_{1(k+1)}^{fb}(t)$ and a TS fuzzy feedback conpensator $\Delta u_{1(k+1)}^{fb}(t)$ control signal such as:

$$u_{1(k+1)}^{fb}(t) + \Delta u_{1(k+1)}^{ff}(t) = (1-\lambda) u_{1k}^{fb}(t) + \lambda u_0(t) + \phi_k e_{1k}(t) + \Gamma_k \int e_{1k}(t) d\tau + \Delta\phi_k \Delta e_{1k}(t) + \Delta\Gamma_k \int \Delta e_{1k}(t) d\tau \tag{4.7}$$

$$\Delta u_{1(k+1)}^{fd}(t) = \Delta\phi_k \Delta e_{1k}(t) + \Delta\Gamma_k \int \Delta e_{1k}(t) d\tau \tag{4.8}$$

It's theoretical description is given in Chapter-3. The controller block diagram is given in Fig 3.4.

4.2.1.5 Limiter

In case of the step change of speed, speed reversal and application of load, the motor torque goes beyond the break down torque of the motor which may be cause of instability and over current. To keep the electromagnetic torque within a reasonable value output of the speed controller is fed to the limiter. Ultimately the torque-producing component of the current is calculated on the basis of reference torque. Therefore, in order to operate the cage induction motor drive in the stable zone with a safe operating current of the limiter after the speed controller is very much desirable. This ensures inverter's output current to remain within safe value and thereby providing the feature of an inherent over current protection in the drive.

4.2.2 Flux Controller

The rotor reference flux ψ_r^* is compared with the estimated flux ψ_r and the flux error is processed in the flux controller. The different flux controllers namely, the proportional integral controller and the sliding mode controller have been designed in this work. In summation block, whose output known as flux error becomes the command input to the flux controller. The flux controller output is new state variable *u2* which is the input to the feedback linearization controller. The rotor reference flux is obtained from field weakening controller.

4.2.2.1 Field Weakening

The field weakening operation of a linearized induction motor drive is similar to the field control of a separately excited dc motor. This operation is implemented when the drive speed is controlled above the base speed. The input to the field-weakening is the feedback speed of the motor. The output of the controller is the rotor reference flux (ψ_r^*). Below the base speed the rotor reference flux remains constant. Above the base speed the rotor reference flux varies in inverse proportion to the speed. Thus, the main function of the field- weakening controller is to achieve the value of the reference flux depending upon the drive speed.

$$\psi_r^* = \psi_r \qquad \text{when} \quad \omega_r < \omega_b \tag{4.9}$$

$$\psi_r^* = (\frac{\omega_0}{\omega_r})\psi_r \qquad \text{when} \quad \omega_r > \omega_b \tag{4.10}$$

where, ψ_r^* = reference rotor flux, ψ_r = rated rotor flux, ω_r = speed of the motor drive, ω_b = base speed of the motor drive system.

4.2.2.2 Proportional Integral Flux Controller

The computed value of the flux error is fed to the flux controller, whose output is a new state variable *u*2. Which is the input of the feedback linearized controller. The flux error at the nth instant of time is given as:

$$e_2(t) = \psi_r^* - \psi_r \tag{4.11}$$

The general equation of PI controller for flux in time domain is

$$u2(t) = k_{p2} e_2(t) + k_{i2} \int_0^t e_2(t)dt \tag{4.12}$$

Where *u*2 *(t)* is the respective controllers output. k_{p2} and k_{i2} are the proportional and integral gain of the flux PI controller. Numerical values of the gains are calculated in Chapter-2.

For simulation purpose this equation needs to be discredited. The discrete input to the PI controller requires a discrete form of PI controller and is given by

$$u2(k) = u2(k-1) + k_{p2}(e_2(k) - e_2(k-1)) + k_{i2} e_2(k) \tag{4.13}$$

The general block diagram of the PI controller is shown in Fig. 4.3.

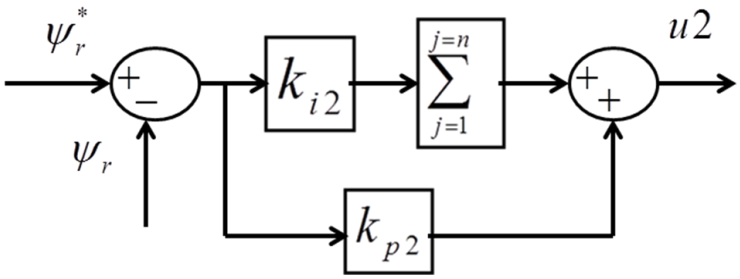

Fig.4.3 Block diagram for proportional integral flux controller

4.2.2.3 Sliding Mode Flux Controller

The algorithm and calculation of controller constants required for designing the sliding mode flux controller for the feedback linearized induction motor system described in Chapter- 3. The sliding mode control law is given below.

$$u2 = \hat{b}_2^{-1}\left[-\hat{f}_2 + \dot{\psi}_r^* - \lambda_2 e_2 - k_2\,\mathrm{sgn}(s_2)\right] \tag{4.14}$$

where, $u2$ is the output of the sliding mode flux controller and the new state variable of the speed control loop, $e_2 = \psi_r - \psi_r^*$ is flux error, k_2 sliding mode switching constants, s_2 is sliding surfaces, $\hat{f}_2$ is approximate estimated state obtained from (3.21), $\hat{b}_2$ is estimated gain (3.18), ψ_r^* is the reference flux and ψ_r is the actual values. The block diagram is given in Fig. 3.2.

4.2.3 Rotor Flux Estimator

The knowledge of rotor flux is essential for the feedback linearization. The direct measurement of flux is practically difficult. Therefore, the voltage model of flux estimation has been preferred [12], where measurement of terminal voltage and stator current are required.

The α-β axis stator voltage components are estimated as

$$V_{\alpha s} = -\frac{V_{bs}}{\sqrt{3}} + \frac{V_{cs}}{\sqrt{3}} \tag{4.15}$$

$$V_{\beta s} = \frac{2}{3}(V_{as} - \frac{V_{bs}}{2} - \frac{V_{cs}}{2}) \tag{4.16}$$

Similarly the α-β axis components of stator currents are estimated as

$$i_{\alpha s} = \frac{2}{3}(-\frac{\sqrt{3}}{2} i_{bs} + \frac{\sqrt{3}}{2} i_{cs}) \tag{4.17}$$

$$i_{\beta s} = \frac{2}{3}(i_{as} - \frac{i_{bs}}{2} - \frac{i_{cs}}{2}) \tag{4.18}$$

Where (V_{as},, $V_{b\,s}$, V_{cs}) and (i_{as} , i_{bs}, i_{cs}) are the sensed stator voltage and stator currents. The *α-β* axis component of stator flux is estimated by using the *α-β* component of

stator voltages and currents. The α-β axis component of stator flux can be estimated by using the *α-β* component of stator voltages and currents.

$$\psi_{\alpha s} = \int (V_{\alpha s} - R_s i_{\alpha s}) dt \tag{4.19}$$

$$\psi_{\beta s} = \int (V_{\beta s} - R_s i_{\beta s}) dt \tag{4.20}$$

The *α-β* component of rotor current referred to stator reference frame is obtained from the *α-β* component of stator fluxes and currents.

$$i_{\alpha r} = \frac{\psi_{\alpha s}}{L_m} - \frac{i_{\alpha s}}{L_m} L_s \tag{4.21}$$

$$i_{\beta r} = \frac{\psi_{\beta s}}{L_m} - \frac{i_{\beta s}}{L_m} L_s \tag{4.22}$$

Finally the *α-β* component of rotor flux is estimated by using the *α-β* component of rotor currents, stator currents and machine parameters.

$$\psi_{\alpha r} = L_r i_{\alpha r} + L_m i_{\alpha s} \tag{4.23}$$

$$\psi_{\beta r} = L_r i_{\beta r} + L_m i_{\beta s} \tag{4.24}$$

where, L_r and L_m are rotor self and magnetizing inductance respectively.

4.2.4 Feedback Linearizing Controller

The output of the speed controller after limiting and output of the flux controller are taken as the new variables $u1$ and $u2$ are the inputs to the feedback linearizing controller, which takes rotor quadrature flux from feedback path, and process to produced complete decoupled currents in stationary (α-β) reference frame. The input-output equation of the state feedback is rewritten in (4.25) and (4.26).

$$i_{\alpha s} = \frac{\psi_{\alpha r}}{\psi_r} u1 - \frac{\psi_{\beta r}}{\psi_r^2} u2 \tag{4.25}$$

$$i_{\beta s} = \frac{\psi_{\beta r}}{\psi_r} u1 + \frac{\psi_{\alpha r}}{\psi_r^2} u2 \tag{4.26}$$

4.2.5 Current Controlled Voltage Source Inverter

In order to insure that three phase motor currents (i_{as}, i_{bs}, and i_{cs}) truly follow the reference currents (i^*_{as}, i^*_{bs} and i^*_{cs}) use of suitable current controlled technique is essential. For this purpose, a current controller voltage source inverter (CC-VSI) is employed where the switching signal for power device of the inverter is generated using hysteresis band current controlled PWM technique. The inverter has a constant voltage source at its input and gives three-phase PWM voltage at its output forcing the 3-phase sinusoidal current in the motor winding. These phase sinusoidal current of variable voltage and variable frequency in the motor winding depending up on the operating condition. The output voltage of the inverter depends on switching state of the IGBT of three legs, as shown in Fig.4.4. The output voltage can be expressed in terms of switching functions SFa, SFb and SFc. The value of switching function can be 0 or 1 depending upon switching state of the IGBT corresponding phase.

Table-4.1

Switching states of inverter IGBT

Device ON	SF_K value
Lower ON	0
Upper ON	1

The mathematical expressions for three phase voltages in terms of dc link voltage and switching functions are [12].

$$V_{as} = V_{dc} (2SF_a – SF_b – SF_c) / 3 \quad (4.27)$$

$$V_{bs} = V_{dc} (-SF_a + 2SF_b – SF_c) / 3 \quad (4.28)$$

$$V_{cs} = V_{dc} (-SF_a – SF_b + 2SF_c) / 3 \quad (4.29)$$

The inverter is simulated with the assumption that the voltage drop in the device, the effect of switching network and the switching delay of individual device including the delay time between the switching instants of the devices in the same lag of the inverter are negligible.

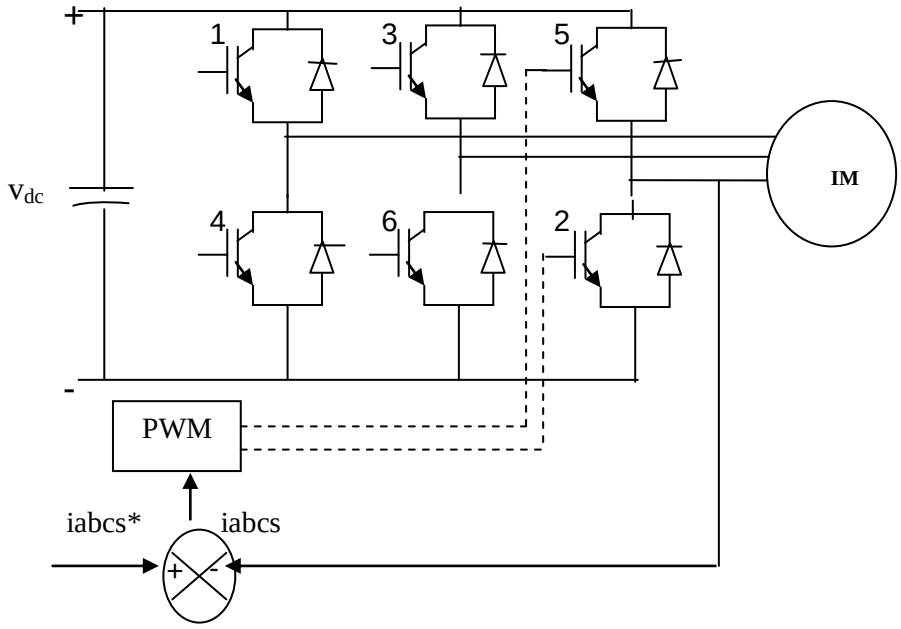

Fig. 4.4 Schematic diagram of current controlled VSI

4.2.6 PWM Current Controller

The switching signal for the inverter devices is obtained by comparison of the motor currents (i_{as}, i_{bs}, i_{cs}) with their reference counter parts (i_{as}^*, i_{bs}^*, i_{cs}^*). Hysteresis band with limits is properly selected for better performance of the current controller. The states of the devices are obtained in the following manner.

If $i_{as} \leq i_{as}^*$ - band limit then T_1 is on (SF_a=1) and $V_{an} = V_{dc}$

If $i_{as} \geq i_{as}^*$ + band limit then T_4 is on (SF_a=0) and $V_{an}=0$

If $i_{bs} \leq i_{bs}^*$ - band limit then T_3 is on (SF_b=1) and $V_{bn}= V_{dc}$

If $i_{bs} \geq i_{bs}^*$ + band limit then T_6 is on (SF_b=0) and $V_{bn}= 0$

If $i_{cs} \leq i_{cs}^*$ - band limit then T_5 is on (SF_c=1) and $V_{cn}=V_{dc}$

If $i_{cs} \geq i_{cs}^*$ + band limit then T_2 is on (SF_c=0) and $V_{cn}=0$ (4.30)

The operating principle of hysteresis band PWM is illustrated in Fig.4.5.

A switching (ON/OFF) signal for the devices of the inverter are generated according to above switching law. Hence the actual motor currents (i_{as}, i_{bs}, & i_{cs}) follow the reference currents (i_{as}^*, i_{bs}^* & i_{cs}^*), produced by the speed controller.

4.3 MATLAB Model of the Induction Motor Drive System

MATLAB is a software package for high performance, numerical computation and visualization. It has become a standard tool in the research environment. It provides an interactive environment with hundreds of built in functions for technical computation, graphics, and animation.

The MATLAB model of the complete drive system is shown in Fig. 4.6, which is used to simulate and test the versatility and reliability of the developed model using different controllers. The description of the different MATLAB submodels are given below.

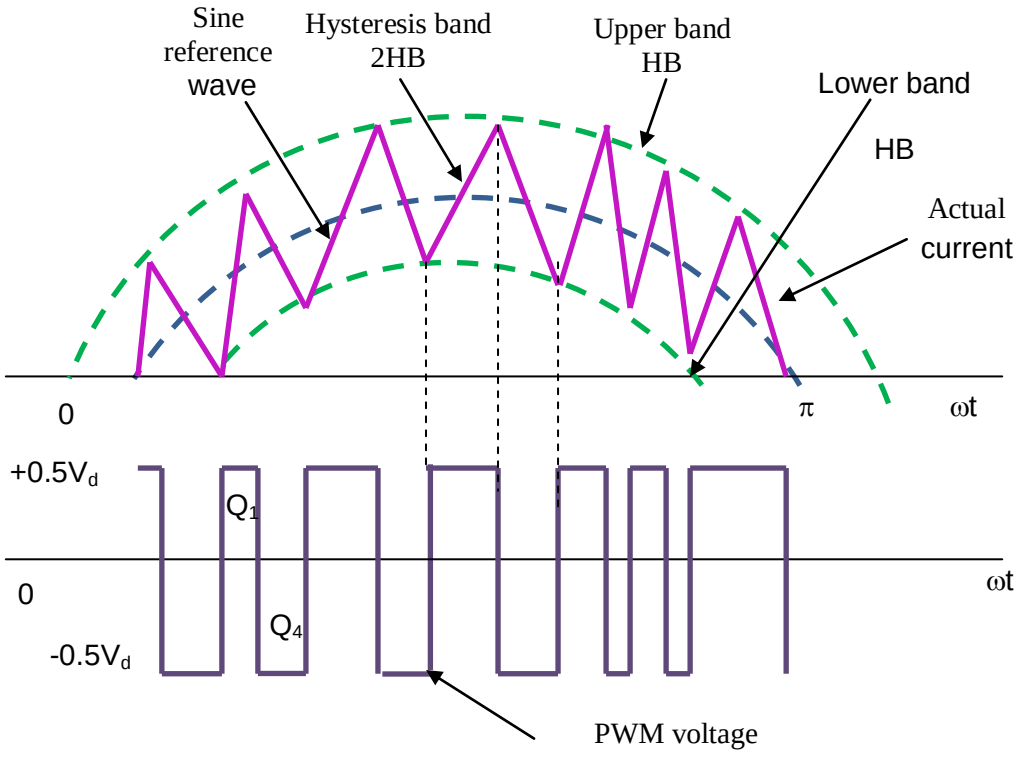

Fig. 4.5 Principle of hysteresis-band current control

4.3.1 Speed and Flux controller

The model of PI speed and flux controller realised using the SIMULINK toolbox. The controller parameter values are given as obtained in Chapter-2.The main function of these controllers are to generate two intermediate state variables $u1$ and $u2$. Fig. 4.7 and Fig. 4.8 show the simulink model of the PI speed and flux controller along with limiter in discrete time frame. These models are based on equations stated in section 4.2

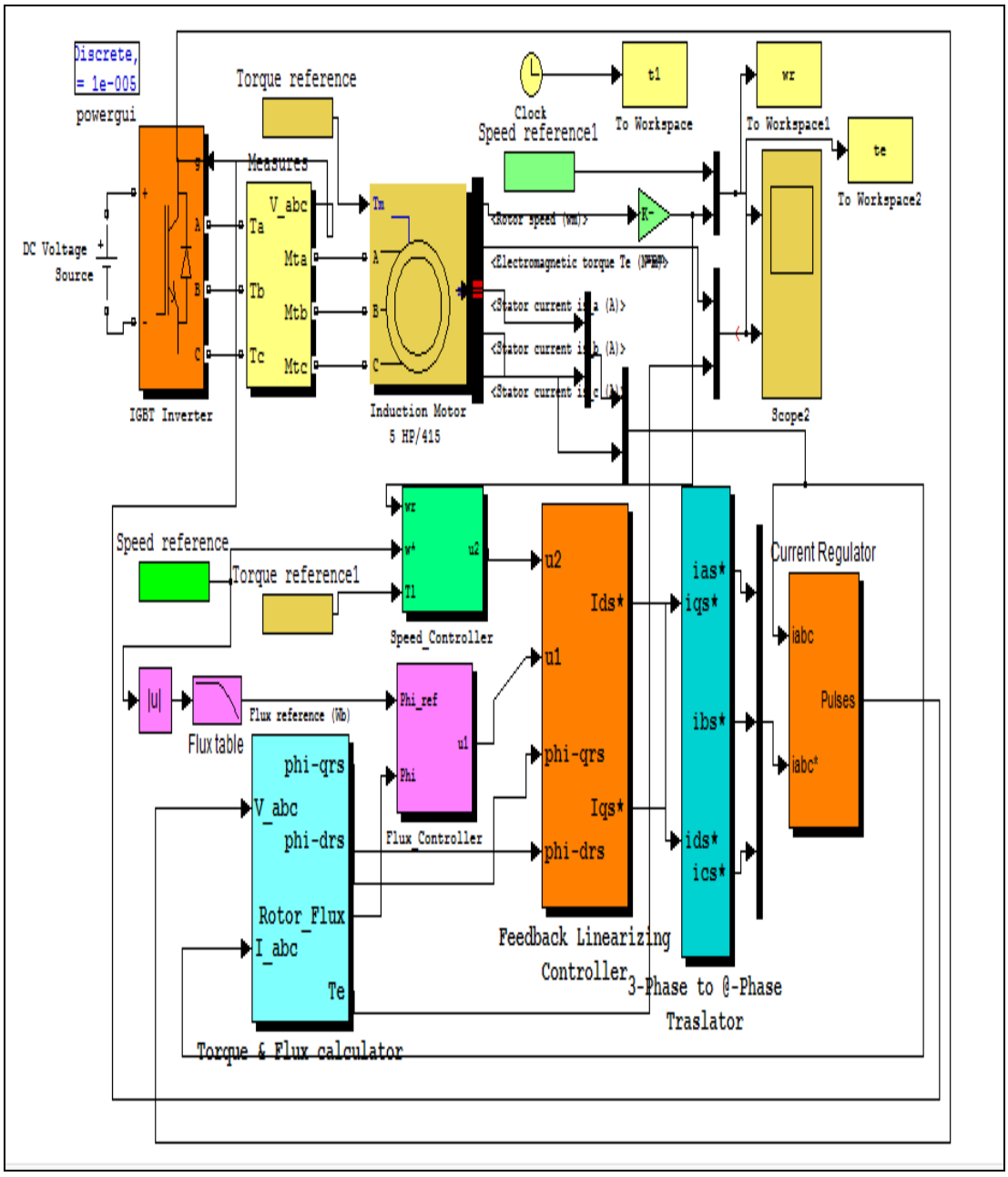

Fig. 4.6 MATLAB model of linearized induction motor drive system

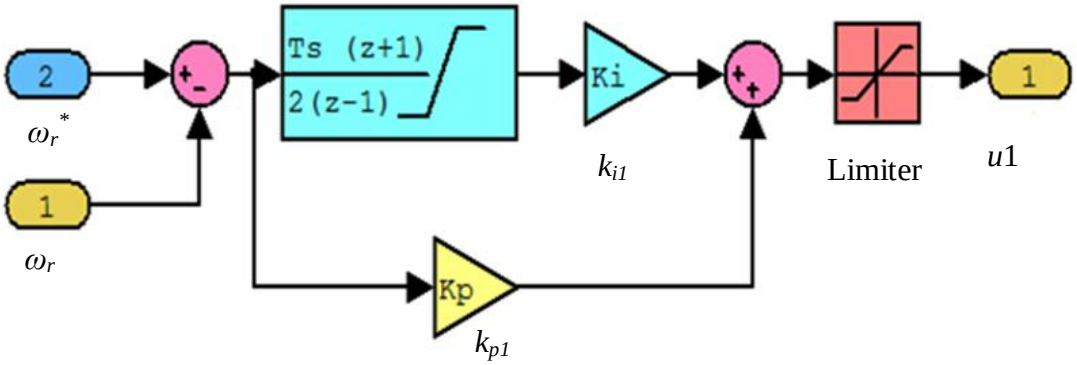

Fig.4.7 MATLAB submodel of PI speed controller

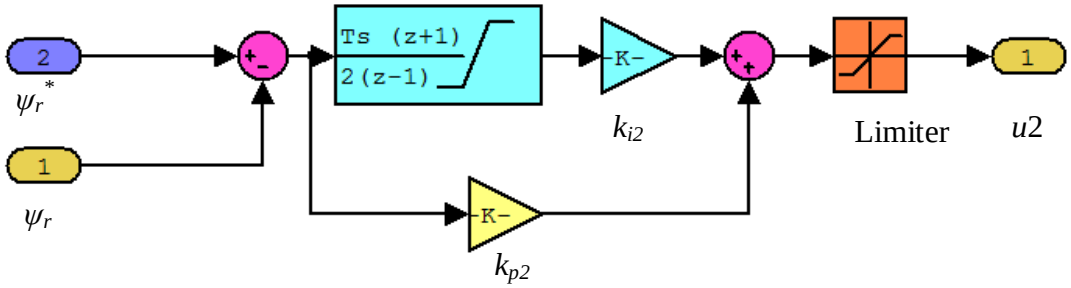

Fig. 4.8 MATLAB submodel of PI Flux controller

4.3.2 Fuzzy Torque Compensator

Fig. 4.9 shows the simulink model block diagram for the fuzzy torque compensator. The two inputs namely: reference torque and estimated torque are compared. The error and the change of error are scaled into the range of -1 to +1. These are input to the decision inference section. The decision switch decides which option to be transmitted out of the torque compensator. The outputs are amplified to obtain corresponding signal $u1$ input for the feedback linearization controller.

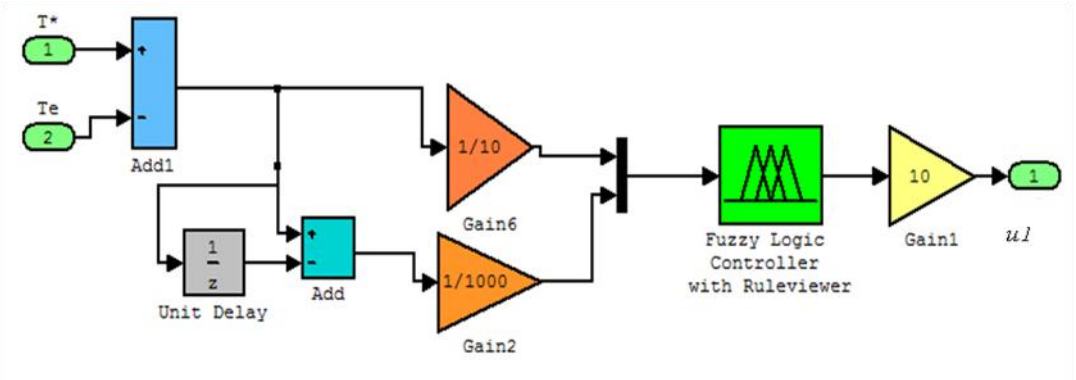

Fig. 4.9 MATLAB submodel of fuzzy torque compensator

4.3.3 Sliding Mode Controller

Fig 4.10 and Fig.4.11 shows the SIMULINK model block diagram for the sliding mode speed and flux controller. Related theory and corresponding controller parameters are described in chapter in Chapter- 3.

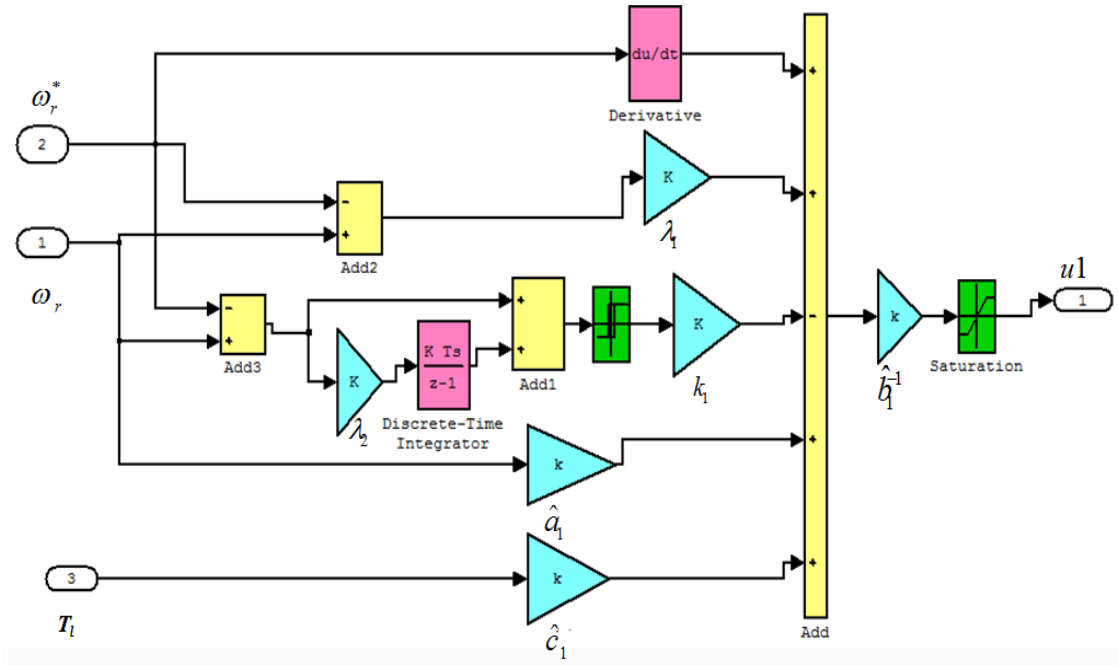

Fig. 4.10 MATLAB submodel of sliding mode speed controller

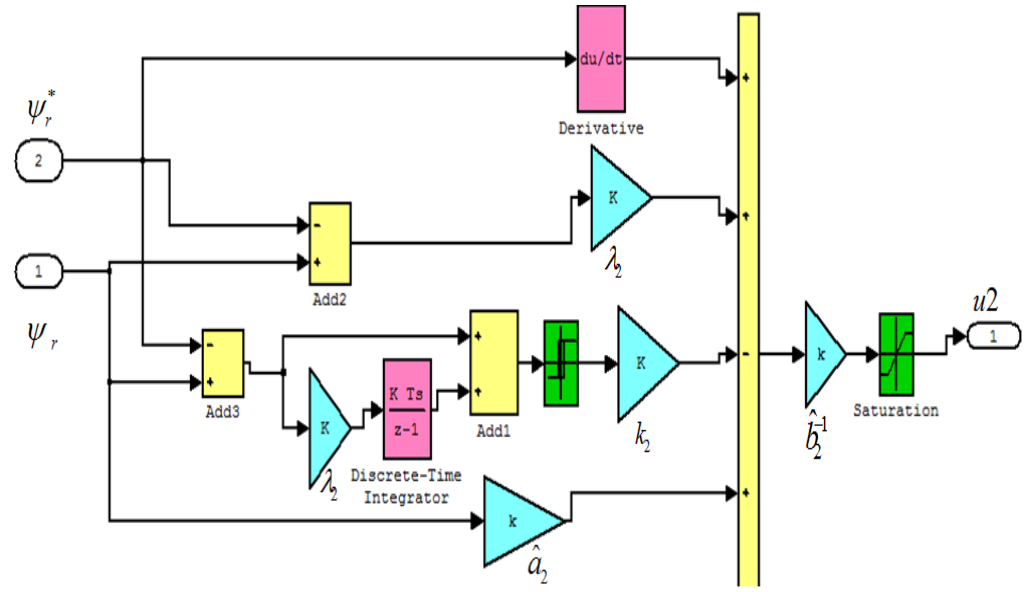

Fig. 4.11 MATLAB submodel of sliding mode flux controller

4.3.4 Iterative Learning Controller

Fig.4.12 Shows the SIMULINK model diagram for based iterative learning controller. It consists of two controllers namely PI type ILC feedback controller and TS fuzzy compensator. The instant output signal is subtracted from the previous signal and fed to the PI type iterative learning controller and controller gain is tuned to eliminate error in each iteration. TS based fuzzy controller connected in feedback path. This controller is modelled on Takahasi Sugeono principle in fuzzy editor tool of the MATLAB library. The gains and weighing of controller is tune to achieve chattering free and exact value control signal required for motor speed appears due to certain or uncertain disturbances appears during practical operation.

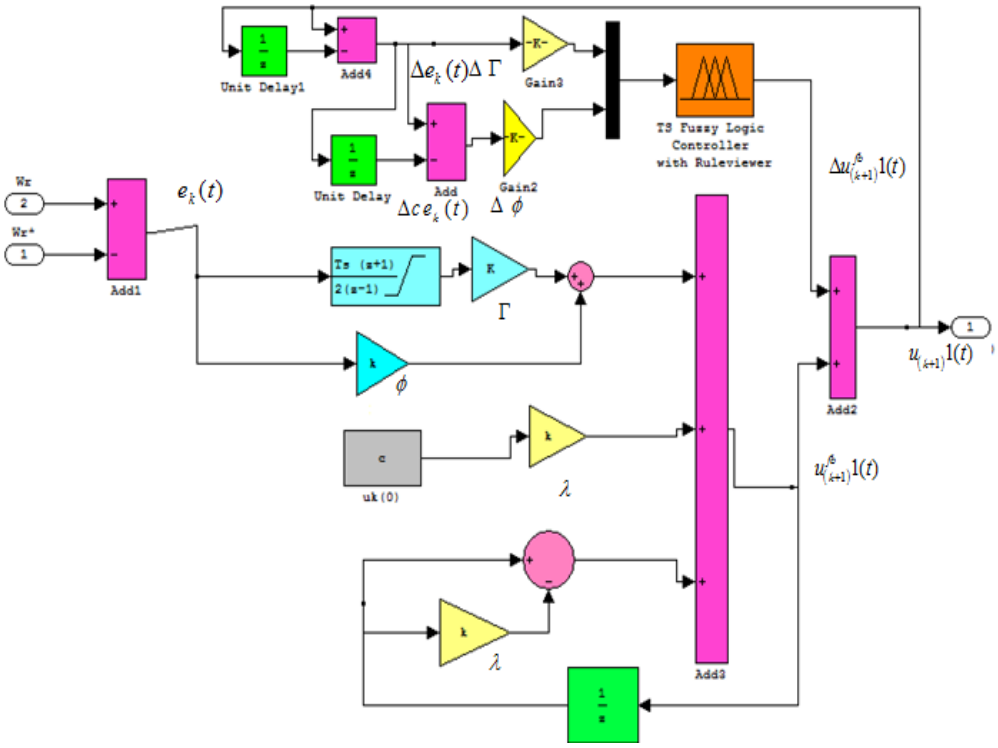

Fig. 4.12 MATLAB submodel of iterative learning controller

4.3.5 Feedback Linearizing Controller

The SIMULINK structure developed for the linearized induction motor is shown in Fig.4.13.The controller operation and related equations are dealt in subsection 4.2. The feedback controller inputs are two new intermediate signals *u*1 and *u*2, coming out from speed controller and flux controller. This feedback controller takes α-β current component from feedback path. By process of inversion nonlinearity present

in the specific control loop is cancelled out. Output of this is the reference α-β stator current components, which are complete decoupled one.

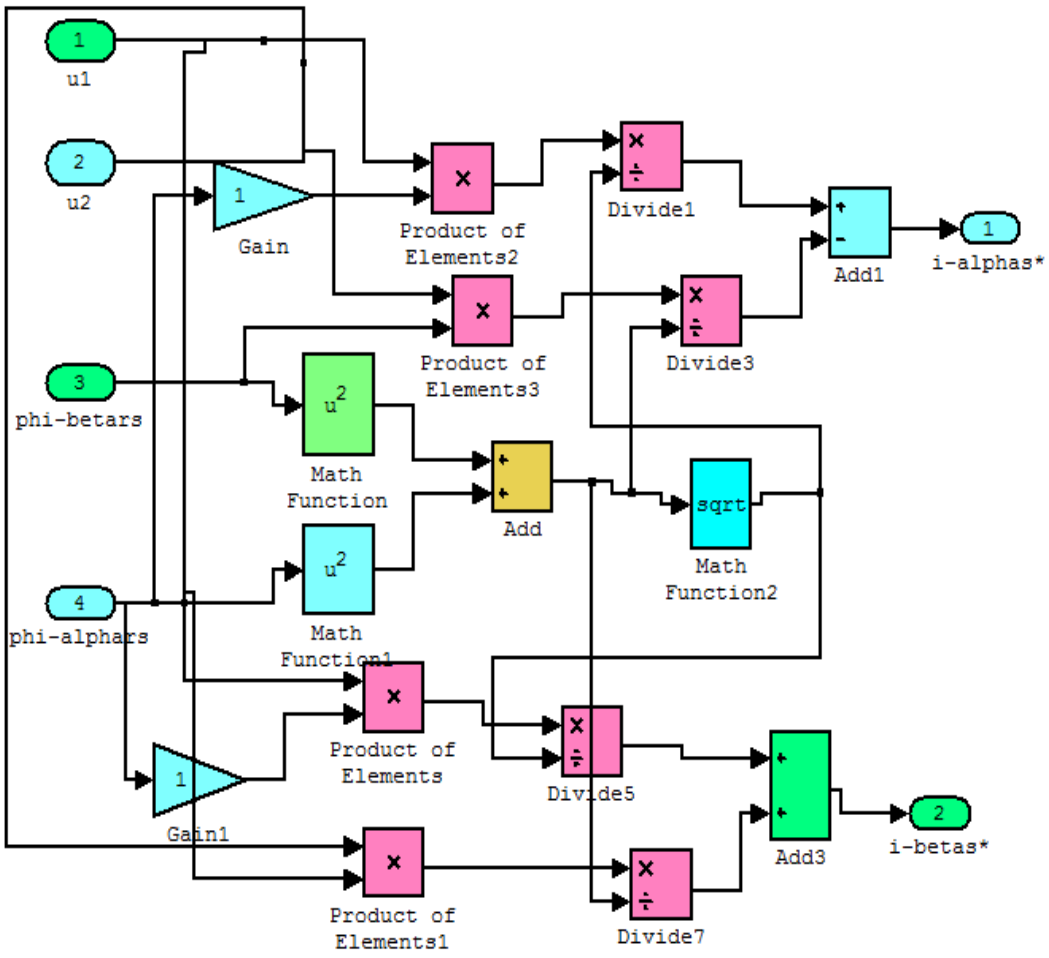

Fig. 4.13 MATLAB submodel of the feedback linearizing decoupling controller

4.3.6 Rotor Flux and Electromagnetic Torque Estimator

The rotor flux linkages are required to be estimated for two reasons in the linearized induction motor drive scheme. First , the magnitude of rotor flux is the input to the flux controller for tracking reference flux command. Second, feedback linearizing controller takes direct and quadrature axis rotor flux linkage component for cancellation of nonlinearity present in speed and flux control loop. The electromagnetic and reference torque, which is obtained from speed control are the inputs to the fuzzy torque compensation scheme, which generates output signal $u1$, minimises the ripples of the control signal. Fig. 4.14 shows the MATLAB submodel of rotor flux and torque estimator.

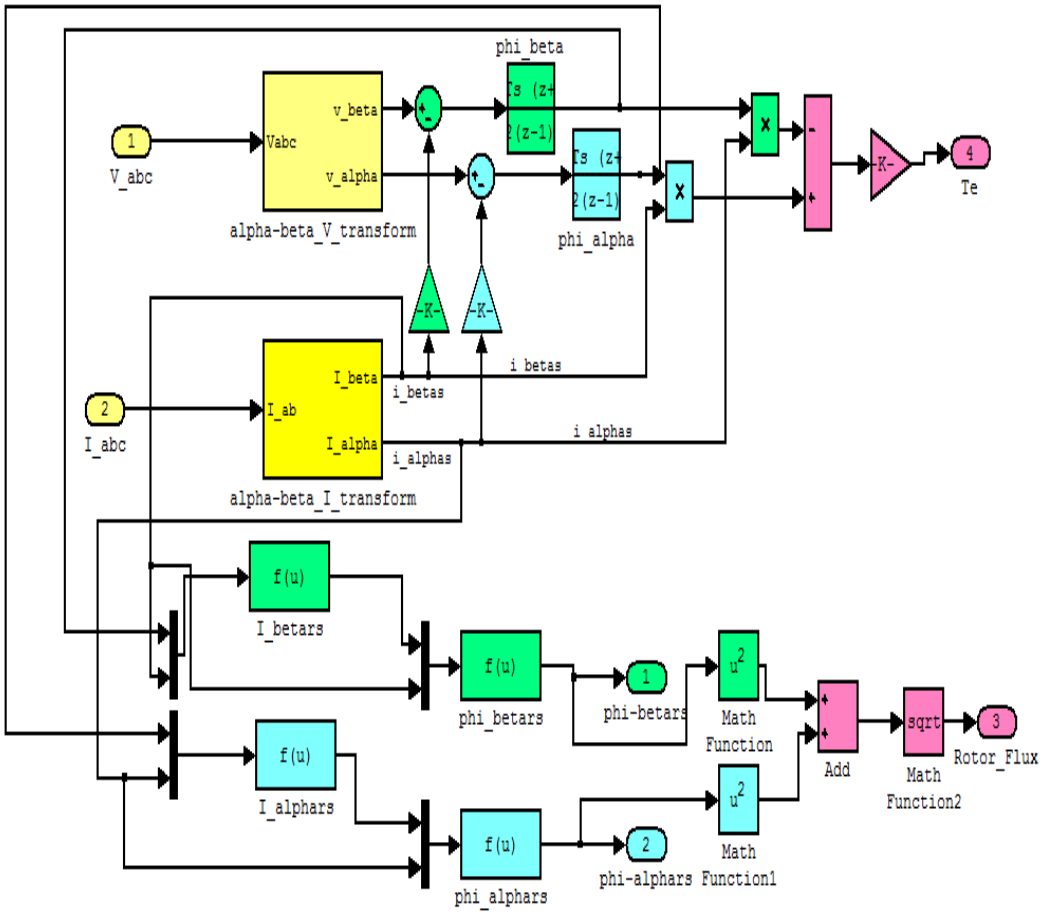

Fig.4.14 MATLAB submodel of rotor flux and torque estimator

4.3.7 Two Phase Stationary to Three Phase Stationary Converter

This subsystem using SIMULINK toolbox carries out conversion of the quantities from the two-phase stationary reference frame to three-phase system. The SIMULINK structure of the subsystem is shown in Fig.4.15.

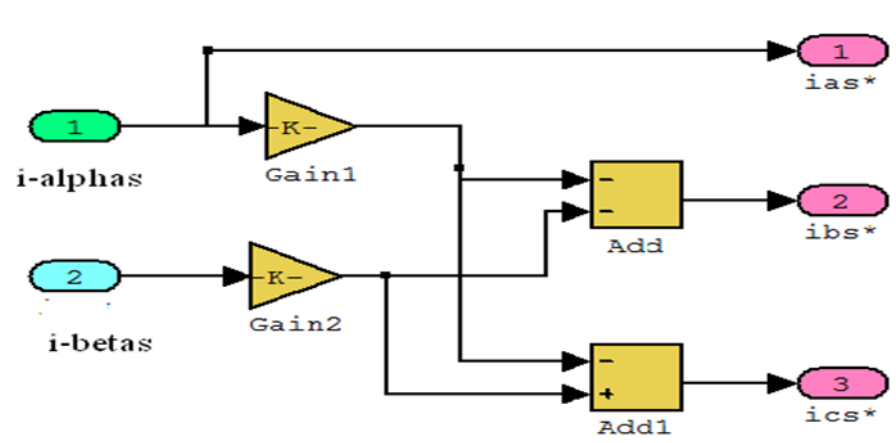

Fig.4.15 MATLAB submodel of two phase to three phase converter

4.3.8 Current Regulator

Input to the current regulator are reference current I^*_{abc} and motor current i_{abc}. Each reference phase current and corresponding motor current are fed to hysteresis comparator. Outputs of three hysteresis comparator are used to produce switching signal for six IGBT of PWM inverter. Inverted signal is used for lower device of the leg of inverter and not inverted signal for upper device. This sub model is shown in Fig.4.16.

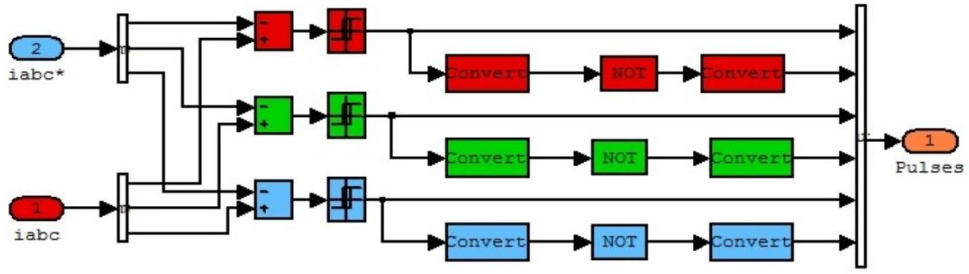

Fig.4.16 MATLAB submodel of current regulator

4.4 Results and Discussions

The performance of the linearized induction motor drive system is simulated in MATLAB/SIMULINK under different dynamic conditions such as starting speed, speed reversal, load perturbation (load application and load removal), periodic speed and load. A set of response comprises of reference speed (ω_r^*) and rotor speed (ω_r) in rpm, developed electromagnetic torque (T_e) and load torque (T_l) in Nm, stator flux ($\psi_{ae}, \psi_{\beta r}$) components in V. s and stator currents($i_{as}, i_{\beta s}$) components in A are taken.

The specifications and parameters of the induction motor used in the simulation are given in Table.2.1.

4.4.1 Performance Comparison between PI and PI with Fuzzy Torque Controller

The simulation responses of the drive with starting acceleration and load perturbation are shown in Fig. 4.17 for PI controller and in Fig. 4.18 for fuzzy torque compensator.

Performance with PI Controller

Starting Dynamics: The three phase squirrel cage induction motor is fed from a controlled voltage and frequency source. The reference speed is set at 500 rpm with a current limit set at the rated value. The starting response is shown in Fig.4.17. The starting current is the rated current when the motor builds up the required starting torque to reach the set speed. The motor reaches its set speed in 0.42sec. When the speed error becomes zero rpm the winding current also reduces to no load value and the developed torque is just no load torque. The rotor flux remains constant throughout. The feedback linearizing controller is apparent as there is clear decoupling between flux and speed.

Load Perturbation: When the motor is running at a steady state speed of 500 rpm, a load torque equal to the 10 Nm is suddenly applied. The application of the external load causes a small drop in speed by 7 rpm. In response to drop in speed, the controller acts and command torque is increased and motor regains the set speed quickly. When the motor is operating at steady state on load, suddenly the applied external load of 10Nm is suddenly removed when motor was running at set speed. Due to sudden removal of the load a small overshoot in motor speed appears. For very short time. These tests clearly indicate good performance of the controller under all conditions.

Performance of PI with Fuzzy Torque Compensator

The same steps as in case of PI controller are repeated, for same speed and load perturbation. The simulation results are shown in Fig.4.18.

Starting Dynamics: It is observed with fuzzy torque compensator the motor speed reaches the set point in 0.37s. This is an improvement over PI controller. The torque ripple is reduced in this case. The fuzzy torque compensator with only 16 fuzzy inference rules improves overall performance of the drive system.

Load Perturbation:. Now the applied torque on the motor is suddenly removed when it was running. A negligible overshoot in motor speed appears, the above described performance clearly indicates improved performance of PI with fuzzy torque compensator.

The performance measures of PI and PI with fuzzy torque compensator is given in table Table 4.2.

Table 4.2

Performance comparison between PI and PI with fuzzy torque compensator

Event	P-I controller	Fuzzy torque compensator
1. Starting acceleration to 500rpm at no load	Starting time = 0.42 s	Starting time = 0.37 s
2. Shaft loading by 10N.m at steady speed of 500rpm	Speed drop on load application = 7 rpm	Speed drop on load application = 0.15 rpm
3. Removal of 10 N.m shaft load torque	Speed overshoot = 1.5 rpm	Speed overshoot = 0 rpm

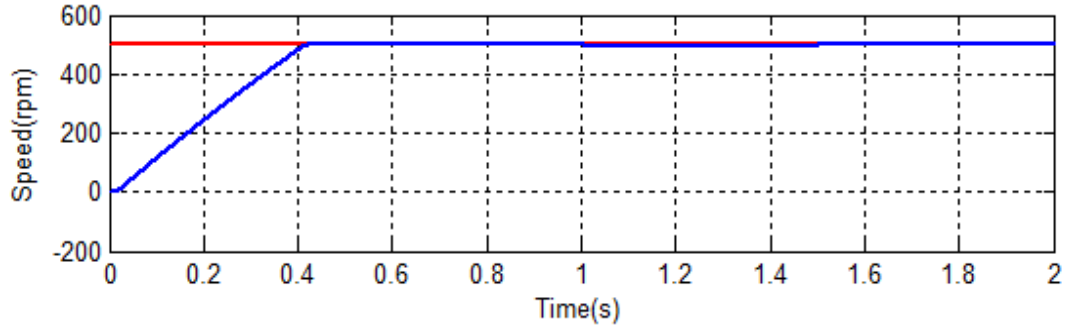

(a)

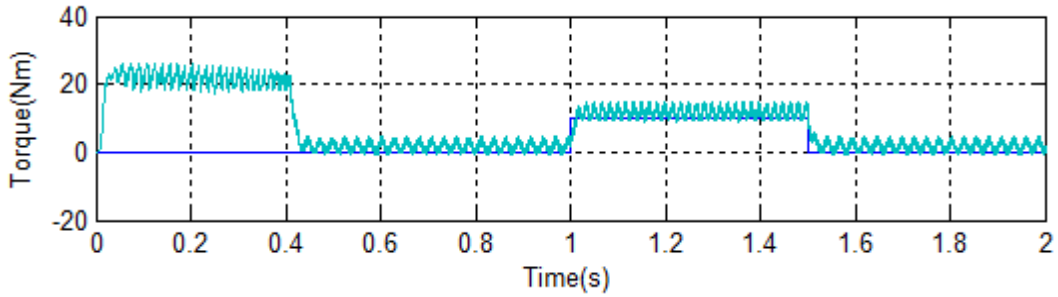

(b)

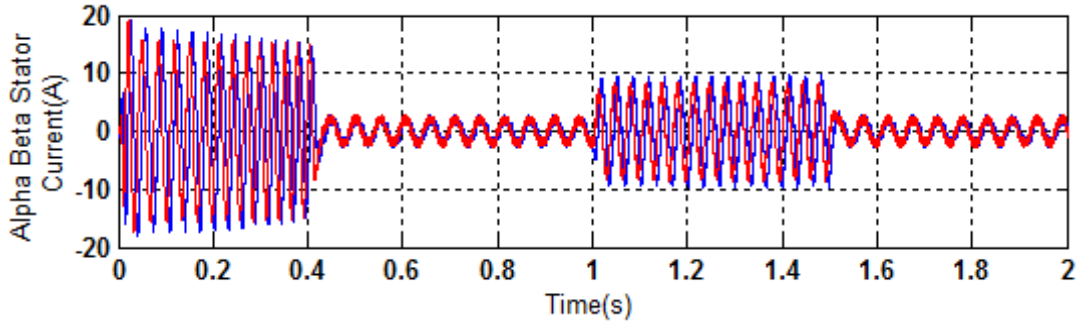

(c)

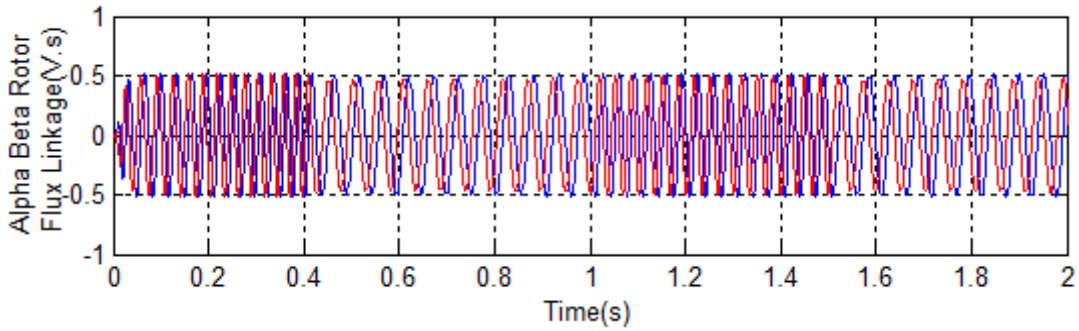

(d)

Fig.4.17. Simulation response of IM drive for step change and loading with PI controller showing: (a) reference and motor speed (b) load torque and electromagnetic torque (c) α-β stator current components (d) α-β rotor flux linkage component

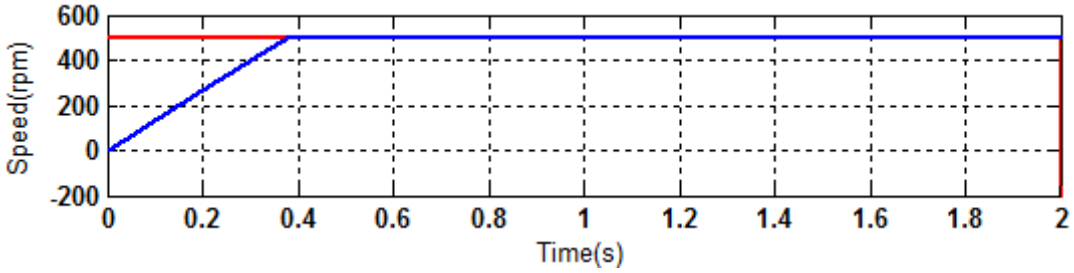

(a)

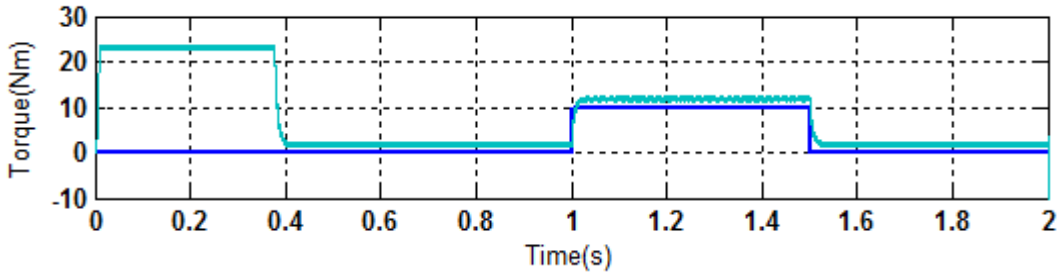

(b)

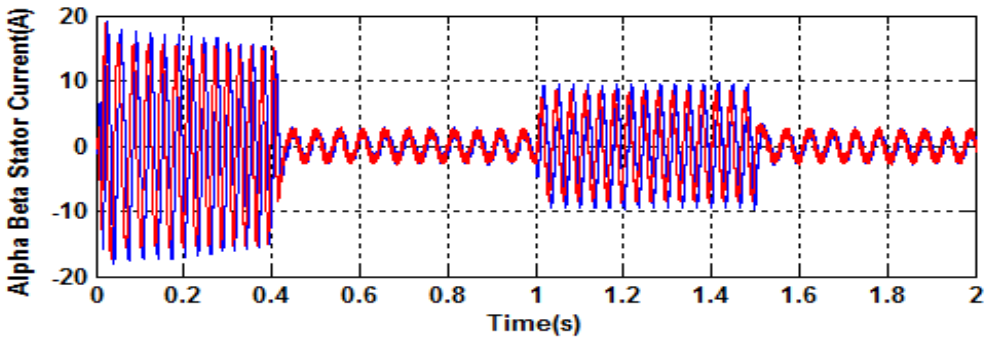

(c)

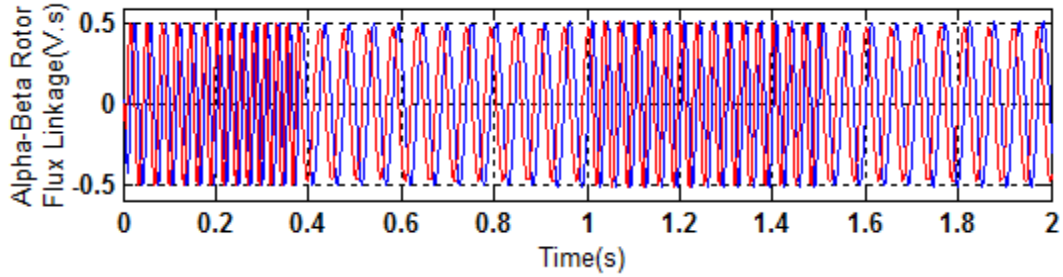

(d)

Fig. 4.18 Simulation response of IM drive for step change and loading using PI with fuzzy torque compensator showing: (a) reference and motor speed (b) load torque and electromagnetic torque (c) α-β stator current components (d) estimated α-β rotor flux linkage components

4.4.2 Performance Analysis of IM Drive with PI, SM and ILC

The performance comparison of the feedback linearized induction motor drive system with proportional integral, sliding mode and iterative learning controller are done in this section The same induction motor is used as described in Table 2.1. The responses with PI, SM and IL controller are shown in Fig. 4.19, Fig. 4.20 and Fig.4.21 respectively. Responses are compared in Table 4.5.

Starting Dynamics: These illustrate that the right from beginning motor picks up speed at constant rate and reaches its set points (zero to 500rpm) in 0.42s with P-I controller, 0.35s with SM and 0.3s with ILC. Remarkable chattering in torque is observed in torque response with PI and SM controller. Although torque ripples appears with all controllers, ILC shows the minimum chattering.

Speed Reversal

Motor accelerates without load from rest at t=0, with a reference spead of 500rpm. While motor is running at steady speed of 500 rpm , then motor speed is reversed from 500 rpm to -500 rpm at=2s. In response to this controller first reduced the frequency of the current demonstrating regenerative breaking followed by phase reversal for starting the motor in the reverse direction. The total reversal time taken by motor drive system with controllers PI, SM and ILC are 0.85s, 0.84s and 0.72s respectively. Again at T=3.0s, when motor is running at -500 rpm, the speed command is changed and set at 1000 rpm. In this situation motor takes 1.3s, 1.15s and 1.1s with PI, SM and ILC. It can be observed that ILC provide better transient performance during starting and speed reversal.

Load Perturbation

When operating at the steady speed of 500 rpm, a load torque of 10N.m is applied at t=1s, which is again removed at t=1.5s. Sudden application of load causes an instantaneous deep in speed. In response to drop of speed , followed by increase in stator currents. Speed drop with PI, SM, IL controllers are 7 rpm, 0.35 rpm and 0.15 rpm respectively.

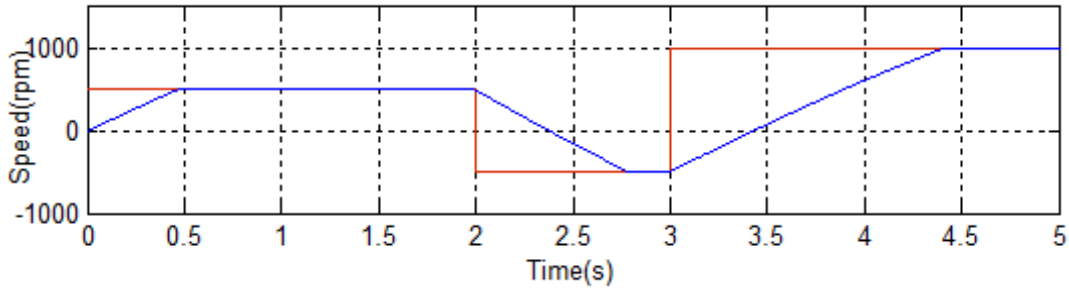

(a)

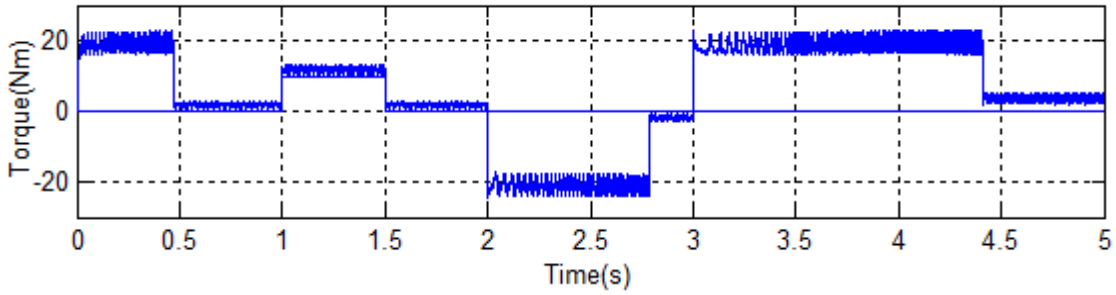

(b)

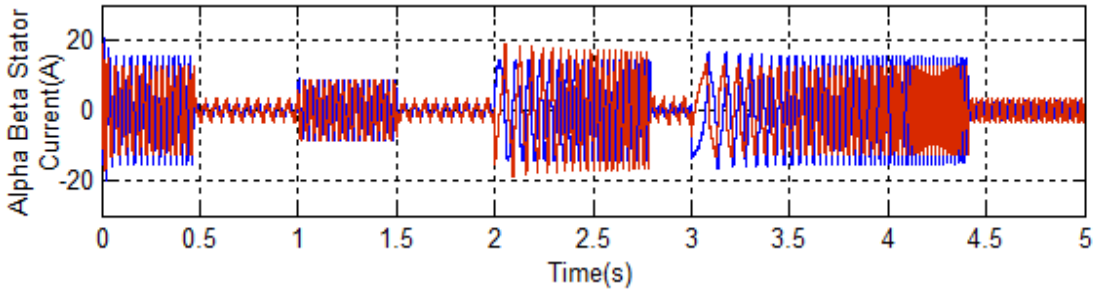

(c)

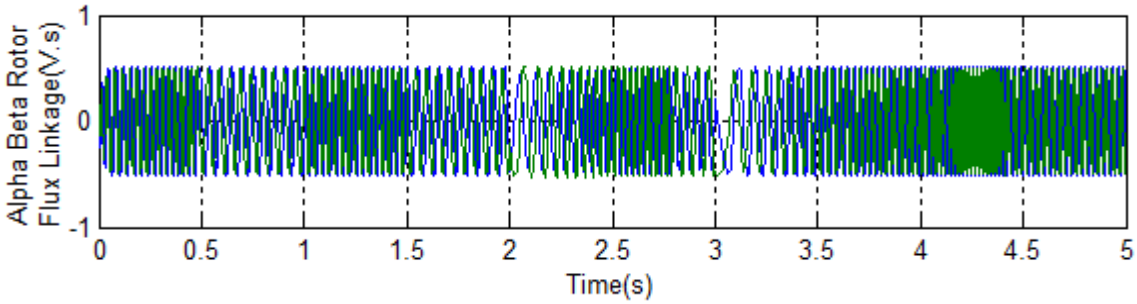

(d)

Fig.4.19. Simulation response of IM drive for starting, speed reversal and load perturbation with PI controller showing: (a) motor speed (b) load torque and electromagnetic torque (c) α-β stator current components (d) α-β rotor flux linkage components

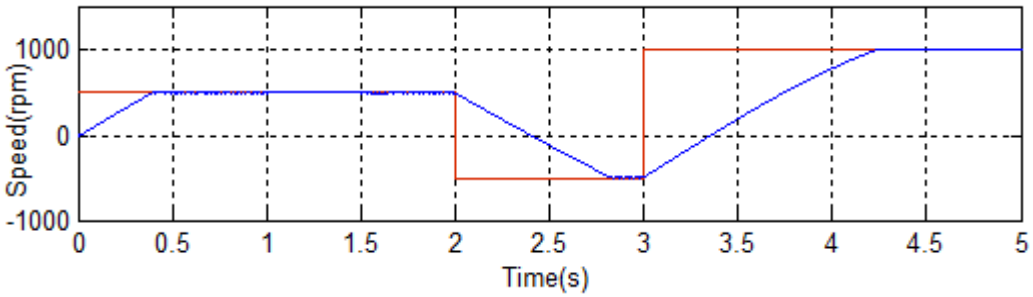

(a)

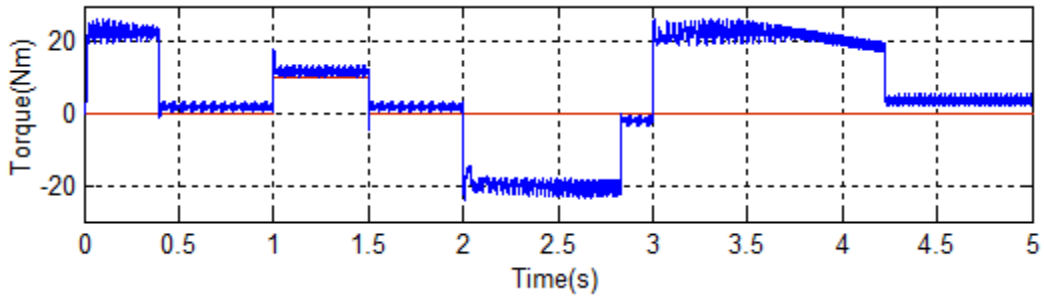

(b)

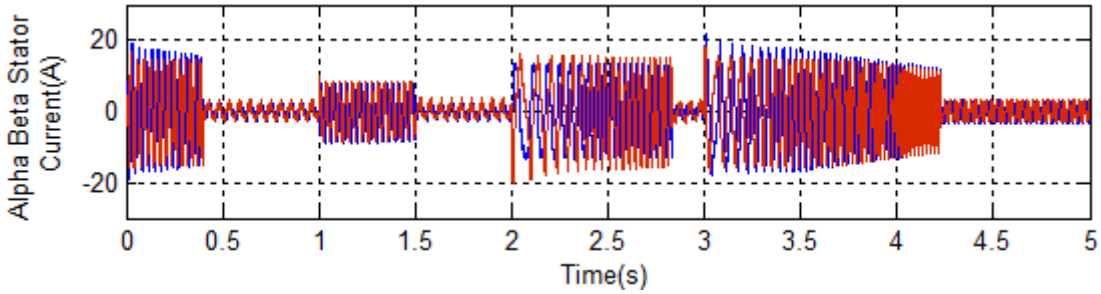

(c)

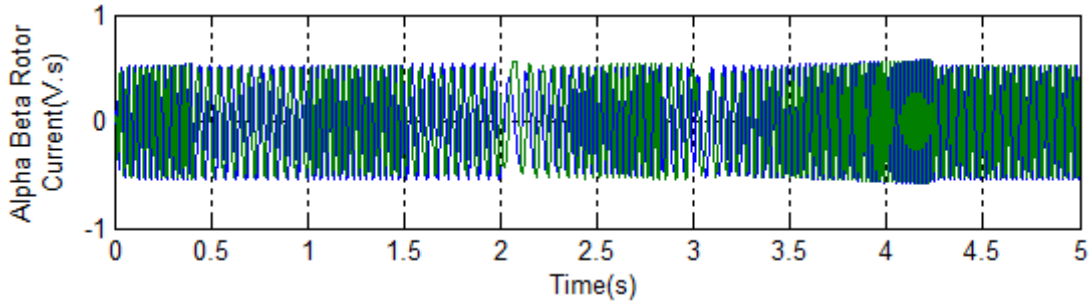

(b)

Fig.4.20 Simulation response of IM drive for starting, speed reversal and load perturbation with SM controller showing: (a) motor speed (b) load torque and electromagnetic torque (c) α-β stator current components (d) α-β rotor flux linkage components

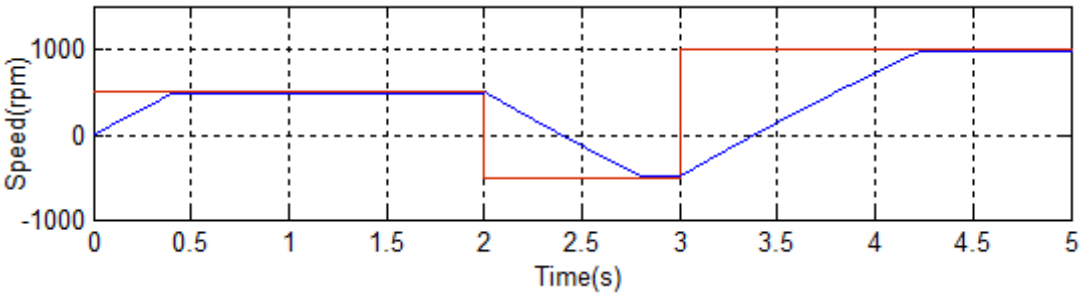

(a)

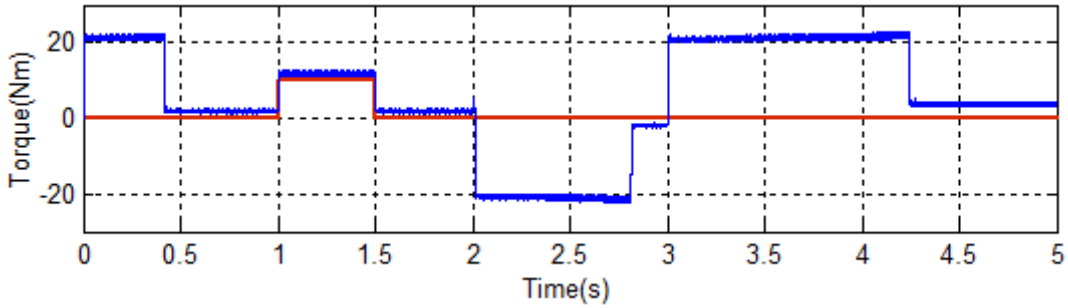

(b)

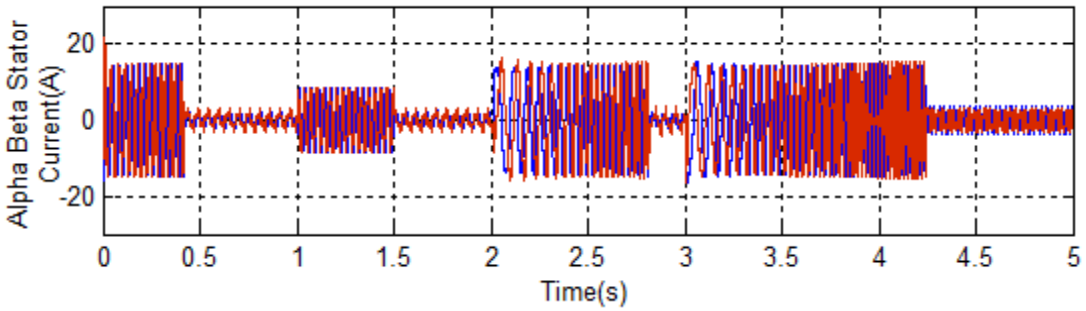

(c)

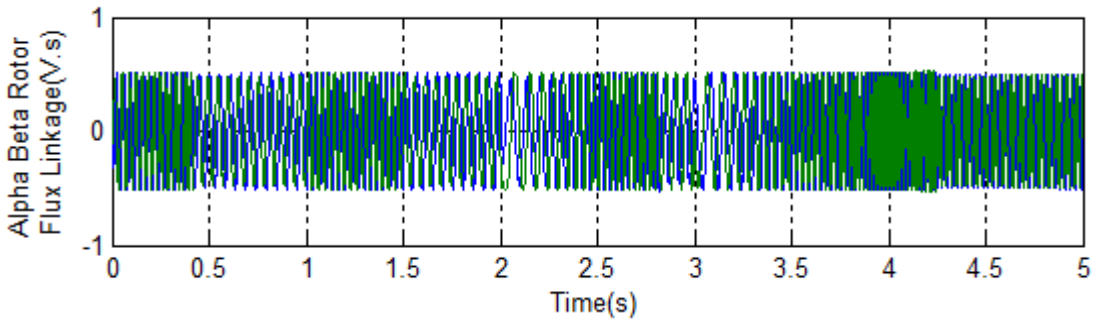

(d)

Fig.4.21 Simulation response of IM drive for starting, speed reversal and load perturbation with ILC showing: (a) motor speed (b) load torque and electromagnetic torque (c) α-β stator current components (d) α-β rotor flux linkage components

Table 4.3

Performance comparison among PI, SM and IL controllers for starting,speed reversal, light load application

Event	PI Controller	Sliding Mode Controller	Iterative learning Controller
1 Starting acceleration to 500 rpm at no load	Starting time= 0.42 s	Starting Time= 0.35s	Starting time=0.3 s
2. Shaft loading by 10N.m at steady speed of 500rpm	Speed drops on load application =7 rpm	Speed drops on load application =0.35 rpm	Speed drops on load application =0.15 rpm
3. Removal of 10 N.m shaft load torque	Speed rises to original value 501.5 rpm	Speed rises to original value 500 rpm	Speed rises to original value 500 rpm
4. Speed reversal from 500rpm to-500rpm at no load	Reversal Time=0.85s	Reversal Time=0.84 s	Reversal Time=0.72s
5. Speed reversal from -500rpm to+1000rpm at no load	Forward peak-up time =1.3s	Forward peak-up time =1.15s	Forward peak-up time =1.1s

Periodic speed and load torque tracking

There are many industrial control applications, where periodic speed and periodic load tracking is required, e.g., reversible drives in rolling mills, repetitive trajectory tracking of robots, servo control system and radar tracking. In this section performance of the feedback linearized induction motor using speed controllers namely PI, sliding mode and iterative learning controller for periodic speed and load torque tracking has been investigated. The periodic reference speed and load torque are taken as:

$\omega_r^* = 30\sin 10t$, $T_l = 10\sin 10t$

The simulation results are shown in Fig. 4.22-4.23. This shows the motor tracks the set speed. It has been observed that the α-β axis current and rotor flux components are completely decoupled even during transient condition. The robustness over external disturbance is also obtained. Chattering of torque, rotor flux and stator current is significant in PI and in sliding mode controller. The proposed ILC controller gives minimum torque ripple with reduced speed error.

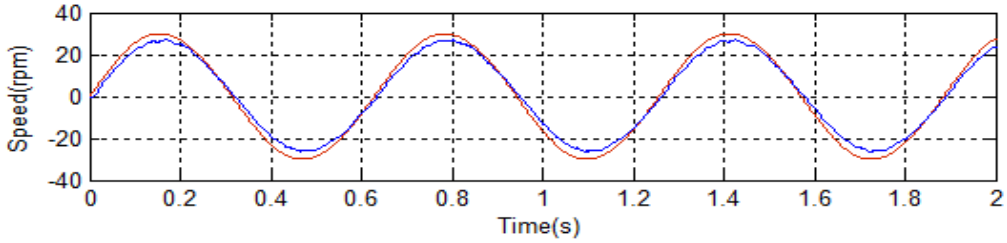

(a)

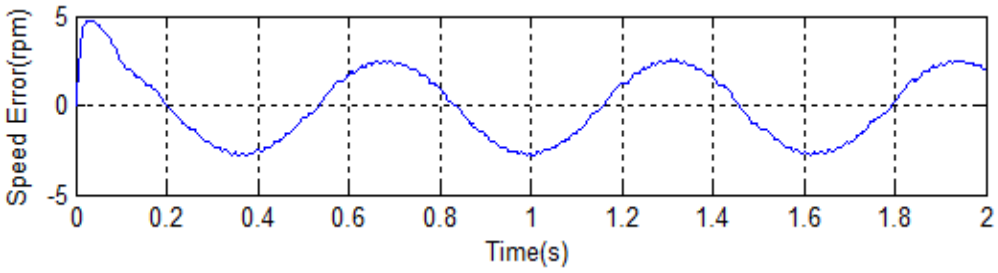

(b)

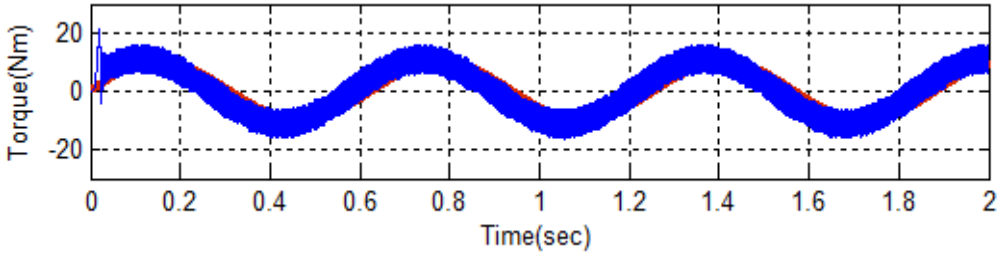

(c)

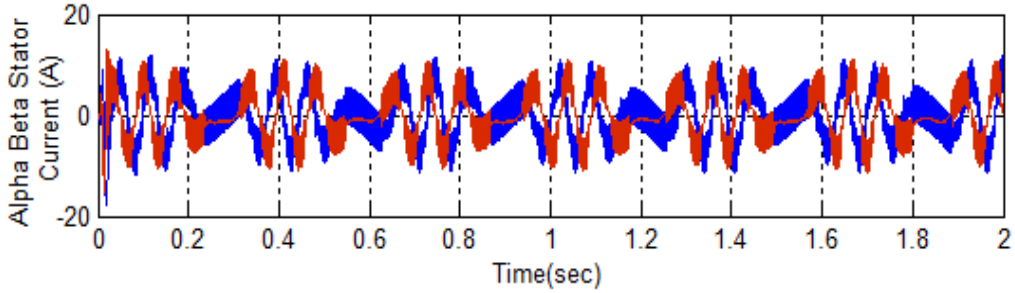

(d)

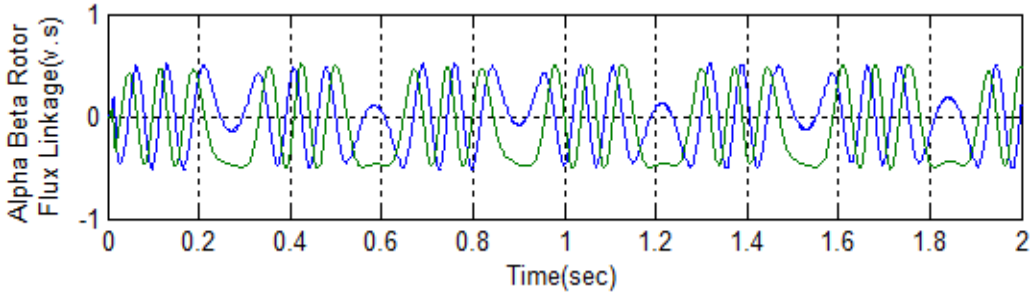

(e)

Fig.4.22 Simulation response of IM drive for periodic speed and periodic load perturbation with PI controller showing: (a) motor speed (b) motor speed error(c) load torque and electromagnetic torque (d) α-β stator current components (e) α-β rotor flux linkage components

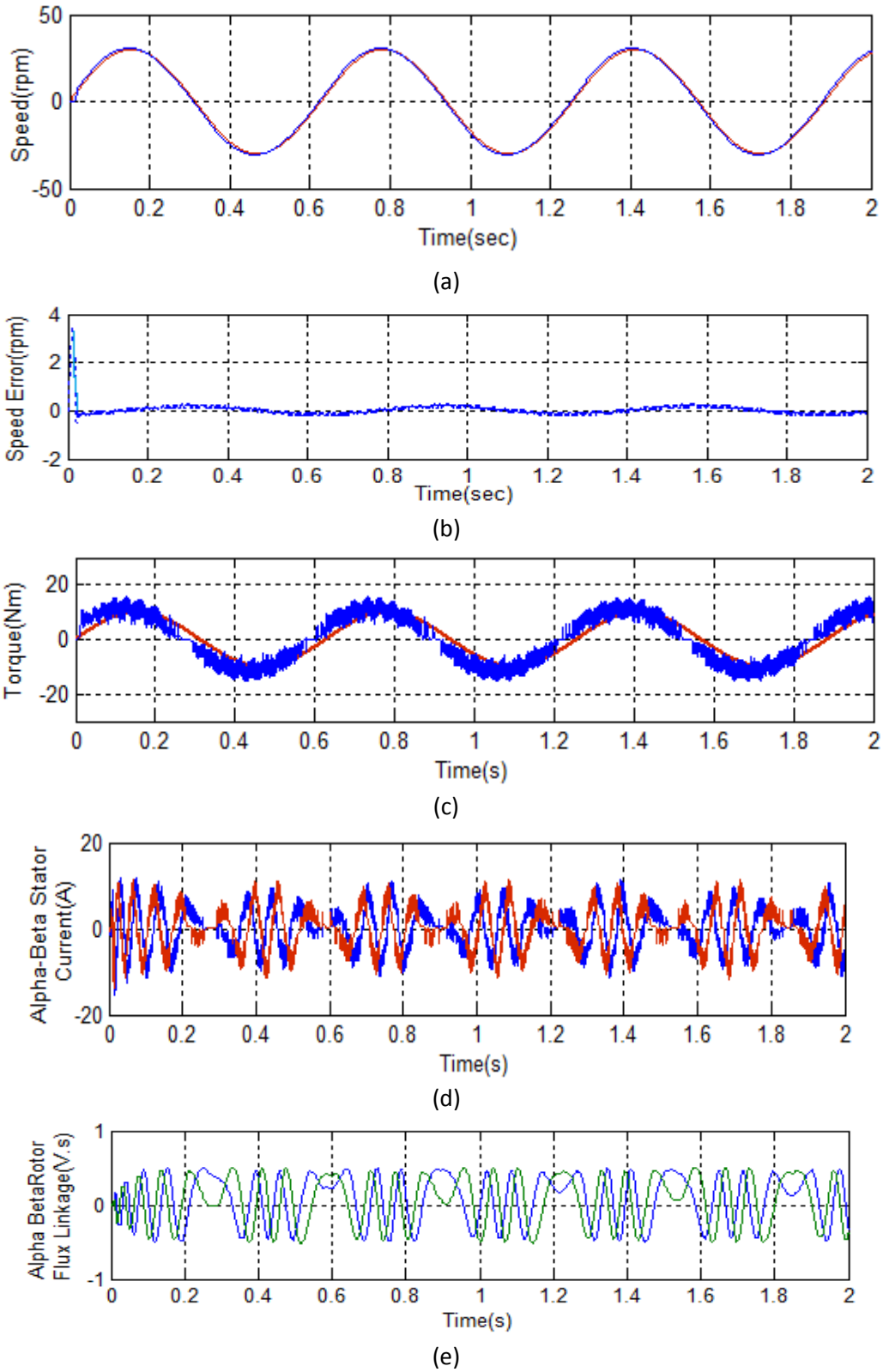

Fig.4.23 Simulation response of IM drive periodic speed and periodic load perturbation with SM controller showing: (a) motor speed (b) motor speed error(c) load torque and electromagnetic torque (d) α-β stator current components (e) α-β rotor flux linkage components

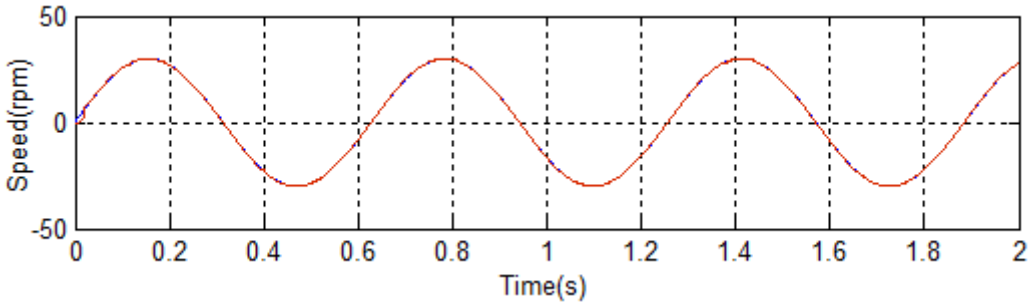

(a)

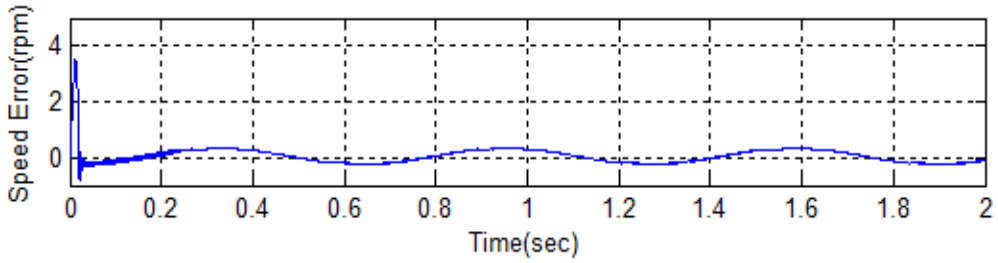

(b)

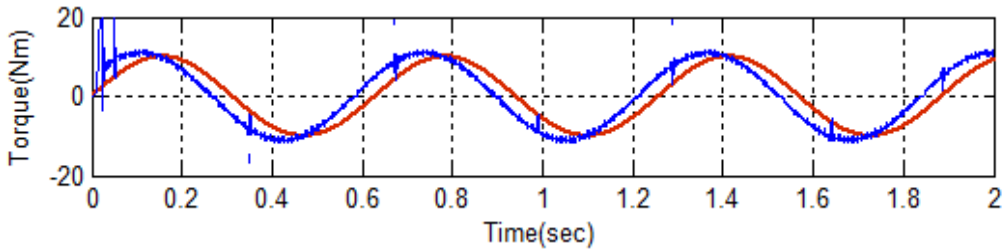

(c)

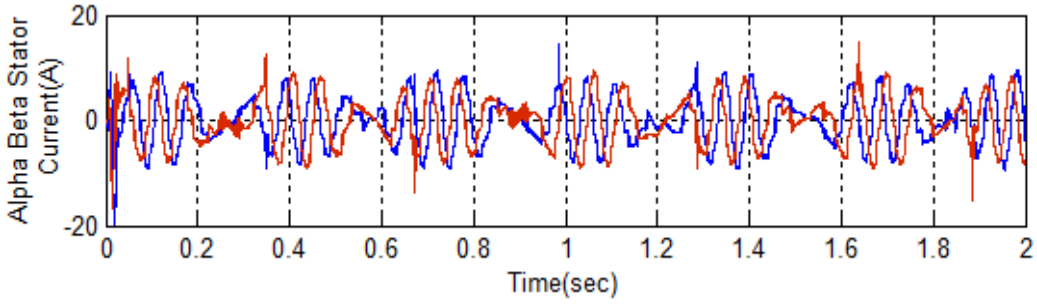

(d)

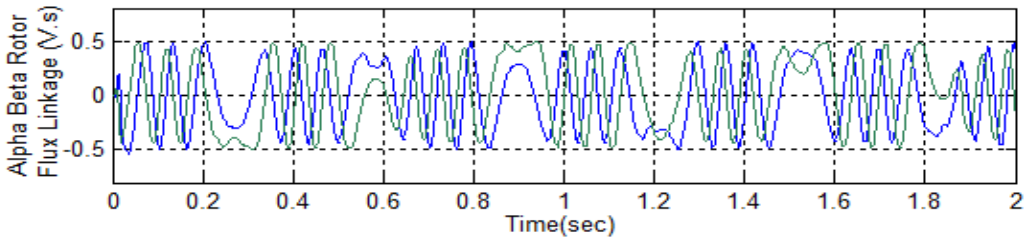

(e)

Fig.4.24 Simulation response of IM drive for periodic speed and periodic load perturbation with ILC showing: (a) motor speed (b) motor speed error (c) load torque and electromagnetic torque (d) α-β stator current components (e) α-β rotor flux linkage component

This proposed IL controller is extremely simple and gives better result in all respect such as speed error, torque, flux and winding current as clearly evident from Fig.4.24.

4.4.2 Performance Analysis of IM Drive with PI, SM and Lyapunov Function Based Controller

The responses with PI, SM and Lyapunov function based controller are shown in Fig. 4.25, Fig. 4.26 and Fig.4.27 respectively. At t=0, the closed loop drive accelerates from standstill with reference speed set at 1000 rpm, without any load. The responses show that the right from beginning motor picks up speed at constant rate and reaches its set points in 1.0s using PI controller, 0.8s with SM controller and 0.9s with Lyapunov Function based controller. Remarkable ripple in torque is observed in torque response with PI controller, SM controller but with Lyapunov controller the ripple is very small. When IM is running at steady state speed of 1000 rpm, a load torque equal to 16 Nm. is applied. The disadvantage in steady state speed error on load is observed in case of PI and sliding mode. In case of Lyapunov function based controller the drop is near to zero on load. It is due instantaneous correction of error. It is clearly established from simulation results that Lyapunov function based controller gives decoupling at all stages, reduces torque ripple and better rotor flux and stator current response and hence better than PI controller and SM controller. The performance comparison among these controllers is shown in Table 4.3.

Table 4.4

Performance comparison among PI, SM and Lyapunov Function based controllers for high speed and heavy load

Event	PI Controller	Sliding Mode Controller	Lyapunov Theory Based Controller
1.Starting acceleration to 1000rpm at no load	Starting time=1 s	Starting Time= 0.8s	Starting Time=0.9s
2. Shaft loading by 16N.m at steady speed of 1000rpm	Speed drops on load application 50rpm	Speed drops on load application 40 rpm	Speed drops on load application rpm=0
3. Removal of 16 N.m shaft load torque	Speed overshoot original value 1.5 rpm	Speed overshoot original value 0.00 rpm	Speed overshoot original value 0.0 rpm

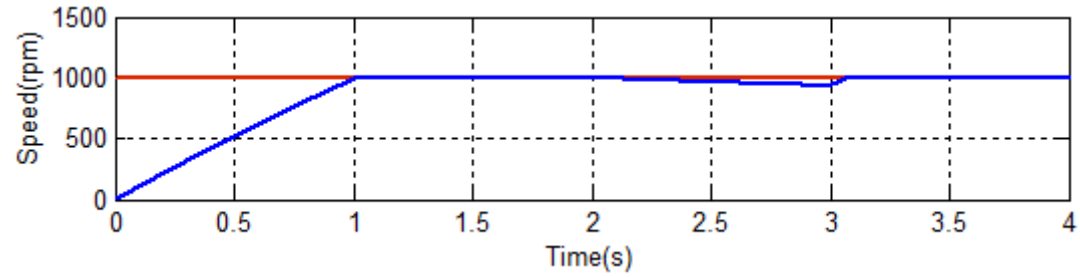

(a)

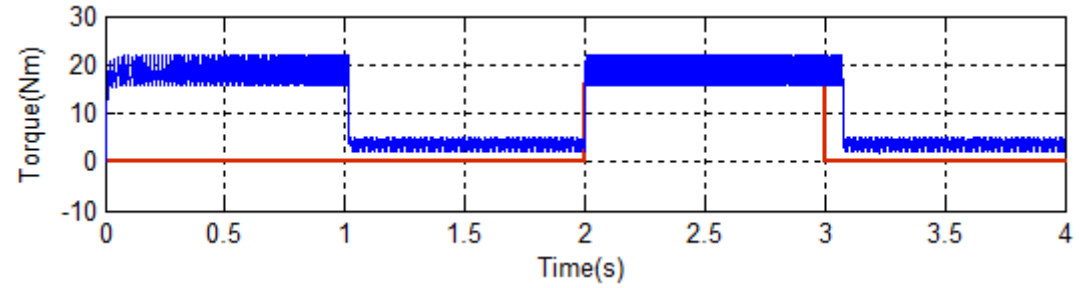

(b)

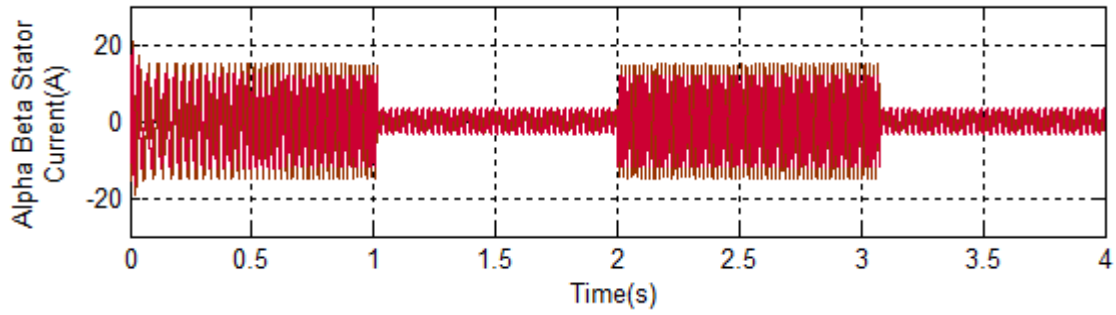

(c)

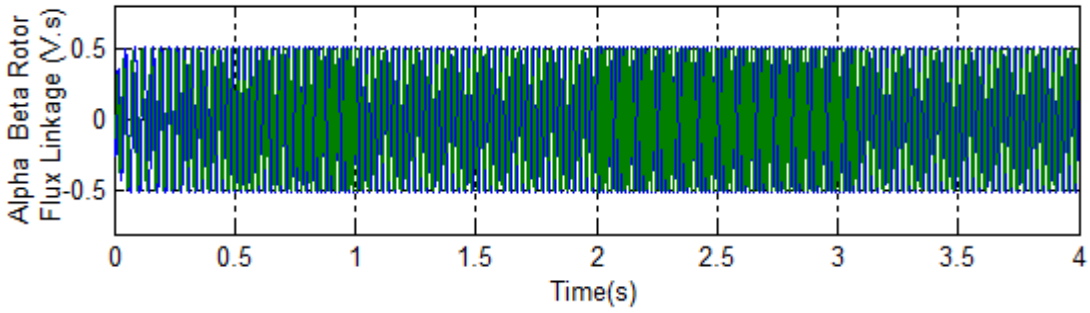

(d)

Fig. 4.25 Simulation response of IM drive for 1000 rpm speed step change and heavy external load application with PI controller showing (a) motor speed (b) load torque and electromagnetic torque (c) α-β stator current components (d) estimated α-β rotor flux linkage components

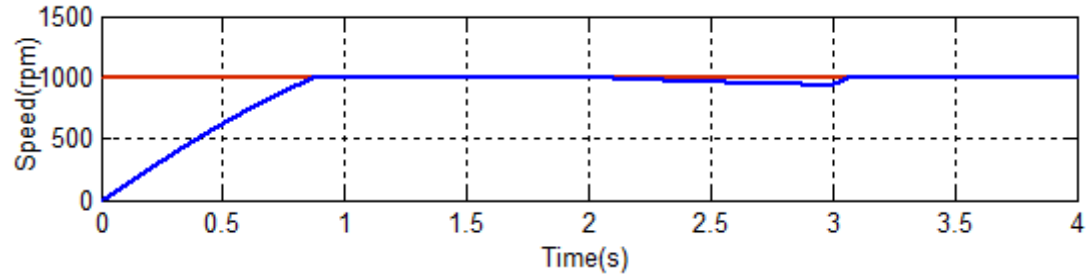

(a)

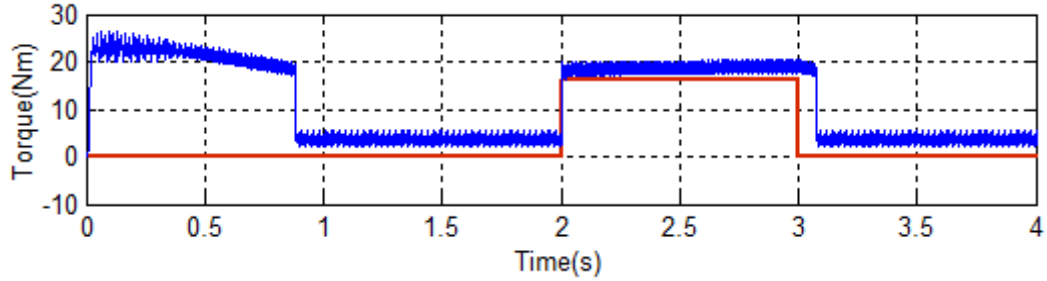

(b)

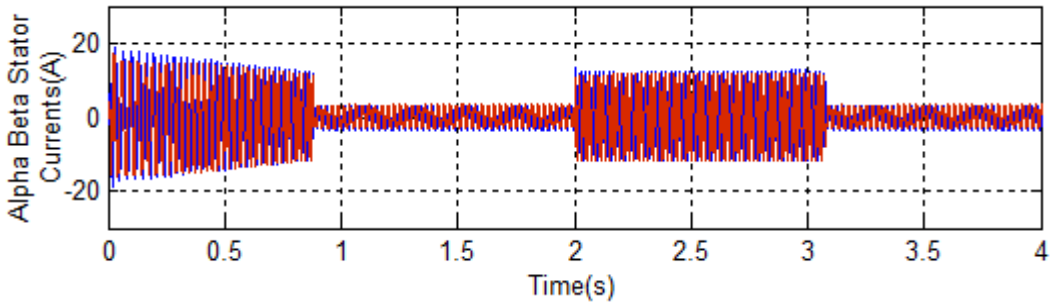

(c)

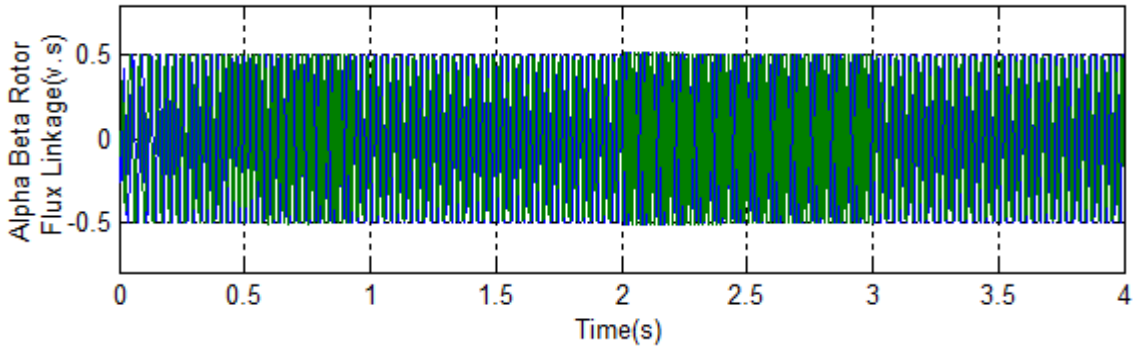

(d)

Fig. 4.26 Simulation response of IM drive for 1000 rpm speed step change and heavy external load application with SM controller showing (a) motor speed (b) load torque and electromagnetic torque (c) α-β stator current components (d) estimated α-β rotor flux linkage components

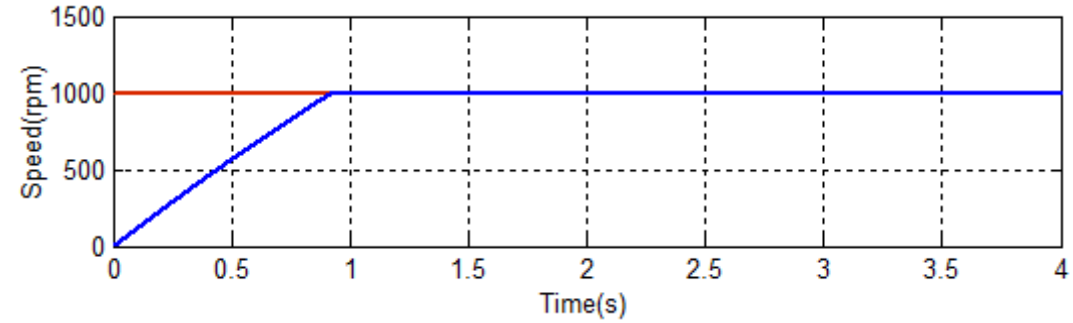

(a)

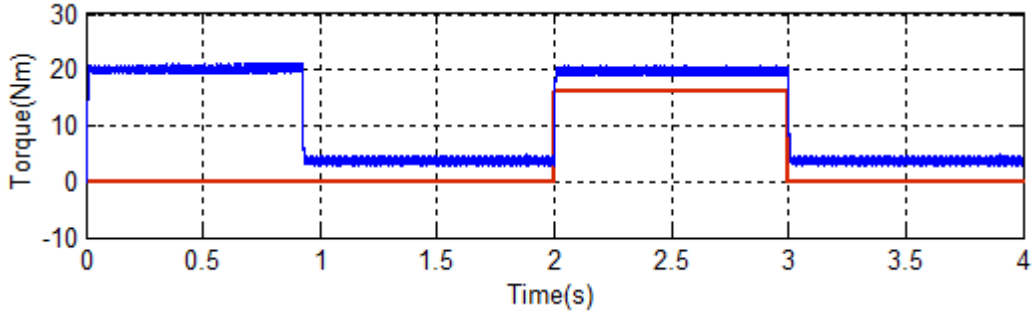

(b)

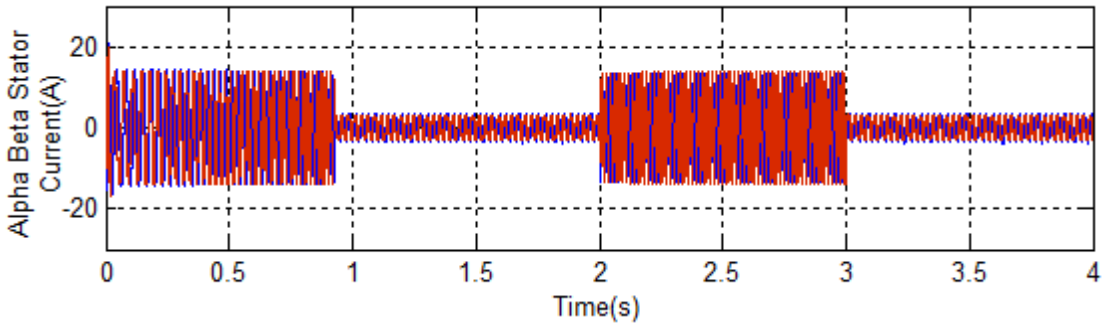

(c)

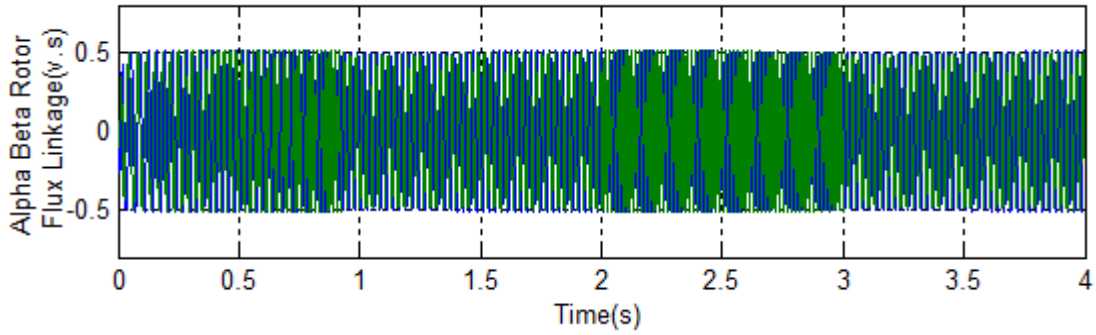

(d)

Fig. 4.27 Simulation response of IM drive for 1000 rpm speed step change and heavy external load application with Lyapunov function based controller showing (a) motor speed (b) load torque and electromagnetic torque (c) α-β stator current components (d) estimated α-β rotor flux linkage components

4.5 Summary of the Chapter

Initially the function of different blocks of the proposed drive system has been presented. The mathematical equations associated with different types of controller have been outlined. MATLAB/SIMULINK model with controllers used in simulation study has been presented. Simulation results obtained has been presented for analysis and comparison. In course of analysis it has been observed that some of the controllers are suitable particular situation. More over simulation results clearly indicates that an iterative learning controller is the most versatile.

Chapter – 5

Real-Time Simulation of the Induction Motor Drive

5.1 General

The traditional model-based simulation packages, such as PSIM, PSCAD, MATLAB can easily handle a small–scale application. When model size and complexity increases, these fail to cop up to the requirements due to either speed accuracy or solution accuracy. This is due to the limitation of underlying solution algorithm, sequential computation and memory restriction. For real implementation of the model based system, the system model is to be first converted into the differential equation or state-space form by programming. It is time consuming when complexity of the system increases. The RT-LAB software has an automatic code generator, which generate code for prototyping and successful implementation of real time execution. Therefore, the RT-LAB tools are desirable necessities, especially in electric motor drives and power electronics [78]-[79].

This chapter describes in brief about RT-LAB real-time simulator and the process of implementation of MATLAB/SIMULINK model on real-time simulation platform. The feedback linearized induction motor using different speed controllers designed in the previous chapters are developed and implemented in real- time simulator. The simulation study under various operating conditions like step change of speed, step change of load torque, periodic change of speed and torque are investigated. Controller performances are compared, analyzed and observations are recorded.

5.2 RT-LAB Simulator

RT-LAB is a powerful, modular, distributed real-time simulator for quick implementation of Simulink model based-design system on real-time platform using hardware-in-loop and off-line simulation. Nearly ten years ago this technology started with huge analog simulator, then improved to hybrid and presently fully digital real-time simulators are available. Simulink model based design methodology is widely used by students, researchers and engineers, because it enables them to focus on their design, algorithms, system topologies and different innovative ideas, rather than dedicating time and effort to the intricacies of writing the real-time code for implementing the software on the real-time platform (microcontroller, DSP, FPGA, etc).The RT-LAB has provision of automatic code generator, for prototyping, implementation and true execution in real –time. Therefore, the RT-LAB tools are no longer a luxury in modern system design, especially in electric motor drives and power system.

The general architecture of RT-LAB is shown in Fig.5.1. It comprises of, the host and a target. The host is a PC, in which RT-LAB and MATLAB packages are loaded. Tools are used to design and develop the system model, first in MATLAB and then with some modification in RT-LAB environment. The MATLAB model processing is sequential where individual block has different step length as per requirements. For real-time execution RT-LAB model works in parallel with fixed step size.

The host PC interfaces and communicates with the target through Ethernet. The target comprises of one or two, Intel or AMD processor, each processor can be single, dual or quard core, so that a single target box can hold as much as 8 processing cores communicating by shared memory, and each core simulating a simulink subsystem. Such a distribution of task makes processing parallel. Thus speed of execution becomes closed to the real system.

In addition, RT-LAB uses Xilinx FPGA time target, and this target requires extra block using Xilinx Blockset, and the VHDL code is then automatically generated from the block diagram, compiled and uploaded to FPGA. The engineer can then design extremely fast control algorithms, or model extremely fast sampling

plant, and target them to FPGA without hand coding and without the need of programmable logic chip expertise.

In order to connect the real-time system with real world hardware devices or physical plant, input/output (I/O) is configured through custom blocks, supplied with RT-LAB as a Simulink toolbox (analog, digital, PWM, encoder etc). One has to drag and drop the I/O block to the graphic model. The RT-LAB manages the automatic code generation so as to direct the model's data flow onto the physical system in order to meet the stringent I/O speed and accuracy requirement of power electronics and drives. It uses digital I/O boards controlled by a 100 Mhz FPGA chip yielding a PWM, encoder with resolution of 10ns, 16- bits simultaneous fast analog-digital converter.

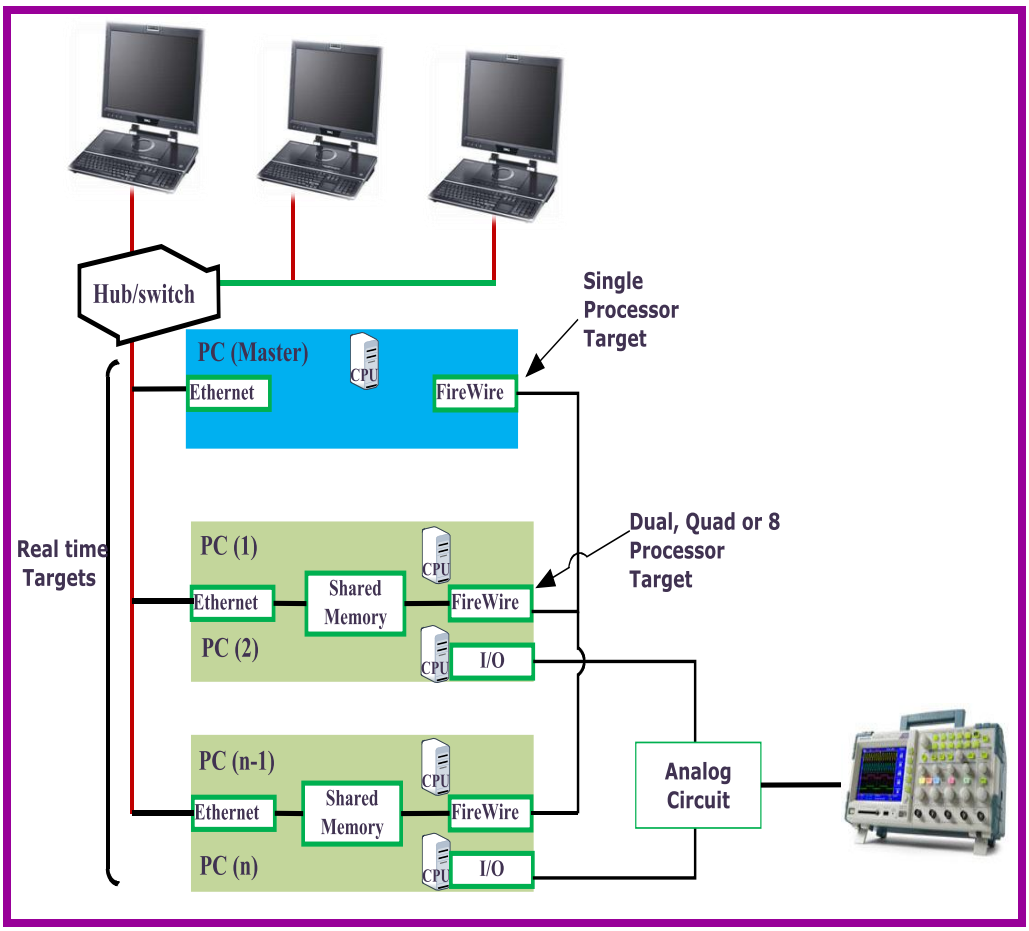

Fig. 5.1 RT-LAB Simulator Architecture

5.3 Real-Time Simulation of an IM Drive

The steps for RTDS implementation of an induction motor drive is Fig. 5.2 to 5.8. The process covers following steps:

- Building a MATLAB block model
- Grouping the computation into subsystems
- Adding OpComm blocks to enable communication
- Identifying state or state-derived variables to maximize parallel execution
- Setting the proper simulation parameters
- Registering initialization function in RT-LAB

All above steps are described in brief as under.

Building a MATLAB block model

The simulink model of the complete system shown in Fig.5.2 is converted to real-time model for uploading to RT-LAB platform to conduct real-time simulation.

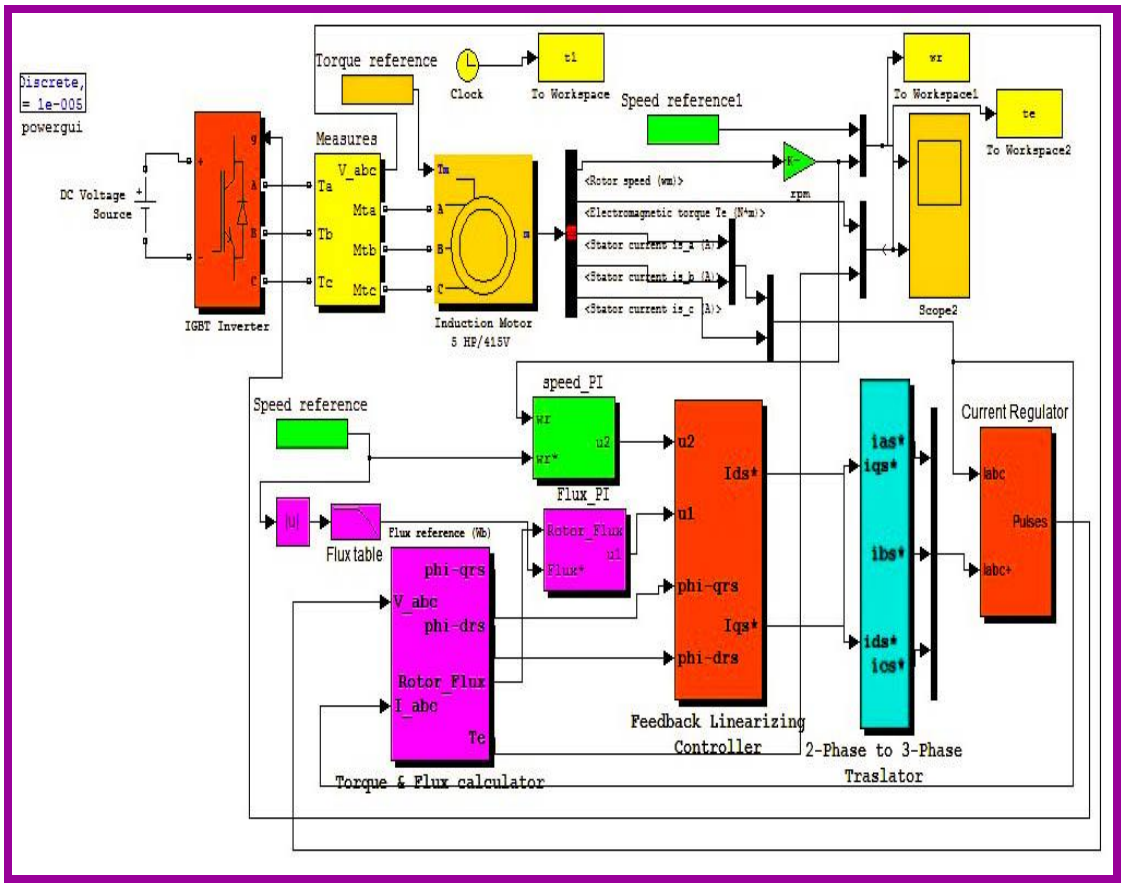

Fig. 5.2 Building of a MATLAB simulink block model of a linearized induction motor using PI speed and flux controller

Grouping the Computation into Subsystems

The three separate subsystems are constructed with the combination of different functional block of the MATLAB model shown in Fig. 5.3. According to the RT-LAB naming convention, these subsystems are named with a prefix identifying their function. The prefixes are described as:

SM_master subsystem (always one): It contains the computational elements of the model. In this scheme, blocks namely induction motor, power supply, voltage, current and flux measurement block, set speed, flux and load torque blocks are assembled to construct sm_ master subsystem (Fig.5.4).

SS_slave subsystem (s) (any number): In general it contains the computational elements of the model when distributing the processing across multiple nodes. In this scheme one ss_slave subsystem is configured by grouping a speed controller, a flux controller, a feedback linearization controller and a flux estimator. The details of ss_slave is shown in Fig.5.5.

SC_console subsystem (at most one): In general it includes all user interface blocks (scope, slider gains, manual switches). For this scheme it contains three scopes. It is shown in Fig.5.6.

These conventional named subsystems are mapped directly to logical nodes. The SC subsystem is the “host” while SM is the target. For distributed computation, the SS subsystems allow us to dispatch additional computation on other targets. Each CPU of a target (physical node) is considered a logical node and distribution of the computation is done as follows:

1 target	SM subsystem only
2 target (2 CPU)	SM and SS subsystems
3 target (3CPU)	SM and 3 SS subsystems

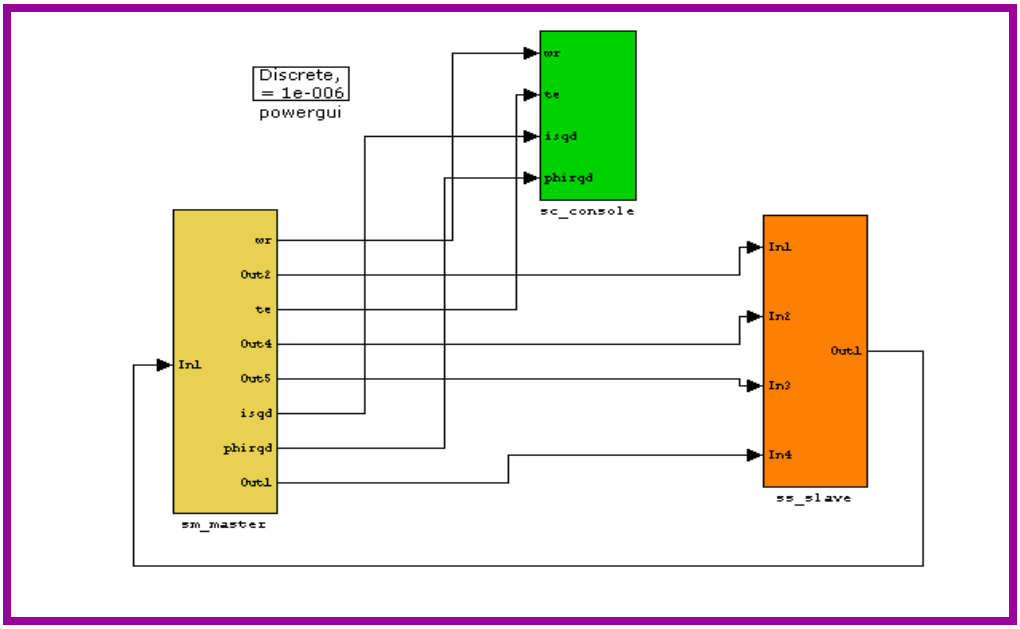

Fig.5.3 Grouping the induction motor MATLAB model into the subsystems namely sm_master, ss_slave and sc_console

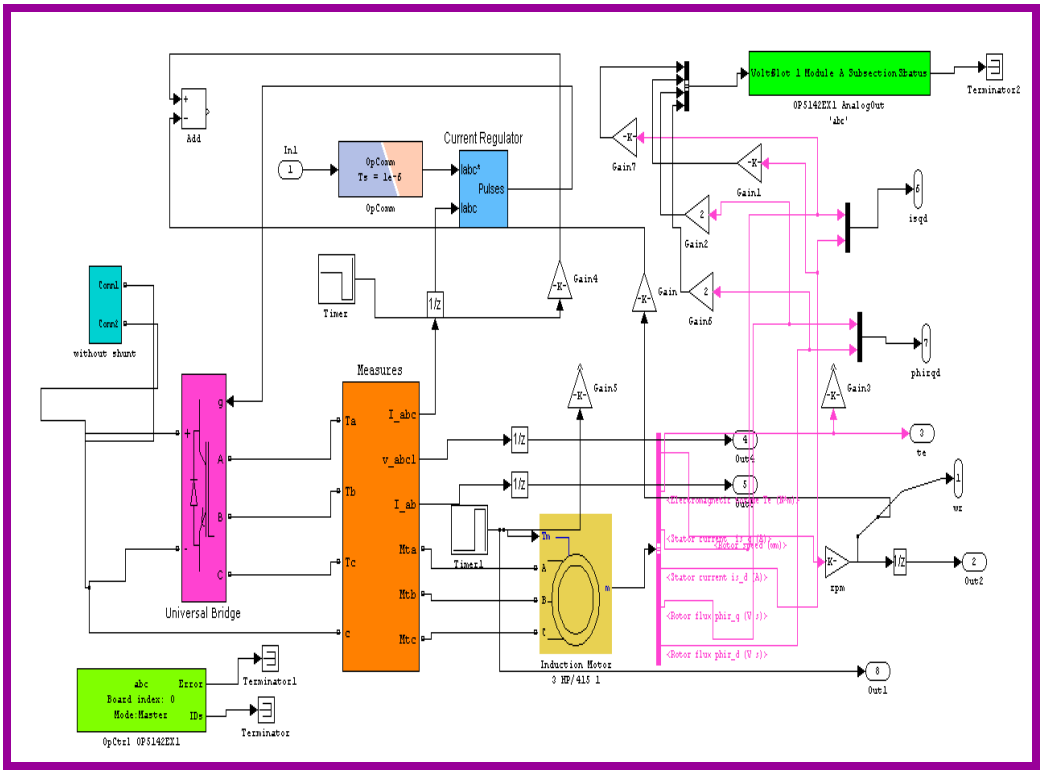

Fig.5.4 Configuration of the sm_master subsystem

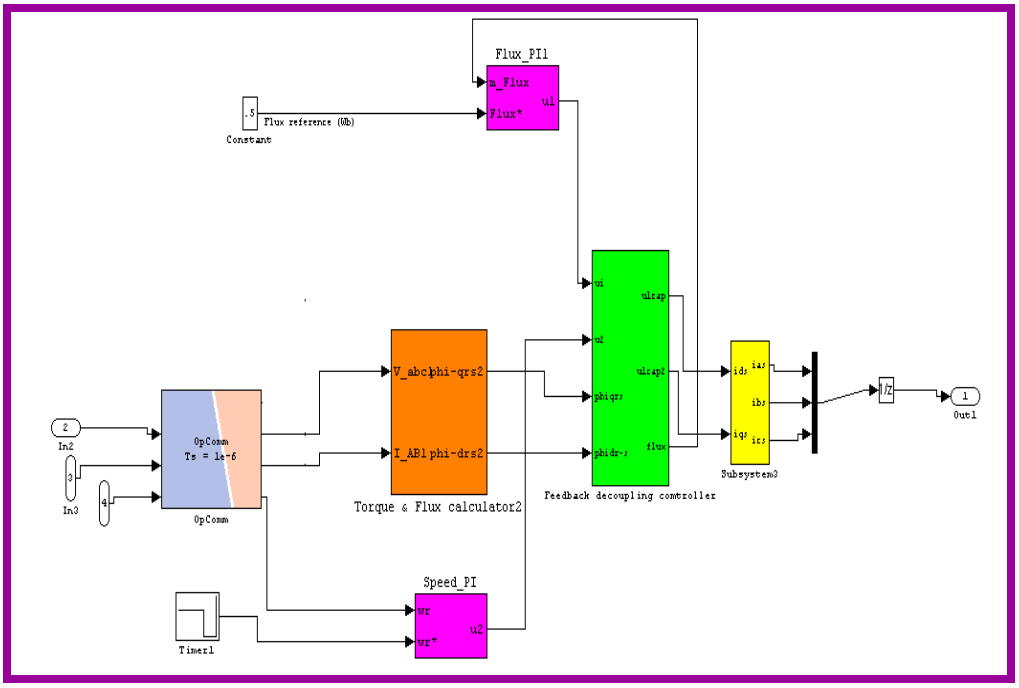

Fig.5.5 Configuration of the ss_slave subsystem

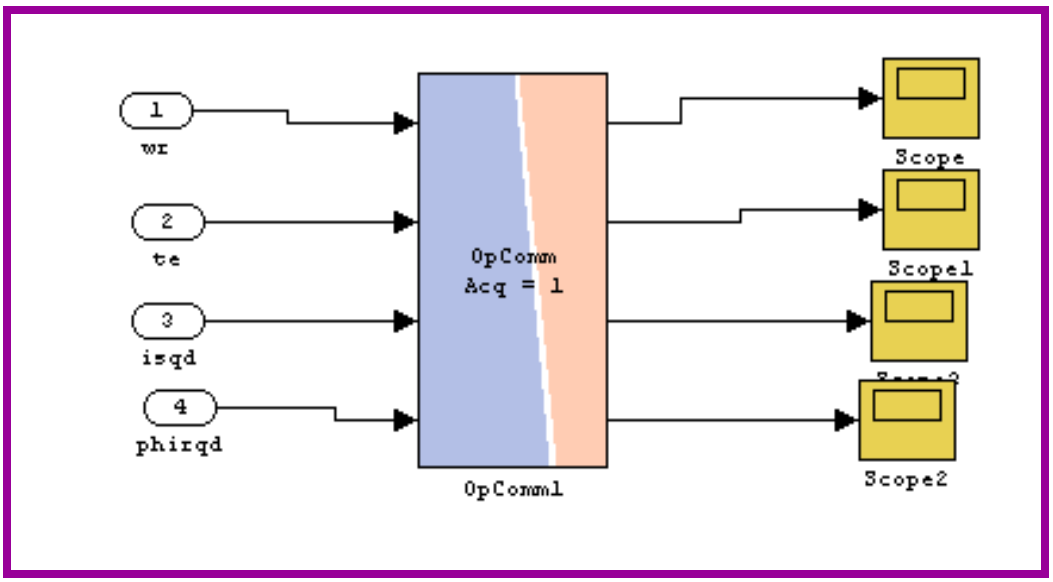

Fig.5.6 Configuration of the sc_console subsystem

- **Adding OpComm blocks to enable communication**

The RT-LAB uses OpComm blocks to enable and to save communication information. It includes both communication between the command station and computation nodes and communication between computation nodes in a distributed simulation scenario. All inputs to the top-level subsystems must first go through an

Opcomm block before they can be used. It is present in the RT-LAB toolbox in Simulink library. The inclusion of OpComm in each subsystems for this work can be seen in Fig 5.3 to Fig. 5.6.

- **Identifying state or state-derived variables to maximize parallel execution**

The RT-LAB maximizes parallelism when computation nodes exchange only priority signals. For this slave and master subsystems must compute and send their outputs before they read their inputs (within the same step). For this identification of state or state –derived signals is needed in order to enable parallel computation of subsystems. The state can be defined as an output (signal) which is computed only from preceding inputs or outputs. The delay by one step is connected to the output signals of each block.

- **Setting the proper simulation parameters**

The real-time simulation should not miss its schedule and it should run as fast as real life. To meet these requirements we should avoid iterative solving methods. As in general we use variable –step in MATLAB simulation, which is iterative. In the RT-LAB, fixed step solver is used, because simulation requires determinism of the computation done at every step. In this work a fixed step solver named ODE4 is selected and 1 microsec is taken for a fixed step size (Fig5.3 to 5.5).

- **Registering initialization function in RT-LAB**

Upto RT-LAB model all process is over. Then it is required to resister the initialization (or load the workspace) from RT-LAB. Then the model becomes ready to run under RT-LAB. The photographs of the experimental setup are shown in Fig. 5.7 and Fig. 5.8.

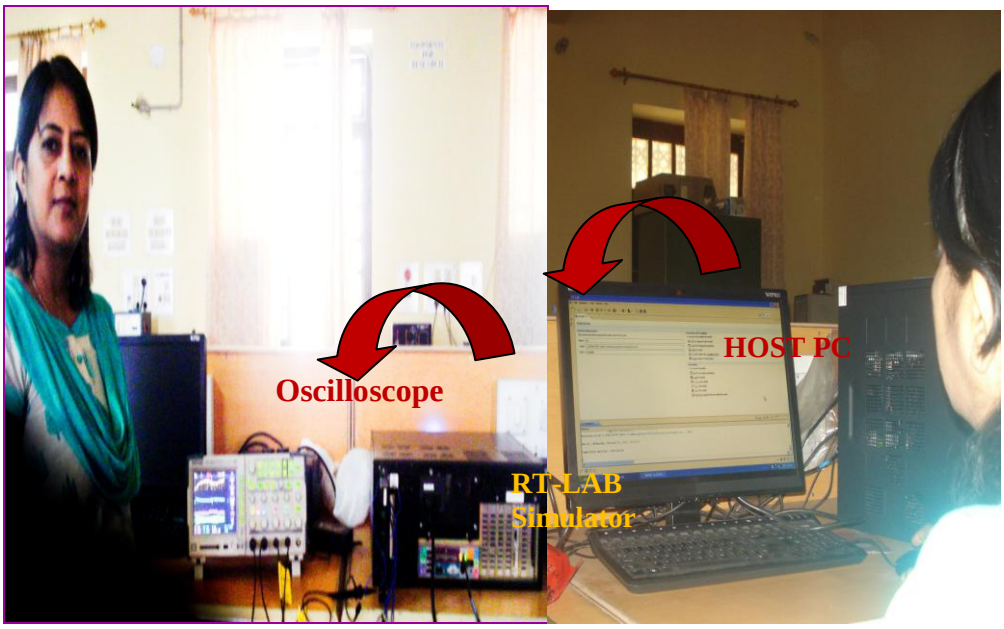

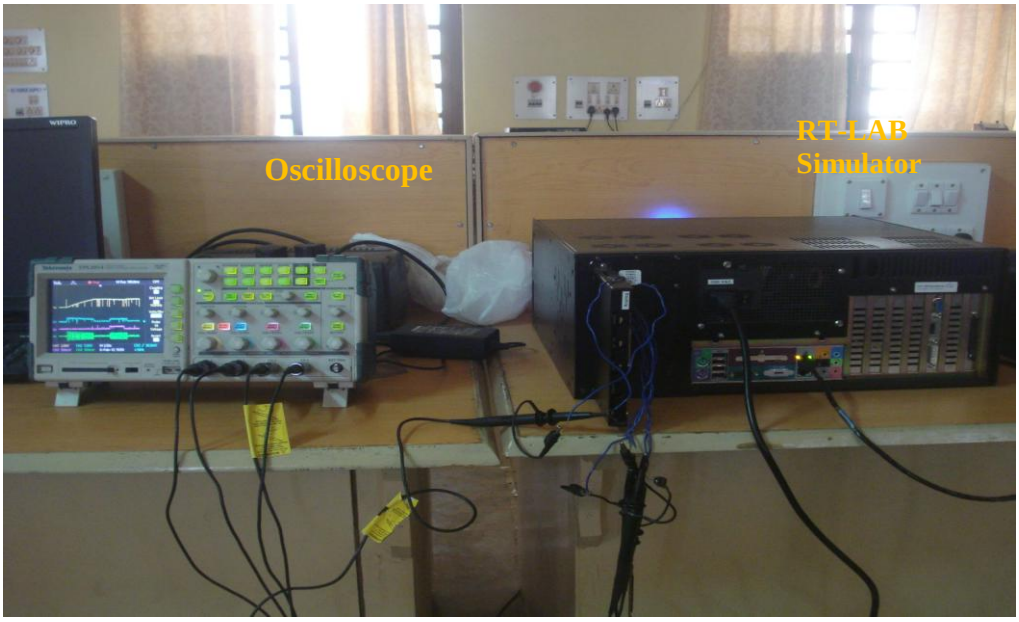

Fig. 5.7 Photographs of experimental setup with RT-LAB simulator interfaced to an oscilloscope and PC

Fig. 5.8 Photographs of experimental setup with RT-LAB simulator interfaced to an oscilloscope performance showing speed reversal tracking

5.4 Real-Time Simulation Results and Discussions

The performance of the feedback linearized induction motor drive system with PI controller, sliding mode controller, iterative learning controller and Lyapunov function based controller are validated by implementation of the schemes on the real-time simulator (RT_LAB). The responses are taken in the oscilloscope connected to the analog I/O terminal of the RT_LAB hardware system. These responses are shown in Fig. 5.9 –Fig. 5.17.

5.4.1 Performance Comparison of IM Drive between PI and PI with Torque Compensator

The feedback linearized induction motor drive system with PI controller and PI with torque compensator are implemented in the real-time simulator. The specifications and parameters of the induction motor used in the experiment are as given in Table 2.1. Simulations are done with a step change in speed from 0 to 500 rpm at t=0, and application of 10 Nm load at t=1s and removal at t=1.5s. Simulation results corresponding to speed response, torque response, rotor flux components and stator current components are presented corresponding to both the schemes. The discussions on the results are given below.

Results with PI controller

Feedback linearized induction motor drive with designed PI controller is simulated and tested in RT-Lab environment. The results are shown in Fig. 5.9-Fig. 5.10.

Starting Dynamics: The reference speed is set at 500 rpm with a current limit set at the rated value. Therefore, the starting current is the rated current when the motor builds up the required starting torque to reach the set speed. The motor reaches its set speed in 0.35 s. When the speed error becomes zero, the winding current also reduces to no load value and the developed torque becomes equal to no load torque as observed in the starting response shown in Fig. 5.9. The rotor flux remains constant throughout. The purpose of feedback linearizing controller is achieved through decoupling between flux and speed control.

Load Perturbation: When the motor is running at steady speed of 500 rpm, a load torque of 10 N.m is applied at t =1.0 s. Sudden application of the load causes an instantaneous fall in the speed of the motor. In response to drop in speed, the output of the speed controller responds by increasing the set current to corresponding value. Therefore, the developed electromagnetic torque of induction motor increases, and the motor speed settles at the reference value with the increased winding currents. When the motor is operating at steady state on load, suddenly load is removed at t=1.5s. Consequently, the stator current also reduces to the no load value. Only negligible speed drop on load application and similarly negligible overshoot on load removal are noted. However the presence significant torque ripples may be seen in T_e.

Results with PI with Fuzzy Torque Compensator

The same set-up is tested with PI with fuzzy torque compensator, for same speed and load changes , and corresponding results are shown in Fig. 5.11 and Fig. 5.12.

Starting Dynamics: It is observed that proposed scheme with fuzzy torque compensator results in a better performance than the PI controller. The torque ripple is reduced significantly compared to only PI controller. The fuzzy torque compensator with only 16 fuzzy inference rules improves overall performance of the drive system. With fuzzy torque compensator the drive reaches the set point in 0.25s compare to 0.35 s without fuzzy torque compensator. Fig 5.12 shows better stator current components, which are than previous result (Fig.5.10).

Load Perturbation: The scheme with fuzzy torque compensator exhibits robustness under external load empact. When motor is loaded with 10 Nm at t=1.0s, the speed deep is smaller compare to the previous scheme. When the motor is running at steady state on load, and suddenly load is removed at t=1.5s, it does not lead to any overshoot. In this RT-Lab implementation results are much closed to SIMULINK results and thus validated.

5.4.2 Performance Analysis of IM Drive with PI, SM and ILC

The feedback linearization scheme is implemented for IM drive in RTDS environment with PI, SM and ILC. The drive performance is recorded under similar condition for all three controllers. The results of various operating conditions are presented and analyzed one by one. The responses of the drive system are shown in Fig. 5.13 (a), Fig.5.13 (b) and Fig.5.13 (c) for PI, SM and ILC respectively.

Starting Dynamics

The response of state change of speed from zero to 500 rpm with rated current limit is shown in Fig. 5.13. The right from beginning motor picks up speed at constant rate and reaches its set points in 0.4s with PI controller, 0.35s with SM and 0.25s with ILC without any overshoot. The speed response with ILC is found to be the best. Remarkable ripple in torque developed can be seen with PI and SM controllers, but comparatively lesser in case of ILC.

Load Perturbation

When the motor is running in steady state at 500 rpm, a load torque of 10 Nm is applied. Sudden application of load tends to cause a small drop in the speed of the motor. The speed controller responds by increasing the reference torque value. Therefore, the developed electromagnetic torque of the induction motor increases, causing the motor speed to settle to the reference value, with the increased stator currents as shown in Fig.5.13.The same load is suddenly removed which causes a small overshoot in rotor speed. The overshoot is present for very short time as speed controller acts immediately reducing the developed torque. In case of all the controllers there is no permanent drop in speed and overshoot when load torque is applied and same is removed. After removal of load, the stator current also reduces to the no load value.

Speed Reversal

The effect of speed reversal on the performance of the drive system with controllers like PI, SM and ILC are recorded. When the induction motor is running at state speed of 500 rpm, the set speed is changed to -500 rpm.The reversal time with PI controller is 0.8s, with SM controller is 0.7s, whereas it is 0.5s for ILC.The performance of the drive system for larger change in speed from -500 rpm to1000 rpm is also recorded with all three controllers. The time taken for speed reversal is larger in this case. The PI controller performance is not as satisfactory as in SM and ILC.

Periodic Speed and Load Change

There are many industrial applications where drive has to meet the periodic nature of speed and the load. The three controllers under test for types of periodic speed and periodic torque.

Set periodic speed (rpm): $\omega_r^* = 30\sin 10t$,

External periodic load torque (Nm): $T_l = 10\sin 10t$

The responses of the drive system with all three controllers are shown in Fig. 5.14 to Fig. 5.16. It shows that the motor tracks the set speed in all cases. During periodic

speed and load tracking operation motor remains always in transient state even then the drive system runs at the set speed in all cases without any deviation. It may also be observed that α-β stator current and rotor flux components are completely decoupled even during transient condition. The robustness over external disturbance can also be noted. Comparatively SM and ILC give better transient response, lesser speed error and smother current waveform than PI controller.

5.4.3 Performance Analysis of IM Drive with PI, SM and Lyaponuv Function based Controllers

The feedback linearization scheme is implemented in RTDS environment individually with PI, SM and Lyapunov function based controllers. The real time results with PI, SM and Lyapunov function based controller are shown in Fig. 5.17 (a), Fig.1.17 (b) and Fig.1.17 (c) for larger step change in speed and heavy load. At t=0, the closed loop drive accelerates from standstill with reference speed set at 1000 rpm, without any load. The responses show that the right from beginning motor picks up speed at constant rate and reaches its set points in 1.0s using PI, with SM 0.75s and 0.6s with Lyapunov function based controller. An overshoot is observed during starting in case of PI and SM. The overshoot is eliminated in Lyapunov function based controller, which is the indication of robustness of this controller. Remarkable ripple in torque is found in torque response with PI and SM, but with Lyapunov function based controller the ripple is very small. When motor is running at steady state speed of 1000 rpm, a load torque equal to 80% Nm is applied at t=2.0s. Sudden application of load causes instantaneous fall in the speed of the motor is significant with PI and SM but speed drop with Lyapunov function based controller is zero.

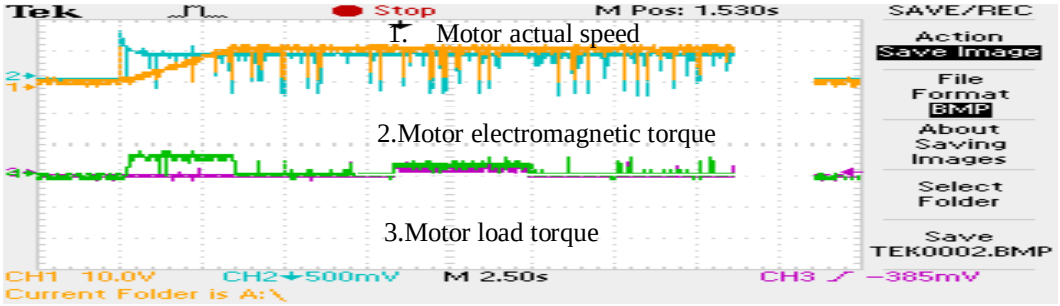

(a)

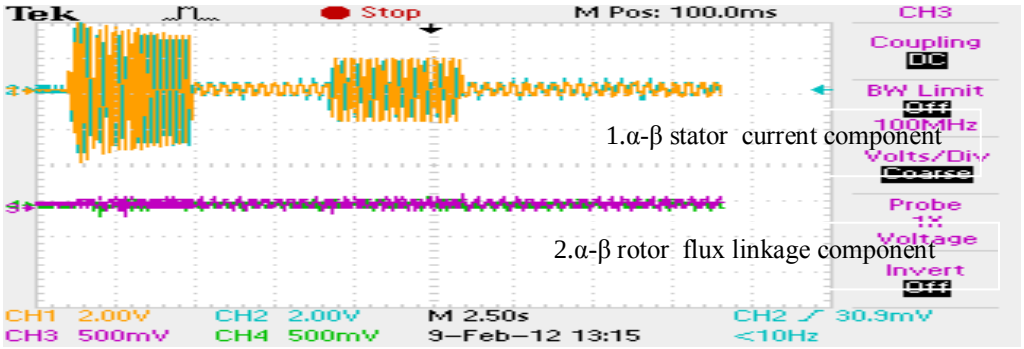

(b)

Fig. 5.9 RTDS Hardware results for starting, and load perturbation of IM drive with PI controller illustrating; (a) 1. motor set speed (rpm), 2. motor actual speed (rpm), 3. electromagnetic and 4. load torque (Nm) ,(b) 1. α-β stator currents (A) and 2. α- β rotor flux linkages (V.s)

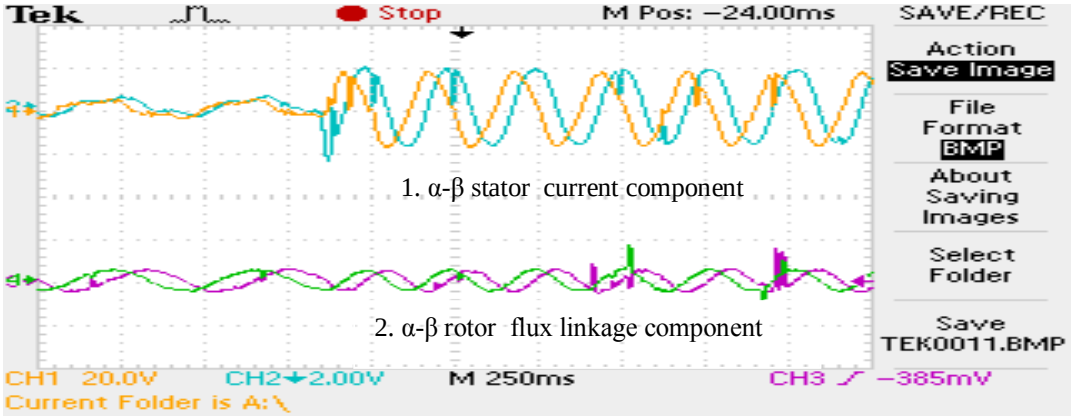

Fig. 5.10 RTDS Hardware results with PI controller for starting dynamics under no load illustrating: 1. α-β stator currents (A) and 2. α- β rotor flux linkages (V.s)

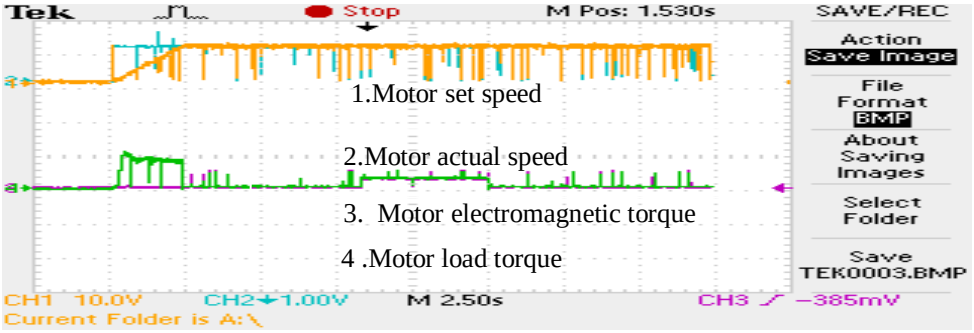

(a)\

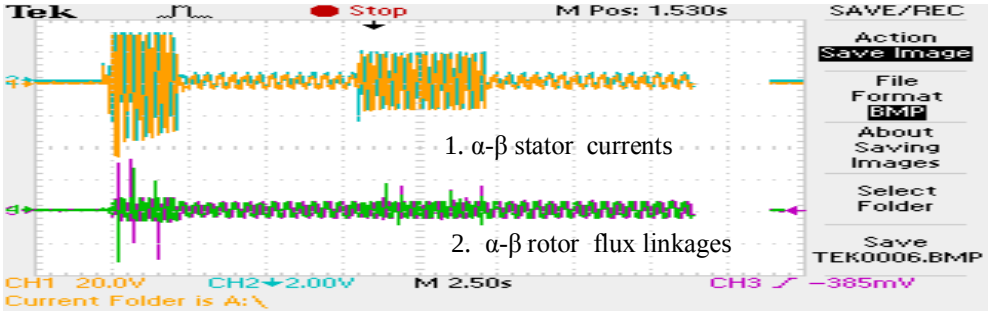

(b)

Fig. 5.11 RTDS Hardware results for starting, and load perturbation of IM drive with PI and fuzzy torque compensator illustrating; (a) 1. motor set speed (rpm), 2. motor actual speed (rpm), 3. electromagnetic and 4. load torque (N.m) (b) 1. α-β stator currents (A) and 2. α- β rotor flux linkages (V.s)

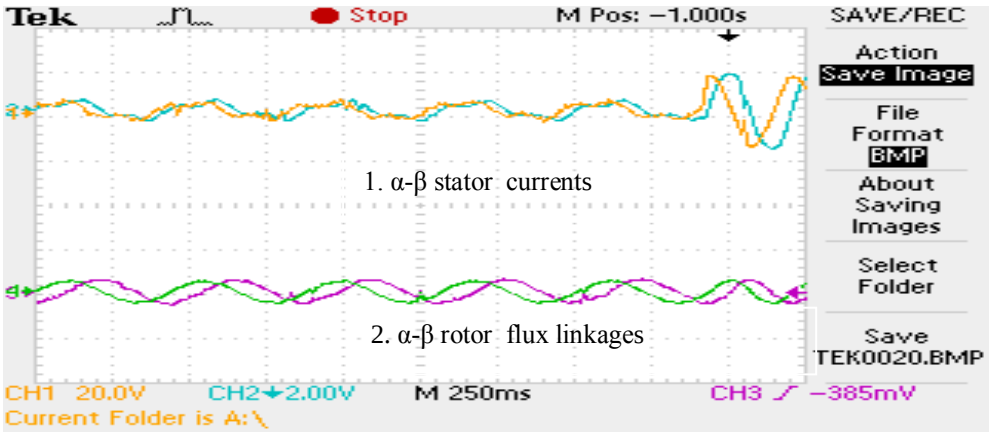

Fig.5.12 RTDS Hardware results for PI with fuzzy torque compensator for starting, dynamics under no load illustrating 1. α-β stator currents (A) and 2. α- β rotor flux linkages (V.s)

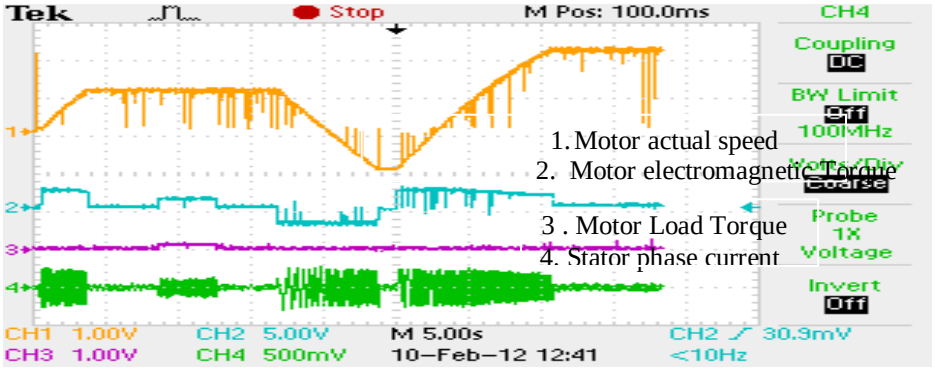

(a)

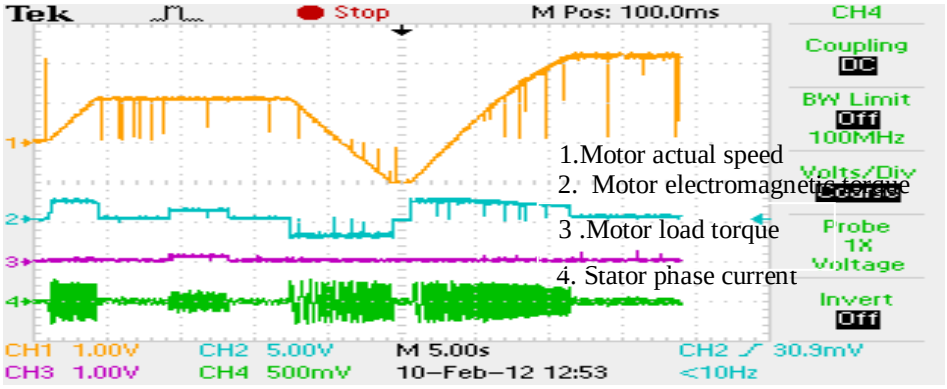

(b)

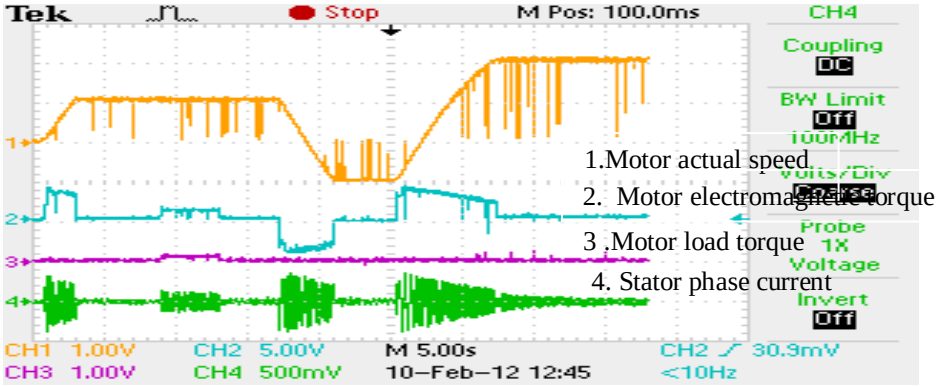

(c)

Fig. 5.13 RTDS Hardware results of IM drive with (a) P-I and (b) SM (c) ILC for speed step change, 10Nm external load and speed reversal; 1. motor speed (rpm), 2. electromagnetic and 3. load torque (N.m) , 4. stator phase current (A)

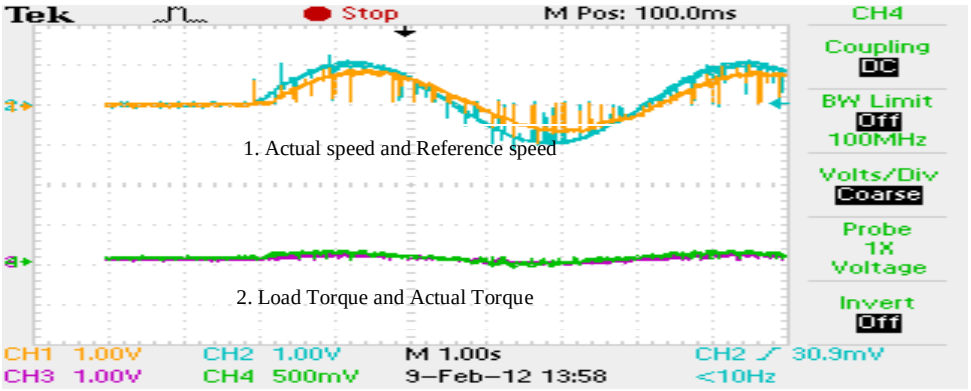

(a)

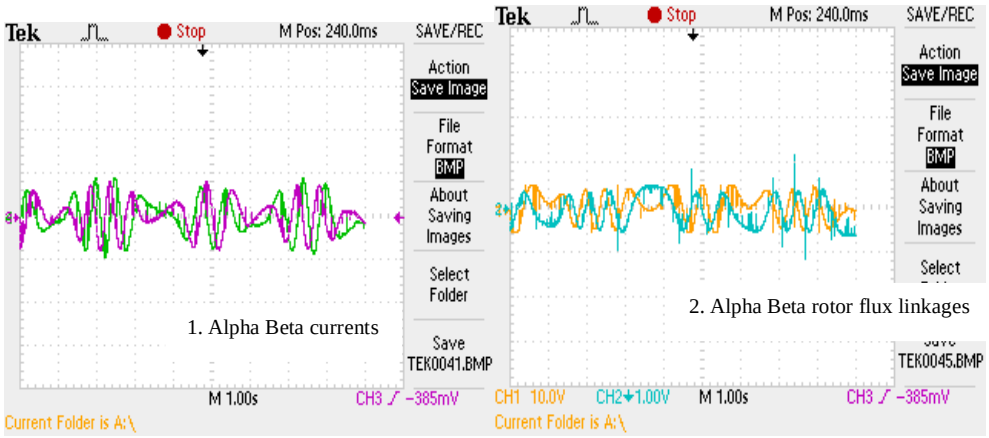

(b)

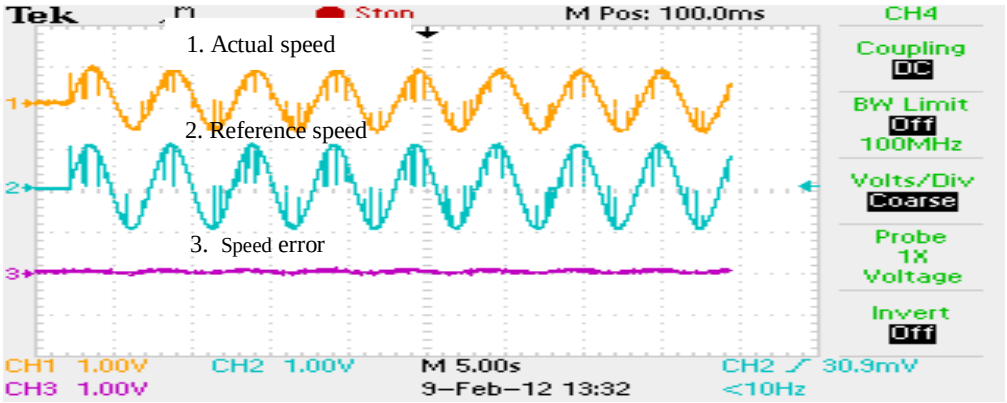

(c)

Fig. 5.14 RTDS Hardware results of IM drive with PI controller for periodic speed and load torque illustrating; (a) 1. motor reference and actual speed (rpm) and 2. electromagnetic and load torque (N.m) (b) 1. α-β stator current (A) and 2. α- β rotor flux linkages (V.s) (c) 1. motor actual speed (rpm), 2. reference speed (rpm) and 3. speed error (rpm)

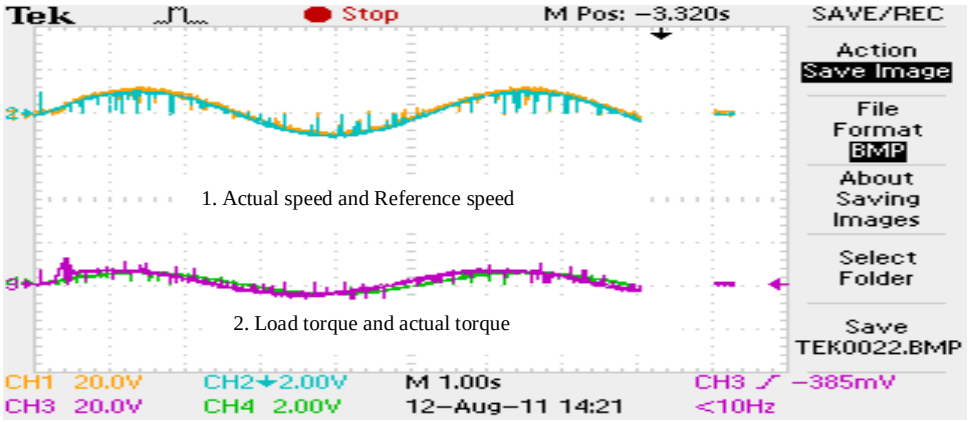

(a)

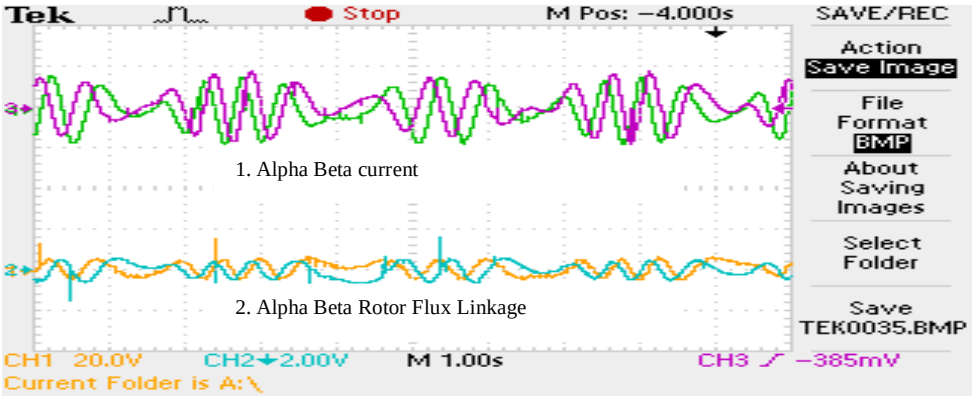

(b)

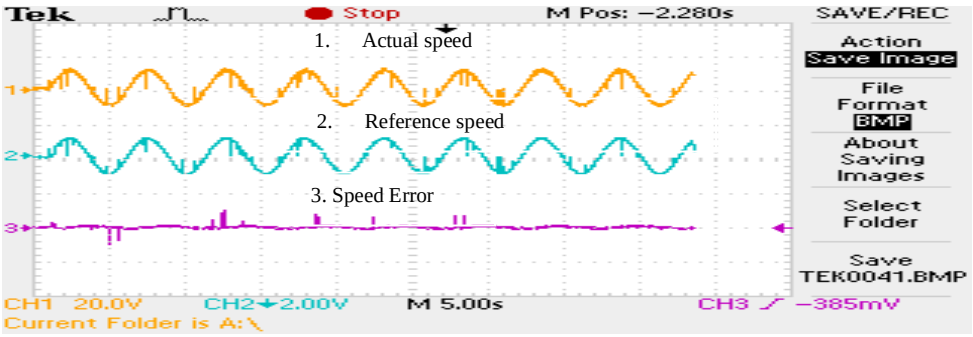

(c)

Fig. 5.15 RTDS Hardware results of IM drive with SM controller for periodic speed and load torque illustrating (a) 1.motor reference and actual speed (rpm) and 2. electromagnetic and load torque (Nm) (b) 1. α-β stator currents (A) and 2. α-β rotor flux linkages (V.s) (c) 1. motor actual speed (rpm) , 2. reference speed (rpm) and 3. speed error (rpm)

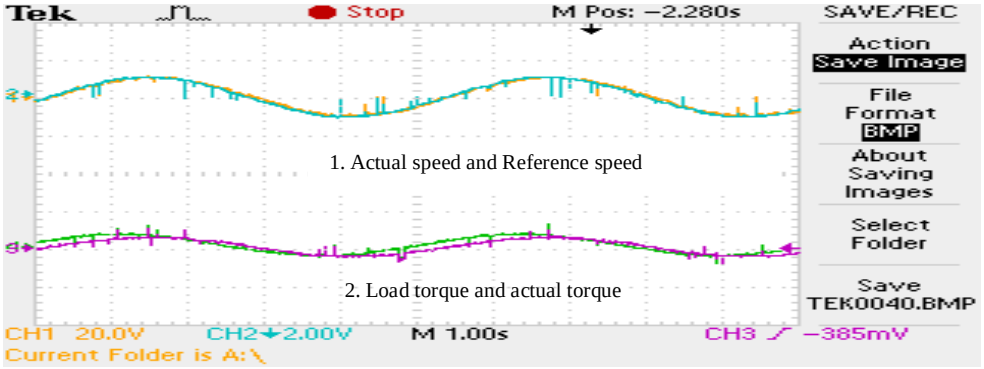

(a)

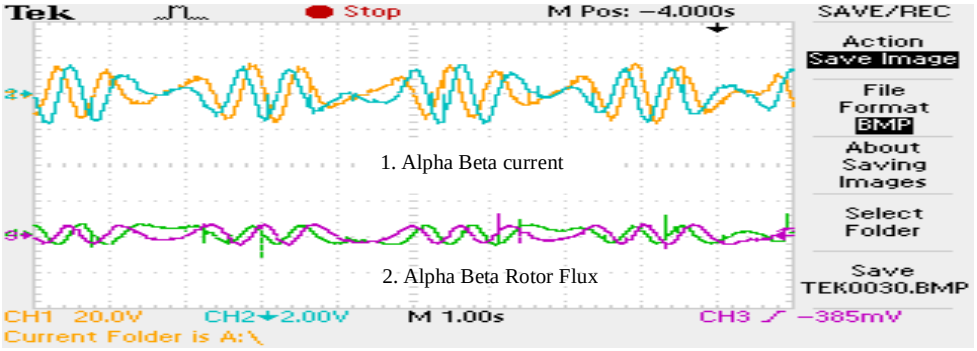

(b)

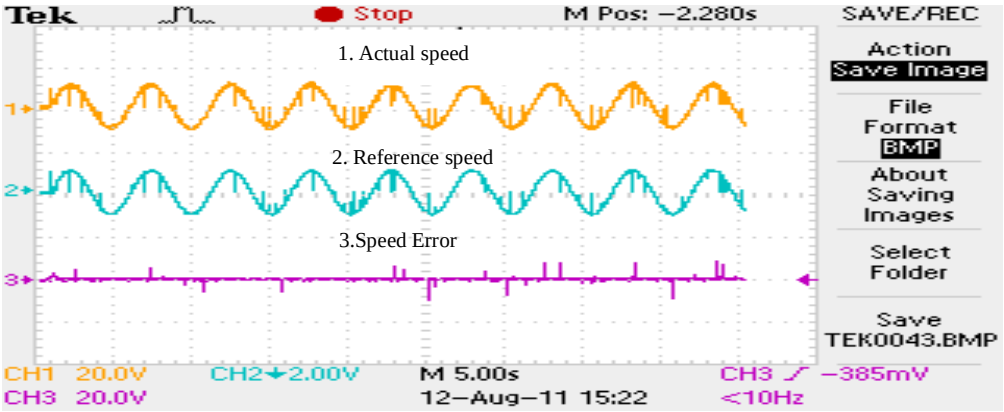

(c)

Fig. 5.16 RTDS Hardware results of IM drive with ILC for periodic speed and load torque illustrating; (a) 1. motor reference and actual speed (rpm) and 2. electromagnetic and load torque (N.m) (b) 1. α-β stator currents (A) and 2. α- β rotor flux linkages (V.s) (c) 1. motor actual speed (rpm) , 2. reference speed (rpm) and 3. speed error (rpm)

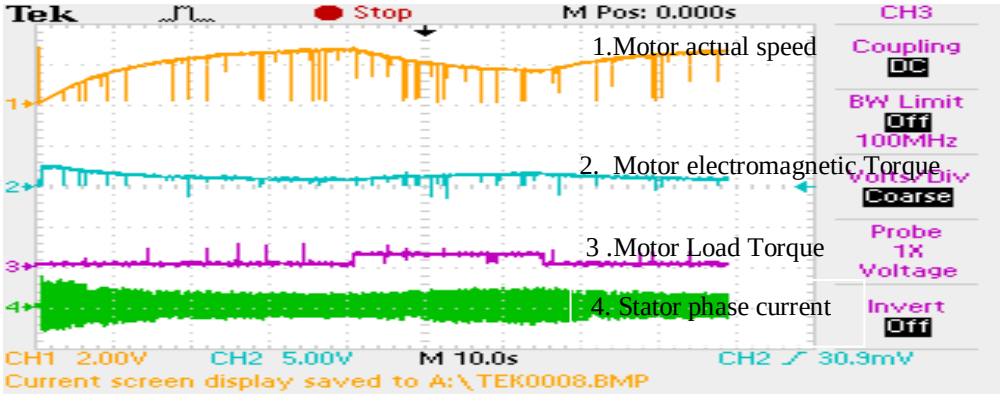

(a)

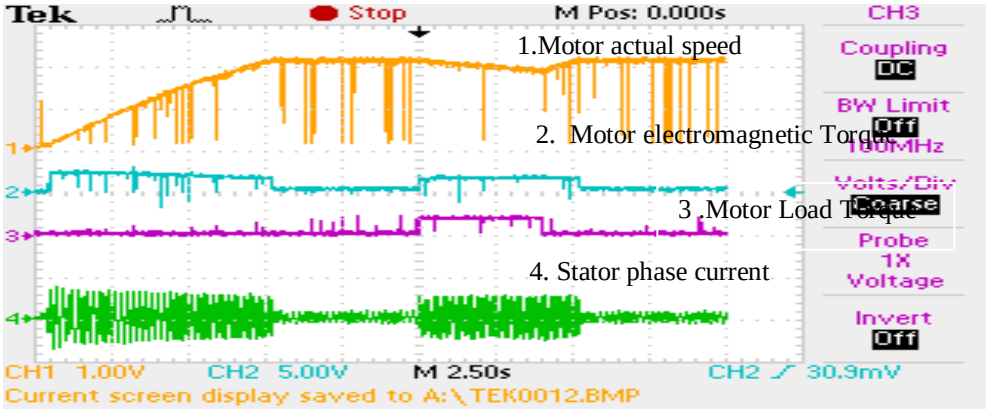

(b)

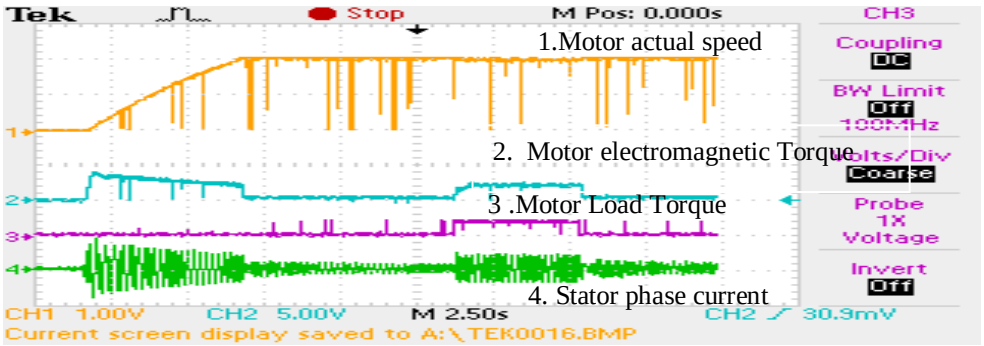

(c)

Fig.5.17 RTDS Hardware results of IM drive with (a) PI and (b) SM and (c) Lyapunov function based controller for 1000 rpm speed step change and heavy external load application illustrating ; 1. motor speed (rpm) , 2. electromagnetic and 3. load torque (N.m) , 4. stator phase current (A)

5.5 Summary of the Chapter

The state feedback linearized induction using PI, SM, ILC and Lyapunov function based controllers is implemented and tested in RT-Lab environment. The results obtained are analyzed and performance of the controllers is compared under the same operating conditions. The three sets of controllers are taken for comparison. The first set is PI and PI with fuzzy torque compensator. The second set is PI, SM and ILC and third set of controllers are PI, SM and Lyapunov function based controller. The set of controllers are tested for medium range of speed and light load. The performance of ILC has been found to be better than PI and SM controller in all the operating conditions. The third set of controllers is tested with larger step change of speed and heavy loads. Here Lyapunov function based controller has been found to be more robust than other two controllers.

Chapter – 6

Power Quality Improvement at AC Mains for the Induction Motor Drive System

6.1 General

Variable voltage and variable frequency induction motor drive is one of the major causes of the deterioration in poor quality of ac mains. Large current harmonics, poor input factor and high total harmonic distortion in ac mains current are some of the common problems. Normally we use rectifier in front-end of ac-dc conversion to reduce the overall cost of the drive system. Such uncontrolled ac-dc conversion results in the injection of current harmonics in the ac mains, leading to distortion of supply voltage at the point of common coupling. All of us are very much aware of such problem but in most cases our investigation remains limited to machine drive. The author wants to express her concern for power quality and wants to dedicate something for power quality improvement through extended research work. With remarkable progress in quality of semiconductor switching device in terms of speed and capacity, an active power filter has become a powerful tool for compensating not only current harmonic but also the reactive power [102]. The problem with active filter is it's high cost and therefore they are not recommended for large power rating. In some cases to enhance performance the combination of filters are used. The passive filters consisting of capacitors, inductors and resistors are comparatively simple and low cost which are connected in parallel with the nonlinear load [91]. Installation of such a passive filter in the vicinity of a nonlinear is to provide to impendence path for specific harmonics frequencies, thus resulting in observing the dominant harmonics current flowing out of load. An attempt is made by the author to look into various aspects of power filters with objective to improve the power quality of the utility.

Initially different types of passive filters such as passive shunt filter, passive series filter and passive hybrid filter are described. There advantages and disadvantages are mentioned. Hybrid passive filter owing constant parameter is not capable for accurate compensation (harmonics and reactive power). Therefore, a TSC-hybrid filter consisting of passive series filter and thyristor switched capacitor is configured, designed and developed. A novel control approach based on model reference adaptive control law is developed for thyristor switched capacitor for variable reactive power compensation connected at the point of common coupling is validated by simulation.

6.2 Classification of Passive Filters

Passive filters are made of capacitors, inductors and resistances. These are tuned for particular frequency. Depending on the connection of different passive filters, the passive filters can be broadly classified in three categories as given below.

6.2.1 Passive Shunt Filter

The schematic diagram of a passive shunt filter consists of two low pass tuned shunt filters at 5^{th} and 7^{th} harmonic frequencies and a high pass tuned for 11^{th} harmonic frequency, connected at input ac mains of the three phase uncontrolled rectifier feeding power to induction motor drive system is shown in Fig.6.1.This is the most commonly used configuration of passive filter. It sinks the more dominant 5^{th} and 7^{th} and other higher order harmonics and thus prevents them from flowing into ac mains. The diversion of harmonic current in the passive filter is primarily governed by the source impedance available in the system. The higher value of source impedance offers better performance of the passive filter.

6.2.2 Passive Series Filter

For voltage source type of harmonic loads (such as diode rectifier with R-L load filter), passive series filter is considered as a potential remedy for harmonic mitigation. Here, the different tuned branches of passive filters are connected in series with the supply and the uncontrolled converter. Fig.6.2 shows the schematic diagram of the passive series filters connected at input ac mains. It consists of a set of two low

block tuned shunt filters at 5th and 7th harmonic frequencies and a high block tuned filter for 11th harmonic frequency. These passive filters blocks most dominant 5th, 7th and other higher order harmonics and thus prevents them from flowing into ac mains. Here, the performance of the series filter is not much dependent on the source impedance [88]. However, it results in reduction in dc bus voltage due to voltage drop across filter components.

6.2.3 Passive Hybrid Filter

The passive series filter suffers from lagging power factor, on other hand the passive shunt filter suffers from leading power factor. To overcome this drawback, a balance combination of both these configurations may give improved power factor and harmonic mitigation. Fig. 6.3 shows the schematic diagram of the hybrid filter consists of three series filters tuned for 5th, 7th and 11th harmonic and a passive shunt filter of 11th order harmonic.

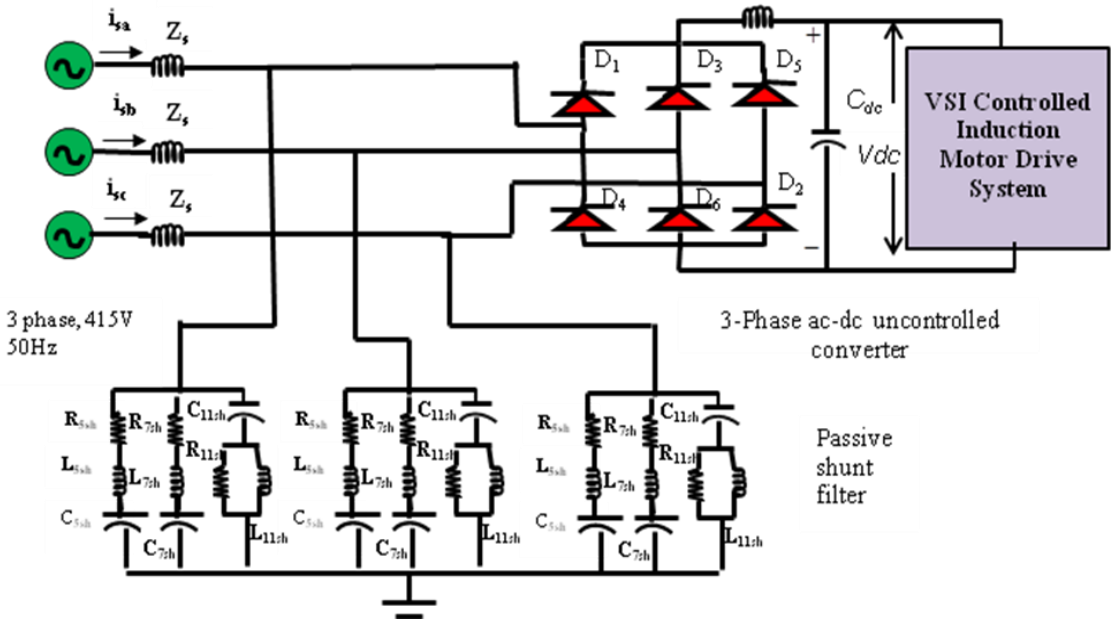

Fig.6.1 Schematic diagram of a 3-phase uncontrolled ac-dc converter fed IM drive with passive shunt filter connected at point of common coupling

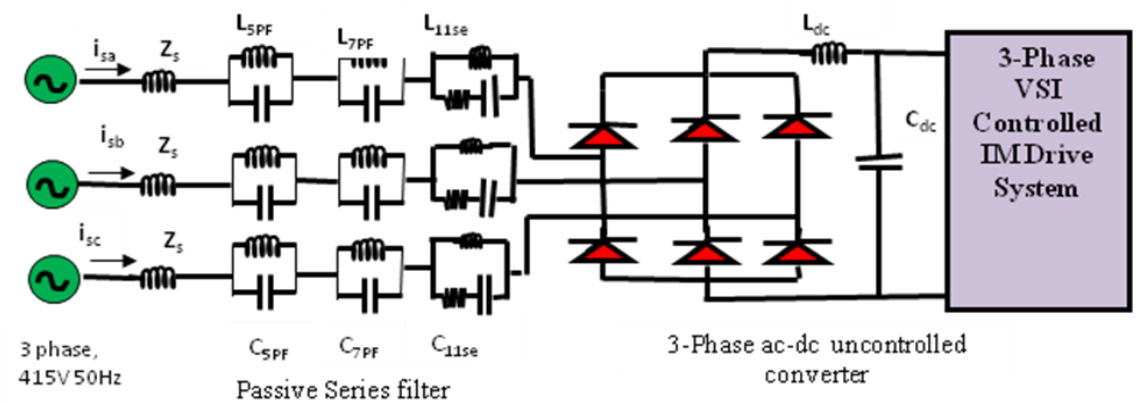

Fig.6.2 Schematic diagram of a 3-phase uncontrolled ac-dc converter fed IM drive with passive series filter connected at point of common coupling

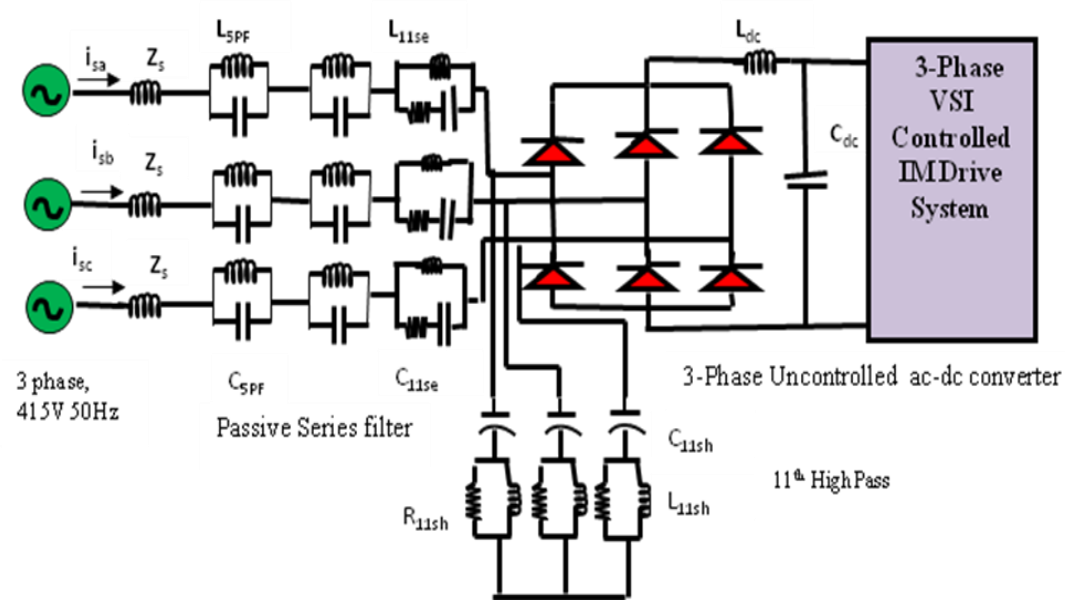

Fig.6.3 Schematic diagram of a 3-phase uncontrolled ac-dc converter fed IM drive with passive hybrid filter connected at point of common coupling

6.3 Compensation Principle and Design of Passive Filters

The basic compensation principle and design procedure of shunt and series filters are given in this section. In this work, mainly first order low pass filters and damped high pass filters are used for shunt configurations. For series configurations, single tuned first order filters and high block damped filters are used to form a composite filter.

6.3.1 Compensation Principle of Passive Shunt Filter

Fig. 6.4 shows the per phase Thevenin's equivalent circuit of a shunt LC filter for harmonic voltage source. Where, the diode rectifier is represented as a harmonic voltage source. The shunt LC filter in the circuit consists of several LCR branches each tuned at a particular frequency. The compensation characteristics of a shunt LC filter for voltage harmonic source can be given as [88]

$$\frac{I_S}{V_l} = \frac{Z_{sh}}{Z_l Z_s + Z_{sh} + Z_s Z_{sh}} \tag{6.1}$$

Where, $Z_{sh,}$ Z_l and Z_s are parallel LC filter impedance, thevenin's equivalent load impedance and source impedance respectively. I_s and V_l represent source (supply) current and thevenin's load voltage. It can be seen from Fig.6.4 and eqn. (6.1), that the performance of parallel LC filter greatly depends on the source impedance and load impendence. If Z_l =0, then eqn. (6.1) reduces to $\frac{I_s}{V_l} = \frac{1}{Zs}$, I_s =I_l, which means that the passive filter is not effective. On the other hand, if Z_s=0, then, $\frac{I_s}{V_l} = \frac{1}{Z_l}$, which means that the filter does not provide harmonic compensation. It is seen that the filter interaction with the source impedance results in a parallel resonance. For inductive source impedance (Z_s), this occurs at a frequency below the frequency at which the filter is tuned. It is given as:

$$f_{sys} = \frac{1}{2\pi(L_s + L)C} \tag{6.2}$$

Moreover, if a filter is exactly tuned at a frequency of concern, then an upward shift in the tuned frequency results in a sharp increase in impedance as seen by the harmonic. The most common mechanisms that may cause filter detuning are:

- Capacitor fuse-blowing, which lowers the total capacitance, thereby raising the frequency at the filter has been tuned.
- Manufacturing tolerances in both inductor as well as capacitor.
- Temperature variations.
- System parameter variations

Therefore, generally, the filter banks are tuned to around 6% below the desired frequency as per IEEE standard 1531[83].

6.3.2 Compensation Principle of Passive Series Filters

Fig.6.5 shows the equivalent thevenin's circuit diagram of a passive tuned series filter for voltage harmonic source. The harmonic compensation is achieved by blocking specific harmonic current with the parallel tuned LCR circuits connected in series path. The compensation characteristics of a passive series filter can be given as [88]

$$\frac{I_S}{V_l} = \frac{1}{Z_s + Z_{se} + Z_l} \tag{6.3}$$

Eqn. (6.3) shows that the harmonic compensation performance of the series filter is virtually independent of the source impedance, since the source impedance is relatively small compared to the LC filter impedance at harmonic frequencies.

6.3.3 Compensation Principle of Passive Hybrid Filters

The passive hybrid filters consists of both passive shunt and passive series filter. Fig.6.6 shows the circuit topology for hybrid filters. The compensation characteristics of the hybrid filter can be given as:

$$\frac{I_S}{V_l} = \frac{Z_{sh}}{Z_l\left(Z_s + Z_{sh} + Z_{se}\right) + Z_s Z_{sh} + Z_{se} + Z_{sh}} \tag{6.4}$$

This filter's harmonics performance is independent of source impedance. It offers both filter's quality. Proper design of this configuration can overcome the limitations of the individual shunt and series filters.

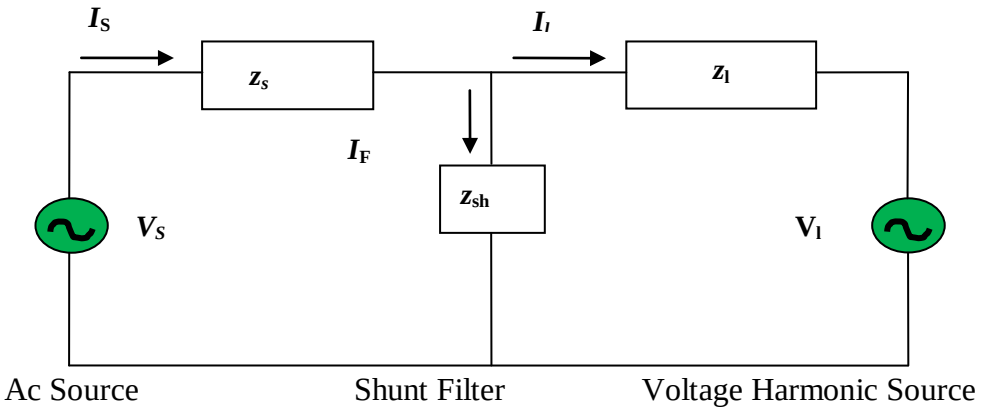

Fig. 6.4 Thevenin's equivalent circuit of a shunt LC filter for harmonic voltage source

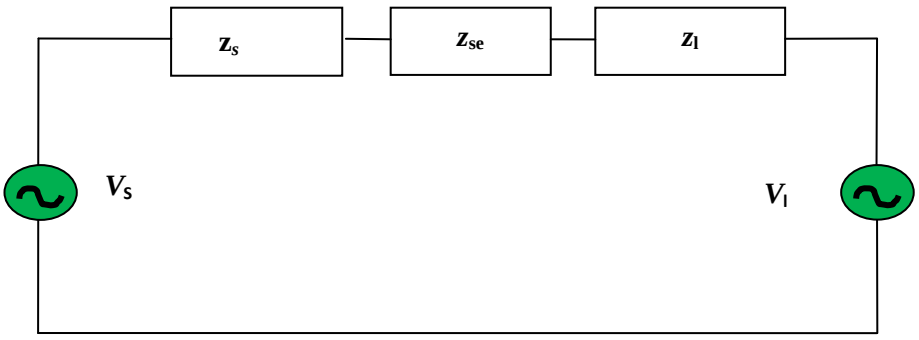

Ac Source Series Filter Voltage Harmonic Source

Fig. 6.5 Thevenin's equivalent circuit of a series LC filter for harmonic voltage source

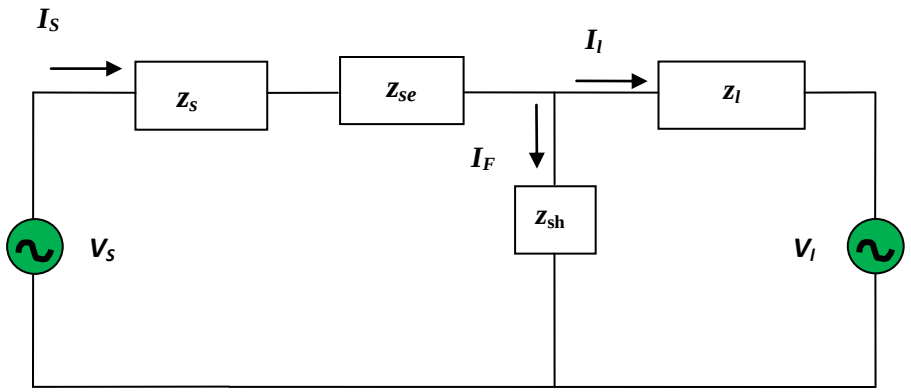

Ac Source Hybride Filter Voltage Harmonic Source

Fig. 6.6 Thevenin's equivalent circuit of a hybrid LC filter for harmonic voltage source

6.4 Design of Passive and TSC-Hybrid Filters

There are many issues involved with the design of the passive filters. Some of the important constrains are discussed first. Then detail procedure of filter design of passive as well as TSC-Hybrid filter are discussed.

6.4.1 Filter design constraints

There are many issues in the design of a passive filter for its proper functioning in harmonic reduction. The key issues are mentioned here:

- Minimizing harmonic source current

The prime objective of the filter design is to minimize the harmonic current in ac mains. This is ensured by minimizing the filter impedance at the harmonic frequencies so that the harmonic filter acts as a sink for the harmonic currents.

- Minimizing fundamental current in passive filter

To ensure that the installation of passive filter does not cause the system loading, the fundamental current in the passive filter is minimized by the maximizing the passive filter impedance at the fundamental frequency.

- Environment and ageing effect

The capacitors with metalized film construction lose capacitance as they age. Similarly the manufacturer tolerance of the harmonic filter reactor may result in tuned frequency higher than the nominal. An IEEE Standard 1531[83] recommends that the passive filters are tuned at 6% below the rated frequency so that it will exhibit acceptable tuning at the end of its 20 year life.

6.4.2 Design of Passive Shunt Filter

The single phase branch configuration for a low pass passive shunt filter consist of capacitor, inductor and resistance (C_{sh}, L_{sh} and R_{sh}) is shown in Fig. 6.7 and a high pass passive shunt filter made of capacitor, inductor and resistance is shown is shown in Fig 6.8. The passive shunt filter consists of first order series tuned low pass filters for 5th and 7th order harmonics. For the series tuned low pass filters, the impedance is given by:

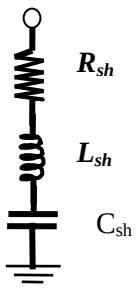

Fig.6.7 Low pass Filter

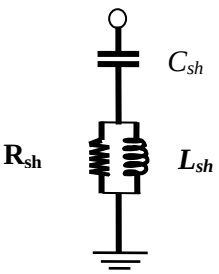

Fig.6.8 High pass Filter

$$Z_{sh(h)} = \left[R_{sh} + j\left(h_n X_{shL} - \frac{X_{shC}}{h_n} \right) \right] \tag{6.5}$$

$$X_{shL} = \frac{X_{shc}}{h_n^2} \tag{6.6}$$

$$X_{shc} = \left(\frac{h_n^2 - 1}{h_n^2} \right) \frac{V^2}{Q_{sh}} \tag{6.7}$$

where, Q_{sh} is the reactive power provided by the passive shunt filter, h_n is the harmonic order of the passive filter; X_{shL} is the reactance of inductor L_{sh}., X_{shc} is the reactance of the capacitor C_{sh} at fundamental frequency. The reactive power requirement may be initially assumed around 25% of the rating of the load [88]. It may be equally divided among different filter branches. The values of series tuned elements may be calculated from eqn. (6.6). The quality factor for low pass filter (defined as $Q_F = X_{shL}/R$), is considered as 30 in this work to calculate the value of the resistive element.

The resonant frequency f_h for the h^{th} harmonic is given as:

$$Z_{sh(h)} = \left[\frac{R_{sh}\left(h_n X_{shL}\right)^2}{R_{sh}{}^2 + \left(h_n X_{shL}\right)^2} + j\left(\frac{R h_n X_{shL}}{R_{sh}^2 + \left(h_n X_{shL}\right)^2} - \frac{X_{shC}}{h_n} \right) \right] \tag{6.8}$$

$$X_{shc} = \left(\frac{h_n^2 - 1}{h_n^2} \right) \frac{V^2}{Q_{sh}} \tag{6.9}$$

$$f_h = \frac{1}{\left(2\pi h_n C_{shL} R_{sh}\right)} \tag{6.10}$$

Quality factor can be defined as:

$$Q_F = \frac{L_{shL}}{\left(C_{shL} R_{sh}^2\right)} \tag{6.11}$$

The values of filter components can be calculated from above equations.

6.4.3 Design of Passive Series Filter

The passive series filter consists of a parallel connection of high impedance LCR circuits each tuned in parallel at a harmonic frequency. Fig. 6.9 shows the basic design for a low frequency and high frequency series passive filter. The harmonic suppression is achieved by blocking specific harmonic currents with the parallel-tuned LCR circuits, which provide high impedance at the specific harmonic. The impedance of first order tuned block filter can be represented as:

$$Z_{se} = \left(\frac{h_n^2 - 1}{h^2 - h_n^2} \right) \frac{hQ_{se}}{I_{se}^2} \tag{6.12}$$

Where, Q_{se} is the reactive power of the series filter. The admittance of the high block can be expressed as:

$$Y_{se} = \left[\frac{h_n X_{seC}}{h_n^2 R_{se}{}^2 + X_{seC}^2} - \left(\frac{1}{h_n . X_{seC}} \right) \right] \tag{6.13}$$

with

$$X_{seC} = h_n^2 X_{seL} . X_{seL} = \left(\frac{h_n^2 - 1}{h_n^2} \right) \frac{Qse}{I_{se}^2} \tag{6.14}$$

The resonance frequency for h^{th} harmonics is given as:

$$f_h = \frac{1}{\left(2\pi h_n C_{se} R_{se} \right)} \tag{6.15}$$

Quality factor can be defined as

$$Q_F = \frac{L_{se}}{\left(C_{se} R_{se}^3 \right)} \tag{6.16}$$

The values of the filter parameters can be obtained from above expressions.

Therefore, the net impedance of the series filter can be represented as:

$$Z_{se} = Z_{5se} + Z_{7se} + Z_{11se} \tag{6.17}$$

The passive series filter is designed to offer minimum impedance at fundamental frequency. So that there should minimum voltage drop across passive filter. If voltage drop becomes significant then system voltage regulation will be adversely effected.

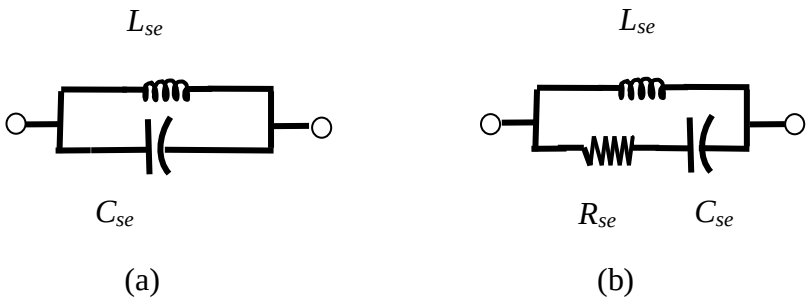

(a) (b)

Fig.6.9 (a) Low block passive series filter and (b) High block passive series filter

6.4.5 Design of Passive Hybrid Filter

The passive hybrid is a combination of shunt and series filter. The passive shunt filter suffers from leading power factor operation and creates the problem of voltage regulation at light loads. On other hand passive series filter suffers from lagging power factor operation as well as voltage drop across the filter. The drawback of the series and shunt can overcome by the passive hybrid filter made of the combination of passive series and passive shunt filter.

6.4.6 Design of TSC-Hybrid Filter

The hybrid filters can be a better choice than either passive shunt filter or passive series filter but for constant reactive power. In case of variable reactive power occurrence it also fails. Then in this situation thyristor switched capacitor can be used. It is a series RLC circuit similar to low pass passive shunt filter with additional two back to back thyristor switches. The TSC provides capacitive reactive power to compensate leading reactive power in the power system. This is achieved by regulating power flow into TCS branch by means of controlling thyristor switches. The combination of the passive series filter and TSC can be an attractive configuration for harmonic mitigation and variable reactive power compensation. As series passive generates leading reactive power which changes with load current and TSC connected to shunt branch, able compensate variable reactive power. For TSC an efficient control technique required to ensure transient free and accurate reactive power compensation. The thyristor switched capacitor system is discussed in Section-6.5.

6.5 Thyristor Switched Capacitor System

The thyristor switched capacitor system comprises of a series RLC circuit, one pair of back-to back thyristor switch and a control unit. The control strategy requires the dynamic model of TSC system. For this the dynamic modelling of the TSC system is first derived in the stationary "abc" reference frame and then transformed into the synchronous orthogonal "dq" reference frame. A model reference adaptive control law is developed for robust dynamic performance for variable reactive power compensation and harmonic mitigation. The control algorithm is implemented on the synchronously orthogonal frame.

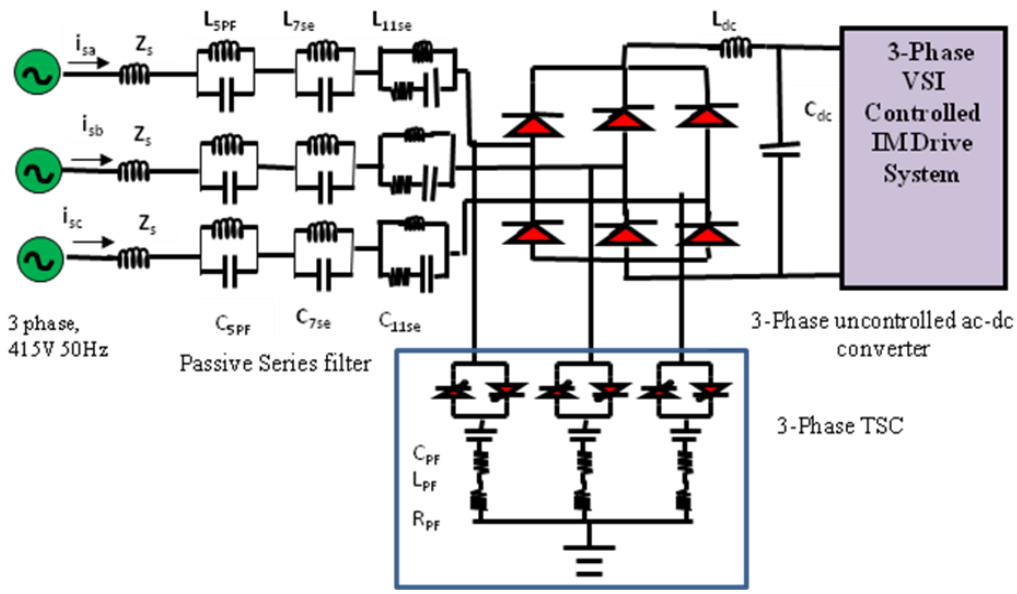

Fig.6.10 Schematic diagram of a 3-phase uncontrolled ac-dc converter fed induction motor drive with TSC- hybrid filter

6.5.1 Dynamic Modeling of Thyristor Switched Capacitor

The dynamic modeling of the TSC at synchronously rotating *(d-q)* reference frame is given below.

The Kirchhoff's voltage equation of TSC circuit can be represented as

$$V_{sk} = L_{PF}\frac{di_{pk}}{dt} + R_{PF}i_{pk} + \frac{1}{C_{PF}}\int i_{pk}dt \qquad (6.18)$$

where, k is index for three phase (a, b, c).

Differentiating (6.18) once result in

$$\frac{dV_{sk}}{dt} = L_{PF}\frac{d^2 i_{pk}}{dt^2} + R_{PF}\frac{di_{pk}}{dt} + \frac{i_{pk}}{C_{PF}} \tag{6.19}$$

The system is transformed into the synchronous orthogonal (*d-q*) frame rotating at the constant supply frequency ω.The two successive matrix conversion performed using (6.19) and (6.20).

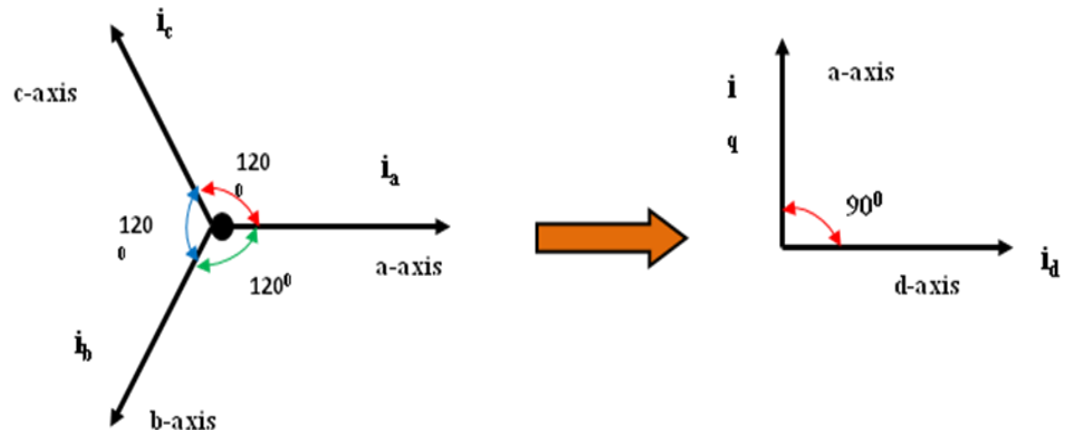

Fig.6.11. a-b-c to d-q-0 transformation

$$M_{\alpha\beta}^{abc} = \sqrt{\frac{2}{3}}\begin{bmatrix} 1 & -\frac{1}{2} & -\frac{1}{2} \\ 0 & -\frac{\sqrt{3}}{2} & \frac{\sqrt{3}}{2} \end{bmatrix} \tag{6.20}$$

$$S_{dq}^{\alpha\beta} = \begin{bmatrix} \cos(\omega t) & -\sin(\omega t) \\ \sin(\omega t) & \cos(\omega t) \end{bmatrix} \tag{6.21}$$

where, (α-β) represents the stationary orthogonal references frame. The equation (6.19) is transformed into (6.22)

$$\frac{d^2}{dt^2}\left[i_{dq}\right] = -\begin{bmatrix} \frac{R_{PF}}{L_{PF}} & -2\omega \\ 2\omega & \frac{R_{PF}}{L_{PF}} \end{bmatrix}\frac{d}{dt}\left[i_{dq}\right] - \begin{bmatrix} -\omega^2 + \frac{1}{C_{PF}L_{PF}} & -\omega\frac{R_{PF}}{L_{PF}} \\ \omega\frac{R_{PF}}{L_{PF}} & -\omega^2 + \frac{1}{C_{PF}L_{PF}} \end{bmatrix}\left[i_{dq}\right] + \frac{1}{L_{PF}}\frac{d}{dt}\left[V_{dq}\right] + \frac{1}{L_{PF}}\begin{bmatrix} 0 & -\omega \\ \omega & 0 \end{bmatrix}\left[V_{dq}\right] \tag{6.22}$$

Finally, the dynamic model of TSC in the synchronously rotating (*d*-*q*) frame becomes:

$$L_{PF}\frac{d^2 i_d}{dt^2}+R_{PF}\frac{di_d}{dt}+\left(-\omega^2 L_{PF}+\frac{1}{C_{PF}}\right)i_d=2\omega L_{PF}\frac{di_q}{dt}+\omega R_{PF}i_q+\frac{dV_d}{dt}-\omega V_q \tag{6.23}$$

$$L_{PF}\frac{d^2 i_q}{dt^2}+R_{PF}\frac{di_q}{dt}+\left(-\omega^2 L_{PF}+\frac{1}{C_{PF}}\right)i_q=-2\omega L_{PF}\frac{di_d}{dt}-\omega R_{PF}i_d+\frac{dV_q}{dt}+\omega V_d \tag{6.24}$$

The above two equations are used for developing control law for operating TSC. It is derived in next section.

6.5.2 Model Reference Adaptive Controller

A model reference adaptive controller is designed which assures stable and robust system dynamic control. It utilises Lyapunov stability theory and Barbalat's lemma [2] theorem.

The reactive power is regulated by the current i_q and the active power is regulated by current i_d.The resistance of TSC is very small, therefore i_d. current will be negligible.

Further, substituting $i_d = 0$ and $\frac{di_d}{dt}=0$ in (6.24), we have

$$L_{PF}\frac{d^2 i_q}{dt^2}+R_{PF}\frac{di_q}{dt}+\left(-\omega^2 L_{PF}+\frac{1}{C_{PF}}\right)i_q=\frac{dV_q}{dt}+\omega V_d \tag{6.25}$$

Here, we take u_q an intermediate control variable to linearize *q* axis dynamic equation. The linearized equation is represented as:

$$L_{PF}\frac{d^2 i_q}{dt^2}+R_{PF}\frac{di_q}{dt}+\left(-\omega^2 L_{PF}+\frac{1}{C_{PF}}\right)i_q=u_q \tag{6.26}$$

where,

$$u_q=\frac{dV_q}{dt}+\omega V_d \tag{6.27}$$

The reactive part is taken that is equation (6.25) is considered and rewritten as follows

$$L_{PF}\frac{d^2 i_q}{dt^2}+R_{PF}\frac{di_q}{dt}+\left(-\omega^2 L_{PF}+\frac{1}{C_{PF}}\right)i_q=u_q \tag{6.28}$$

The state-space representation of (6.28) can be written as

$$\dot{x}=-a_p x+b_p u_q \tag{6.29}$$

Where $\dot{x}=\left[\dot{x}_1\dot{x}_2\right]^T$ with $x_1=i_q$ and $x_2=\dot{x}_1$

$$a_p=\begin{bmatrix} 0 & 1 \\ \left(\frac{1}{L_{PF}C_{PF}}-\omega^2\right) & \frac{R_{PF}}{L_{PF}} \end{bmatrix} \text{ and } b_p=\begin{bmatrix} 0 \\ \frac{1}{L_{PF}} \end{bmatrix}$$

A model reference adaptive control law for the system is defined as [2]

$$u_q=\hat{a}_{x1}x_1+\hat{a}_{x2}x_2+\hat{b}_r r(t) \tag{6.30}$$

where $\hat{a}_{x1},\hat{a}_{x2}$ and $\hat{b}_r$ are variable feedback gains and $r(t)$ is the bounded external reference signal and for reactive power compensation it taken $r(t)=-Q(t)$, the measured reactive component. Substituting the control law (6.30) into equation (6.29).

The new state-space representation becomes

$$\dot{x}=-a_{pc}x+b_{pc}r(t) \tag{6.31}$$

And

$$a_{pc}=\begin{bmatrix} 0 & 1 \\ \left(\left(\frac{1}{L_{PF}C_{PF}}-\omega^2\right)-\frac{\hat{a}_{x1}}{L_{PF}}\right) & \left(\frac{R_{PF}}{L_{PF}}-\frac{\hat{a}_{x2}}{L_{PF}}\right) \end{bmatrix} \text{ and } b_{pc}=\begin{bmatrix} 0 \\ \frac{\hat{b}_r}{L_{PF}} \end{bmatrix}$$

To obtain perfect control, a linear second order reference model is taken and compared with actual system .The controller is designed for measures the steady-state error zero or system to track the reference model. The transfer function of the linear reference model is taken, the damping ratio ζ=1, and the natural frequency 225 rad/s and defined as:

$$G(s) = \frac{{\omega_n}^2}{s^2 + 2\xi\omega_n s + {\omega_n}^2} \tag{6.32}$$

It's state space representation is expressed as

$$\dot{x} = -a_{rm}x + b_{rm}r(t) \tag{6.33}$$

where $\dot{x} = \left[\dot{x}_{1rm}\dot{x}_{2rm}\right]$ with $x_{1rm} = i_{qrm}$, $x_{2rm} = \dot{x}_{1rm}$

with

$$a_{rm} = \begin{bmatrix} 0 & 1 \\ \left(\omega_n^2\right) & \left(2\zeta\omega_n\right) \end{bmatrix} \text{and} \, b_{rm} = \begin{bmatrix} 0 \\ \omega_n^2 \end{bmatrix}$$

And *r(t)* is input reference signal to the reference model. Next, passive filter error state model is obtained for derivation of control law which guaranteed the system stability along with improved dynamic performance. The filter state error model is analysed. It is obtained by subtracting (6.31) from (6.33).

$$\dot{e} = a(e)e + b(e) \tag{6.34}$$

where $\dot{x} = \left[\dot{e}_1\dot{e}_2\right]^T = \left[\left(\dot{x}_1 - \dot{x}_{1rm}\right)\left(\dot{x}_2 - \dot{x}_{2rm}\right)\right]^T$

with

$$a(e) = \begin{bmatrix} 0 & 1 \\ \left(-\omega_n^2\right) & \left(-2\zeta\omega_n\right) \end{bmatrix} . \quad b(e) = \begin{bmatrix} 0 \\ b_e \end{bmatrix} \quad \text{and}$$

$$b_e = \left(\omega_n^2 - \left(\frac{1}{L_{PF}C_{PF}} - \omega^2\right) + \frac{\hat{a}_{x1}}{L_{PF}}\right)x_1 + \left(2\zeta\omega_n - \frac{R_{PF}}{L_{PF}} + \frac{\hat{a}_{x2}}{L_{PF}}\right)x_2 + \left(\frac{\hat{b}_r}{L_{PF}} - \omega_n^2\right)r(t)$$

Next, For design of a stable controller,a Lyapunov function is taken and defined in (6.35)

$$V(e) = e^T Pe + \frac{L_{PF}}{2\gamma}\left(a_{r1}^2 + a_{r2}^2 + a_{r3}^2\right) \tag{6.35}$$

Where γ is a positive constant and P is a symmetric definite constant matrix, and P should satisfy

$$a^T(e)P + Pa(e) = -I \tag{6.36}$$

where

$$P = \begin{bmatrix} p_{11} & p_{12} \\ p_{21} & p_{22} \end{bmatrix} = \begin{bmatrix} \dfrac{1+\omega_n^2+4\zeta^2}{4\zeta\omega_n} & \dfrac{1}{2\omega_n^2} \\ \dfrac{1}{2\omega_n^2} & \dfrac{1+\omega_n^2}{4\zeta\omega_n^3} \end{bmatrix}, I = \begin{bmatrix} 1 & 0 \\ 0 & 1 \end{bmatrix} ,$$

$$a_{r1} = \left(\omega_n^2 - \left(\frac{1}{L_{PF}C_{PF}} - \omega^2\right) + \frac{\hat{a}_{x1}}{L_{PF}}\right), a_{r2} = \left(2\zeta\omega_n - \frac{R_{PF}}{L_{PF}} + \frac{\hat{a}_{x2}}{L_{PF}}\right), a_{r3} = \left(\frac{\hat{b}_r}{L_{PF}} - \omega_n^2\right)$$

According to The Lyapunov global stability , if any function *V(x)* is positive definite and has continuous partial derivatives in a Region , if its time derivative along any state trajectory of system $\dot{x} = f(x)$ is negative semi-definite, i.e. a scalar function *V* of the state x, with continuous first order derivatives such that

- $V(x)$ is positive definite
- $\dot{V}(x)$ is negative definite
- $V(x) \to \infty$ as $\|x\| \to \infty$

then the equilibrium at the origin is globally asymptotically stable.

In order to satisfy the above condition the derivative of the Lyapunov function *V* (e) is taken as

$$\dot{V}(e) = \frac{d}{dt}\left(e^T Pe\right) + \frac{L_{PF}}{2\gamma}\frac{d}{dt}\left(a_{r1}^2 + a_{r2}^2 + a_{r3}^2\right)$$

$$= \frac{d}{dt}\left(p_{11}e_1^2 + p_{21}e_1e_2 + p_{12}e_1e_2 + p_{22}e_2^2\right) + \frac{L_{PF}}{2\gamma}\frac{d}{dt}\left(a_{r1}^2 + a_{r2}^2 + a_{r3}^2\right)$$

$$= 2p_{11}e_1\dot{e}_1 + 2p_{21}\left(\dot{e}_1e_2 + e_1\dot{e}_2\right) + 2p_{22}e_2\dot{e}_2 + \frac{L_{PF}}{\gamma}\left(a_{r1}\dot{a}_{r1} + a_{r2}\dot{a}_{r2} + a_{r3}\dot{a}_{r3}\right)$$

$$= -e_1^2 - e_2^2$$

$$+\left(\left(\omega_n^2-\left(\frac{1}{L_{PF}C_{PF}}-\omega^2\right)+\frac{\hat{a}_{x1}}{L_{PF}}\right)2x_1+\left(2\zeta\omega_n-\frac{R_{PF}}{L_{PF}}+\frac{\hat{a}_{x2}}{L_{PF}}\right)2x_2+\left(\frac{\hat{b}_r}{L_{PF}}-\omega_n^2\right)2r(t)\right)\left(p_{21}e_1+p_{22}e_2\right)$$

$$+\frac{L_{PF}}{\gamma}\left(\frac{d\hat{a}_{x1}}{dt}\left(\omega_n^2-\left(\frac{1}{L_{PF}C_{PF}}-\omega^2\right)+\frac{\hat{a}_{x1}}{L_{PF}}\right)+\frac{d\hat{a}_{x2}}{dt}\left(2\zeta\omega_n-\frac{R_{PF}}{L_{PF}}+\frac{\hat{a}_{x2}}{L_{PF}}\right)+\frac{d\hat{b}_r}{dt}\left(\frac{\hat{b}_r}{L_{PF}}-\omega_n^2\right)\right)$$

$$=-e^TIe+\left(\omega_n^2-\left(\frac{1}{L_{PF}C_{PF}}-\omega^2\right)+\frac{\hat{a}_{x1}}{L_{PF}}\right)\left(2x_1\left(p_{21}e_1+p_{22}e_2\right)+\frac{L_{PF}}{\gamma}\frac{d\hat{a}_{x1}}{dt}\right)$$

$$+\left(2\zeta\omega_n-\frac{R_{PF}}{L_{PF}}+\frac{\hat{a}_{x2}}{L_{PF}}\right)\left(2x_2\left(p_{21}e_1+p_{22}e_2\right)+\frac{L_{PF}}{\gamma}\frac{d\hat{a}_{x2}}{dt}\right)$$

$$+\left(\frac{\hat{b}_r}{L_{PF}}-\omega_n^2\right)\left(2r(t)\left(p_{21}e_1+p_{22}e_2\right)+\frac{L_{PF}}{\gamma}\frac{d\hat{b}_r}{dt}\right) \tag{6.37}$$

Here the adaption law is chosen as

$$\frac{d\hat{a}_{x1}}{dt}=-\left(2x_1\frac{\gamma}{L}\left(p_{21}e_1+p_{22}e_2\right)\right)$$

$$\frac{d\hat{a}_{x2}}{dt}=-\left(2x_2\frac{\gamma}{L}\left(p_{21}e_1+p_{22}e_2\right)\right)$$

$$\frac{d\hat{b}_r}{dt}=-\left(2r\frac{\gamma}{L}\left(p_{21}e_1+p_{22}e_2\right)\right) \tag{6.38}$$

And equation (6.37) leads to

$$\dot{V}=-e^TIe \tag{6.39}$$

Thus, the adaptive control law (6.38) is globally stable, i.e, the variables $e_1, e_2, \dot{a}_{x1}, \dot{a}_{x2}$ and $\hat{b}_r$ are bounded. The tracking error *e(t)* is guaranteed by Barbarat's Law[1] , because the boundness of $e_1, e_2, \dot{a}_{x1}, \dot{a}_{x2}$ and $\hat{b}_r$ imply the boundness of $\dot{e}$ according to equation (6.39).

$$u_q=\hat{a}_{x1}x_1+\hat{a}_{x2}x_2+\hat{b}_r r(t) \tag{6.40}$$

By substituting u_q and V_d into (6.27), one can get V_q. The three phase equivalent voltage in stationary reference frame is obtained through inverse coordinate transformation. This voltage is passed through the PWM pulse generator to generator to gate pulse for thyristor switch. The schematic block of model adaptive control scheme for TSC is shown in Fig. 6.12.

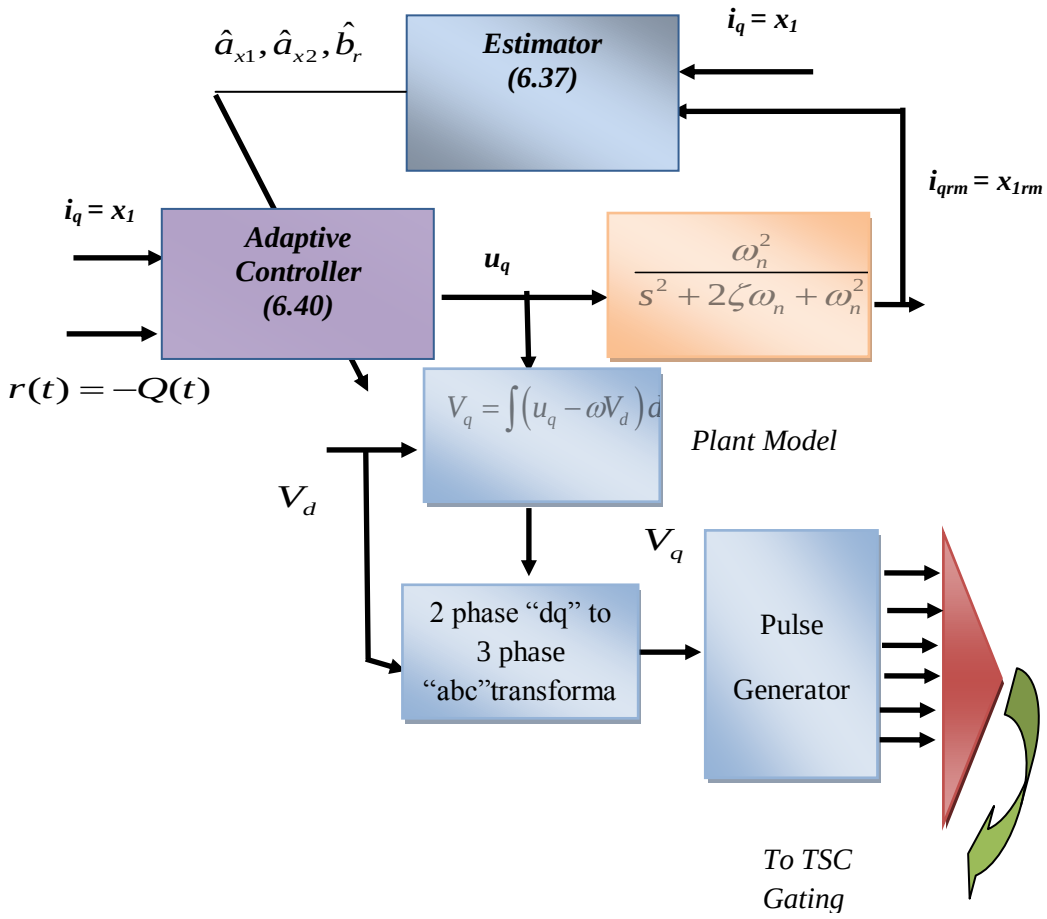

Fig.6.12 Model reference adaptive control scheme for the proposed TSC system

6.6 MATLAB Model of the IM Drive System fed from Three-Phase Uncontrolled AC-DC Converter without and with Filter

In most of the cases, uncontrolled ac-dc converters are used in front end for ac-dc conversion to reduce the cost of the induction motor drive system. To demonstrate the performance of passive filters and TSC-hybrid filter connected at the ac mains side of the uncontrolled ac-dc converter feeding induction motor, the schemes are modelled in MATLAB/ SIMULINK environment.

6.6.1 MATLAB Model of the IM Drive System fed from Three-Phase Uncontrolled AC-DC Converter without Filter

Fig.6.13 shows the MATLAB models of three-phase uncontrolled ac-dc converter without filter feeding power to induction motor drive system.

6.3.2 MATLAB Model of the IM Drive System fed from Three-Phase Uncontrolled AC-DC Converter with Passive Shunt Filter

Fig. 6.14 shows the MATLAB model of the three-phase uncontrolled ac-dc converter with shunt passive filter at the supply end feeding power to an induction motor drive system. Depending on the presence of harmonics in supply current, the passive shunt filter is designed. The low pass filters are tuned for 5 th and 7 th harmonic frequency and a high pass filter is tuned for 11 th harmonics frequency. The series RLC circuits are used and tuned for 5th order and 7th order harmonic filters. The high pass filter consists of a capacitor connected in series with a paraller RL circuit as shown in Fig. 6.8 and tunned for 11th order harmonic. By proper design and tuning of the passive shunt filtes, the ac supply current in each of the three phase is improved to sinusoidal in nature. The design parameters of the passive shunt filter to eliminate 5th, 7th and 11 th order harmonics are given in Table 6.1.

Table 6.1

Parameters of passive shunt filters

5thorder filter	C_{5sh}=20.39e-6F	L_{5sh}=19.86e-3H	R_{5sh}=0.23Ω
7thorder filter	C_{7sh}=20.8e-6F	L_{7sh}=10e-3H	R_{7sh}=0.1Ω
11thorder filter	C_{11sh}=14e-6F	L_{11sh}=6e-3H	R_{11sh}=18.6 Ω

6.3.3 MATLAB Model of the IM Drive System fed from Three-Phase Uncontrolled ac-dc Converter with Passive Series Filter

The MATLAB model of the three phase uncontrolled ac-dc converter with a passive series filter feeding induction motor drive system is shown in Fig.6.15. The passive series filter consists of two low block filters designed and tunned for 5th and 7 th order harmonic and a high block filter designed tuned for 11th order harmonic

frequency. The parameter values of the 5^{th}, 7^{th} and 11^{th} order passive series filter are given in Table 6.2.

Table 6.2

Parameters of passive series filters

5^{th}order filter	C_{5se}=40e-6F	L_{5se}=10e-3H	R_5=0.32Ω
7^{th}order filter	C_{7se}=51.7e-6F	L_{7se}=4e-3H	R_{7se}=0.29Ω
11^{th}order filter	C_{11se}=14e-6F	L_{11se}=10e-3H	R_{11se}=12 Ω

6.3.4 MATLAB Model of the IM Drive System fed from Three-Phase Uncontrolled AC-DC Converter with Passive Hybrid Filter

Fig. 6.16 shows the MATLAB model of a passive hybrid filter consists of two low block filters tuned at 5^{th} and 7^{th} harmonic frequencies and a high block filter tuned at11^{th} harmonic frequency and one high pass passive shunt filter tuned for 11^{th} harmonic frequency. The parameters values of the passive hybrid filter are given in Table 6.3.

Table 6.3

Parameters of passive hybrid filters

5^{th}order series filter	C_{5se}=40e-6F	L_{5se}=10e-3H	R_5=0.32Ω
7^{th}order series filter	C_{7se}=51.7e-6F	L_{7se}=4e-3H	R_{7se}=0.29Ω
11^{th}order series filter	C_{11se}=14e-6F	L_{11se}=10e-3H	R_{11se}=12 Ω
11^{th}order shunt filter	C_{11sh}=14e-6F	L_{11sh}=6e-3H	R_{11sh}=18.6 Ω

6.3.5 MATLAB Model of the IM Drive System fed from Three-Phase Uncontrolled AC-DC Converter with TSC-Hybrid Filter

MATLAB model of three-phase uncontrolled ac-dc rectifier with passive series filters and thyristor switched capacitor are shown in Fig.6.17. The drawback of passive hybrid filter is tried to solve in this scheme. The thyristor switch capacitor consists of series RLC circuit with bidirectional thyristor switches. The TSC circuit is designed

and tuned for 5^{th} order harmonics filter. With this configuration, TSC performs two tasks. First it compensate reactive power and simultaneously improves supply current harmonics. The TSC – hybrid filter parameter values are given in Table 6.4.

Table 6.4

Parameters of TSC-Hybrid filter

5^{th}order series filter	C_{5se}=40e-6F	L_{5se}=10e-3H	R_5=0.32Ω
7^{th}order series filter	C_{7se}=51.7e-6F	L_{7se}=4e-3H	R_{7se}=0.29Ω
11^{th}order series filter	C_{11se}=14e-6F	L_{11se}=10e-3H	R_{11se}=12 Ω
TSC	C_{PF}=20e-6F	L_{PF}=10e-3H	R_{PF}=0.18 Ω

6.7 Results and Discussions

The different configurations of the passive filter and TSC-hybrid filter combination are discussed and presented above. These are modelled and simulated in MATLAB /SIMULINK environment. The specifications and the parameters of the IM are given in Table. 2.1. To compare the power quality indices with different slandered filters and proposed TSC hybrid combination filter, A three phase uncontrolled ac-dc converter feeding power to three phase VSI fed IM drive is simulated without filter and with filter. The simulation results are analyzed and compared to identify the suitability of particular filter. The following five cases are taken-up for simulation and performance analysis.

1. Three phase uncontrolled AC-DC Converter supplying 3-phase VSI fed IM drive (without any filter)
2. Three phase uncontrolled AC-DC Converter supplying 3-phase VSI fed IM drive with passive shunt filter
3. Three phase uncontrolled AC-DC Converter supplying 3-phase VSI fed IM drive with passive series filter
4. Three phase uncontrolled AC-DC Converter supplying 3-phase VSI fed IM drive with passive hybrid filter

5. Three phase uncontrolled AC-DC Converter supplying 3-phase VSI fed IM drive with TSC hybrid combination filter

Case 1: Here the three-phase uncontrolled ac-dc converter feeding 3-phase induction motor is simulated without filter. The simulation results are shown in Fig.6.19-Fig.6.21.The set of response consists of reference speed ω_r^*(rpm), rotor speed ω_r (rpm), developed torque T_e (Nm), applied torque T_l (Nm), active power P (kW). reactive power Q (kVAR), dc-link voltage V_{dc} (V), phase supply voltage V_{sabc} (V), phase supply current i_{sabc} (A), magnified supply phase voltage V_{sa} (V) and phase current i_{sa} (A) and supply current harmonics spectrum. The motor speed's reference speed is set at 500 rpm and it achieves steady state condition at 0.39s. In entire the transient period motor draws full load current. Hence during this period active power drawn by the motor drive system is high and approximately equal to the 7.2KW (Fig.6.19). As soon as the motor achieves set speed 500 rpm at no load, the active power decreases to 2KW. When the full load is given to the motor, the active power rises to 7.2KW and when load is halved at 1.0s, the active power is reduced to 3.5KW. The input power factor under full load, under half load and under no load are 0.98, 0.88 and 0.801(Fig.6.20). The supply current harmonic spectrum is shown in Fig 6.21. The THD is 33.34% at full load , 48.23% at half load and 74.89% at no load. The power quality indices are poor and needs to be improved using suitable filter.

Case 2: Performance of the induction motor drive system fed from uncontrolled converter with passive shunt filter (5^{th}, 7^{th} and 11^{th} order) connected on the supply side at the point of common coupling (PCC) has been simulated under same condition as above. A set of responses are illustrated in Fig.6.22 –Fig.6.25. It has been observed on connecting the shunt filters at the PCC. There is no significant change in the active during step change of speed but reactive power demands decreases in all other operating conditions. The supply current waveform is remarkably improved and more towards sinusoidal. The THD reduced to 9.97% under full load, under half load 10.71% and 9.10% at no load. The input power factor improves to 0.97 at full load but deteriorates as load on motor decreases. Fig.6.23 shows the filter 5^{th}, 7^{th} and 11^{th} order filters. During full load condition reactive power demand decreases and it becomes 2KVAR in all operating conditions. As parameters of the filters remains constant.

Case 3: The performance of passive series filter based scheme is shown in Fig.6.26-Fig. 6.28. Here it can be observed that at full load the THD of the supply current is 6.04%, at half load, it is 9.30% and at no load, it is 14.73%. The THD under full load improves. In half load remains nearly unchanged but deteriorates under no load conditions. The reactive power demand has different story. The demand is high in full but decreases with load. The drop in dc link voltage V_{dc} (V) is also observed at full load. The input power factor is poor with increased load.

Case 4: The performance of passive hybrid filter connected at PCC of uncontrolled ac-dc converter feeding power to induction motor drive system is depicted in Fig.6.29-Fig.6.31. With passive hybrid filter the THD of ac mains current reduces to 3.28% under full load, 4.75% under half load and 5.34% under no load. The power factor indices are 0.99, 0.99 and 0.91 under full load, half load and no load respectively. This shows with this configuration of the hybrid filter power quality able to the limit of IEEE standard 519 throughout the load variation. The effect of passive hybrid filter under full load is similar to passive series filter but it changes under no load condition and exhibits nature of shunt filter. As the hybrid filter is composed of constant filter parameter therefore reactive power of variable nature cannot be accurately compensated. So, there is need of variable reactive power compensator with harmonic compensation.

Case 5: In this case TSC hybrid filter combination has been used. As the passive hybrid filter has different nature under different load conditions. Therefore here to manage the reactive power demand condition the hybrid TSC combination has been opted to examine it's performance (Fig.6.32-Fig.6.34). With this combination of filter it may be noted that reactive power demand has decreased drastically and input power factor is nearly unity. The THD of supply current at full load is 3.83%, at half load THD is 3.81% and at no load, it is 3.49%. The results confirm good performance compare to all other filters considered here. In case TSC connected to ac mains the switching current of capacitor required to be managed. Model adaptive control technique has been used for this purpose and the results have been obtained as desired. The nature and amplitude of capacitor current at the time of switching is large which can be seen in Fig.6.22 and Fig.6.26 and it is moderate in case of passive

hybrid filter (Fig.6.29). But TSC with model reference adaptive controller the input inrush current is got reduced to tolerable range (6.32).

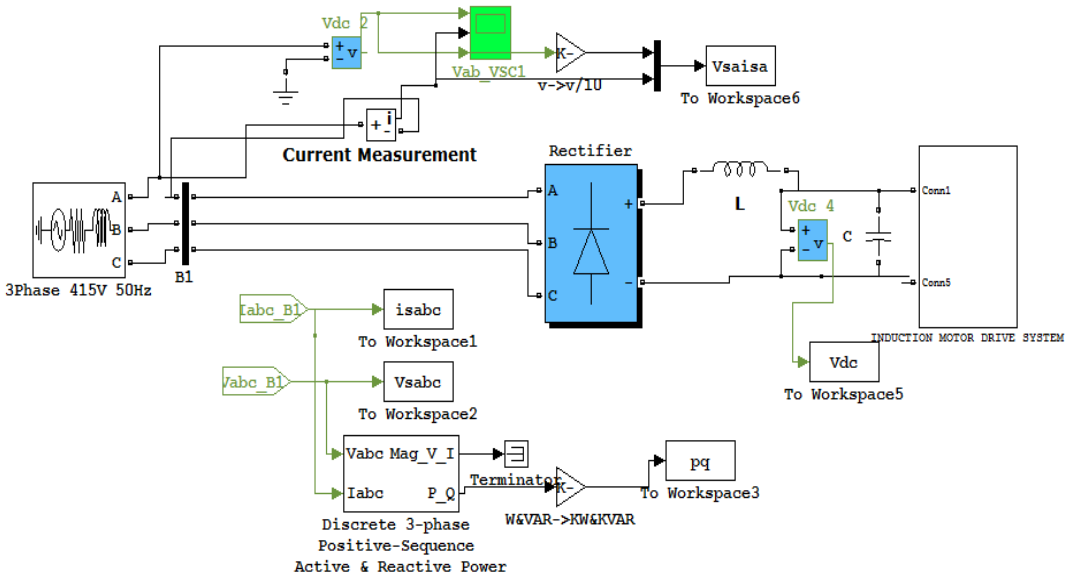

Fig.6.13 MATLAB model for three- phase uncontrolled ac-dc converter feeding induction motor drive

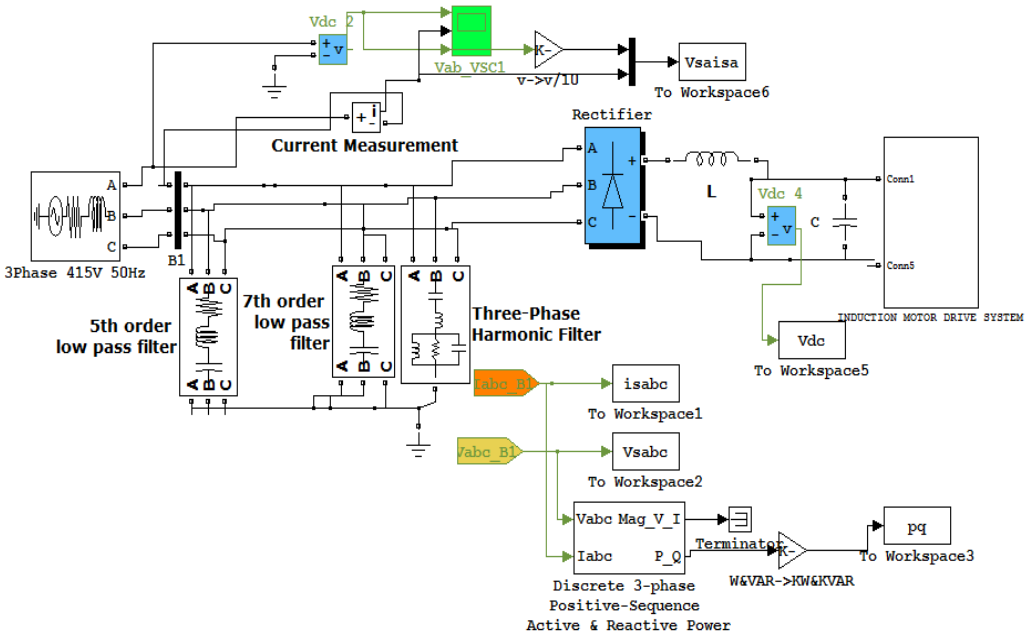

Fig. 6.14 MATLAB model for three- phase uncontrolled ac-dc converter feeding induction motor drive with passive shunt filter connected at PCC

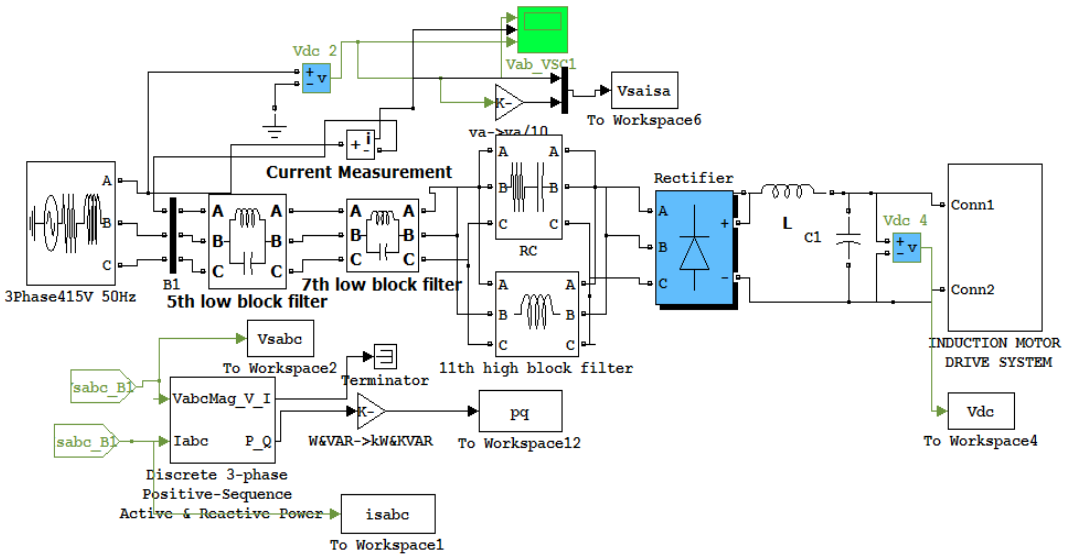

Fig.6.15 MATLAB model for three- phase uncontrolled ac-dc converter feeding induction motor drive with passive series filter connected at PCC

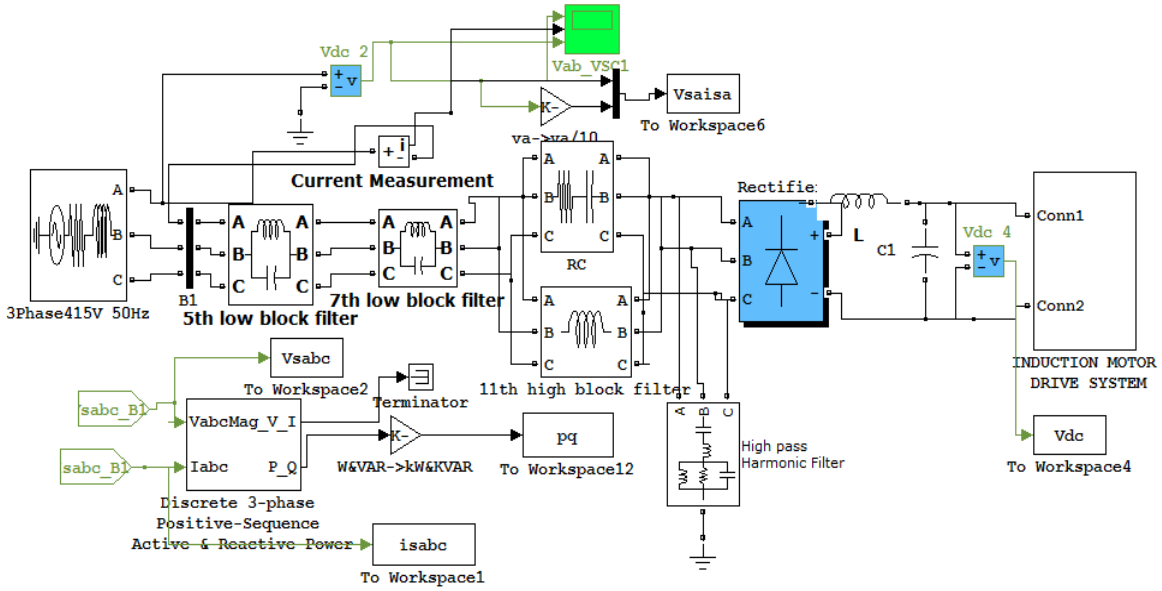

Fig.6.16 MATLAB model for three- phase uncontrolled ac-dc converter feeding induction motor drive with TSC-hybrid filter connected at PCC

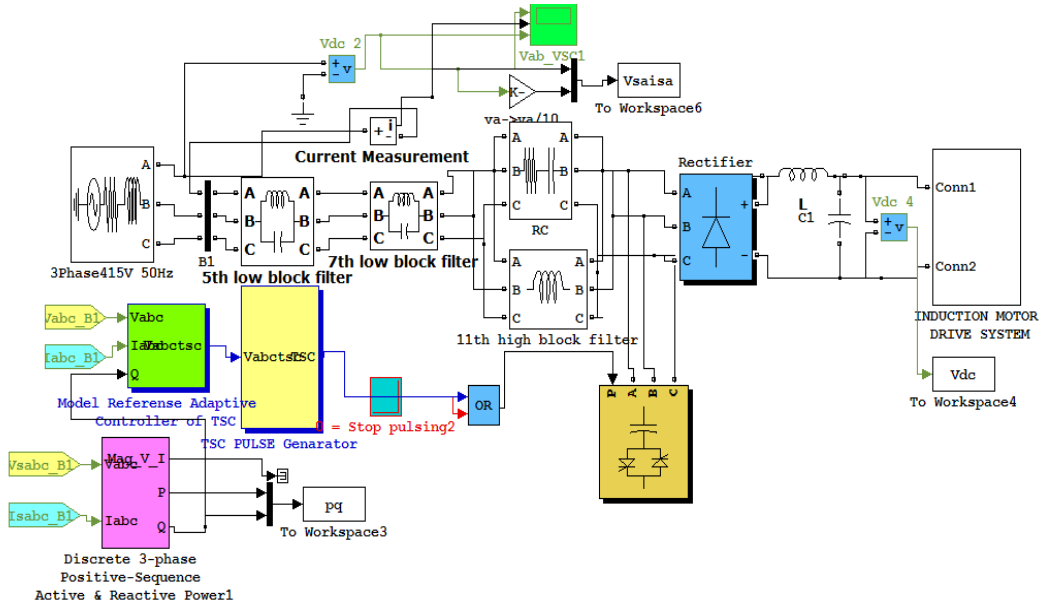

Fig.6.17 MATLAB model of the three-phase uncontrolled ac-dc converter with TSC-hybrid filter

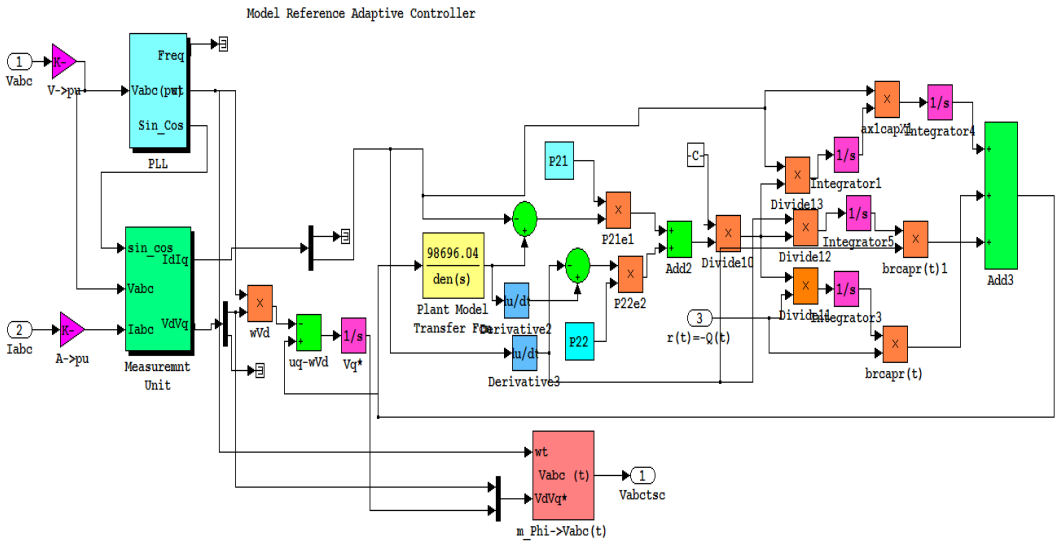

Fig. 6.18 MATLAB model of the model adaptive reference controller design for thyristor switched capacitor

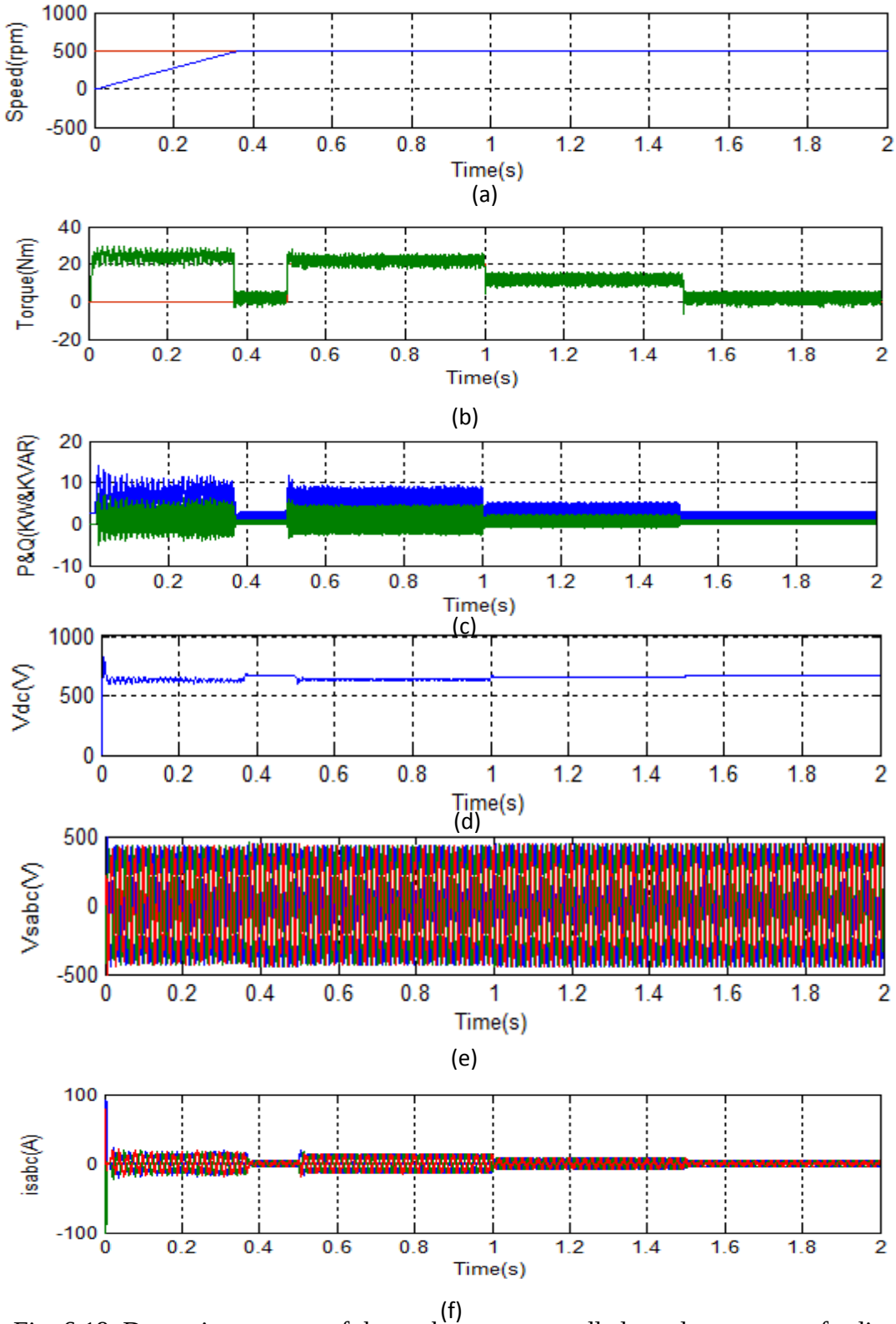

Fig. 6.19 Dynamic response of three-phase uncontrolled ac-dc converter feeding induction motor drive system illustrating: (a) motor speed, (b) actual torque and electromagnética torque (c) active power and reactive power (d) dc link voltage (e) supply phase voltage (f) supply phase current full load, half load and no load

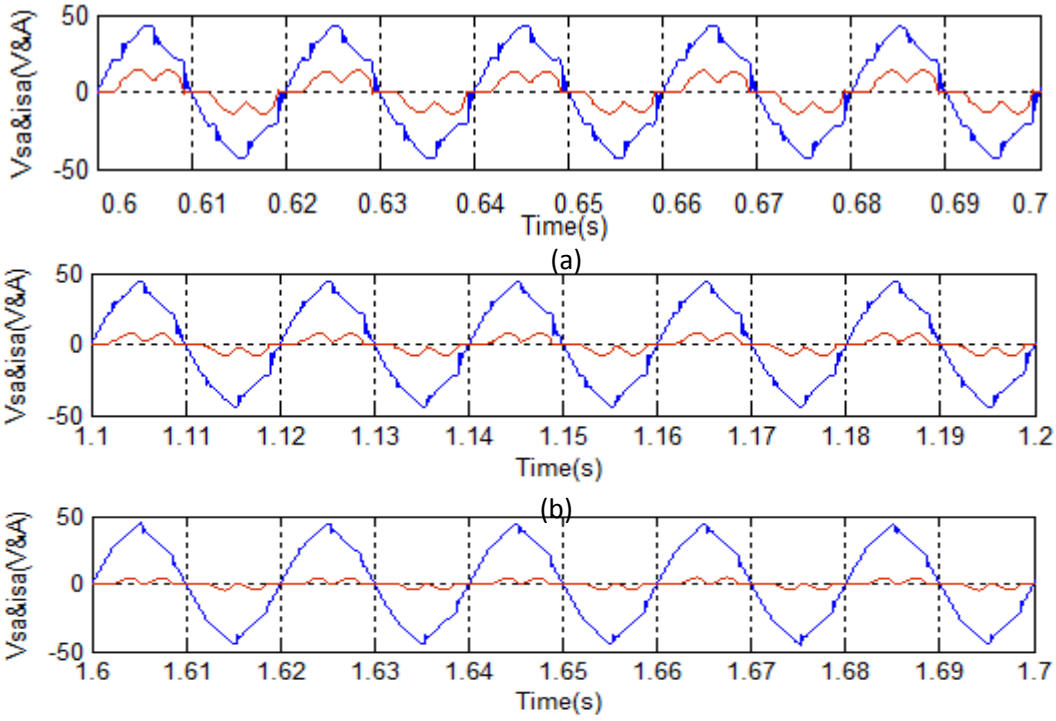

Fig.6 20 Supply voltage and current of three-phase uncontrolled ac-dc converter feeding induction motor drive system at (a) full load, (b) half load and (c) no load

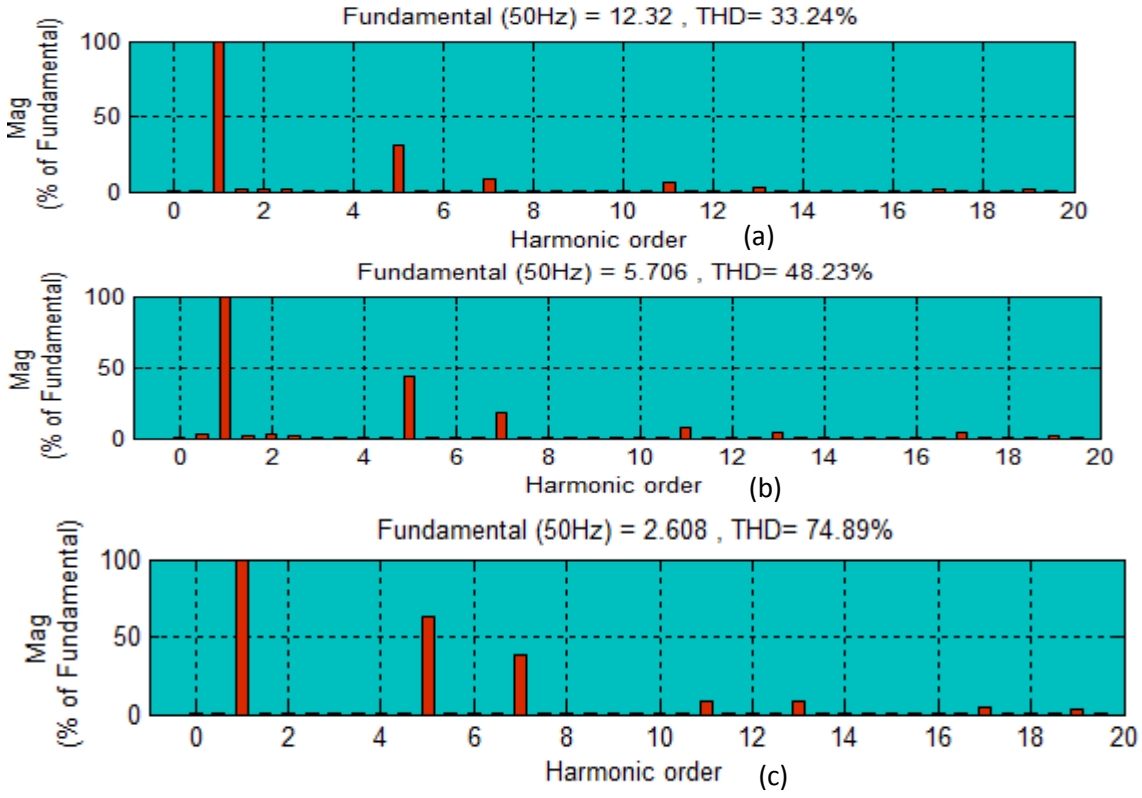

Fig.6.21 Supply current harmonic spectrum of three-phase uncontrolled ac-dc converter feeding induction motor drive system at (a) full load, (b) half load and (c) no load

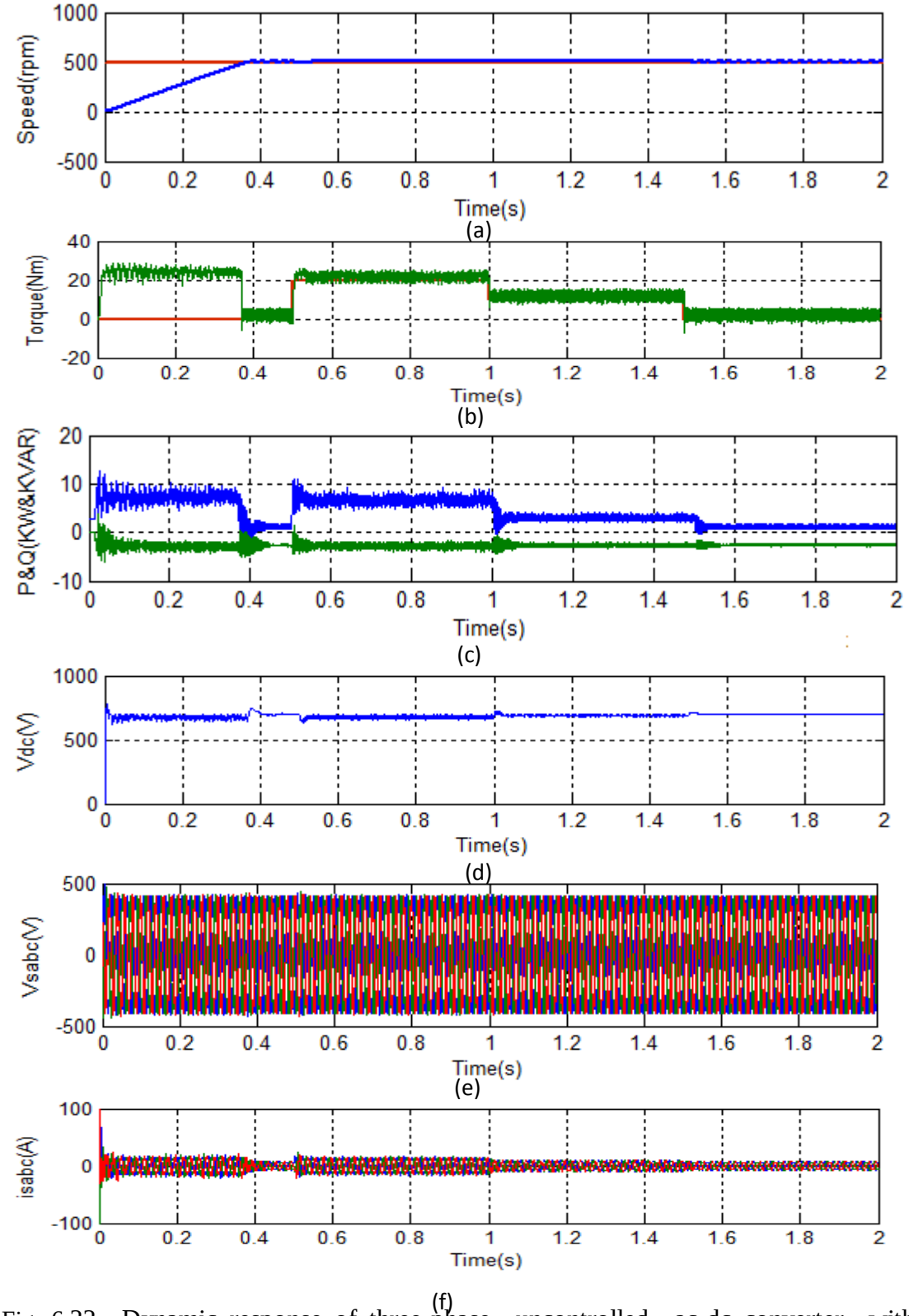

Fig. 6.22 Dynamic response of three-phase uncontrolled ac-dc converter with passive shunt filter feeding induction motor illustrated for (a) motor speed, (b) actual torque and electromagnética torque (c) active power and reactive power (d) dc link voltage (e) supply phase voltage (f) supply phase current at full load, at half load and no load

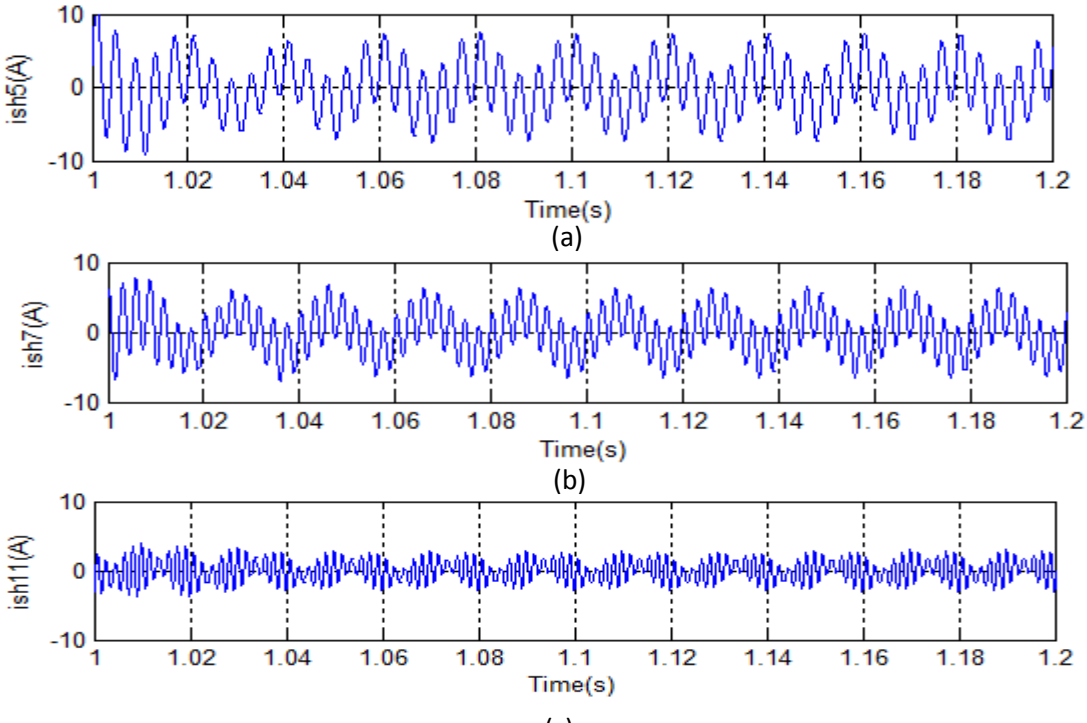

Fig. 6.23 5th , 7 th and 11th harmonic current

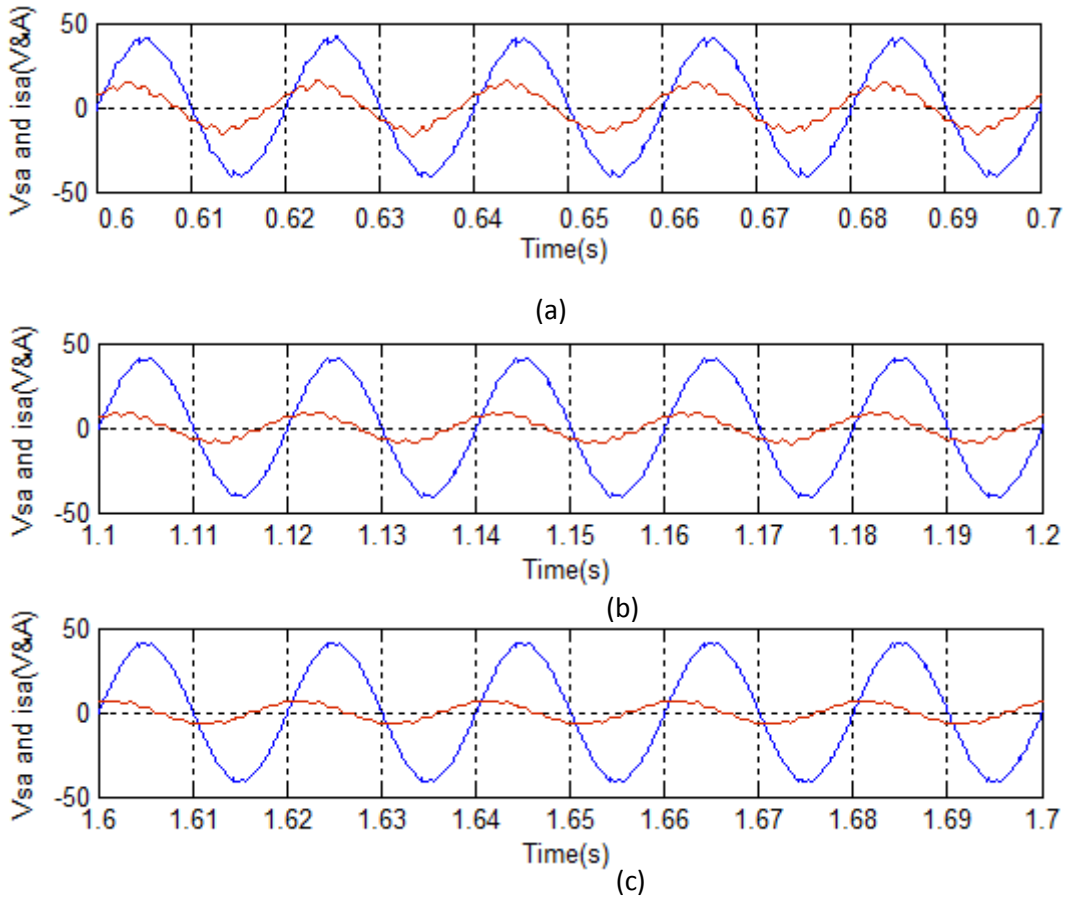

Fig.6.24 Supply voltage and current of three-phase uncontrolled ac-dc converter with passive shunt filter at (a) full load, (b) half load and (c) no load

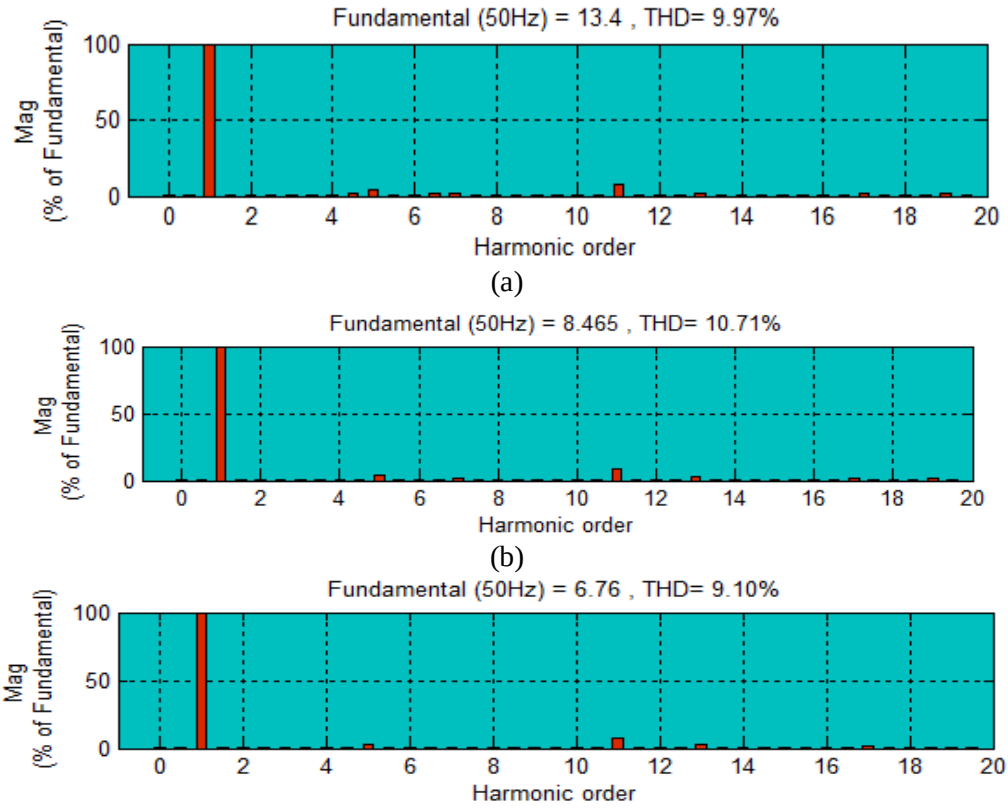

Fig.6.25 Supply current harmonic spectrum of three-phase uncontrolled rectifier with passive shunt filter at (a) full load, (b) half load and (c) no load

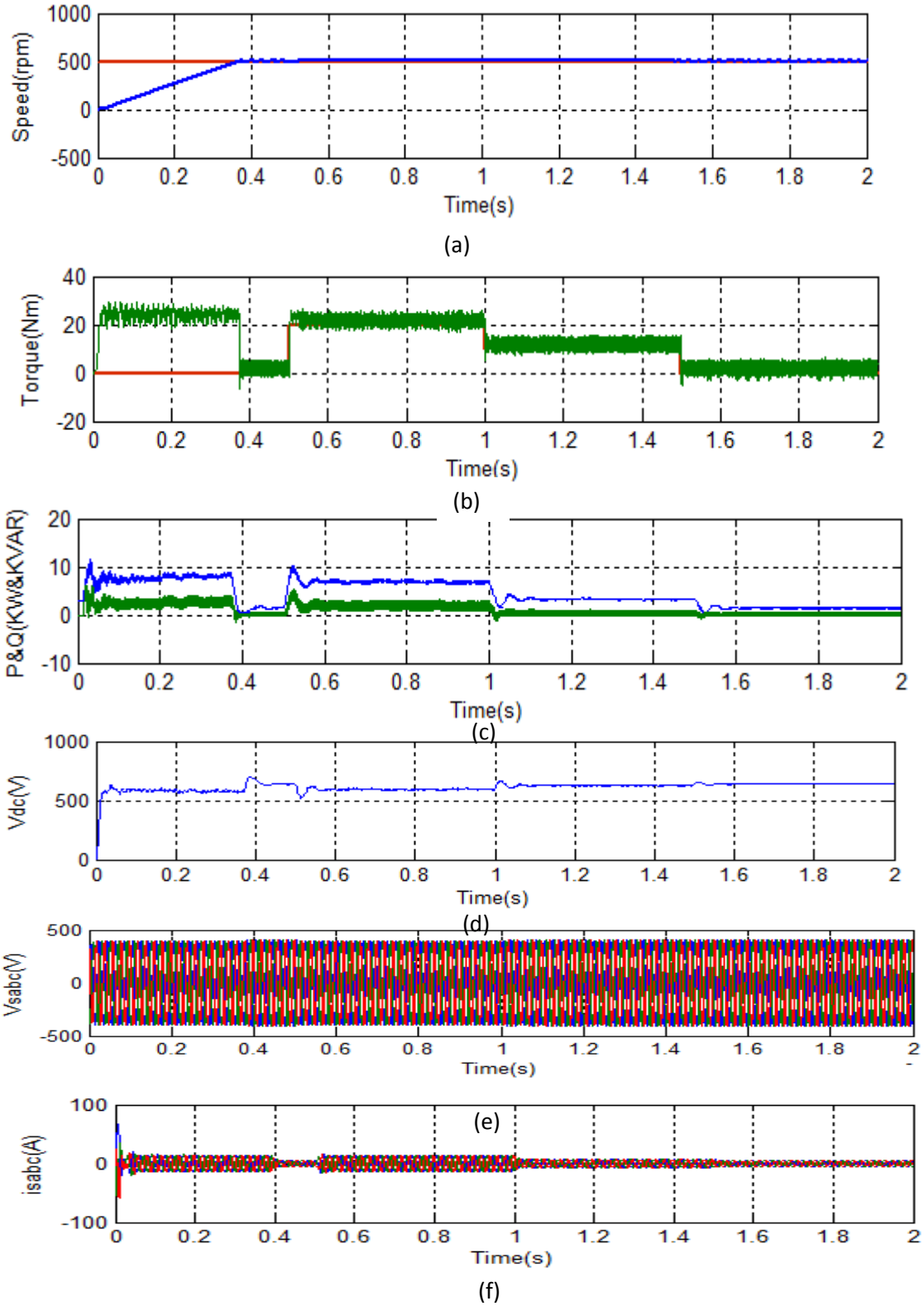

Fig. 6.26 Dynamic response of three-phase uncontrolled ac-dc converter with passive series filter feeding induction motor illustrated for (a) motor speed, (b) actual torque and electromagnética torque (c) active power and reactive power (d) dc link voltage (e) supply phase voltage (f) supply phase current at full load, at half load and no load

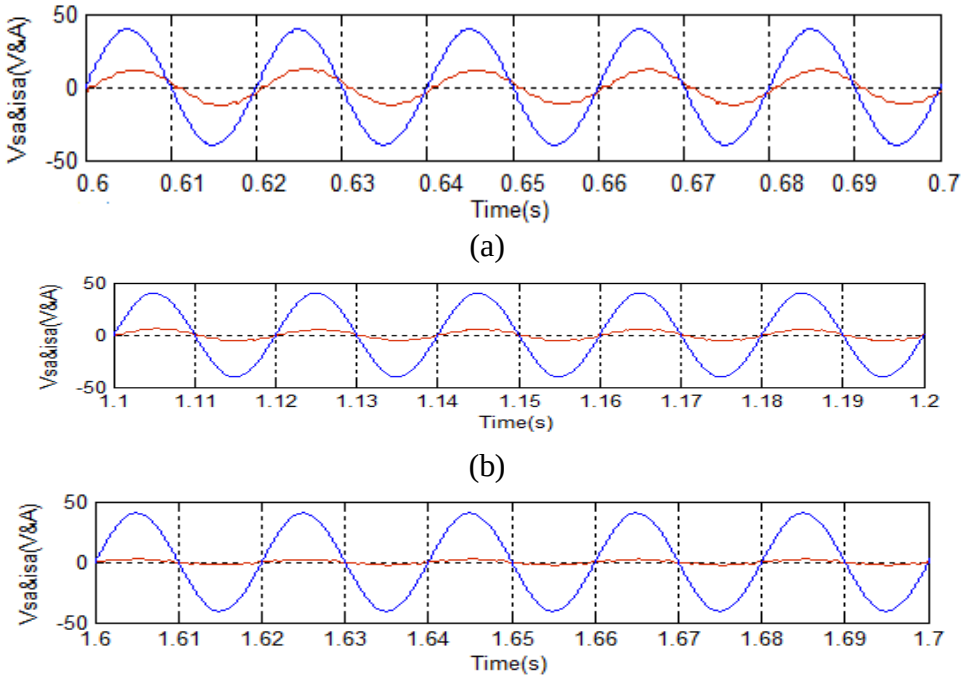

Fig.6.27 Supply voltage and current of three-phase uncontrolled ac-dc converter with passive series filter at (a) full load, (b) half load and (c) no load

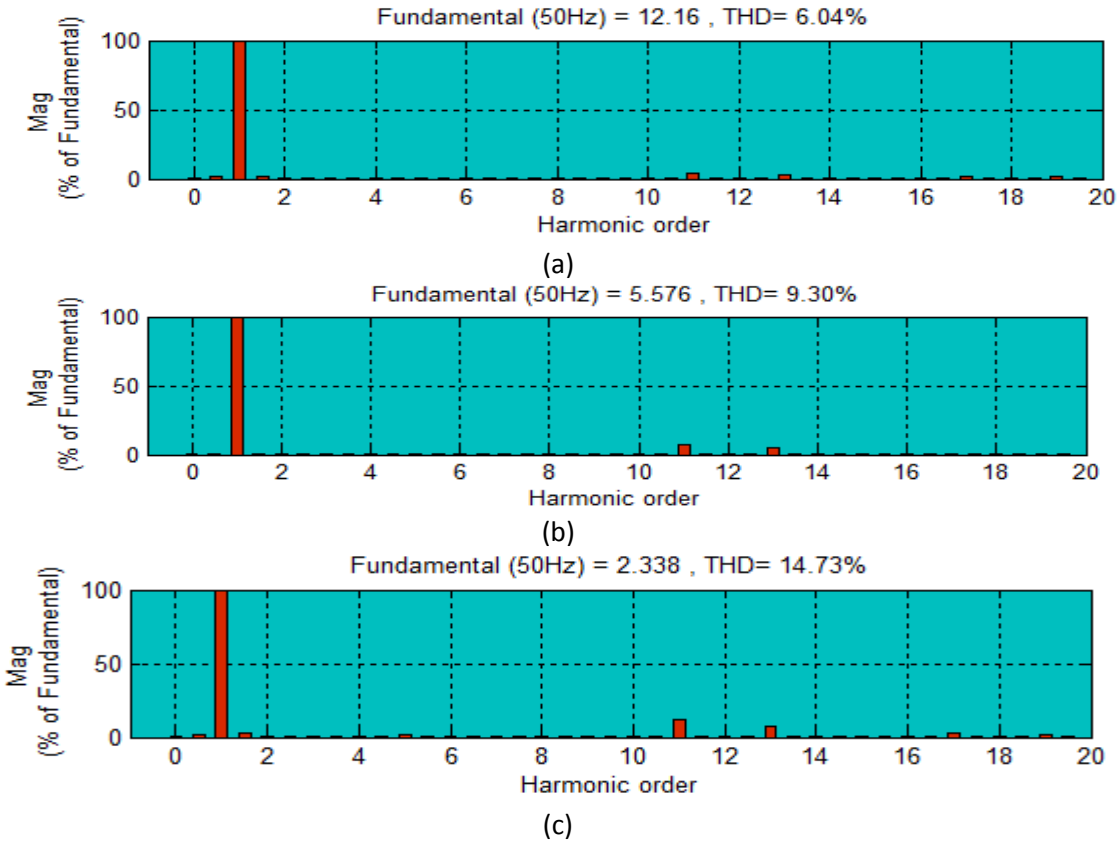

Fig.6.28 Supply current harmonic spectrum of three-phase uncontrolled ac-dc converter with passive series filter feeding induction motor drive at (a) full load, (b) half load and (c) no load

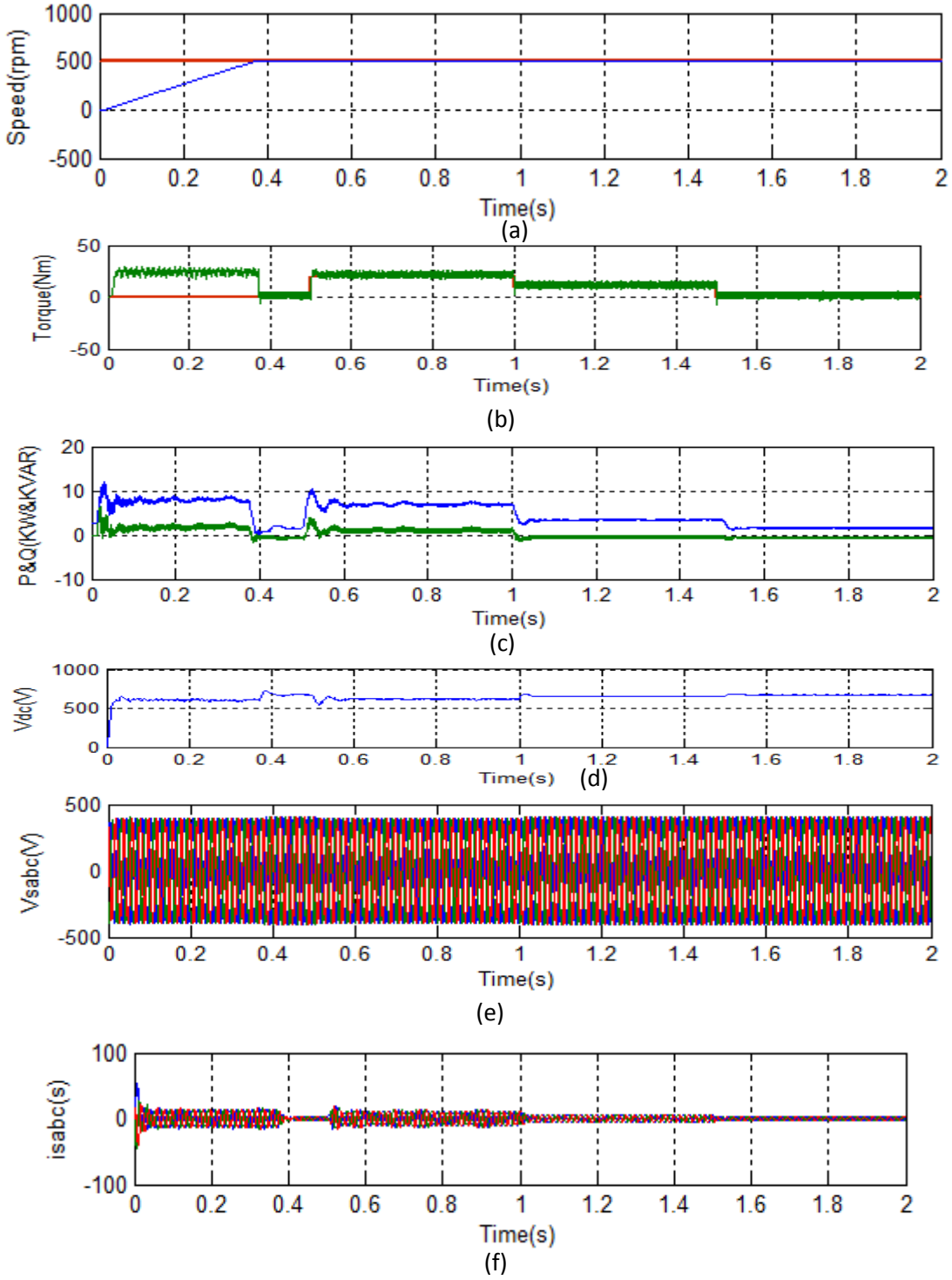

Fig. 6.29 Dynamic response of three-phase uncontrolled ac-dc converter with passive hybrid filter with line inductor feeding induction motor illustrated for (a) motor speed, (b) actual torque and electromagnética torque (c) active power and reactive power (d) dc link voltage (e) supply phase voltage (f) supply phase current at full load, at half load and no load

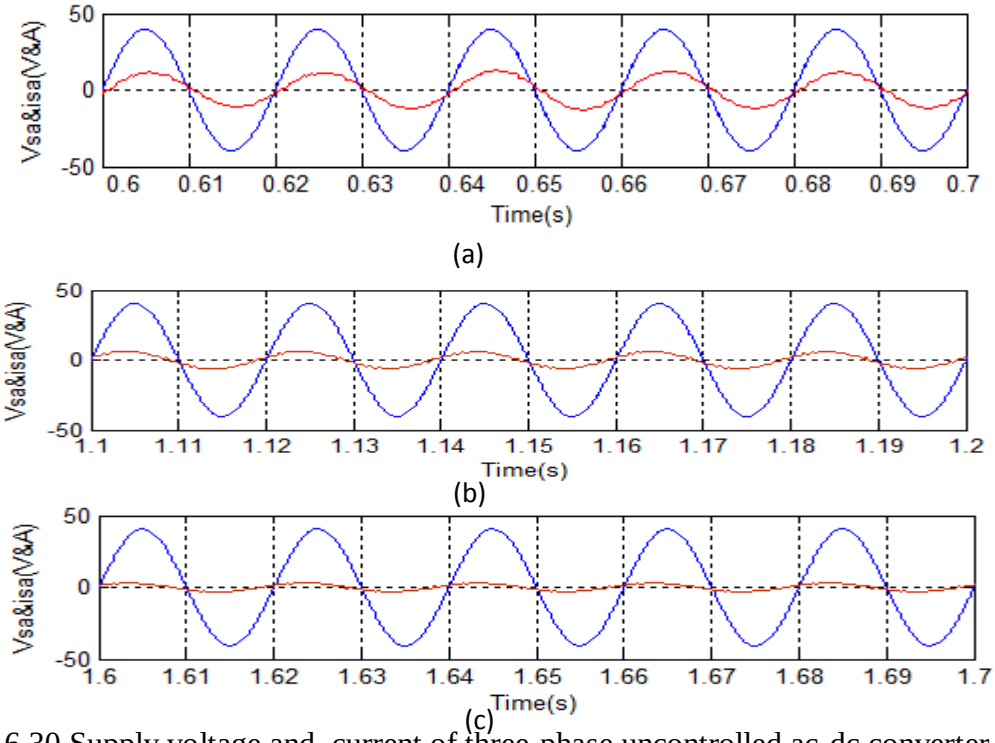

Fig.6.30 Supply voltage and current of three-phase uncontrolled ac-dc converter with passive hybrid filter at (a) full load, (b) half load and (c) no load

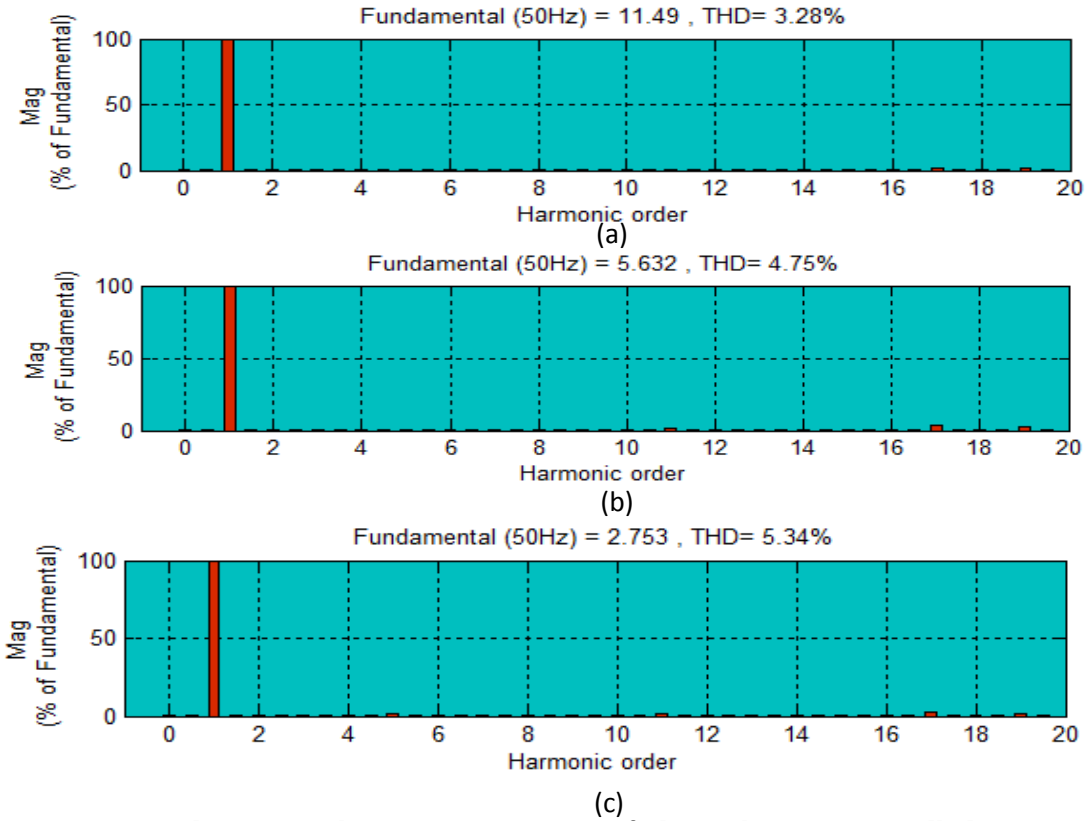

Fig.6.31 Supply current harmonic spectrum of three-phase uncontrolled converter with passive hybrid filter feeding induction motor drive at (a) full load, (b) half load and (b) no load

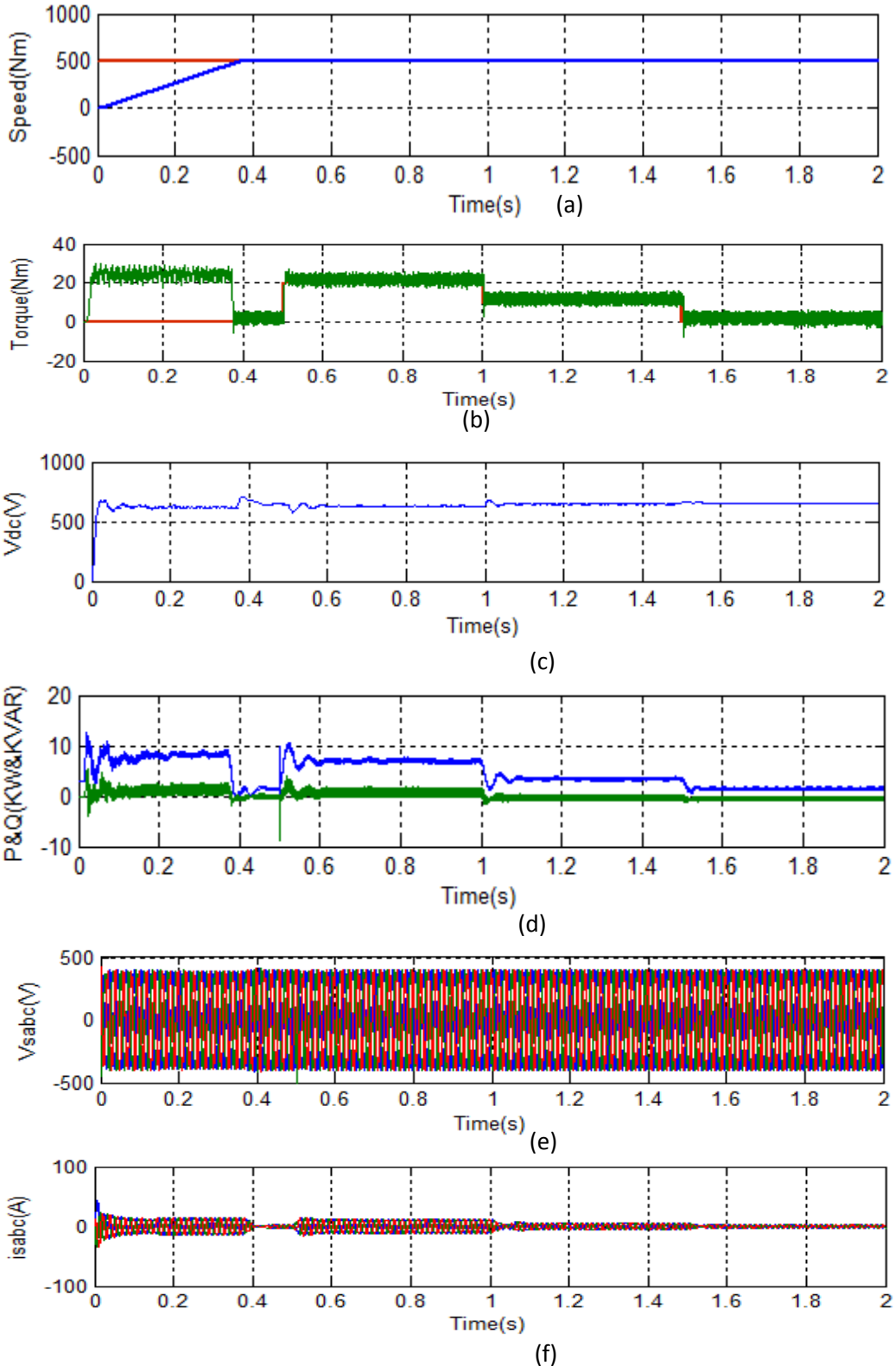

Fig. 6.32 Dynamic response of three-phase uncontrolled converter with TSC-hybrid filter feeding induction motor illustrated for (a) motor speed, (b) actual torque and electromagnética torque (c) active power and reactive power (d) dc link voltage (e) supply phase voltage (f) supply phase current at full load, at half load and no load

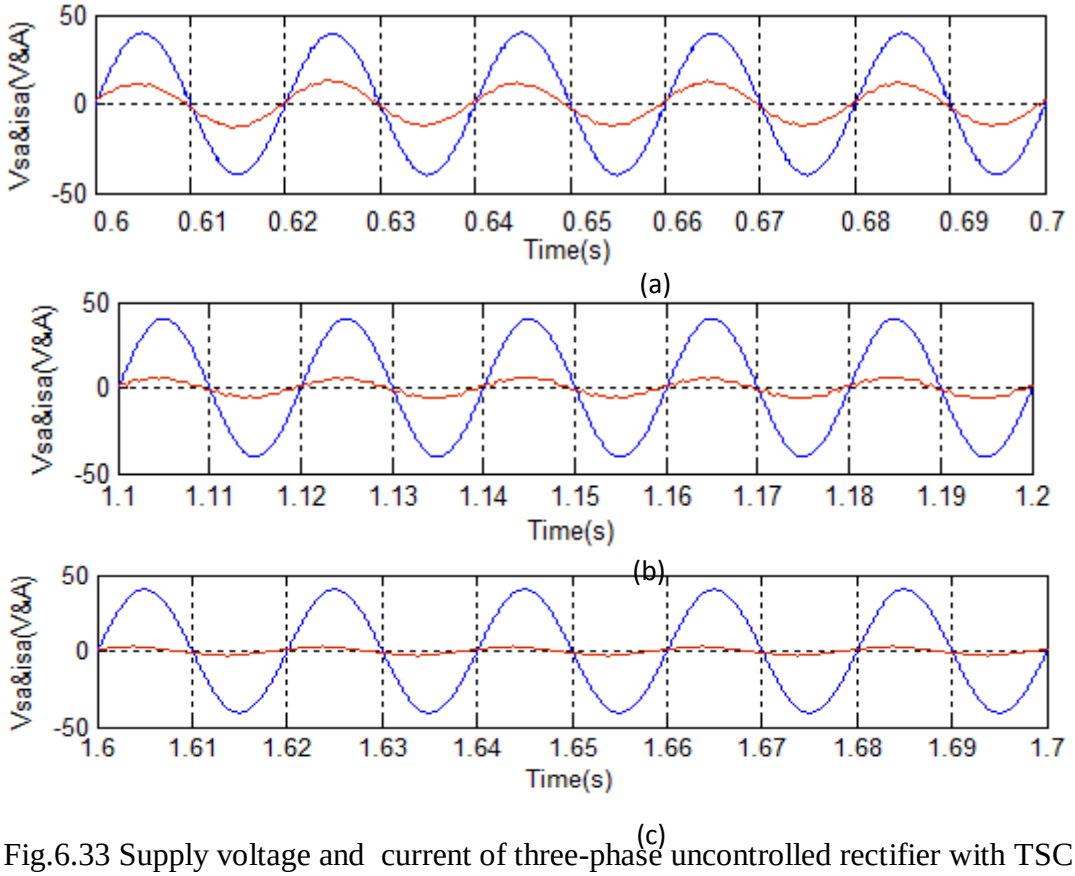

Fig.6.33 Supply voltage and current of three-phase uncontrolled rectifier with TSC hybrid filter at (a) full load, (b) half load and (c) no load

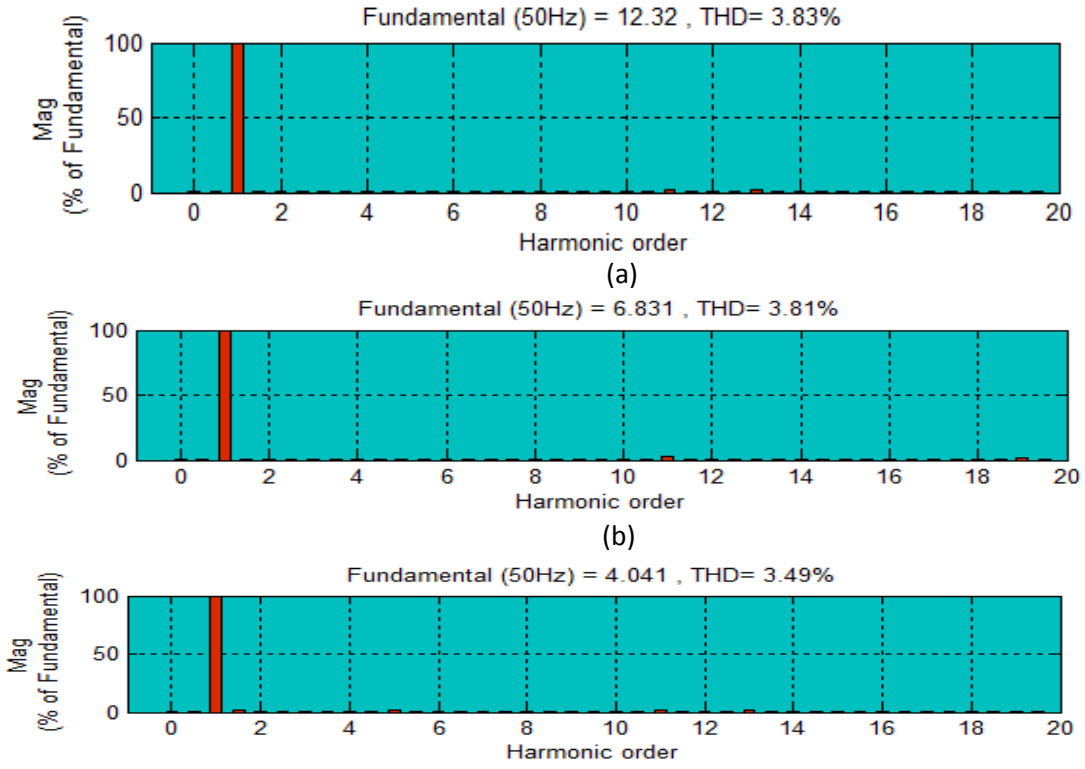

Fig.6.34 Supply current harmonic spectrum of three-phase uncontrolled ac-dc converter with TSC- hybrid filter feeding induction motor drive at (a) full load, (b) half load and (c) no load

Table 6.5
Power quality indices comparison of 3-phase uncontrolled ac-dc converter with various passive filter and active hybrid filter

Sl. No.	Configuration	Load on IM (Nm)	THD(%)Supply Current	THD(%)Supply Voltage	PF	P (KW)	Q (KVAR)	DC link Voltage Vdc(V)
1.	3-phase uncontrolled ac-dc converter	a. Full Load b. Half Load c. No load	33.24 48.23 74.89	4.72 2.99 1.18	0.98 0.99 0.97	7 3.5 2	1.5 1.00 0.5	635 655 670
2.	3-phase uncontrolled ac-dc converter with passive shunt filter	a. Full Load b. Half Load c. No load	9.97 10.71 9.10	3.00 1.5 1.38	0.955 0.83 0.45	6.5 3.0 1..2	-2.0 -2.0 -2.6	680 690 700
3.	3-phase uncontrolled ac-dc converter with passive series filter	a. Full Load b. Half Load c. No load	6.04 9.30 14.73	0.58 0.49 0.32	0.96 .99 0.99	6.5 3.2 1.5	2.0 0.5 0.25	600 630 640
4.	3-phase uncontrolled ac-dc converter with passive hybrid filter	a. Full Load b. Half Load c. No load	3.28 5.34 4.75	1.14 0.85 0.55	0.99 0.99 0.91	6.5 3.5 1.52	1 -0.5 -0.7	625 640 675
5.	3-phase uncontrolled ac-dc converter with TSC hybrid filter	a. Full Load b. Half Load c. No load	3.83 3.81 3.49	1.03 0.7 .42	1 1 1	6 3.0 1.25	0.00 -0.2 -0.2	630 645 655

6.5 Summary of the Chapter

Different configurations of passive filter and TSC hybrid filter combination have been designed, modeled and simulated to study and for comparison of power quality indices. It has been observed that the passive shunt filter is not suitable for voltage source type harmonic producing load, as it's performance deteriorate under light load condition. The passive series filter has been observed to be better suited for such loads as its performance is better than the passive shunt filter. However, the performance of passive series filter is not satisfactory, as it results in the reduction of dc link voltage. The passive hybrid filter has been observed to be a better solution, as it performs well in varying load condition on the drive. But due to constant filter parameter it does not provide smooth control over varying load application. The TSC hybrid filter combination with control strategy meets this requirement with excellent overall power quality indices.

Chapter – 7

Main Conclusions and Suggestions for Future Works

7.1 General

Induction motor drives have started providing solution for medium speed motor control in place of dc drive. The application of field oriented control theory well established over the last two decades [31]]52][56][62] to induction motor drives leads to good dynamic torque and speed control as required by high performance industrial applications. The revolutionary progress in digital signal processing technology provide an easy hand for implementation of advanced and sophisticated control strategy such as state feedback control, sliding mode control, adaptive control and also emerging technology such as fuzzy logic and neural networks. In course of literature survey it has been observed that the above mentioned controlled theory have used along for performance improvement of the drive system. The study analysis design of controllers from comparison point of view is rare in literature. A comparative study of controllers for IM drive may be a good contribution and helpful in selection of suitable drive system for particular application. Normally it has also been noted that the investigations are either concentrated to motion control and it's impact on ac mains is ignored. The author is of the view that the research work should not remain limited to improving drive performance rather it should have wide scope including point of common coupling to be taken care of.

7.2 Summary of the Present Research

The present research work has aimed at study, design and development of some controllers for induction motor drive for performance improvement and their comparison to find the best option. The effect of converter based drive at the point of

common coupling and majors being taken to reduce the deterioration of power quality have also been studied. Initially a comprehensive mathematical model of induction motor is developed in stationary (α-β) reference frame, with state current and rotor flux as state variables. The state feedback linearization for decoupling control principle as applied to the induction motor drive is developed [27]. The linearized induction motor drive system has been splited into two linear subsystem: Electrical and Mechanical [14]. Systematic procedure has been developed to determine the gains of the PI controller for electrical and mechanical subsystem. To take care of model uncertainties and parameter variation a robust control strategy based on sliding mode principle has been designed and developed for IM drive system. The induction motor model is organized to make it suitable for the sliding mode control algorithm. The torque ripple problem of sliding mode controller has been solved by implementing iterative learning controller. Three control schemes: PI, SM and ILC have been simulated in MATLAB/SIMULINK environment and also at real time digital simulator (RT-LAB). The result obtained are analysed and performance have been compared to identify the best performer in similar conditions. Condition for global asymptotic stability in the sense of Lyapunov theorem for close loop IM in stationing α-β reference frame has been derived considering power balance equation. One more control strategy based on this theorem has been designed for improved performance and stability. The strategy has been tested for high speed and heavy load and finally performance have been compared with PI and SM.

The different types of filters connected at the PCC have been modelled with uncontrolled ac-dc converter for power quality improvement. TSC and hybrid filter combination have been designed for harmonic mitigation and reactive power compensation under variable load. The model reference adaptive control law has been implemented for transient free switching and to meet variable reactive power. The designed system has been simulated for evaluation. The test results have been found satisfactory and this combination of filter has been found to be the best among all.

7.3 Main Contributions of the Thesis

This thesis has the following main contributions.

a. Study of PI, PI with Fuzzy logic, Sliding Mode, Iterative Learning, Model Reference Adaptive, and Lyapunov Criteria based Controllers for performance improvement of induction motor drive and also the Power filter.

b. Design of PI controllers and fuzzy torque compensator for the electrical and mechanical subsystems, obtained through decoupling control.

c. Decoupling control of induction motor drive and its stability study using Lyapunov's theorem.

d. Simplified designed approach for developing controllers like sliding mode controller, iterative learning controller and Lyapunov based controller and their analysis.

e. Simulation of the induction motor drive with designed controllers and performance comparison.

f. Implementation and testing of the various designed controllers in RT-LAB simulator, and validation of simulation results.

g. Systematic design of passive shunt, series and hybrid filter for harmonic mitigation.

h. Design of active power filter with thyristor switch capacitor based on model reference adaptive control principle for variable reactive power compensation.

i. Designed filters are simulated in MATLAB/SIMULINK environment. The simulated results are justifying the set objective.

7.4 Scope for Future Research

The present research work has successfully designed and developed some controllers for performance improvement of induction motor drive and power quality at the point of common coupling. The MATLAB/SIMULINK model of the drive system has been developed with designed controllers for performance analysis and comparison. The study of some power filters connected at the front end of ac-dc converter for harmonic mitigation and reactive power compensation has also been taken up.

There is no end of investigation. There exist scope for further research work to exploit the features of modern control theory for developing simple design procedure and improving the performance of not only the IM drive rather power filter for ac mains to be connected at the point of common coupling.

- Intelligent parameter adaptation approach can be added to feedback linearization technique.
- Scope of chattering reduction using a hybrid controller consisting of fuzzy-neural-network can be investigated.
- Stability study of IM drive in low speed range using Lyapunov theorem to identify critical load.
- Design of sliding mode controller takes the variation of rotor resistance into consideration. But complete investigation on system performance with rotor resistance variation should be done.
- The THD at point of common coupling can be further reduced. The application of neural network for accurate switching can be worked out.
- Soft computation techniques can be used to identify the type and optimum size of power filter to be connected at PCC for performance improvement of IM drive as well as harmonic mitigation plus reactive power compensation.

References

[1] W. Leonhard, "Microcomputer control of high dynamic performance as drives – a survey", *Automatic*, Vol. 22, NO.1, pp.1-19, 1986.

[2] J. J. E. Slotine and W.Li, *Applied Nonlinear Control*, Prentice Hall, 1991.

[3] F. Blaschke, "The principle of field orientation as applied to the new TRANSVEKTOR closed- loop control system for rotating-field machines," Siemens review, vol. 39, pp. 217-220, May 1972.

[4] K. Hasse, "On the dynamic behavior of induction machine driven by variable frequency and voltage source," *ETZ Arch. Bd. 89*, H.4, pp. 77-81, 1968.

[5] W. Leonhard, *Control of Electrical Drives*, New Delhi, Narosa Publication, 1985.

[6] G. S. Kim, I. J. Ha and M. S. Ko. "Control of induction motors for both high dynamic performance and high power efficiency," *IEEE Trans. On Industrial Electronics*, vol. 39, no.4, pp. 323-333, Aug. 1992.

[7] D. S. Kischen, D. W. Novotony, and T. A. Lipo, "Optimal efficiency control of an induction motor drive," *IEEE Trans. On Energy Conversion*, vol.2, no.1, pp.75-75, 1990.

[8] A. Isidori, A. J. Krener, C. Gori-Giorgi, and S. Monaco, " Nonlinear decoupling via feedback: A differential-geometric approach," *IEEE trans. AC*, vol. 26, pp. 331-345, April 1981.

[9] A. Isidori, J. W. Grizzle, "Fixed modes and nonlinear noninteracting control with stability," *IEEE Trans. Automatic Control*, vol.33, no.10, pp.907-913, November 1988.

[10] A. Isidori, C. I. Byrnes, "Output regulation of nonlinear systems," *IEEE Trans. Automatic Control*, vol.35, no.2,pp. 131-140, February1990.

[11] C. I. Byrnes, A. Isidori, "Asysmptotic stabilization of minimum phase nonlinear systems," *IEEE Trans. Automatic Control*, vol.36,no.10, pp.1122-1137, October 1991.

[12] B.K. Bose, Modern Power Electronics And AC Drives, *Prentice Hall Of India*, New Delhi, 2008

[13] Z. Krezminski, "Nonlinear control of induction motor," *Proc. Of 10th IFAC World Congress on Automatic Control*, vol. 3, Munic, Germany , pp.349-354, 1987.

[14] A. De Luca, and G. Ulivi, "Design of exact nonlinear controller for induction motors," *IEEE Trans. on Automatic Control*, vol. 34, no.12, pp1304-1307, Dec.1989.

[15] A. De Luca, and G. Ulivi, "Dynamic decoupling of voltage frequency controlled induction motors," in *Proc.of the IEEE*, IAS, vol.82(8), pp 1215-1240, August 1994.

[16] D. I. Kim, I. J. Ha and M. S. Ko, "Control of induction motors via feedback linearization with input-output decoupling," *Int. Journal of Control*, vol.51.no.4, pp.863-883, 1990.

[17] D. I. Kim, I. J. Ha and M. S. Ko, "Control of induction motors for both high dynamic performance and high power efficiency," *IEEE Trans. on Industrial Electronics* , vol.39, no.4, pp.323-333, Aug. 1992.

[18] D. I. Kim, I. J. Ha and M. S. Ko, " Speed sensorless vector control of induction motor using extended Kalman filter," *IEEE Trans. on Ind. Appl*., vol. 30, no.5, pp.1225-1233, 1994.

[19] R. Marino, S. Peresada, and P. Valigi, " Adaptive partial feedback linearization of induction motor," in *Conf.Decision and Control Proc.29th*, Honolulu, HI,Dec.1990.

[20] R. Marino, S. Peresada, and P. Valigi, " Nonlinear control of induction motors: a simulation study," in *Proc 1991 Eurq control conf*. Grenoble, France, 1991.

[21] R. Marino, S. Peresada, and P. Valigi, "Adaptive input-output linearizing control of induction motors," *IEEE Trans. AC*, vol.38, no.2, pp.208-221, 1993.

[22] R. Marino, and P. Tomei, " Global adaptive output-feedback control of nonlinear systems, part1: Linear parameterization," *IEEE AC* , vol.38, no.1, pp. 18-32, January 1993

[23] R. Marino, and P. Tomei, "An adaptive output feedback control for a class of nonlinear systems with time varying parameters," *IEEE Trans. AC* , vol.44, no.11, pp.2190-2194, November 1999.

[24] R. Marino, S. Peresada and P. Tomei, "Output feedback control of current-fed induction motors with unknown rotor resistance," *IEEE Trans. Control Systems Technology*, vol.4, no.4, pp.336-346, July1996.

[25] S. Liuzzo, R. Marino, and P. Tomei, "Adaptive learning control of nonlinear systems by output error feedback," *IEEE Trans. AC*, vol.52,no.7, July 2007.

[26] J. Chiasson, A. Chaudhari, and M. Bodoson, "Nonlinear controllers for the induction motor," *in Proc. IFAC Nonlinear Control System Design Symp.*, Bordeaux France, pp.150-155, June 1992.

[27] J. Chiasson, "Dynamic feedback linearization of the induction motor," *IEEE Trans. Auto. Control*, vol.38, Oct. 1993.

[28] J. Chaiasson, "A new approach to dynamic feedback linearization control of an induction motor," *IEEE Trans. AC* , vol. 43, no. 3 , pp.391-397, March 1998.

[29] R. Ortega and G. Canudas, "A controller design methology for systems with physical structures: applications to induction motors," *Automatica*, vol.29, no.3, pp.621-633, 1993.

[30] R. Ortega, C. Canudas, and S. I. Seleme, "Nonlinear control of induction motors:torque tracking with unknown load disturbances," *IEEE Trans. on Automatic Control*, vol.38, no. 11, pp.1675-1680, Nov.1993.

[31] C.C. Chan, W.S.Leung, and C.W,Ng, "Adaptive decoupling control of induction motor drives," *IEEE Trans. on Industrial Electronics* , vol.35, no.1, pp.41-47, Feb. 1990.

[32] K. B. Mohanty and N. K. De, "Nonlinear controller for induction motor drive," *Proc. of IEEE Int. Conf. on Industrial Technology(ICIT)*, Goa, pp.382-387, Jan 2000.

[33] K. J. Astrom and T. Hagglund, *PID Controllers: Theory, Design, and Tuning*, Second Edition, Instrument Society of America, The International society for Measurement and Control, pp.166, 1995.

[34] A. Sabanovic and D. B. Izosimov, "Application of sliding modes to induction motor control," *IEEE Trans. Ind. App*. Jan./Feb.1981.

[35] J. J. E. Slotine," Sliding controller design for nonlinear systems," *Int. Journal of Control*, vol.40, no. 2, pp. 421-434, 1984.

[36] J. J. E. Slotine and S. S. Sastry ,"Tracking control of nonlinear systems using sliding surfaces with application to robot manipulators," *Int. Journal of Control*, vol.38, no. 2, pp. 465-492, 1984.

[37] R. Soto and K. S. Yeung, " Sliding mode control of an induction motor without flux measurement." *IEEE Trans. on Ind. Appl*., vol. 31. no.4, pp.744-751, July/Aug. 1995.

[38] H. J. Shieh and K. K. Shyu, "Nonlinear sliding-mode torque control of induction motor with adaptive backstepping approach for induction motor drive," *IEEE Trans. on Industrial Electronics*, vol.46, no.2, pp.380-389, April 1999.

[39] R. J Wai and W. K. Liu. "Nonlinear decoupling control for induction motor servo-drive using sliding mode technique," *IEEE Proc. Control Theory Application*, vol. 48, no3, May2001.

[40] F. J. Lin and R .J Wai, "Robust control using neural network uncertainty observer for linear induction motor servo drive ," *IEEE Trans. on Power Electronics* , vol. 17, pp.241-254, March 2002.

[41] R. J. Wai, R. Y. Duan and L. J. Chang , "Grey feedback linearization speed control for induction servo motor drive ," *IECON Proceedings (Industrial Electronics Conference)* , vol. 3, pp. 580-585, 2001.

[42] R. J. Wai, C. M. Lin and C. F. Hsu, "Adaptive fuzzy position controller for induction servomotor drive using sliding-mode technique ," *IEEE International Conference on Fuzzy Systems* , vol. 2, pp. 570-573, 2001.

[43] R. J. Wai and F. J. Lin, "Adaptive recurrent-neural-network control for linear induction motor ," *IEEE Trans. on Aerospace and Electronic Systems* , vol. 2, pp.570-573, 2001.

[44] R. J. Wai and W. K. Liu, "Nonlinear decoupled control for linear induction motor servo-drive using the sliding-mode technique," *IEE Proceedings: Control Theory and Applications* , vol. 148, pp. 217-232, May 2001.

[45] R. J. Wai, F. J. Lin and S. P. Hsu, "Intelligent backstepping control for linear induction motor drive ," *IEE Proceedings: Control Theory and Applications*, vol.3, issue 3, pp 193-202, May 2001.

[46] F. J. Lin and R. J. Wai , "Hybrid control using recurrent fuzzy neural network for linear-induction motor servo drive," IEEE Trans. on Fuzzy Systems, vol. 9, pp. 102-115, February 2001.

[47] R. J. Wai and C. C Chu ,"Robust Petri fuzzy-neural-network control for linear induction motor drive," *IEEE Transactions on Industrial Electronics* , vol. 54, February pp.177-189, 2007.

[48] J. Soltani, N. R. Abjadi, Gh. R. A. Markadeh and H. W. Ping, "Adaptive Sliding-Mode control of a two five-phase series-connected induction motors drive,"

Proceeding of International Conference on Electrical Machines and Systems, pp. 1496-1501, 2007.

[49] J. Soltani and M. A. Abbasian, "Robust nonlinear control of linear induction motor taking into account the primary end effects," in *Proceedings 5th International Power Electronics and Motion Control Conference* , vol.2, pp. 1043-1048, 2007.

[50] J. Soltani, N. R. Abjadi and G. R. A. Markadeh , "Nonlinear decoupled control for a six-phase series-connected two induction motor drive using the sliding-mode technique," *Proceedings of the International Conference on Power Electronics and Drive Systems*, pp. 1267-1273, 2007.

[51] G. R. A. Markadeh and J. Soltani, "A current-based output feedback Sliding Mode control for speed sensorless induction machine drive using adaptive Sliding Mode flux observer," International Journal of Engineering, Transactions A: Basics, vol. 19, Issue 1, pp.21-34, November 2006.

[52] J. Soltani, Y. Abdolmaleki and M. Hajian, "Adaptive fuzzy sliding-mode control of speed sensorless universal field oriented induction motor drive with on-line stator resistance tuning," *Iranian Journal of Science and Technology,Transaction B: Engineering* , vol.29, Issue 4, pp. 425-442, 2005.

[53] Arab Markadeh, G.R. Yazdanpanah, andJ. Soltani, "Input-output feedback linearization control of induction motor with adaptive backstepping observer," *European Power Electronics and Drives Journal* , vol. 18, issue 2, pp. 33-40, April 2008.

[54] R.Yazdanpanah, J. Soltani and G.R. Arab Markadeh, "Nonlinear torque and stator flux controller for induction motor drive based on adaptive input-output feedback linearization and sliding mode control," *Energy Conversion and Management* , vol. 49, Issue 4, pp. 541-550, April 2008.

[55] N.R. Abjadi, G.R. Arab Markadeh, and J. Soltani, " Model following sliding-mode control of a six-phase induction motor drive ," *Journal of Power Electronics*, vol. 10, Issue 6, pp. 694-701, November 2010.

[56] S. M .N Hassan and I. Hussain, " A laurenberger sliding mode observer for on line parameter estimation and adaptation in high performnce induction motor drives," *IEEE Trans. on Industry Application*, vol.45, pp.772-781, 2009.

[57] O.Kowalska, T.,M. Dybkowski, K. Szabat, "Adaptive sliding –mode neuro-fuzzy control of the two-mass induction motor drive without mechanical sensors," *IEEE Trans. on Industrial Electronics*, vol.57, pp.553-564, Feb.2010.

[58] P. Liutanakul, S. Pierfederici, and F. M.- Tabar, " Application of smc with i/o feedback linearization to the control of the cascade controlled- rectifier/inverter-motor drive system with small dc-link capacitor ," *IEEE Trans. Power Electronics*, vol. 23, no.5, pp.2489-2499, September 2008

[59] P. Liutanakul, S. Pierfederici and F. Meibody-Tabar , "Nonlinear control techniques of a controllable rectifier/inverter-motor drive system with a small dc-link capacitor ," *Energy Conversion and Management* , vol. 49, Issue 12, pp.3541-3549, December 2008.

[60] L.A. Zadeh. "Fuzzy sets ," *Infom. Control*. vol.8, pp.338-335, 1965.

[61] T. Takagi, M. Sugeno, "Fuzzy identification of systems and its application to modeling and control," *IEEE. Trans Syst. Man Cybern*, vol. 15, no.1, pp.116-132, 1985.

[62] C. C. Lee, "Fuzzy Logic on Control System-PartI, *IEEE Trans on Systems, Man and Cybernetics*," vol. 20, no2. pp.404-418, March/April 1990.

[63] C C Lee, "Fuzzy Logic on Control System-PartII," *IEEE Trans. on Systems, Man and Cybernetics*, vol 20, no2. pp.419-435, March/April 1990.

[64] B. N. Singh, B. Singh and B. P. Singh, "Fuzzy control of integrated current – controlled converter _inverter _fed cage induction motor drive," *IEEE Trans on Industry Applications*, vol. 35, .no.2, pp.405-412, March/April 1999.

[65] M. M. Krishan, L. Barazane and A. Knwaldeh, " Using an adaptive fuzzy-logic system to optimize the performance and the reduction of chattering phenomenon in the control of induction motor," *American Journal of Applied Sciences*, vol.7, pp.110-119, 2010.

[66] A. Moez, S. Mansour and C. Mananed, " Takagi-sugeno fuzzy control of induction motor," *Wold Academy of science, Engineering and Technology*, vol.68, pp. 479-485, Aug. 2010.

[67] A. K. Sichani, G. R. A. Markadeh and S. H. Esjahani, " Design of optimal-robust speed T-S fuzzy controller for a wounded rotor induction motor coupled with a nonlinear load," *IEEE International symposium on Industrial Electronics*, article no. 5637609, pp.148-156, 2010.

[68] Y Li. , X.Zhang and Y.Wang, " H_∞ fuzzy variable structure control for TS-model based induction motor drive system," *International review on computers and software*, vol.6, pp.219-226, March 2011.

[69] J. B. Edwards and D. H. Owens, *Analysis and Control of Multipass Processes*, Taunton, Chichester: Research Studies, 1982.

[70] S. Arimoto, S. Kawamura, and F. Miyazaki, "Bettering operation of robots by learning," *J. Robotic Systems*, vol. 1, no. 2, pp. 123–140, 1984.

[71] Casalino and B. Bartolini, "A learning procedure for the control of movements of robotic manipulators," in *Proc. IASTED Symp. Robotics and Automation*, Amsterdam, Netherlands, pp. 108–111, 1984.

[72] N. Amann, D.H. Owens, E. Rogers, "Iterative learning control using optimal feedback and feedforward actions," *International Journal of Control* 65 ,277–293, 1996.

[73] D.A. Bristow, M. Tharayil, A.G. Alleyne, "A survey of iterative learning control," *IEEE Control Systems Magazine* 26 pp.96–114, 2006.

[74] W. Qian, S. K. Panda and J. X. Xu, "Torque ripple minimization in PM synchronous motor using iterative learning control," *IEEE Trans. on Power Electronics*, vol.19, no.2, March 2004.

[75] S. A. Saab, "A stochastic iterative learning control algorithm with application to an induction motor," *Int.J.Contr*., vol.77, no.2, pp.144-163, 2004.

[76] A. Oteafy and J. Chiasson, "Lyapunov stability of an open-loop induction machine," in *Proc. Amer. Control Conf.*, St. Louis, MO, pp.3452–3457, 2009.

[77] C. M. Verrelli ,"Global exponential convergence properties for the open-loop induction motor," *IEEE Trans on Control System Technology, vol. 20, no. 6*, pp. 1647-1650, Nov. 2012.

[78] L. F. Pak, M. O. Faruque, X. Nie and V. Danivahi, "A versatile cluster based real-time digital simulator for power engineering research", *IEEE Trans on Power System, vol. 21, no. 2,* May 2006, pp. 455-465.

[79] C. Dufour, S. Abourida and J. Belanger, "Real-time simulation of induction motor IGBT drive on a pc-cluster", *Procc. of the Int. Conf. on Power System Transients*, 2003, Hong Kong.

[80] A. Kusko and M.T. Thompsom, "Power quality in electrical systems", *The McGraw-Hill Professional*, New York, 2007.

[81] R.S. Vedam and M.S. Sharma, "Power quality in electrical system," *Taylor &Francis Group*, Florida, 2009.

[82] *IEEE Recommended Practices and Requirements for Harmonics Control in Electric Power Systems*, IEEE Std. 519, 1992.

[83] *IEEE Guide for Application and Specification of Harmonic Filters, IEEE Std.1531,* 2003.

[84] *IEEE recommended practice for monitoring electric power quality, IEEE Std. 1159-1995,* June 14, 1995.

[85] *Electromagnetic Compability (EMC)-Part 4-30: Testing and Measurement Techniques-Power Quality Measurement Methods*, IEC Std. 6100-4-30, 2003.

[86] Damian, A. Gonzalez and J. C. Mccall, "Design of filter to reduce harmonic distortion in industrial power systems," *IEEE Trans. on Industry Applications*, vol.23, no.3, pp.504-511, May/June.1987.

[87] S. M. Peeran and C.W.P. Cascadden, "Application, design and specification of harmonic filters for variable frequency drives," *IEEE Tras. on Industry Applications*, vol.31, no.4, pp.841-847, July/ August 1995.

[88] F. Z. Peng, G. J. Su, and G. Farquharson, "A series LC filter for harmonic compensation of AC drives," in *Proc. IEEE PESC 1999,* vol.1, pp213-218, June/July 1999

[89] J. K. Phipps, "A transfer function approach to harmonic filter design," *IEEE Industry Application*, vol.1A-40, no.1, pp.232-241, Jan./Feb.2004.

[90] J. C. Das, " Passive filters-Potential and limitations." *IEEE Trans, on Industry Applications*, vol. IA-40, no.1, pp.232-241, Jan/Feb.2004.

[91] B. Singh, V. Verma, A. Chandra and K. Al. Haddad, "Hybrid filters for power quality improvement," *IEE Proc. Gener. Transm. Distrib*. vol.152, no.3, pp365-378, May 05.

[92] K. K. Shyu, M. J. Yang, Y. M. Chen, and Y. F. Lin, "Model reference adaptive control design for a shunt active-power-filter system," *IEEE Trans. Ind. Electron.*, vol. 55, no. 1, pp. 97–106, Jan. 2008

[93] C. C. Hua, C. H.Li, and C. S. Lee, "Control analysis of an active power filter using Lyapunov candidate," *IET Power Electron*. vol.2, no.4, pp.325-334, Jul.2008.

[94] L. Asiminoaei, P. Rodriguez, F. Blaabjerg, and M. Malinowski, "Reduction of switching losses in active power filters with a new generalized discontinuous-PWM strategy," *IEEE Trans. Ind. Electron.*, vol. 55, no. 1,pp. 467–471, Jan. 2008.

[95] Z. Shu, Y. Guo, and J. Lian, “Steady-state and dynamic study of active power filter with efficient FPGA-based control algorithm,” *IEEE Trans.Ind. Electron.*, vol. 55, no. 4, pp. 1527–1536, Apr. 2008.

[96] C. Lascu, L. Asiminoaei, I. Boldea, and F. Blaabjerg, “Frequency response analysis of current controllers for selective harmonic compensation in active power filters,” *IEEE Trans. Ind. Electron.*, vol. 56, no. 2, pp. 337–347, Feb. 2009.

[97]] S. Rahmani, K. Al-Haddad, and H. Y. Kanaan, “A comparative study of two PWM techniques for single-phase shunt active power filters employing direct current control strategy,” *J. IET Proc.—Electr. Power Appl.*,vol. 1, no. 3, pp. 376–385, Sep. 2008.

[98] S. Orts-Grau, F. J. Gimeno-Sales, S. Segui-Chilet, A. Abellan-Garcia, M. Alcaniz-Fillol, and R. Masot-Peris, “Selective compensation in four-wire electric systems based on a new equivalent conductance approach,” *IEEE Trans. Ind. Electron.*, vol. 56, no. 8, pp. 2862–2874,Aug. 2009.

[99] E. Lavopa, P. Zanchetta, M. Sumner, and F. Cupertino, “Real-time estimation of fundamental frequency and harmonics for active shunt power filters in aircraft electrical systems,” *IEEE Trans. Ind. Electron.*, vol. 56,no. 8, pp. 2875–2884, Aug. 2009.

[100] W. Lenwari, M. Sumner, and P. Zanchetta, “The use of genetic algorithms for the design of resonant compensators for active filters,” *IEEE Trans.Ind. Electron.*, vol. 56, no. 8, pp. 2852–2861, Aug. 2009.

[101] J. Miret, M. Castilla, J. Matas, J. M. Guerrero, and J. C. Vasquez, “Selective harmonic-compensation control for single-phase active power filter with high harmonic rejection,” *IEEE Trans. Ind. Electron.*, vol. 56, no. 8, pp. 3117–3127, Aug. 2009.

[102] R. S. Herrera, P. Salmeron, and H. Kim, “Instantaneous reactive power theory applied to active power filter compensation: Different approaches, assessment, and experimental results,” *IEEE Trans. Ind. Electron.*, vol. 55,no. 1, pp. 184–196, Jan. 2008.

[103] F. Defay, A. M. Llor, and M. Fadel, “A predictive control with flying capacitor balancing of a multicell active power filter,” *IEEE Trans. Ind.Electron.*, vol. 55, no. 9, pp. 3212–3220, Sep. 2008.

[104] K. Drobnic, M. Nemec, D. Nedeljkovic, and V. Ambrozic, "Predictive direct control applied to AC drives and active power filter," *IEEE Trans. Ind. Electron.*, vol. 56, no. 6, pp. 1884–1893, Jun. 2009.

[105] M. Cirrincione, M. Pucci, G. Vitale, and A. Miraoui, "Current harmonic compensation by a single-phase shunt active power filter controlled by adaptive neural filtering," *IEEE Trans. Ind. Electron.*, vol. 56, no. 8,pp. 3128–3143, Aug. 2009.

[106] B. Singh and J. Solanki, "An implementation of an adaptive control algorithm for a three-phase shunt active filter," *IEEE Trans. Ind. Electron*, vol. 56, no. 8, pp. 2811–2820, Aug. 2009.

[107] B. Kedjar and K. Al-Haddad, "DSP-based implementation of an LQR with integral action for a three-phase three-wire shunt active power filter," *IEEE Trans. Ind. Electron.*, vol. 56, no. 8, pp. 2821–2828, Aug. 2009.

[108] N. He, D. Xu, and L. Huang, "The application of particle swarm optimization to passive and hybrid active power filter design," *IEEE Trans.Ind. Electron.*, vol. 56, no. 8, pp. 2841–2851, Aug. 2009.

[109] S. Rahmani, N. Mendalek, and K.AI-Haddad, "Experimental design of a nonlinear control technique for three-phase shunt active power filter," *IEEE Trans. Ind. Electron*, vol.57, no.10, pp.3364-3375, Oct.2010.

[110] S. Rahmani, A. Hamadi, and K. Al-Haddad, "A new three phase hybrid passive filter to dampen resonances and compensate harmonics and reactive power for any type of load under distorted source conditions," in *Proc. IEEE Power Electron. Sep.*2007, pp.2594-99.

[111] V. F. Corasaniti, M. B. Barbieri, P. L. Arnera, and M. I. Valla, "Hybrid active filter for reactive and harmonics compensation in a distribution network," *IEEE Trans. Ind. Electron.*, vol. 56, no. 3, pp. 670–677,Mar. 2009.

[112] A. Hamadi, S. Rahmani, and K. Al-Hadad, "A hybrid passive filter configuration for VAR control and harmonic compensation," *IEEE Trans. Industrial Electronics*, vol. 57, no. 7, pp. 2419-2434, July 2010.

[113] A. Luo, X.Xu, L Fang., H.Fang, J Wu., and C, Wu. "Feedback feedforward PI- type iterative learning control for hybrid active filter with injection circuit," *IEEE Trans.Ind. Electron.*, vol.57,pp.3767-3779, Nov. 2010.

[114] S. Rahmani, A. Hamadi and Kamal Al-Haddad, "A Lyapunov- function –based control for a three-phase shunt hybrid active filter," *IEEE Trans. Ind. Electronics* vol.no.3,March 2012.

[115] L. Gyugyi, "Reactive Power Generation and Control by Thyristor circuits, " *IEEE Trans. Ind. Appl*. vol.IA-15, no.5, pp.521-532, Sept./Oct.1979.

[116] S. Lee, "Development of an input power factor corrected variable speed motor drive system for the electric motor drives," *ASEE Annual Conference and Exposition. Vancouver*, pp18, 26 -29 June 2011.

[117] A. Sarijali and M. Farsadi , " Application of D-STATCOM to improve the power quality and transient operation of induction motor," *International review on modeling and simulations* vol. 4, issue 1, pp. 318-324, February 2011.

[118] A. Hamadi, S. Rahmani, and K. Al-Haddad, " A hybrid passive filter configuration for VAR control and harmonic compensation," *IEEE Trans.Ind. Electron*., vol. 57, no. 7, pp. 2419–2434, Jul. 2010.

[119] I. R. Smith, G. K. Creighton, "Reactive-Current compensation by switched capacitors", *IEEE Transactions on Industrial Electronics and Control Instrumentation*, vol.IECI-22, issue 1, pp.75-78, February 1975.

[120] A. Olwegard, K. Walve, G. Waglund, H. Frank, S. Torseng, "Improvement of Transmission Capacity by Thyristor Controlled Reactive Power," *IEEE Transaction on Power Apparatus and Systems*, vol. PAS-100, no.8, pp. 75-78, August 1981.

[121] T. Ohyama, K.Yamashita, T. Maeda, H.Sujuki, S.Mine, "Effective Application of Static Var Compensation to Damp Oscillations," *IEEE Transactions on Power Apparatus Systems*, vol. PAS-104, issue 6, pp. 1405-1410, June1985.

[122] G. G. Karady, "Continuous regulation of Capacitive reactive power," *IEEE Transaction on Power Delivery*, vol.7, no.3, July 1992.

[123] M. Tabandeh, M. H.Alavi, M. Marami and G. R.Dehnavi, "Design and implementation of TSC type SVC Using a new approach for electrical quantities measurement", *Power Tech Proceedings*, vol.2, p. 6, 10-13 September 2001.

[124] Z. Jianhua, D. Guanping, X. Gang, Z. Jie, Z. Hui and W. Shuying, "Design of the control system for thyristor switched capacitor devices", *Trans-mission and Distribution Conference and Exposition*, vol.2, pp. 606{610, 7-12 September 2003.

[125] H. Ai-jun., S.Fei and C.Wen-jin, "Zero-Cross Triggering Technology of Series SCRs with optical fiber at medium voltage: application for thyristor switched capacitor",

Transmission and Distribution Conference and Exhibition: Asia and Pacific, 2005 IEEE/PES, pp. 1, 2005.

[126] G. Celli, F.Pilo and S.B.Tennakoon, "Voltage Regulation on 25 kV AC railway systems by Using thyristor switched capacitor", *Ninth International Conference on Harmonics and Quality of Power*, vol. 2, pp. 633{638, 2000.

[127] X. Yuqin, W. Zengping, Z. Hai, "The automatic following control of arc suppression coil with thyristor switched capacitors", *IEEE Conference on Industrial Electronics and Applications*, pp. 15, 24-26 May 2006.

[128] A. Kallaste.,L. Kutt,V. Bolgov, K. Janson, "Reactive power compensation for spot welding machine using thyristor switched capacitor", *Power Quality and Supply Reliability Conference*, pp. 241,245, 27-29 Aug. 2008.

[129] M. A. M. Radzi and N. A. Rahim, "Neural network and bandless hysteresis approach to control switched capacitor active power filter for reduction of harmonics," *IEEE Trans. Ind. Electron.*, vol. 56, no. 5, pp. 1477–1484, May 2009.

[130] M. H. Rashid, Power Electronocs Circuits, Devices, and Applications, Pearson Prentice Hall, 2004.

List of Publications

1. K. B. Mohanty, Madhu Singh, "RTDS implementation and induction motor drive performance comparison with P-I, sliding Mode and iterative learning controller," *International Review of Electrical Engineering (IREE)*, vol. 8, no. 1, Feb. 2013, pp.144-156.
2. K. B. Mohanty, Madhu Singh, "Performance improvement of induction motor drive using feedback linearization and fuzzy torque compensator with RTDS implementation," *International Review of Electrical Engineering (IREE)*, vol. 7, no. 3, June 2012, pp.4374-4382.
3. K. B. Mohanty, Madhu Singh, "Stability analysis and RTDS implementation of the induction motor controller based on Lyapunov theorem," Under review of *IET Electric Power Applications*.
4. K. B. Mohanty, Madhu Singh, "Modeling of induction motor in stationary reference frame and Lyapunov analysis," Under review of *Int. Journal of Modeling and Simulation*, ACTA Press.
5. K. B. Mohanty, Madhu Singh, "Feedback linearizing control of induction motor drive by P-I controllers in RTDS environment," *Journal of Automation and Control Engineering*, 2013.
6. Madhu Singh, K. B. Mohanty, and B. Subudhi, "Sliding mode control of a feedback linearized induction motor using TS fuzzy based adaptive iterative learning controller," *Procc. of 9th IEEE Int. Conf. on Power Electronics and Drive Systems, Singapore*, Dec., 2011, pp. 625-630.
7. K. B. Mohanty, Madhu Singh, "Input Power Conditioning of a Linearized Induction Motor Drive using Three Level Front-End Converter and Passive Filter," *Procc. of IEEE INDICON*, Dec. 2011, Hyderabad, pp. 1-6.
8. K. B. Mohanty, Madhu Singh, "Robust control of a feedback linearized induction motor through sliding mode," *Procc. of IEEE PEDES 2010 and Power India Joint Conf.*, New Delhi, Dec. 2010, pp. 1-7.
9. K. B. Mohanty, Madhu Singh, "Performance improvement of an induction motor drive using feedback linearization and fuzzy torque compensator," *Procc. of IEEE PEDES 2010 and Power India Joint Conf.*, New Delhi, Dec. 2010, pp. 1-7.